IAEA TECDOC SERIES

IAEA-TECDOC-1764

IAEA-TECDOC-1764

Radiation Curing of Composites for Enhancing Their Features and Utility in Health Care and Industry

IAEA
International Atomic Energy Agency

RADIATION CURING OF COMPOSITES FOR ENHANCING THEIR FEATURES AND UTILITY IN HEALTH CARE AND INDUSTRY

The following States are Members of the International Atomic Energy Agency:

AFGHANISTAN
ALBANIA
ALGERIA
ANGOLA
ARGENTINA
ARMENIA
AUSTRALIA
AUSTRIA
AZERBAIJAN
BAHAMAS
BAHRAIN
BANGLADESH
BELARUS
BELGIUM
BELIZE
BENIN
BOLIVIA, PLURINATIONAL STATE OF
BOSNIA AND HERZEGOVINA
BOTSWANA
BRAZIL
BRUNEI DARUSSALAM
BULGARIA
BURKINA FASO
BURUNDI
CAMBODIA
CAMEROON
CANADA
CENTRAL AFRICAN REPUBLIC
CHAD
CHILE
CHINA
COLOMBIA
CONGO
COSTA RICA
CÔTE D'IVOIRE
CROATIA
CUBA
CYPRUS
CZECH REPUBLIC
DEMOCRATIC REPUBLIC OF THE CONGO
DENMARK
DJIBOUTI
DOMINICA
DOMINICAN REPUBLIC
ECUADOR
EGYPT
EL SALVADOR
ERITREA
ESTONIA
ETHIOPIA
FIJI
FINLAND
FRANCE
GABON
GEORGIA
GERMANY
GHANA
GREECE
GUATEMALA
GUYANA
HAITI
HOLY SEE
HONDURAS
HUNGARY
ICELAND
INDIA
INDONESIA
IRAN, ISLAMIC REPUBLIC OF
IRAQ
IRELAND
ISRAEL
ITALY
JAMAICA
JAPAN
JORDAN
KAZAKHSTAN
KENYA
KOREA, REPUBLIC OF
KUWAIT
KYRGYZSTAN
LAO PEOPLE'S DEMOCRATIC REPUBLIC
LATVIA
LEBANON
LESOTHO
LIBERIA
LIBYA
LIECHTENSTEIN
LITHUANIA
LUXEMBOURG
MADAGASCAR
MALAWI
MALAYSIA
MALI
MALTA
MARSHALL ISLANDS
MAURITANIA
MAURITIUS
MEXICO
MONACO
MONGOLIA
MONTENEGRO
MOROCCO
MOZAMBIQUE
MYANMAR
NAMIBIA
NEPAL
NETHERLANDS
NEW ZEALAND
NICARAGUA
NIGER
NIGERIA
NORWAY
OMAN
PAKISTAN
PALAU
PANAMA
PAPUA NEW GUINEA
PARAGUAY
PERU
PHILIPPINES
POLAND
PORTUGAL
QATAR
REPUBLIC OF MOLDOVA
ROMANIA
RUSSIAN FEDERATION
RWANDA
SAN MARINO
SAUDI ARABIA
SENEGAL
SERBIA
SEYCHELLES
SIERRA LEONE
SINGAPORE
SLOVAKIA
SLOVENIA
SOUTH AFRICA
SPAIN
SRI LANKA
SUDAN
SWAZILAND
SWEDEN
SWITZERLAND
SYRIAN ARAB REPUBLIC
TAJIKISTAN
THAILAND
THE FORMER YUGOSLAV REPUBLIC OF MACEDONIA
TOGO
TRINIDAD AND TOBAGO
TUNISIA
TURKEY
UGANDA
UKRAINE
UNITED ARAB EMIRATES
UNITED KINGDOM OF GREAT BRITAIN AND NORTHERN IRELAND
UNITED REPUBLIC OF TANZANIA
UNITED STATES OF AMERICA
URUGUAY
UZBEKISTAN
VENEZUELA, BOLIVARIAN REPUBLIC OF
VIET NAM
YEMEN
ZAMBIA
ZIMBABWE

The Agency's Statute was approved on 23 October 1956 by the Conference on the Statute of the IAEA held at United Nations Headquarters, New York; it entered into force on 29 July 1957. The Headquarters of the Agency are situated in Vienna. Its principal objective is "to accelerate and enlarge the contribution of atomic energy to peace, health and prosperity throughout the world''.

IAEA-TECDOC-1764

RADIATION CURING OF COMPOSITES FOR ENHANCING THEIR FEATURES AND UTILITY IN HEALTH CARE AND INDUSTRY

INTERNATIONAL ATOMIC ENERGY AGENCY
VIENNA, 2015

COPYRIGHT NOTICE

For further information on this publication, please contact:

Radioisotope Products and Radiation Technology Section
International Atomic Energy Agency
Vienna International Centre
PO Box 100
1400 Vienna, Austria
Email: Official.Mail@iaea.org

Printed by the IAEA in Austria
April 2015

IAEA Library Cataloguing in Publication Data

Radiation curing of composites for enhancing their features and utility in health care and industry. — Vienna : International Atomic Energy Agency, 2015.
p. ; 30 cm. — (IAEA-TECDOC series, ISSN 1011–4289 ; no. 1764)
ISBN 978–92–0–103815–9
Includes bibliographical references.

1. Composite materials — Curing. 2. Radiation — Industrial applications. 3. Radiation curing. I. International Atomic Energy Agency. II. Series.

IAEAL 15–00964

FOREWORD

Composite materials combine the properties of the individual components to produce a variety of materials in an efficient and cost effective manner. Composite materials are used in various applications, including sports equipment, automotive and aerospace industries, food packaging and artificial organs. Materials reinforced with nanoscale components add new dimensions to composite materials and enable further major improvements in functional and structural properties. The incorporation of only a small number of nano-sized particles can result in dramatic property changes of the composite.

Several major issues need to be addressed to utilize the full potential of such nanofillers. Among them are the incompatibility or weak interfacial bonding between the matrix and the nanoscale component, and the agglomeration of nano-sized component during processing, resulting in inhomogeneous distribution. According to the results of ongoing investigation and product preparation at several Member State institutions, radiation technology offers a way of overcoming these challenges by grafting appropriate monomers and polymers onto the nanofiller surface, thereby fixing their morphology and making them compatible with the host polymer. Radiation techniques also offer the possibility for simultaneous synthesis of the nanoparticle component and crosslinking of the matrix of the composite, which is not possible with other techniques. With the availability of lower cost, self-shielded low energy electron beam accelerators, this process is becoming an option for developing countries.

In order to use the advantages of radiation techniques and to address the needs of Member States producing advanced composite materials, the Coordinated Research Project (CRP) on Radiation Curing of Composites for Enhancing their Features and Utility in Health Care and Industry supported participating institutions in the development of methodologies and protocols for new abrasion resistant coating formulations, radiation curable nanocomposites from natural polymers, new biodegradable packaging materials suitable for radiation sterilization and new methods to modify surface characteristic of nano-sized materials to enhance polymer fillers interaction. This CRP provided a forum for knowledge and technology transfer among the participating institutions, and promoted early involvement of developing countries in knowledge intensive R&D programmes. This publication is the final report of the CRP, with detailed reports from each participating institution.

The IAEA wishes to thank all participants for their valuable contributions. The IAEA officer responsible for this publication was A. Safrany of the Division of Physical and Chemical Sciences.

EDITORIAL NOTE

This publication has been prepared from the original material as submitted by the contributors and has not been edited by the editorial, staff of the IAEA. The views expressed remain the responsibility of the contributors and do not necessarily represent the views of the IAEA or its Member States.

Neither the IAEA nor its Member States assume any responsibility for consequences which may arise from the use of this publication.

This publication does not address questions of responsibility, legal or otherwise, for acts or omissions on the part of any person.

The use of particular designations of countries or territories does not imply any judgement by the publisher, the IAEA, as to the legal status of such countries or territories, of their authorities and institutions or of the delimitation of their boundaries.

The mention of names of specific companies or products (whether or not indicated as registered) does not imply any intention to infringe proprietary rights, nor should it be construed as an endorsement or recommendation on the part of the IAEA.

The IAEA has no responsibility for the persistence or accuracy of URLs for external or third party Internet web sites referred to in this publication and does not guarantee that any content on such web sites is, or will remain, accurate or appropriate.

CONTENTS

Chapter 1

1.1. INTRODUCTION

1.1.1. Composite and nanocomposite materials

Composite materials combine properties of the individual components in a synergetic manner to produce a variety of materials in an efficient and cost effective manner. Thus, composite materials today are being used in various applications from sports equipment, automotive and aerospace industries to artificial organs. Their utilization is expected to further increase in the next decades since multi-functional composites are the key for advanced structures and devices.

The incorporation of micro-size inorganic particulate materials is an established method of enhancing specific properties of polymeric materials for many industrial products. However, high concentrations (typically 20 – 30% by volume) of these additives are required to achieve the targeted properties. In some cases this high filler loadings adversely affects the processability of the composite, energy demands for processing are increased and the weight of the end material is much higher as compared to the neat polymer. Nano-size materials, like carbon nano-tubes (CNTs), possess much superior mechanical and thermal properties and incorporation of such materials in the polymer composites is expected to increase the mechanical and thermal characteristics of the polymers at extremely low filler concentrations. Additionally, nanofillers may impart other, either bulk or surface, desired properties, such as shrinkage control, lighting strikes protection, radiation resistance or shielding, erosion or corrosion protection, controlled wetting and adhesion.

Similarly blend of polymers such as natural rubber and ethylene-vinyl acetate (NR/EVA), natural rubber polypropylene (NR/PP) and polypropylene (PP) with the incorporation of nanoclay as specialty materials are being investigated for application in automotive parts and packaging. Radiation curable nanocomposites containing nano silica can give additional benefits, and their potential to be utilized as coating materials for flooring, wall panel, and furniture products with high scratch and abrasion resistance properties has already been shown. Other improvements like self-cleaning properties can be reached by changing the nature of particles.

One of the important areas where nanocomposites are expected to play an important part is their use as catalysts in industrial applications due to their very high surface area.

There are significant opportunities for future developments of nanocomposites in health care as advanced delivery devices that include site specific or self-regulated drug delivery, targeted radiotherapy, targeted imaging systems and integrated diagnostic and therapeutic micro-/nanodevices.

1.1.2. Challenges

Several major issues need to be addressed to utilize the full potential of such nanocomposites, and among them:

— Due to the incompatible surface properties, the interfacial bonding between the polymer segments and nanofiller is weak and needs to be improved by chemically modification of the nanofiller,

— Due to their high surface area, that is several orders of magnitude higher than the conventional fillers, they tend to agglomerate in the polymer matrices during processing and the full potential of their expected properties is not achieved;

— Due to their high surface area, the nanoparticles may exhibit unwanted catalytic activity;

— There are numerous health and toxicity concerns associated with nanofillers;

— There are unmet clinical needs for safer and better-tolerated drugs and "active" nanoparticles as tags in the diagnosis and treatments of various diseases integrated into scaffolds for tissue engineering, embedded or attached to fibres and fabrics to obtain smart patches, smart bandages or bed linens, etc.

1.1.3. The role of radiation in addressing the challenges

Radiation technology offers an excellent way of overcoming some of these challenges as the characteristics of these nanosized fillers can be suitably modified by grafting of appropriate monomers/polymers onto their surface thereby altering their morphology and at the same time making them compatible with the host polymers. Unlike conventional methods, radiation grafting can be carried out at room temperature and without any initiators, avoiding the incorporation of toxic chemical byproducts. Nanoparticles can more easily be homogeneously dispersed in liquid media (monomers, solvent plus monomers, sol/gels, etc.) followed by a quick polymerization step by radiation at ambient temperature thereby retaining the initially obtained homogeneous distribution resulting in a better dispersion of the nano-filler materials. The desired characteristics of the product thus can be achieved at lower filler content resulting in the formation of a light-weight material with superior mechanical properties in an energy efficient manner. Additionally, keeping the nanoparticles in solution may eliminate some toxicity concerns too.

1.1.4. Scope of this CRP

In order to use the advantages of radiation techniques and address the needs of Member States for producing advanced composite materials for various applications, this CRP started in 2010. The CRP aimed to support IAEA Member States to develop methodologies and protocols for new abrasion resistant coating formulations, radiation curable nano-composites from natural polymers, new biodegradable packaging materials suitable for radiation sterilization, and new methods to modify surface characteristic of nano-sized materials to enhance polymer fillers interaction. This CRP also provided a forum for knowledge and technology transfer among the participating institutions, as well as promoted early involvement of developing countries in knowledge-intensive R&D programs was to enhance their level of competence and confidence and promote the local spin-off initiatives.

1.2. CRP OVERALL OBJECTIVE

To enhance Member States capability in the use of radiation technology for production of nano-composites with enhanced safety, stability and functionality for advanced applications.

1.2.1. Specific research objectives

Support the production and technology transfer of advanced polymer nano-composites by using the demonstrated advantages of radiation technology for:

— Protocols for preparation of new scratch and abrasion resistant coating formulations with enhanced surface finishing;

— Preparation methods for radiation curable nano-composites from natural polymers;

— Preparation of protocols and specifications for new biodegradable packaging materials suitable for radiation sterilization;

— New methods to modify surface characteristic of nano-sized materials to enhance polymer fillers interaction.

1.2.2. Expected research output

— Protocols for scratch and abrasion resistant coating formulations with enhanced surface finishing

— Preparation methods for new radiation curable nano-composites from natural polymers

— Specification and protocols for biodegradable packaging materials suitable for radiation sterilization

— New methods to modify surface characteristic of nano-sized materials to enhance polymer fillers interaction

The participating institutions were expected to contribute to one or more specific research objectives. The results were presented in international conferences and published in scientific journals.

1.2.3. Achievements

The first RCM was held 18–22 July 2011 in Vienna, Austria, where the 14 participants presented and discussed the status in the field, agreed on the work plan for the first 18 months and indicated collaboration possibilities. The report from this meeting is available as working material at http://www-naweb.iaea.org/napc/iachem/working_materials/RC-1207-1-report.pdf.

The second RCM was convened on 26–30 November 2012 in Cairo, Egypt, and was attended by 14 participants, who presented their achievements and agreed on the work plan for the next period. The meeting report is available as working material at http://www-naweb.iaea.org/napc/iachem/working_materials/RC-1207-2-report.pdf.

The third RCM was held on 9–13 June 2014 in Palermo, Italy. The participants reviewed the achievements of the CRP, and highlighted them organized around the categories matching the planned expected outrputs:

1.2.3.1. Protocols for scratch and abrasion resistant coating formulations with enhanced surface finishing were developed as follows:

— Transparent, scratch and abrasion resistant topcoats are the essential requirements of automotive and wood flooring products. To maximize mechanical, optical and chemical performance, a proper selection of lacquer as well as nanofiller components is very important and various protocols for different applications have been developed. Large scale production of five nanocomposite formulations has been set up (Germany);

— For curing such high solid content formulations, UV induced polymerization is an effective approach owing to its advantages such as fast curing, energy saving, curing at

ambient temperature, and environmental friendly technology by avoiding volatile organic solvents. Acrylate based silica containing nanocomposites have been preferred because of their superior reactivity and properties;

— For photoinitiator-free curing of acrylate-based coatings a VUV/UV lamp set-up has been tested and successfully applied on pilot scale.

1.2.3.2. Preparation methods for new radiation curable nano-composites from natural polymers:

— Nanocomposites with Ag nanoparticles (NP), incorporated in poly(vinyl alcohol) (PVA) and chitosan (CS) based polymer matrix, were prepared using gamma irradiation. The synthesis of hydrogel nanocomposites was done by two different pathways: (1) Ag NPs were incorporated in previously crosslinked PVA/wsCS matrix; (2) simultaneous crosslinking of polymers and *in situ* synthesis of Ag NPs by γ-irradiation. (Serbia);

— Radiation (UV/EB) was used to cure coatings of acrylated epoxidized palm oil (EPOLA) containing various proportions of silica nanoparticles. The nanoparticles induced increase in both: gel contents and surface hardness. These polymeric materials showed excellent resistance toward scratch and abrasion. (Malaysia);

— Significant improvement of the tensile properties of radiation-cured (UV/EB) PUR acrylate aqueous emulsions was achieved by introducing 1 wt-% of cellulose nanocrystals (aqueous CNC suspension originating from ramie). Attempts to further improve the tensile properties by enhancing the CNC content led to several difficulties for achieving the preparation of defect-free samples and/or induced nanoparticle aggregation. (France).

1.2.3.3. Specification and protocols for biodegradable packaging materials suitable for radiation sterilization were reported by Canada, Pakistan, Poland and Egypt. Examples include:

— Protocols for preparation of biodegradable nanocomposite films with good mechanical and barrier properties from cellulose acetate (CA), chitosan or polycaprolactone (PLC) were developed using a small amount of graphene oxide nano-sheets and silver nano-particles as nano-scale additives;

— Protocol for PCL-based films reinforced by carbone nanotube (CNT) using gamma radiation;

— Development of a methodology to encapsulate antimicrobial compounds, as well as microfluidisation and irradiation treatment for better dispersion of nanofibers in suspension;

— Development of a protocol for measuring the controlled release of active compounds;

— Development of a methodology to encapsulate antimicrobial compounds in polymers and combination with irradiation;

— Preparation and characterization of bioactive polylactic acid-nanocrystalline cellulose poly-lactic acid –nanocrystalline nanocellulose supramolecular nanocomposite films;

— Hydrophilicity of the biodegradable and edible films constructed from potato starch and lipids was reduced by the addition of NCC and NFC, followed by gamma-radiation. 25 kGy dose improves additionally stress-strain features the final product;

— Partially bio-based thermoplastic packgaing materials suitable for radiation sterilizable products containing high density polyethylene/starch/nano-clay blends was developed. The obtained results of these composites at sterilization dose of 25 kGy are quite encouraging and will have potential as packaging materials for food, drug and other disposable items etc.

1.2.3.4. New methods to modify surface characteristic of nano-sized materials to enhance polymer fillers interaction:

— Methyl-cellulose (MC)-based films grafted with TMPTMA monomer by gamma radiation, in combination with nanocrystalline cellulose filling;
— Chitosan-based composites films grafted with silane by gamma radiation, in combination with polycaprolactone (PCL) reinforcement;
— Effect of hema and silane monomers using gamma irradiation on the mechanical and barrier properties of methylcellulose-based films.(Canada);
— Functional groups were successfully introduced onto carbon nanofiber surface via ionizing radiation, which led to a significant increase in the percentage of oxygen. These functionalized nanofibers in composites improved the interactions with an epoxy resin system. (Brazil);
— The polypropylene (PP) irradiated in air was successfully used as a compatibilizer in the preparation of PP/montmorillonite(MMT) nanocomposites with about 25% improvement in elastic modulus at very low MMT loading. The compatibilizing effect of radiation modified PP was found to be comparable with commercially available maleic acid (MA) grafted PP. The second approach was to modify MMT by in-situ radiation induced polymerization of a charged vinyl monomer. Radiation-modified MMT was found to be fully exfoliated when used in the preparation of nanocomposites based on ethylene-vinyl acetate copolymer. The improvement achieved in mechanical properties of nanocomposites was better than when organo-modified MMTs were used. (Turkey);
— The concept of radiation–induced compatibilization of polymers for the preparation of nanocomposites has been successfully applied in composites prepared from vegetable fibers as well as rubber.

1.2.3.5. Additional achievements

New methods to modify polymer-filler/fiber interfaces in composite materials

Besides methods to modify the nanofiller surface for better compatibility with the matrix, several institutions from Italy, India, France and Thailand reported achievements as follows:

— Admicellar polymerization was used to coat ultra-thin (nanoscale) film of poly(methyl methacrylate) (PMMA) onto starch surface to make it more compatible with poly(lactic acid) (PLA). The PMMA-modified starch was successfully prepared as confirmed by Fourier-transform infrared spectroscopy (FTIR), scannin electron microscopy (SEM), floating test and iodine test. The prepared modified starch resulted in improved compatibility with PLA as well as enhanced mechanical properties, compared with unmodified starch;
— The main features of the inhibition mechanisms affecting the radiation-induced free radical polymerization of unsaturated monomers in carbon fibre-reinforced composites were established by using various analytical methods and model reactions. Convenient methods for achieving the surface modification of the carbon fibres are based on sulfur chemistry. This approach significantly improved the mechanical performances of composite samples;
— Innovative strategies such as selective percolation, multiple fillers and percolation in percolation were employed to develop highly conducting nanocomposites at relatively lower loading of conducting fillers. Applications of thus prepared conducting nanocomposites in strain sensing, detection of toxic volatile organic compounds, over current protection devices, high-dielectrics and low positive-temperature-coefficient materials for electro-magnetic

irradiation shielding were explored, and significant improvement in the properties of interest was observed with the use of high energy radiation;

— Applicability of poly(tetrafluoroethylene) (PTFE) microparticles, produced through radiation degradation of PTFE waste, as reinforcing filler was demonstrated in elastomeric and thermoplastic matrices;

- High energy irradiation in air of a partially degalactosylated xyloglucan (Deg-XG) was demonstrated to be a useful tool reduce the size of its polymeric clusters when dispersed in water, without impairing the thermally induced self-aggregation behavior of the polymer. Colloidally stable Deg-XG nanoparticle dispersions showed propensity to incorporate hydrophobic guest molecules and dispersed homogeneously onto native xyloglucan films.

Radiation induced synthesis of metal nanoparticles was reported by several participating institutions from Egypt, France, Poland, Serbia, Turkey, USA, and Vietnam:

— Silver nanoclusters were synthesized in molecular sieves by using gamma-rays. Depending on the geometry of the cages as well as the presence of water molecules and/or anions in the porous structure the dimension of the cluster might be adapted for use in catalysis;

— Colloidal silver nano-particles and graphene nano-sheets were synthesized by gamma irradiation using carboxy methyl cellulose (CMC) and poly(vynil pirrolidone) (PVP) as stabilizers or capping agents;

— Large scale production of silver nanoparticle solution by gamma irradiation method has been set up. Antimicrobial porous ceramic candle filters containing silver nanoparticles have been produced for point of use drinking water treatment;

— Silver nanoparticles were synthesized by gamma irradiation in the presence of PVA and chitosan. The obtained nanoparticles are spherical in the shape with the size less than 15 nm, which can be controlled by changing the composition of polymer matrix. The smallest Ag NPs were obtained in the case of simultaneously crosslinking of polymers and *in situ* synthesis of Ag NPs;

— The formation of gold nanoparticles by radiolysis of Au (III) solutions in the presence of chitosan was achieved by gamma and EB irradiation. The obtained results allow for concluding to (i) the effective complexation of Au (III) by chitosan in the solution prior to irradiation, (ii) the dose rate effects on the nanoparticle formation, (iii) the significant contribution of chitosan-mediated reduction of Au (III) to the overall process of nanoparticle formation;

— Polymer thin film composites embedded with copper metal nanoclusters were synthesized by gamma and X-ray irradiation of binary and ternary complexes of poly(acrylic acid), poly(allyl amine) and Cu(II). The metallic copper nanoclusters with a size range of 2-20 nm were obtained in thin films. Copper nanoclusters were found to be stable, not oxidizing in air for a period of more than one year;

— Radiation synthesis of ethyl hexyl acrylate (EHA) and acrylic acid (AA) copolymer-ferric ionomer, and 20-30 nm Fe_3O_4 (magnetite) nanoparticles encapsulated in EHA-AA copolymer was achieved. The magnetization results of $(EHA\text{-}AA\text{-}Fe_3O_4)_n$ nano composite show a combination of ferromagnetic behavior (hysteresis) at relatively small magnetic fields with superparamagnetic behavior at large fields. The $(EHA\text{-}AA\text{-}Fe^{3+})_n$ ionomer exhibits a positive deviation from the Curie's Law dependence at low temperature, attributed to a mutual spin alignment contribution to the magnetization.

New matrix for nanocomposites was developed by Serbia from water soluble chitosan prepared by gamma irradiation induced acidic degradation of commercially available

product, and used in further preparation of crosslinked PVA/CS matrix for incorporation of silver nanoparticles.

A new initiator for radiation-induced curing of epoxy resin nanocomposites was synthesized based on a coumarine derivative (Poland). The product reduces the thermal effect of curing, thus mitigating undesirable internal stress.

New methods for development of electrically conductive nanocomposites were shown by India, Italy and Egypt:

— Reusable PVA/AAc-TiO_2 composite microgels for dye photo-catalytic degradation were successfully prepared. The introduction of polyaniline (PANI) nano-particles greatly enhanced the photo-catalytic activities of TiO_2 nano-particles for the organic dyes degradation under visible light irradiation. Further improvement in organic dye photocatalytic activity of TiO_2 nano-composites under visible light irradiation was achieved by exposing the prepared PANI-TiO_2 nano-composites to different gamma irradiation doses up to 25 kGy;

— Radiation grafting of a functional monomer onto an otherwise chemically inert polypropylene substrate enabled the in-situ polymerization and grafting of a conducting polymer on the surface as well as in the bulk of the insulating polymer. The obtained skin-core nanocomposites showed up to nine order of magnitude increases in bulk conductivity and amenability to be used as flexible electrodes to promote a further growth of the conducting polymer.

1.2.3.6.Collaborations

Participants have realized numerous collaboration and joint actions, as listed in Table 1.1.

TABLE 1.1. COLLABORATION BETWEEN PARTICIPANTS OF THE CRP

No.	Country / Representative	Collaborating Countries	Topics	Description
1	BRAZIL L. GONDIM de ANDRADE e SILVA M. C. EVORA	USA	Characterization of carbon based nanofibers (EPR, Raman)	1-week scientific visit at the University of Maryland
2	CANADA M. LACROIX	Egypt	Reinforcement of PLA with CNC and encapsulation of active compounds	Providing training to a researcher
3	EGYPT H. ABD-EL-REHIM	Canada	Reinforcement of PLA with CNC and encapsulation of active compounds	3-month fellowship 4-month fellowship / Preparation and characterization of materials
		Italy	Nanocomposite films	
4	FRANCE X. COQUERET	Vietnam	Dose rate effects on Au nanoparticles	1 Ph.D. completed / 1-week scientific visit
		USA	Tailored polymers for magnetic nanoparticles	Supplying polymer samples
		Malaysia	Cellulose nanocrystal	Application for a Ph.D. fellowship
		Serbia	Composites containing silver nanoparticles	Structural characterization / microscopy
5	GERMANY F. BAUER	Malaysia	Waterborne nanocomposites	Providing training to a researcher /

				Preparation and characterization of materials / 2-week scientific visit to ANM
6	INDIA K. ABHINAV DUBEY			
7	ITALY C. DISPENZA	Egypt	Nanocomposite films	Providing training to a researcher/Preparation and characterization of materials
		Malaysia	Radiation formation of nanoparticles as bioactive compounds carriers	1-week scientific visit
		Poland	Radiation engineering of polysaccharaide chaperones	Gamma and E-Beam irradiation of polymers/Three 1-week visits of two researchers/Samples prepared and sent/Joint publication in progress
		Turkey	PALS of cured samples	6-month visit for a Ph.D. student 6-month training of an undergrad student
		USA	AAc-grafted-PVP nanoparticles for imaging Nanocomposites for fuel cell	
8	MALAYSIA N. G. NIK SALLEH	Germany	Waterborne nanocomposites	3-month fellowship to IOM, Germany
9	PAKISTAN T. YASIN	Turkey	GPC Characterization	Characterization of irradiated samples
		Thailand	Gamma irradiation	Irradiation of composite samples
		Serbia	Polymer samples	Structural characterization / spectroscopy
10	POLAND G. PRZYBYTNIAK	Italy	Radiation engineering of polysaccharaide chaperones	Providing electron beam and gamma irradiation Scientific discussion
		Turkey	Radiation grafting	
11	SERBIA A. RADOSAVLJEVIC	France	Composites containing silver nanoparticles	Samples prepared and sent
		Pakistan	Polymer matrices	Samples prepared and sent Scientific discussion / consultation
		Turkey	Polymer nanocomposites	
12	THAILAND K. HEMVICHIAN	Turkey	PMMA-modified starch	Samples prepared and sent/Joint publication in progress
		Pakistan	Gamma irradiation	Samples prepared and sent/Joint publication in progress

13	TURKEY O. GÜVEN	Thailand	PMMA-modified starch	XPS characterization/Scientific discussion/consultation/Joint publication in progress
		Pakistan	Polymer Characterization	GPC analysis 1-week scientific visit/ Providing lectures for 15 hr
		Poland	Radiation grafting	
14	USA M. AL-SHEIKHLY	Brazil	Characterization of carbon-based nanofibers (EPR, Raman)	2-week scientific visit to IPEN, Brazil
		Italy	AAc-grafted-PVP nanoparticles for imaging	Support for material characterization
			Nanocomposites for fuel cell	Training for undergrad student
		France	Tailored polymers for magnetic nanoparticles	4-week scientific visit
15	VIETNAM Q. H. NGUYEN	France	Dose rate effects on Au nanoparticles	Gamma irradiation / characterization (TEM and spectroscopy) / 1-week scientific visit

In addition to the collaboration listed in the Table 1.1., the participants have established additional collaborations relevant to this CRP. In particular:

France, Italy, Poland and Turkey, together with other external partners, prepared and submitted a proposal under the framework of EU Erasmus+ KA2 –Strategic partnership for higher education with the purpose of organising and delivering a joint innovative training and teaching/learning programme in enhancing development and transfer knowledge of application of ionizing radiation in materials processing.

A research collaboration was established between Hacettepe University (Turkey) and Moscow State University (Russian Federation) on the generation of metallic cupper nanoclusters and binary and ternary polymer/Cu(II) systems. The papers published from this work are given in the list of publications.

Two IAEA research fellows from Egypt, one from Bangladesh and one from Philippines were received by the Canadian Irradiation Centre, INRS-Institute Armand-Frappier (Canada) for the development of grafted and reinforced natural polymers using irradiation methodologies.

Collaborations generated between France and Poland during a previous CRP on “Radiation processing of natural polymers” offered the opportunity to involve MSc students in the frame of the Erasmus exchange programme (Technical University of Lodz, University Marie Curie Sklodowska Lublin, Universite de Reims Champagne Ardenne). A number of research internships with projects on the radiation processing of nanomaterials and nanocomposites provided the students with education and training to that topic of growing importance.

1.3. SUMMARY OF THE WORK DONE IN PARTICIPATING INSTITUTIONS

1.3.1. Brazil

Radiation can be used to modify and improve the properties of materials. Electron beam and gamma ray irradiation has potential application in modifying the structure of carbon fibers in order to produce useful defects in the graphite structure and create reactive sites. At the Radiation Technology Center (IPEN-CNEN), the methodology to functionalize carbon nanofiber (CNF) via radiation process using acrylic acid as a source of oxygen functional groups was investigated. The samples were submitted to direct grafting radiation process with electron beam and gamma source. Several parameters were changed such as acrylic acid concentration, radiation dose and percentage of inhibitor to achieve functionalization with higher percentage of oxygen functional groups on carbon nanofiber surface and better dispersion. The better results achieved was mixing CNF in a solution of acrylic acid with 6% of inhibitor ($FeSO_4$.7H2O) and irradiated at 100 kGy. The samples were characterized by X-ray Photoelectron Spectroscopy and the dispersion stability upon storage was visually investigated. The functionalized samples under this methodology, had an increase of 20% of oxygen content onto CNF surface. The Auger D-parameter for the samples functionalized ranged between 17.0-17.7 compared to 21.1-18.9 of the unirradiated ones. This indicated that these samples had less sp^2 and more sp^3 bonding characteristics than non irradiated samples. This can be an indication of C=C bond breaking leading to the formation of new sp^3 carbon atoms on carbon nanofiber surface with oxygen functional groups grafted. The grafted samples were stable in dispersion. The application of these functionalized nanofibers in composites showed promising results. The best results seem to be those that were made by 3 roll mill method. Despite the difficulties that each manufacture methodology, the 3 roll mill process was the most efficient process for providing composites with less bubbles and promoted greater interaction between functionalized nanofiber and the polymer matrix. From the results of DMA and flexural tests, an increase on the storage modulus and flexural strength on the CNF functionalized nanocomposites was observed. The stability of the dispersion of the functionalized CNF in water during months was a good indication that the functionalization via ionizing radiation was successful. The functionalized nanofiber promoted better interface in the composites, but different mechanical tests will still be conducted. This interaction can be confirmed by SEM images where it was observed that the nanocomposites manufactured with functionalized CNF presented better interaction between CNF and resin system.

1.3.2. Canada

At the Canadian Irradiation Centre, INRS-Institute Armand-Frappier, the focus of the research was on the development of a variety of advanced packaging materials. In order to improve the functionality of bio-polysaccharide based films, addition of active reinforcements has been proposed. Crystalline nanocellulose (CNC) has the advantage of having an abundance of hydroxyl groups at its surface, thus, chemical modifications of these functional sites could be performed. Also, CNC can reinforce the physico-chemical properties of natural polymers. Cellulosic materials are biodegradable and can be alternative of synthetic polymers.
Grafting of antioxidant gallic acid (GA) on CNC was developed using different ɣ-radiation doses. A reaction of gallic acid on CNC surface was carried out under a free radical grafting by using hydrogen peroxide/ascorbic acid (AA) as redox couple initiator. GA was incorporated at different ratios with respect to molar ratios CNC/GA (R1=0.66 and R2=8). Gamma radiation was applied from 0 to 20 kGy. Results indicated that increasing radiation

doses allowed improving the radical scavenging properties of CNC-*g*-GA from 0.18 to 1.27 TEAC (Trolox Equivalent Antiradical Capacity; mM Trolox eq/mg CNC). Higher TEAC value was obtained with R1=0.66 at 20 kGy (1.27 Trolox eq). Covalent attachment of GA on CNC was characterized by FTIR analysis with typical vibrations of aromatic ester linkage (1730 cm^{-1}).

The aim of this project was to develop and optimize a grafting method using gamma irradiation to produce antioxidant coating and packaging for food application. In addition, development and application of antioxidant CNC based film formulations were done and verified *in situ* using mushrooms as a food model. Quality and characteristic of coated mushrooms with antioxidant based films were analyzed during food storage time.

1.3.3. Egypt

At the National Centre for Radiation Research (NCRRT) nanocompoiste were developed by incorporating nano silver into cellulose acetate (CA) films. Radiation is an effective tool to produce nano silver from silver salt solution. In order to obtain highly dispersed and stable nano silver, a small amount of stabilizing agents like natural polymer was added during the irradiation process of $AgNO_3$ solution. The obtained nano- silver was investigated and mixed with CA polymer solution. However, the color of prepared nano composite changed from colorless to brown, whil the film remained transparent. Mechanical properties of irradiated films were not significantly affected by radiation. The CA-Ag nano composites showed biological activity towards different microorganisms and the activity increased as the Ag content in the composite increased. Efforts were also made to improve the mechanical and barrier properties of polycaprolactone (PCL) and chitosan for food packaging purposes by addition of reinforcing compounds (fillers like graphene oxide). The addition of low amount of graphene oxide (GO) or graphen to PCL and chitosan, respectively, significantly improved both mechanical strength and barrier properties of PCL- and chitosan based films, while the oxygen transmission rate (OT) and water vapor permeability (WVP) decreased significantly with the increment of GO amount in PCL films. Biodegradability of the PCl and chitosan was not affected by adding GO or grapheme. Twenty five kGy irradiation dose slightly improved the strength and barrier properties of PCL/GO nano-composite films. PCL- GO and chitosan – G films could be used as a high load bearing films in food packaging. Polyaniline nano-fibers (PANFS-HCl) were synthesized and blended with biodegradable polymer like polycaprolactone to obtained green color nano-composite films. Polyanilines in a protonated conductive form (green) are rapidly interact with basic solutes or vapours associated with sea food decay likes amines and change to neutral non-conductive form (blue). Gamma rays have no significant effect on the green color of PANFS-HCl /polycaprolactone films as well as their mechanical properties. The prepared sheet could be used as smart packaging for sea food products which are permissible to be treated with ionizing radiation. Immobilization of nano scale titanium dioxide (TiO_2) on the surface of the prepared PVA-AA microgel was carried out. Photo-degradation efficiency of TiO_2/ PVA-AA microgel against metanil yellow dyes was studied. Easy recovery and better reproducibility made TiO_2/PVA/AA of great important in practice use as a photo-catalytic degradation composite materials for safe treatment of textile wastewater. Additionally, Polyaniline–TiO_2 (PANI–TiO_2) nanocomposites were studied and showed better photocatalytic degradation activity against methyl orange aqueous solution under sunlight than TiO_2 nanoparticles. In order to improve the photocatalytic activity of the prepared photocatalysts, PANI-TiO_2 nanocomposites had been exposed to different gamma irradiation doses. It was found that gamma radiation plays an important role in improving photocatalytic activity of PANI-TiO_2 nanocomposites.

1.3.4. France

The chemical and physico-chemical interactions between the radiation-curable matrix and the reinforcing fibres or fillers are of outmost importance for obtaining beneficial effects in composites with demanding mechanical properties. The research at the Univeristy of Reims Champagne-ardenne (UMR-CNRS) has been focused on two types of composites based on radiation-curable acrylate-based matrices, one including high modulus carbon fibres, the second one containing cellulose nanocrystals.

— (i) The influence of surface functions present at the surface of carbon fibres was investigated. The inhibiting effect of aromatic hydroxylic and amino groups as well as the sensitizing effect of thiol groups were evaluated by comparing the dose dependence of butyl acrylate samples submitted to EB irradiation in the presence of various additives. We have proposed and evaluated sulfur-based surface modifications and/or sizing application to carbon fibers for inducing the formation of cohesive interfaces. Significant improvements of the transverse strength of unidirectional composites were achieved by implementing this approach.

— (ii) Cellulose nanocrystals prepared from ramie (CNC) were introduced in a radiation-curable polyurethane acrylate emulsion. The influence of the amount of introduced CNC (1 to 10 w t-%) on the reactivity under UV or EB-radiation as well as the thermomechanical and tensile properties of the resulting materials was studied. FT-MIR and NIR spectroscopies were used to control the degree of monomers conversion of series of samples. Significant enhancement of the Young's modulus and of the strength at break was observed with 1 wt-% of CNC. The profile of the reaction kinetics measured during UV- or EB-initiated polymerization was not significantly altered by the presence the nanocrystals in the coalesced material.

Besides this research that was conducted with students, scientists and institutions from Poland, several interactions and other joint projects have been conducted on a cooperative basis, particularly:

— with USA, on new functional copolymers for designing magnetic nanocomposites;

— with Vietnam, on the synthesis of gold nanoparticles by radiation-induced reduction of Au(III) salts in the presence of chitosan, with one PhD defended.

The development of new interactions is in progress with Malaysia (1 PhD application for the grafting of cellulose nanocrystals) and Serbia (characterization of composites including metallic nanoparticles).

1.3.5. Germany

At the University of Leipzig, hybrid nanocomposites, which offer unique advantage to enable multi-functionalisation of coatings used in various applications from automotive to furniture industries were developed. To utilize the full potential of such nanocomposites, several issues need to be addressed such as the functionalization of nanofillers (SiO_2, Al_2O_3, TiO_2, and ZnO), their homogeneous embedding of into miscellaneous resins and radiation/thermal curing of such high solid content formulations. For typical UV curing using Hg lamps, the photoinitiator required can lead to unpleasant yellowing and harmful toxicity originated from the presence of unconverted/residual photoinitiator molecules and low-molecular photocleavage fragments trapped in the photocured coatings. Therefore, real-time ATR FTIR and lab-scale curing studies of photoinitiator-free acrylate based nanocomposites were performed using a dual VUV/UV lamp system. For SiO_2 nanofillers, through cure of 50 µm thick, photoinitiator-free acrylate formulations by the VUV/UV lamp system has been

observed. Moreover, VUV irradiation of cured acrylate coatings yields a higher network density within surface-near layers due to radical formation of C=O groups. The lab-scale comparison between UV, VUV/UV and EB curing of silica nanocomposites proofed that the VUV/UV curing/matting technique is a practical alternative for photoinitiator-free photo-polymerization.

1.3.6. India

At the Radiation Technology Development Division of the Bhabha Atomic Researh Centre (BARC) high energy radiation was used for the property enhancement of conducting polymer nanocomposites, improving their efficacies in applications such as strain sensors, chemiresistive sensors, over current protection devices, EMI shielding and high dielectric constant materials. Innovative strategies such as selective percolation, multiple fillers and percolation in percolation were used to develop highly conducting nanocomposites at relatively lower loading of conducting fillers. In addition, applicability of PTFE powder – generated through CCl_4 assisted radiation degradation of PTFE waste (RPTFE)—as reinforcing filler was explored for developing high-modulus composites. Extensive studies on the radiation processing of polymer blends and coatings containing nanoparticulate fillers were also carried out and ozone resistant SBR/EPDM blends, oil resistant EPDM/neoprene rubber blends, and abrasion resistant polyurethane coatings were developed. The radiation dose was found to have a profound effect on the sensing range as well as on the sensitivity (gauge factor) of the strain sensors. Cyclic strain sensing response was also found to be affected by crosslinking density and the best results were observed for a crosslinking density of 73.2 mol/g, corresponding to 50 kGy of Co-60 radiation dose. The effect of graphene on the strain sensing characteristics of a radiation crosslinked thermoplastic-elastomeric blend/ conducting carbon nano black (CCNB) nanocomposites was also investigated. The graphene content was found to have profound effect on the electromechanical response; the sensitivity of the sensor was the highest for 0.02 weight fraction of graphene and was around 3 times of that observed in nanocomposites without graphene. RPTFE was found to act as a reinforcing filler for Polydimethylsiloxane (PDMS), improving not only elastic modulus but also coefficient of friction. With the use of RPTFE, exceptional synergistic effects observed in ethylene vinyl acetate (EVA)/organoclay composites. Mechanical properties of ternary composites demonstrated high synergy between fillers, leading to manifold increase in the modulus of dual filler filled composites in comparison to single filler systems. Nielsen model fitted well with EVA/ RPTFE system; however it predicted remarkably low values for EVA/ RPTFE /organoclay system, confirming exceptional synergy between two fillers. X-ray diffraction studies revealed around 10% intergallery expansion in organoclay, in the composites having high loading of PTFEMP. Applications of radiation crosslinked conducting nanocomposites for detection of toxic volatile organic compounds, over current protection devices, high dielectrics materials and low PTC sheets for EMI shielding were also explored and significant improvement in the properties of interest was observed with the use of high energy radiation.

1.3.7. Italy

In recent years, polymer nanocomposites have fascinated scientists, engineers and industrialists on the premise that the creation of new and more performing polymeric materials is possible by the combination of different building blocks with controlled dimensions at the nanoscale. Unfortunately, uniform dispersion and stability of the hetero-phase domains within the plastic matrix or on its surface often fail due to unfavorable thermodynamics and resulting irreversible aggregation phenomena.

In-situ generation of a dispersed hetero-phase within the same polymer matrix or its precursors increases the chances of achieving a better control of morphology by eliminating the often critical harvesting and re-dispersion steps in the manufacturing process. Strong interaction at the interface is also required to avoid aggregation and coarse phase-separation in usage.

At the University of Palermo, radiation grafting of a functional monomer onto polypropylene film has been applied to modify the molecular structure and properties of the otherwise chemically inert film. The radiation-grafted film has become permeable to the precursors of polymerization of a conducting polymer, namely polyaniline that can grow as a thin skin from its surface as well as an interpenetrated network into the film. Chemical attachment of the conducting polymer to the polyolefin has been demonstrated. The nanocomposite film shows an increase of electrical conductivity of several orders of magnitudes and amenability to be used as flexible electrode. In consideration of the well-known possibility of controlling the extent and depth of chemical modification of a substrate by radiation grafting, by tuning both system composition and irradiation conditions, this approach can enable a good degree of control of the morphology of the heterophase that forms on or within the substrate and thereby of the nanocomposite film.

Reducing the interfacial tension and the interfacial area of the dispersed phase in the matrix by recourse to suitable carriers, as chaperones of active molecules or nanoparticles to vehicle into structurally different polymer matrices, is another possible strategy to obtain more uniform and stable dispersions. For this purpose, radiation processing has been applied to tailor the aggregation propensity in water of a polysaccharide selected as a potential carrier of hydrophobic additives into hydrophilic polysaccharide-based films.

In particular, the possibility of obtaining colloidally stable micro-/nanoparticles from a partially degalactosylated xyloglucan (Deg-XG) was investigated. ^{60}Co γ-irradiation was applied to reduce the size of polymeric in clusters in water. Irradiation was performed on the solid powder in air, and up to a maximum dose of 60 kGy. Fourier transform infrared spectroscopy (FTIR) and gel permeation chromatography (GPC) analyses do not evidence any significant change of functional groups of the polymer or its average molecular, respectively. Deconvolution of CPC curves suggests a change only in the proportion between two main fractions of different molecular weight (MW) clusters, with a prevailing contribution of the smaller over the higher MW clusters at the increase of the absorbed dose. Aqueous dispersions of the irradiated materials at low concentrations were characterized by dynamic light scattering measurements as function of the time and at different temperatures. For all systems an increase of scattered light intensity as function of the time at 37°C was observed, which is likely due to the same reversible temperature-triggered aggregation process at the basis of the temperature-induced gelation observed in the high concentration regimes (above 2 wt%). The fastest kinetics and the highest pseudo-plateau were shown by the 20 kGy irradiated system. Globular particles with 300-400 nm hydrodynamic diameters are formed. Their propensity to incorporate hydrophobic small guest molecules or high molecular weight biomolecules was tested. The possibility of preparing optically transparent native xyloglucan films incorporating these particles by solvent casting was demonstrated.

1.3.8. Malaysia

At the Malaysian Nuclear Agency, the properties of coating film prepared from the incorporation of acrylated palm oil (EPOLA) in commercial epoxy acrylate have been

studied. A series of different amount of EPOLA was mixed with commercial epoxy acrylate. The blended acrylates passed through non-ionizing radiation to produce a non-tacky film. The conversion of acrylate double bond was monitored by FTIR. The effect of EPOLA concentration onto coated films was investigated by determination of the pendulum hardness and gel content. By increasing the amount of EPOLA in the mixtures will lower the pendulum hardness and the gel content but to a level acceptable for usage in the high-end applications.

In this work, ultraviolet (UV) light and electron beam (EB) radiation were used to cure coatings of acrylated epoxidized palm oil (EPOLA) containing different proportions of silica nanoparticle (SiO2). The influence of various factors such as addition of photoinitiators and other additives in the formulations were also been investigated. The coating materials were cured by UV light and low energy EB radiation. The cured materials were characterized by gel fraction and swelling techniques. The effect of nanoparticles on the performance and properties of the coating materials such as scratch resistance, pencil hardness, pendulum hardness, abrasion resistance were been investigated. The nanoparticle induced both a bulk and a surface modification of cured coatings with an increase gel content and surface hardness by increasing the amount of silica into radiation curable material. The strong decrease on water uptake in the presence of SiO2 makes these nanocomposites particularly interesting for our investigation.

1.3.9. Pakistan

The project proposed by the Pakistan Institute of Engineering and Applied Sciences (PIEAS) aimed to develop a polysaccharide based biodegradable packaging material for radiation sterilizable products in order to mitigate the environmental pollution resulted by biostable polymers. Mostly, these biostable polymers are petroleum based which are becoming expensive and their reserves are also depleting with time. The blend of polyethylene and starch were prepared with different amount of functionalized sepiolite using melt mixing technique. Both the electron beam and Co-60 were used to irradiate the composites in air at different doses up to maximum of 100 kGy. The effect of different amount of functionalized sepiolite and ionizing radiation on thermo-mechanical properties of high density polyethylene (HDPE)/starch were investigated. The intensities of XRD peaks of polyethylene appeared at 21.6^{o} and 24.0^{o} decreased with increasing amount of sepiolite. Scanning electron microscopy revealed good dispersion and interfacial adhesion of the additives in the polymer matrix. Both the sepiolite and irradiation dose improved the tensile strength and thermal stability of the composites. The solvent uptake study of EB irradiated composites showed the following order: chloroform > xylene > kerosene oil > acetone > water > methanol > NaOH > H_2SO_4. The sample irradiated at high gamma dose as well as electron beam showed comparable properties. The obtained results are quite encouraging and will have good potential as packaging materials for food, drug and other disposable items etc.

1.3.10. Poland

In the framework of this CRP the studies on radiation supporting synthesis and curing of nanocomcosites suitable for practical use were conducted at the Institute of Nuclear Chemistry and Technology (ICHTJ). The first part of the work was focused on the stabilization of micro- and nanostructures of metal centres and their halides in various systems. For the matrix constructed from radiation crosslinked copolymer of acrylic acid/acrylamide it was confirmed that the diffusion of aqueous solutions is determined by intra- and intermolecular hydrogen bonding system, density of crosslinking dependent on

dose absorbed and metal (Ag^+ and Cu^{2+}) complexes that play a role of additional network nodes. Such a pH responsive inorganic-organic hybrid system might be potentially used in medicine and catalysis.

The silver agglomerates and silver halides synthesis was supported by ionizing radiation and the products were stabilized in sodalites and track membranes, respectively. Molecular sieve were applied as matrices stabilizing silver clusters produced by gamma radiation. It was confirmed that dimension and charge of the products depend on the geometry of sodalite cages as well as the presence of water molecules and/or anions in the porous structure. Two mechanisms of the cluster creation were proposed – via gradual addition of cations to silver atom and though reduction of pre-arranged cations localized in the sodalite cage. It was also proved that track-etched membranes produced by heavy ion beam can be applied as templates for obtaining silver halides in the form of nano/micro rods and grains.

Carbon nanostructures incorporated into thermoset might considerably improve some important properties of the final product. However, they also significantly influence curing of the resins, including the processes induced by ionizing radiation. The main goal of the studies was to obtain higher performance composites for more demanding applications by: optimization of curing conditions, reinforcement of the epoxy resin by carbon nanoparticles, evaluation of the final product and conducting tests of the new synthesized cationic initiator based on cumarine derivatives. In the frame of the project tests of the influence of accelerated electrons on grahene oxide (GO) as a potential nanofiller of epoxy resin were conducted. It was found that (i) there are at least two types of paramagnetic centres in GO, (ii) upon radiation treatment the concentration of such defects increases up to 200 kGy and then remains almost constant to 1200 kGy, (iii) the changes are inconsistent with total population of defects (diamagnetic and paramagnetic ones) determined on the basis of Raman spectroscopy thus free electrons are probably localized in the pre-existing non-paramagnetic defects. In the second part of the work radiation cured epoxy resin and its nanocarbon composites based on nanotubes and GO were investigated. We concluded that the thermal effects recorded during radiation curing of epoxy resins in the presence of cationic photoinitiators and selected carbon nanofillers were influenced predominantly by the type of radiation and dose rates, the concentration of initiator and the nature of nanofillers. The induction time of curing is even twice longer for graphene based composites than for non-filled matrix due to limited availability of the initiator absorbed on the surface of dispersed phase. It was confirmed that cheap and easy to synthesize cumarine based initiators might be used instead of commercially available Rhodosil. The maximum thermal effect is then achieved after longer time but its intensity is over 100 ^oC lower, which is a desirable phenomenon reducing resin shrinkage and diminishing internal stress occurring in the case of high temperature polymerization. The composites containing MWCNT and RGO show at elevated temperatures significant increase in deflection force as compare to the epoxy resin and its CNT and graphite composites.

Third part of our studies was related to the assessment of applicability of starch based films in food packaging and pharmacy. Improvement of their properties as a barrier or a carrier for active components might be achieved by the alteration of composition and by radiation induced modification of the interaction between particular components of the multicomposite system. Hydrophobic/ hydrophilic properties were modified by three surfactants: cetyltrimethylammonium bromide (CTAB, cationic), sodium laurate (Na-Lau, anionic) and mono-lauroyl glycerol (MLG, non-ionic) and two lipids: lauric acid (Lau) and palmitic acid (Pam). Differences of the interaction between all examined ligands and irradiated/non-

irradiated starch were followed. For CTAB and Lau, decrease in the inclusion complex symmetry was found upon irradiation of the starch. Moreover, improvement of the coordination arrangement was confirmed after further thermal treatment of the complex formed with the non-irradiated starch. The irradiated starch is capable to bind less ligands but the interaction between both components is stronger. When used as a film component increases homogeneity of the final material. It was confirmed that radiation treatment can support production of potato starch nanoparticles.

1.3.11. Serbia

The objective of the project carried out at the Vinca Institute of Nuclear Sciences was to develop simple, one-step radiolytic methodology to obtain noble metal/natural polymer based hybrid composite nanosystems with the goal of exploring favorable characteristics of radiation technology for nanoscale engineering of materials, especially for biomedical application. The crosslinking of polymers and reduction of metal ions were performed by means of radiation chemistry method due to its advantage over chemical methods. To achieve project goals the research activities were focused on developing synthesis strategies of formation of silver nanoparticles (Ag NPs) and crosslinking of polymer matrix consisting of poly(vinyl alcohol)/chitosan (PVA/CS) blend system, or only chitosan (CS). Noble metal NPs are generally considered as environmentally friendly antibacterial materials, and these two polymers have been used successfully in many biomedical applications.

To achieve the project outputs, research activities were divided in several sections:

- The investigation of *in vitro* silver release by the simple nano-Ag/PVA hydrogel device as a model system. This study was aimed to quantify the amount of Ag^+ ions released in an *in vitro* medium and to use the elements of pharmacokinetic drug delivery paradigm to the nano-Ag/PVA hydrogel as a model system for the evaluation of the release kinetics and the release mechanism.
- The investigation of possibility of radiolytic method to control the size of Ag NPs by changing the composition of CS/PVA blends as a matrix.
- The investigation of the radiation chemical pathways for the synthesis of Ag/PVA/CS hydrogel nanocomposites. First, the Ag NPs were *in situ* incorporated in previously crosslinked matrix consisting of PVA and water soluble CS (obtained also by γ-irradiation). Second, the simultaneously crosslinking of polymers and *in situ* synthesis of Ag NPs by γ-irradiation was performed.

The antimicrobial testing of obtained hydrogel nanocomposites has shown the correlation between the observed Ag^+ ions release potential and the antimicrobial properties against gram-positive *Staphylococcus aureus* and gram-negative *Escherichia coli*. Moreover, the antibacterial activity of nanocomposites based on wsCS, show enhanced antibacterial potential in comparing with Ag-PVA nanocomposites or PVA/wsCS matrix only.

1.3.12. Thailand

At the Thailand Institute of Nuclear Technology (TINT) the research project aimed to apply the use of radiation processing to prepare biodegradable composites from poly(lactic acid) or polylactide (PLA) and cassava starch. The major problem of blending PLA with starch is a very poor compatibility between hydrophilic starch and hydrophobic PLA. Our previous research has succeeded to improve the compatibility between hydrophobic natural rubber and hydrophilic silica by radiation-induced admicellar polymerization of isoprene on the silica surface. The results showed that the modified silica is more compatible to natural rubber,

resulting in improved properties of the rubber compounds. The results strongly confirm the effectiveness of surface modification of silica through admicellar polymerization. Hence, this research intended to improve the compatibility between PLA and starch by similar concept. The summary can be given as follows:

— Radiation-induced crosslinking of PLA was investigated. Results showed that the presence of a suitable crosslinking agent (TAIC) enables PLA to undergo crosslinking induced by gamma radiation. The optimum condition for radiation-induced crosslinking of PLA was determined;

— PLA grafted cassava starch (PLA-g-CS) was synthesized to be used as a compatibilizer between PLA and cassava starch (CS). Thermoplastic starch (TPS) was prepared from CS and glycerol. The prepared TPS was blended with PLA, with and without the compatibilizer. Results from mechanical tests of PLA-CS blends showed that the compatibilizer did hot help improve the mechanical properties of the blends;

— In addition to the synthesis of the compatibilizer, an alternative method to increase the compatibility between PLA and CS was investigated. Admicellar polymerization was used to coat ultra-thin (nanoscale) film of poly(methyl methacrylate) (PMMA) on the surface of CS to make it more hydrophobic and hence more compatible with PLA. Results from FTIR, SEM, floating test as well as iodine test have shown that PMMA film was successfully coated on the surface of CS. PMMA-modified starch (MS) was subsequently blended with PLA. Results have shown that, at the same TPS content, mechanical properties of PLA-MS blends were much better than those of PLA-CS blends, confirming the improved compatibility between PLA and MS.

1.3.13. Turkey

Nanocomposites are a new class of materials that are filled with particulate or fibrous materials at least one dimension of the dispersed phase to be in nanometer range. The addition of nanoclays to a polymer matrix has been proven to bring large improvement in the mechanical properties, thermal stability, fire resistance, gas barrier properties of starting polymeric materials. Polymers and clay are not generally fully interspersed to form nanocomposites and modification of either the clay or the polymer is mostly necessary. Montmorillonite (MMT), a frequently used clay for example in polymer/clay nanocomposites is modified by quaternary ammonium compounds to make an intercalated nanocomposite exfoliate. Clays are generally modified by cation exchange. As for the modification of polymers, grafting of maleic anhydride onto PE or PP enhances the compatibility of these fully hydrophobic polymers with unmodified clay. In either approach the main goal is to increase the dispersion of polymer chains within the layered structure of silicates. The significant improvement in mechanical properties of nanocomposites was explained to be due to the presence of an exceptionally high interfacial surface area generated by exfoliation and to the formation of ionic and/or hydrogen bonding between the organic polymer and inorganic silicate.

In the first part of this work carried out at the Department of Chemistry, Hacettepe University, ionizing radiation has been used to modify polypropylene to make it compatible with montmorillonite and in the second, montmorillonite was radiation modified to make it compatible with ethylene-vinyl acetate copolymer. In this first case radiation-induced chain scission together with oxidation converted a high molecular weight and totally hydrophobic polypropylene into a structure that is compatible with hydrophilic nanofiller. In the second case irradiation of montmorillonite swollen with a cationic monomer resulted with a modified clay with silicate layers separated from each other for easy diffusion of EVA copolymer.

Thus in both approaches we obtained polymer/clay nanocomposites with exfoliated structures. Exfoliation of clay particles was proven by XRD and TEM measurements as well as PALS studies. Up to 50% improvement in some of the mechanical properties was observed in 3-5% clay loading.

The second part of this Project dealt with the in-situ formation of metallic copper nanoparticles in polymer thin films for the preparation of polymer-metal nanocomposites. Polymer thin films prepared by interpolymer complexation of poly(acrylic acid) and poly(allyl amin) were loaded with Cu(II) ions by dipping into $CuSO_4$ solution and irradiated with X- and gamma rays in 10% alcohol solutions. Hydrated electrons generated in aqueous solution converted copper ions into metallic nanoparticles. The effects of complex stochiometry, concentration, type of irradiation and absorbed dose were investigated and it was shown that by controlling these factors it was possible to control the size and distribution of copper nanoparticles inside the polymer matrices.

1.3.14. USA

Magnetic nanocomposites, in which magnetic nanoparticles are encapsulated in polymeric matrices, have important applications in medicine, imaging, electronics and mechanical devices. At the University of Maryland, radiation synthesis of ethyl hexyl acrylate (EHA) and acrylic acid (AA) copolymer-ferric ionomer, and 20-30 nm Fe_3O_4 (magnetite) nanoparticles encapsulated in EHA-AA copolymer were achieved. The kinetics of copolymerization were measured by pulse radiolysis technique. Pulse radiolysis of 2-EHA shows that transient absorption at 330 nm, attributable to 2-EHA$^{\bullet}$ radicals, forms within 0.01 μs, probably due to reaction of trace amounts of water present in the 2-EHA with 2-EHA$^{-\bullet}$ radicals. The decay of the absorption over a time scale of $1 \cdot 10^{-8}$ to $1 \cdot 10^{-4}$ s follows second order kinetics that slow as the polymer radical grows in mass. At very short durations the rate constant reaches an upper limit of $(2.0 \pm 0.2) \cdot 10^{10}$ $M^{-1}s^{-1}$. The magnetic properties of $(EHA\text{-}AA\text{-}Fe^{3+})_n$ ionomer and $(EHA\text{-}AA\text{-}Fe_3O_4)_n$ nano composite exhibit interesting magnetic properties.
The magnetization results of $(EHA\text{-}AA\text{-}Fe_3O_4)_n$ nano composite show a combination of ferromagnetic behavior (hysteresis) at relatively small magnetic fields with superparamagnetic behavior at large fields. The ferromagnetic behavior can be attributed to the presence of larger nanoparticles and the superparamagnetic behavior to smaller nanoparticles. As expected, the magnetization increases with magnetite concentration up to about 10% Fe (in the form of Fe_3O_4). Above this concentration, the magnetite apparently no longer forms a uniform suspension in the 2-EHA/AA copolymer.

Our results also show that $(EHA\text{-}AA\text{-}Fe^{3+})_n$ ionomer exhibit a positive deviation from the Curie's Law dependence at low temperature. This deviation can be attributed to a mutual spin alignment contribution to the magnetization. In nano particulate materials both a superparamagnetic behavior (due to very small particles) and cooperative behavior (due to larger particles) contribute to the total magnetization; such combined effect is indeed clearly visible in our results. The ferromagnetic behavior is expected to be more noticeable at lower temperatures, where thermal motion is least likely to disrupt mutual spin orientation. This is indeed reflected in our results. It should be noted that that specific magnetization of the $FeCl_3$ ionomers is much lower than the one observed with the $(EHA\text{-}AA\text{-}Fe_3O_4)_n$ nano composite. This is to be expected in view of the strong tendency of magnetite to exhibit ferromagnetic behavior. However, it is remarkable that some mutual spin alignment takes place within the $FeCl_3$ ionomers.

1.3.15. Vietnam

At the Research and Development Centre for Radiation Technology, colloidal silver nanoparticles (AgNPs) solution with concentration of 500 mg/L and the AgNPs diameter of 10-15 nm was synthesized on pilot scale of 100 L/batch by gamma irradiation method using polyvinylpyrrolidone as stabilizer. Porous ceramic (PC) samples and porous ceramic candle filter (PCCF) product with the specific surface area of 1.83 m^2/g and the average pore size of 61.9 Å were functionalized by treatment with an aminosilane (AS) agent (3-aminopropyltriethoxysilane) and then impregnated in AgNPs solution for fixing through coordination bonds between $–NH_2$ groups of the AS and the silver atoms. The AgNPs content attached in PC (AgNPs/PC) and in PCCF (AgNPs/PCCF) was of about 200 – 250 mg/kg. Owing to strong bonding of silver atoms to the wall of PC, the contents of silver released from AgNPs/PCCF into filtrated water by flow test were less than 10 μg/L, it is satisfactory to the WHO guideline of under 100 μg/L for drinking water. The antimicrobial effect of AgNPs/PCCF for *E. coli* was carried out by flow test with an inoculated initial contamination of *E. coli* in water of about 10^6 CFU/100ml. Results showed that the contamination of *E. coli* in filtrated water through AgNPs/PCCF (up to 500 L) was less than 1 CFU/100ml compared to 3×10^4 CFU/100ml for bare PCCF (only up to 40 L). Thus, AgNPs/PCCF with the silver content of 200 – 250 mg/kg, the specific surface area of 1.51 m^2/g and the average pore size of 48.2 Å has highly antimicrobial effect and suitably released silver content that can be applied for point-of-use drinking water treatment.

1.4. CONCLUSIONS

The participants concluded that the CRP was very successful in fully achieving its objective. All specific objectives had also been fully achieved, with numerous additional outputs. It was also concluded that:

— The CRP was very successful in establishing collaboration among the members in terms of scientific visits, training fellowships, exchange of samples for characterization, providing support for irradiation and characterization of materials. This is reflected in joint publications and proposals for new joint research projects.

— The results of research works carried out under this CRP have proven that radiation processing is a technically and economically viable tool for the preparation of nanocomposites and nanomaterials, such as scratch and abrasion resistant top coats containing modified nanosilica particles and antimicrobial porous ceramic water filter containing silver nanoparticles. The research also demonstrated that radiation processing offers unique approaches to improve physico-chemical properties of composite materials in their final physical forms, without impairing other desirable properties such as crystallinity and morphology.

— Radiation-induced modification and functionalization of bio-based monomers and polymers was demonstrated as an efficient method for producing materials with new functionalities exhibiting an increasing content of renewable carbon, such as palm oil acrylates, modified polysaccharides, PLA blends and biomass.

— The presence of carbon materials (graphene, carbon nanotubes, carbon fibers, carbon black) in radiation processable matrices affects the chemical reactions taking place under irradiation driving the needs for new approaches in the developments of advanced materials.

— The CRP members have agreed to publish the results of this CRP in the form of an IAEA TECDOC.

PUBLICATIONS RESULTING FROM THE COORDINATED RESEARCH PROJECT

Journal Articles:

AKTER, N., KHAN, R., SALMIERI, S., SHARMIN, N., DUSSAULT, D., LACROIX, M. Fabrication And Mechanical Characterization Of Biodegradable And Synthetic Polymeric Films: Effect Of Γ-Irradiation. *Rad. Phys. Chem*., 81 (2012) 995-998.

ALESSI S, SPINELLA A, CAPONETTI E, DISPENZA C, SPADARO G. Structural investigation of e-beam cured epoxy resins through solid state NMR. Radiat. Phys. Chem. 81 (2012) 1328-1331.

BAKAR, A., GÜVEN, O., ZEZIN, A.A., FELDMAN, V.I., Controlling the size and distribution of copper nanoparticles in double and triple polymer-metal complexes by X-ray irradiation, Rad. Phys. Chem.,94(2014)62-65.

BAKAR, A., DE, V.V., ZEZIN, A.A., ABRAMCHUK, S.S., GÜVEN,O., FELDMAN,V.I., "Spatial organization of a metal-polymer nanocomposite obtained by radiation-induced reduction of copper ions in the poly(allyl amin)-poly(acrylic acid)-Cu2+ system" Mendeleev Commun., 22(2012)211.

BAUER, F., DECKER, U., NAUMOV, S., RIEDEL, C. (2014). Photoinitiator-free UV curing and matting of acrylate-based nanocomposite coatings: Part 3. Progress in Organic Coatings 77 (2014) 1085-1094.

BAUER, F., DECKER, U., NAUMOV, S., RIEDEL, C. (2012). Photoinitiator-free UV curing of acrylate-based nanocomposites. Proceedings of II ESPS, Torino (Italy), September 2012

CIEŚLA, K., SARTOWSKA, B, KRÓLAK, E., Gamma irradiation influence on the structure of potato starch gels studied by SEM. Radiat. Phys. Chem., accepted for publication

CIEŚLA, K., RAHIER, H., DSC studies of the influence of gamma irradiation on the structural properties of the complexes formed with cetyl-trimethyl-ammonium bromide, Radiation Physics and Chemistry, in preparation.

CHAUDHARI, C. V., K. A. DUBEY, Y. K. BHARDWAJ AND S. SABHARWAL, Radiation processed styrene-butadiene rubber/ethylene-propylene diene rubber/multiple-walled carbon nanotubes nanocomposites: Effect of MWNT addition on solvent permeability behavior, Journal of Macromolecular Science, Part B: Physics **51**(5)(2014) 839-859

CRIADO, P., FRASCHINI, C., SALMIERI, S., BECHER, D., SAFRANY, A., LACROIX, M. Free radical grafting via gamma-irradiation of antioxidant gallic acid (GA) on cellulose nanocrystals (CNC) in gellan gum films (under preparation).

DUBEY, K. A., Y. K. BHARDWAJ, C. V. CHAUDHARI, N. K. GOEL, S. SABHARWAL, K. RAJKUMAR AND S. K. CHAKRABORTY, Radiation effects on styrene-butadiene-ethylene-propylene diene monomer-multiple walled carbon nanotube nanocomposites: Vulcanization and characterization, Polymers for Advanced Technologies**,** **22**(12)(2011)1888-1897.

DISPENZA C, SABATINO MA, NICONOV A, CHMIELEWSKA D, SPADARO G. E-beam crosslinked, biocompatible, functional hydrogels incorporating polyaniline nanoparticles. Radiat. Phys. Chem. 81 (2012) 1456-1459.

DISPENZA C, SABATINO MA, DEGHIEDI N, CASALETTO MP, ALESSI S, PIAZZA S, EL RHEIM H., Conductive polyaniline skins grown onto radiation grafted polypropylene films, *in preparation*.

DUBEY, K. A., Y. K. BHARDWAJ, C. V. CHAUDHARI AND S. SABHARWAL, LDPE/EVA/PCR/MWNT nanocomposites: Radiation crosslinking and physicomechanical characteristics, Polymer Composites **32**(5) (2011) 737-746

DUBEY, K. A., Y. K. BHARDWAJ, K. RAJKUMAR, L. PANICKER, C. V. CHAUDHARI, S. K. CHAKRABORTY AND S. SABHARWAL, Polychloroprene rubber/ethylene-propylene diene monomer/multiple walled carbon nanotube nanocomposites: Synergistic effects of radiation crosslinking and MWNT addition, Journal of Polymer Research **19**(5)(2012).
DUBEY, K. A., S. K. SINHA, Y. K. BHARDWAJ, L. PANICKER AND L. VARSHNEY, Carbon Black-Filled PE/PP/EPDM Blends: Phase Selective Localization of Carbon Black and EPDM-Induced Phase Stabilization." Polymer - Plastics Technology and Engineering **53**(5) (2014) 442-450.
DUBEY, K. A., S. MAJJI, S. K. SINHA, Y. K. BHARDWAJ, S. ACHARYA, C. V. CHAUDHARI AND L. VARSHNEY, Synergetic effects of radiolytically degraded PTFE microparticles and organoclay in PTFE-reinforced ethylene vinyl acetate composites, Materials Chemistry and Physics **143**(1) (2013) 149-154.
FARAHANI,.M., CLOCHARD, M.C., GIFFORD, I., BARKATT, A. AND AL-SHEIKHLY, M., Differences in Fundamental Reaction Mechanisms between High and Low-LET in Recent Advancements and Applications of Ionizing Radiation, Rad. Phys. Chem., 105 (2014) 39–47.
FERREIRA,M.S., SARTORI,M.N., OLIVEIRA,R.R., GÜVEN,O., MOURA, E.A.B., Short vegetable-fiber reinforced HDPE: A study of electron-beam radiation treatment effects on mechanical and morphological properties, Appl. Surf. Scien., xxx(2014)xxx
HUQ, T., KHAN, A., DUSSAULT, D., SALMIERI, S., KHAN, R.A., LACROIX, M. Effect of γ-irradiation on the physico-chemical properties of alginate-based films and beads. Rad. Phys. Chem. 81 (2012) 945-48.
KARSLI, N.,G., AYTAÇ, A., AKBULUT, M., DENIZ, V., GÜVEN,O., "Effect of irradiated polypropylene compatibilizer on the properties of short carbon fiber reinforced polypropylene composites" Rad. Phys. Chem.,84(2013)74-78.
KHAN, R.A., BECK, S., DUSSAULT, D., SALMIERI, S., BOUCHARD, J., LACROIX, M. Mechanical and barrier properties of nanocrystalline cellulose reinforced poly (caprolactone) composites: effect of gamma radiation. *J. Appl. Polymer Sc*., 129 (2013) 3038-3046.
KHAN, R. A., BECK, S., DUSSAULT, D., SALMIERI, S., BOUCHARD, J., LACROIX, M. Mechanical and barrier properties of carbon nanotubes-reinforced PCL-based composite films: effect of gamma radiation. *J. Appl. Polym. Sci.* 127 (2013) 3962-9.
KHAN, A., HUQ, T., KHAN, R.A., DUSSAULT, D., SALMIERI, S., LACORIX, M. Effect of γ-irradiation on the mechanical and barrier properties of HEMA grafted chitosan-based films. *Rad. Phys. Chem*., 81 (2012) 941-44.
KHAN, R., DUSSAULT D., SALMIERI, S., SAFRANY, A., LACROIX, M., Improvement of the mechanical and barrier properties of methylcellulose-based films by treatment with HEMA and silane monomers under gamma radiation. *Rad. Phys. Chem.*, 81 (2012) 927-931.
KHAN, R., SALMIERI, S., DUSSAULT, D., URIBE-CALDERON, J., KAMAL, M.R., SAFRANY, A., LACROIX, M. Preparation, gamma-irradiation and thermo-mechanical characterization of chitosan loaded methylcellulose films. *J. Polym. Environ.* 20 (2012) 43-52.
KHAN, R., SALMIERI, S., DUSSAULT, D., CALDERON, J.U., KAMAL, M.R., SAFRANY, A., LACROIX, M. Production and Properties of Nanocellulose Reinforced Methylcellulose-Based Biodegradable Films. *J. Agric. Food Chem*., 58 (2010) 7878-7885
KHAN, A., MEHMOOD, S., SHAFIQ, M., YASIN, T., AKHTER, Z., AHMAD, S. "Structural and Antimicrobial Properties of Irradiated Chitosan and its Complexes with Zinc". Radiat Phys Chem, **91** (2013) 138–142
KRSTIC, J., SPASOJEVIC, J., RADOSAVLJEVIC, A., SILJEGOVIC, M., KACAREVIC-POPOVIC, Z., Optical and structural properties of radiolytically *in situ* synthesized silver

nanoparticles stabilized by chitosan/poly(vinyl alcohol) blends, Rad. Phys. Chem. **96** (2014) 158-166.
KRSTIC, J., SPASOJEVIC, J., RADOSAVLJEVIC, A., PERIC-GRUJIC, A., DJURIC, M., KACAREVIC-POPOVIC, Z., POPOVIC, S., *In vitro* silver ion release kinetics from nanosilver/poly(vinyl alcohol) hydrogels synthesized by gamma irradiation, J. Appl. Polym. Sci. **131** (2014) Article No. 40321.
LACROIX, M., KHAN, R., SENNA, M., SHARMIN, N., SALMIERI, S., SAFRANY, A, Radiation grafting on natural films. Rad. Phys. Chem., 94 (2014) 88-92.
MAJJI, S., K. A. DUBEY, R. K. MONDAL, Y. K. BHARDWAJ AND S. ACHARYA, Development of Electron Beam Cross-Linked PDMS/PTFEM Composites with Low Coefficient of Friction and High Elastic Modulus, Polymer - Plastics Technology and Engineering **53**(5) (2014) 435-441.
MARTIN A., PIETRAS-OZGA D., PONSAUD P., KOWANDY C., BARCZAK M., DEFOORT B., COQUERET X., Radiation-curing of acrylate composites including carbon fibres: a customized surface modification for improving mechanical performances, Radiat. Phys. Chem. (2014), in press
NIK GHAZALI NIK SALLEH, MOHD SOFIAN ALIAS, H-J.GLÄSEL & R.MEHNERT. High performance radiation curable hybrid coatings, Radiation Physics and Chemistry Journal, 84 (2013) 70-73.
NIK GHAZALI NIK SALLEH, MOHD FIRDAUS YHAYA, AZMAN HASSAN, AZNIZAM ABU BAKAR AND MUNIRAH MOKHTAR, Effect of radiation dosages on the properties of nanocomposite coatings. Radiation Physics and Chemistry Journal 80 (2011) 136-141.
NOWICKI A, G. PRZYBYTNIAK, K. MIRKOWSKI, "Radiacyjne sieciowanie żywic epoksydowych z napełniaczami nanowęglowymi" in „Modyfikacja polimerów. Stan i perspektywy w roku 2013" Ed. Ryszarda Stellera i Danuty Żuchowskiej, Wrocław 2013, TEMPO s.c., ISBN 978-83-85520-19-0, p. 382-385.
PHU, D.V., TRINH, N.T.A., DU, B.D., HIEN, N.Q., Gamma-irradiation synthesis of silver nanoparticles fixing in porous ceramic for application in water treatment, Vietnam Journal of Chemistry, 51 (2013) 653-657.
PRZYBYTNIAK, G., L. LIPIŃSKA, J. SADŁO, Paramagnetic defects in electron beam irradiated graphene oxide, in preparation
PRZYBYTNIAK, G., NOWICKI, A., Radiation-induced curing of epoxy resin composites filled with nanocarbon particles, in preparation.
QUOC, L.A, PHU, D.V, DUY, N.N, LANG, V.T.K, LAN, N.T.K., TRINH, N.T.A., HIEN, N.Q., Study on antibacterial activity (*Escherichia coli)* of porous ceramic fixed with silver nanoparticles, Nuclear Science and Technology, VINATOM, 3 (2013) 25-30.
RIEDEL, C., MEHNERT, R., SCHUBERT, R., BAUER, F., PRAGER, L. (2012). UV curing systems using 172 nm excimer lamps. Proceedings of II ESPS, Torino (Italy), September 2012.
SALMIERI, S., KHAN, R. A., SAFRANY, A., LACROIX, M. Influence of 2-hydroxyethyl methacrylate and gamma radiation on the mechanical and barrier properties of methylcellulose-based films. J. Appl. Polym. Sci. (2014) APP-2013-11-3807.
SALMIERI. S., ISLAM, F., KHAN, R. A., HOSSAIN, F. M., IBRAHIM, H. M. M., MIAO, C., HAMAD, W. Y., LACROIX, M., Antimicrobial nanocomposite films made of poly(lactic acid)-cellulose nanocrystals (PLA-CNC) in food applications. Part B: Effect of oregano essential oil release on the inactivation of *Listeria monocytogenes* in mixed vegetables. Cellulose. (2014) CELS-D-13-00484R2.
SALMIERI, S., ISLAM, F., KHAN, R., HOSSAIN, F., IBRAHIM, H., MIAO, C., WADOOD, C.M., HAMAD, Y., LACROIX, M., Antimicrobial nanocomposite films made

of poly(lactic acid)-cellulose nanocrystals (PLA-CNC) in food applications: part A—effect of nisin release on the inactivation of *Listeria monocytogenes* in ham. Cellulose 21 (2014) 1837-1850.
SHARMIN, N., KHAN, R., SALMIERI, S., DUSSAULT, D., BOUCHARD, J., LACROIX, M. Mechanical and barrier properties of methylcellulose-based films grafted with trimethylolpropane trimethacrylate by gamma irradiation: effect of filling with cellulose nanocrystals, J. Sc. Technol. For Forest Products and Processes 2 (2012) 24-31.
SHARMIN, N., KHAN, R.A., SALMIERI, S., DUSSAULT, D., BOUCHARD, J., LACROIX, M. Modification and characterization of biodegradable methylcellulose films with trimethylolpropane trimethacrylate (TMPTMA) by gamma radiation: effect of nanocrystalline cellulose. J. Agric. Food Chem., 60 (2012) 623-629.
SHARMIN, N., KHAN, R., DUSSAULT, D., SALMIERI, S., AKTER, N., LACROIX, M. Effectiveness of silane monomer and gamma radiation on chitosan films and PCL-based composites. Rad. Phys. Chem., 81 (2012) 932-935.
SENNA M.M., SALMIERI S, EL-NAGGAR AW, SAFRANY A, LACROIX M. Improving the compatibility of Zein / Polyvinyl alcohol blends by gamma irradiation and graft copolymerization of acrylic acid. *J. Agric. Food Chem.*, 58 (2010) 4470-4476.
SINHA, S. K., K. A. DUBEY, V. GROVER, P. SASTRY, Y. K. BHARDWAJ, L. PANICKER, A. K. TYAGI, P. A. MAHANWAR AND V. A. BAMBOLE, Selective interfacial localization in conducting polycaprolactam/ethylene vinyl acetate/carbon black composites, Polymer Composites **34**(6) (2013) 912-919.
SPADARO G, ALESSI S, DISPENZA C, SABATINO MA, PITARRESI G, TUMINO D, PRYZBYTNIAK G, Radiation curing of carbon fibre composites. Radiat. Phys. Chem. 94 (2014) 14-17.
TODARO S, SABATINO MA, WALO M, MANGIONE MR, BULONE D, DISPENZA C. Influence of gamma-irradiation on the thermally-induced mesoscopic gelation of degalactosylated xyloglucans. Radiat. Phys. Chem., 94 (2014) 245-248.
VO K. D. N., KOWANDY C., DUPONT L., NGUYEN Q. H., COQUERET X., Radiation synthesis of chitosan-stabilized gold nanoparticles: comparison between e(-) beam and gamma irradiation, Radiat. Phys. Chem. (2014), 94, 84-87
VO K. D. N., GUILLON E., DUPONT L., KOWANDY C., COQUERET X., Influence of Au(III) interactions with chitosan on gold nanoparticles formation, J. Phys Chem. (C) (2014), *118* (8), 4465–4474
YASIN, T., NISAR, M., SHAFIQ, M., NHO, Y.C., AHMAD, R. Influence of Sepiolite and Electron Beam Irradiation on the Structural and Physicochemical Properties of Polyethylene/Starch Nanocomposites, Polym. Composites, **34/3** (2013) 408–416.

Conference Abstracts and Proceedings

CIEŚLA, K., RAHIER, H., ŁYCZKO, K., The influence of gamma irradiation on the physico-chemical properties of the complexes formed by potato starch with cetyl-trimethyl ammonium bromide, Polysaccharides and polysacharide derived products, from basic science to application" (EPNOE 2013), Nicea 21.10 - 24.10.2013, poster P76, Book of Abstracts p 328.
CIEŚLA, H. RAHIER, H. LUNDQVIST, DSC studies of the influence of gamma irradiation on the structural properties of the complexes formed with cetyl-trimethyl-ammonium bromide. 10th meeting of the Ionising Radiation and Polymers Symposium IRAP 2012, Cracow, Poland 1 4- 19 October 2012: Poster nr. 58. Book of Abstracts of str 166 (2012).

CIEŚLA, A NOWICKI, M. BUCZKOWSKI, B. SARTOWSKA, K. ŁYCZKO: „Modification of the structure and the functional properties of the biodegradable films based on starch by radiation treatment and addition of lipids/surfactants**.** Multifunctional, Hybrid and Nanomaterials (Hybrid Materials 2013) 3-7.03.2013 Sorrento, Włochy. Poster nr A3.10.3.
KACAREVIC-POPOVIC, Z., RADOSAVLJEVIC, A., KRSTIC, J., SPASOJEVIC, J., On the use of gamma irradiation for the nanoengineering of the Ag and Au/hydrogel based nanosystems for the potential biomedical applications, The 28th Miller Conference on Radiation Chemistry, Dead Sea, Israel, March 14-19, 2013, Scientific Programme and Abstracts, p.25.
KORNACKA, E., PRZYBYTNIAK, G., MIRKOWSKI, K., Interaction between inorganic and polymeric components in a hybrid system. 28th Miller Conference on Radiation Chemistry, Dead Sea, Israel 13-19. 03. 2013.
KRSTIC, J., SPASOJEVIC, J., KRKLJES, A., KACAREVIC-POPOVIC, Z., Non-isothermal kinetics of dehydration of Ag/PVA hydrogel nanocomposite synthesized by γ-irradiation, 11th International Conference of Fundamental and Applied Aspects of Physical Chemistry, PHYSICAL CHEMISTRY 2012, September 24-28, 2012, Belgrade, Serbia, *Proceedings*, p.212-214.
KRSTIC, J., SPASOJEVIC, J., RADOSAVLJEVIC, A., ABAZOVIC, N., JOVANOVIC, U., KACAREVIC-POPOVIC, Z., Ag-PVA/wsCS blend hydrogel nanocomposite synthesized by γ-irradiation followed by freeze/thawing method, 12th International Conference of Fundamental and Applied Aspects of Physical Chemistry, PHYSICAL CHEMISTRY 2014, September 22-26, 2014, Belgrade, Serbia, Proceedings, manuscript submitted.
KRSTIC, J., SPASOJEVIC, J., RADOSAVLJEVIC, A., MITRIC, M., KACAREVIC-POPOVIC, Z., Chitosan/poly(vinyl alcohol) blend as a capping agent for gamma irradiation induced *in situ* synthesis of silver nanoparticles, Tenth Young Researchers' Conference - Materials Science and Engineering, Serbian Academy of Sciences and Arts (SASA), Belgrade, Serbia, December 21-23, 2011, Program and the Book of Abstracts, XI/3, p.45.
KRSTIC, J.I., SPASOJEVIC, J.P., RADOSAVLJEVIC, A.N., SILJEGOVIC, M.Z., KACAREVIC-POPOVIC, Z.M., Silver-Chitosan/Poly(vinyl alcohol) Nanocomposites Obtained by Gamma Irradiation Induced *In Situ* Synthesis, First International Conference on Pocessing, characterization and application of nanostructured mateials and nanotechology NanoBelgrade 2012, Belgrade, Serbia, September 26-28, 2012, Book of Abstracts, p.95
NIK GHAZALI NIK SALLEH, MOHD SOFIAN ALIAS, H-J. GLASEL, R. MEHNERT, MEK ZAH SALLEH, RIDA TAJAU & NURLIYANA ABD RAHMAN, Development of high performance radiation curable hybrid coatings. Proceeding of RadTech Asia 2013, The 13th International Conference on Radiation Curing in Asia (RadTech Asia 2013), Shanghai China, 20-24 Mai 2013.
NIK GHAZALI NIK SALLEH, MOHD SOFIAN ALIAS, H-J. GLASEL, R. MEHNERT, MEK ZAH SALLEH, RIDA TAJAU & NURLIYANA ABD RAHMAN, Development of high performance UV/EB curable hybrid coatings. The 8th International Conference on Surfaces, Coatings and Nanostructured Materials (NANOSMAT), Granada Spain, 22-25 September 2013.
NIK GHAZALI NIK SALLEH, MOHD SOFIAN ALIAS, H-J.GLÄSEL AND R. MEHNERT, 2012. UV/EB curing of nanocomposites for enhancing their functionality and utility in the coatings industry. Proceedings of RadTech International North America 2012, 30 April-2 May 2012, Chicago USA.
NIK GHAZALI NIK SALLEH, MOHD SOFIAN ALIAS, KHAIRIAH HJ BADRI, H-J.GLÄSEL AND R. MEHNERT, 2011. High performance of clear coatings using

nanoparticles for wood based products. Proceedings of RadTech Asia 2011, 20-23 June 2011, Yokohama Japan.
NOWICKI, A., PRZYBYTNIAK, G., MIRKOWSKI, K., Radiacyjne sieciowanie żywic epoksydowych z napełniaczami nanowęglowymi, XXI Conference „Modyfikacja Polimerów", 18-20.09.2013, Kudowa Zdrój.
PRZYBYTNIAK, G., NOWICKI, A., Radiation cured epoxy resins composites filled with nanocarbon particles" NUTECH, Warszawa 21-24.09.2014

Chapter 2

DEVELOPMENT OF RADIATION PROCESSING TO FUNCTIONALIZE CARBON NANOFIBER TO USE IN NANOCOMPOSITE FOR INDUSTRIAL APPLICATION

L. GONDIM DE ANDRADE E SILVA
Institute for Nuclear and Energy Research – IPEN/CNEN-SP,
Cidade Universitária

M. C. EVORA
Institute for Advanced Studies- IEAV/DCTA,
Av. Cel. Jose Alberto Albano do Amarante,
São Jose dos Campos-SP

Brazil

Abstract

Radiation can be used to modify and improve the properties of materials. Electron beam and gamma ray irradiation has potential application in modifying the structure of carbon fibers in order to produce useful defects in the graphite structure and create reactive sites. In this study was investigated the methodology to functionalize carbon nanofiber (CNF) via radiation process using acrylic acid as a source of oxygen functional groups. The samples were submitted to direct grafting radiation process with electron beam and gamma source. Several parameters were changed such as acrylic acid concentration, radiation dose and percentage of inhibitor to achieve functionalization with higher percentage of oxygen functional groups on carbon nanofiber surface and better dispersion. The better results achieved was mixing CNF in a solution of acrylic acid with 6% of inhibitor ($FeSO_4.7H_2O$) and irradiated at 100 kGy. The samples were characterized by X-ray Photoelectron Spectroscopy and had an increase of 20% of oxygen content onto CNF surface. The Auger D-parameter for the samples functionalized ranged between 17.0-17.7 compared to 21.1-18.9 of the non irradiated ones. This indicated that these samples had less sp^2 and more sp^3 bonding characteristics than non irradiated samples. The samples functionalized presented a good and stable dispersion. Nanocomposites were manufactured from functionalized CNF and it was observed from DMA and flexural tests, an increase on the storage modulus and flexural strength. The interaction could be confirmed by SEM images where it was observed that the nanocomposites manufactured with functionalized CNF presented better interaction between functionalized CNF and resin system. The stability of the dispersion of the functionalized CNF in water during months was a good indication that the functionalization via ionizing radiation was successful.

2.1. INTRODUCTION

Carbon nanofibers (CNFs) are being thoroughly investigated for application in structural composites for the aerospace industry. This requires careful control of their surfaces to promote properties required for end use, because CNFs are not compatible with most polymers.

Carbon nanofibers (CNFs) are cylindrical nanostructures composed by graphene layers that may take one of several arrangements such as stacked cones. CNFs have also attracted attention in the last ten years because they offer somewhat comparable electrical, mechanical, and thermal properties, at a lower production cost than SWCNTs and MWCNTs [2.1]. CNFs differ from SWCNT and MWCNT in the following respects: carbon nanofibers have an average diameter of 60-200 nm while carbon nanotubes have an average diameter of 10-20

nm, they are longer (30-100 micrometers) and they have a different surface morphology [2.2, 2.3].

Advanced CNFs-polymer nanocomposites can be obtained combining two specific properties: uniform dispersion of CNFs in the polymeric matrix and strong interfacial adhesion for efficient tension transfer from the polymeric matrix to the CNFs [2.4, 2.5]. Likewise CNFs, without any surface treatment, may have a weak interfacial adhesion with the polymeric matrix. Therefore, it is necessary to modify their surfaces through chemical or physical techniques to produce optimized polymer nanocomposites of a mechanical properties view.

There are several methods to functionalize carbon based materials and these modifications may promote changes on nanostructure surface [2.6-2.12]. There are some works in the literature investigating the impact of the process conditions on nanostructures and, consequently, on the technological applications of the final product. The main effects investigated are: composition of monomers and solvents employed on the functionalization [2.12-2.14], reaction temperature [2.12, 2.15], additives [2.16], and dispersion of carbon materials in solvents and water [2.17-2.19].

Radiation process, with the aim to modify carbon based materials, has been used for a long time and is a subject that still has plenty to explore [2.20-2.28]. Ionizing radiation has high enough energy to convert at least one neutral atom or molecule into an ion pair. The energy deposited by this radiation is localized in individual atoms or molecules, and it is sufficiently high to break and induce chemical reactions in a short time period. This is the basic principle of using ionizing radiation to modify materials chemically. Therefore, radiation grafting polymerization may be an alternative way to induce surface modification, and it is a uniform, effective and environment-friendly method. It can be conduct at room temperature and in gaseous, liquid and solid state phase. To date, there are some published papers related to radiation grafting polymerization to functionalize graphitic nanostructures [2.2, 2.9, 2.11, 2.22] but it still has been subject of investigation due to show a variety of structural transformations under radiation process. Adding to that, the difficulties to controlling the product are greatly magnifies when the particle size is in the nanometer range. Characterization, control and reprodutibility are still a challenge when particle size is in nanometer range and it is not an easy task to compare methods of characterization which are usually not in agreement with each other.

The aim of this work was investigate and propose the methodology to functionalize CNFs and compare two different methods to promote grafting reactions: gamma ray and electron beam irradiation. Different parameters, as inhibitor concentration in acrylic acid solution, were applied to the samples during the process to establish this methodology. Fourier-Transform Infrared Spectroscopy (FTIR) and X ray Photoelectron Spectroscopy (XPS) were used to evaluate the functionalization degree of CNFs while Auger spectroscopy was used to evaluate the Csp^2/Csp^3 ratios of CNFs comparing the different methods of irradiation. XPS and Auger spectroscopies provide an average for the content of functional groups of the first 10 – 15 molecules layer. Raman spectroscopy was used to investigate the nanostructure of carbon samples after irradiation and is a popular nondestructive tool for structural characterization of carbon materials. Scanning electron microscopy (SEM), thermogravimetric analysis (TGA), dynamic mechanical analysis (DMA) were used to characterize the functionalized samples. Composites were prepared by different methods and characterized by flexion tests and DMA.

2.2. EXPERIMENTAL

2.2.1. Carbon Nanofiber

CNFs used in this study were obtained from Applied Sciences Inc. Cedarville Ohio (under licenses from General Motors Coorp. and Applied Science Inc.) and they are manufactured in a continuous vapor phase growth process that contributes to a significantly lower cost compared to most carbon nanotubes, and they are readily available in large quantities and in several grades.

CNFs (PR-25-PS grade) were selected for the investigation in this work because, in a previous work, showed less resistant under electron beam process and it was able to promote surface oxidation. Carbon nanofiber has a chemically vapor deposited (CVD) layer of carbon on the surface of the fiber over a graphitic tubular core fiber. CNFs are available in different grades. The PS grade is produced at 1100°C by pyrolytically stripping the as produced CNF to remove polyaromatic hydrocarbons from the surface.

In Table 2.1 is showed the samples submitted to direct radiation grafting process. As received PR-25-PS-XT samples were weighed, and then immersed in solutions of 10 % of acrylic acid (MERK / stabilized with 200 ppm of hydroquinone) with 1, 6 or 10 % of inhibitor metal salt ($FeSO_4.7H_2O$). One part of the samples were poured into petri dishes and irradiated with a direct accelerator operated by the Institute for Nuclear and Energy Research (IPEN/CNEN-SP/Brazil). These samples were irradiated with an industrial electron accelerator Dynamitron, from Radiation Dynamics Inc., model DC 1500/25-JOB 188 that was operated with the following parameters: beam energy 1.5 MeV, pulse current 5.62 mA, 5 kGy/pass with dose rate of 22.42 kGy/sec. Other part of the samples, with the same amount of acrylic acid and $FeSO_4.7H_2O$, were irradiated by gamma radiation process in a Cobalt-60 irradiator, Gammacell model 220, series 142, manufactured by Atomic Energy of Canada Limited which activity is 64.946 TBq (1755.1 Ci) - 06/2012. The Gammacell design provides uniform gamma field and the samples were irradiated at a dose rate of 1.48 kGy/h. The mixtures were purged with dry nitrogen for 10 min to remove dissolved oxygen and then sealed.

TABLE 2.1. SAMPLES PREPARED WITH ACRYLIC ACID SUBMITTED TO DIRECT RADIATION GRAFTING PROCESS

Samples Name	Samples PR-25-PS-XT	Dose (kGy)		$FeSO_4.7H_2O$ (%)
GA-1	pristine	0	-	None
Blank-1	pristine	0	-	1 %
Blank-2	pristine	0	-	6 %
GA-11	pristine	50 kGy	e-beam	6 %
GA12	pristine	100 kGy	e-beam	6 %
GA-13	pristine	100 kGy	gamma	6 %
GA-14	pristine	100 kGy	gamma	10%
GA-16	pristine	90 kGy	gamma	6 %
GA-17	pristine	90 kGy	e-beam	6 %
GA-18	Pre-irradiated at 1000 kGy	90kGy	e-beam	6 %

The surface oxygen content of the nanofibers was characterized with X-ray Photoelectron Spectroscopy (XPS) analysis. GA-1, Blank-1, GA 12, GA-13 and GA-14 were conducted in K- Alpha XPS equipment from ThermoFisher Scientific, with a 400 μm X-ray spot size and with the low energy electron/argon ion charge neutralization system turned on. XPS survey spectra (0-1350 eV) were collected for all samples to provide qualitative and quantitative

surface analysis information. The XPS analysis for GA-1, Blank-2, GA-16, GA-17 and GA-18 were carried out in National Institute of Metrology, Quality and Technology (Inmetro). X-ray photoelectron spectroscopy (ESCAplus P System; Omicron Nanotechnology; Taunusstein, Germany) was used in order to study the chemical composition and chemical groups in carbon nanofibers before and after an irradiation process. The XPS analyses were performed in an ultra-high vacuum medium using an Al Kα=1486.7 eV X-ray source, with a 20 mA emission at a voltage of 13.5 kV. Survey spectra were acquire in the range of 1350-0 eV, step of – 0.8 eV, dweel time of 0.2 eV, and resolution of 70 eV. For carbon and oxygen elements, the high resolution spectra were obtained with analyzer pass energy of 30 eV. The binding energies were referenced to the carbon 1s level at 284.6 eV. The Shirley background and a least-squares routine, as implemented in the Casa XPS software (licensed by Omicron Nanotechnology, Taunusstein, Germany), were used for peak fitting. The FTIR analyses were performed in a Perkin-Elmer Spectrum GX spectrometer (Perkin-Elmer, Massachusetts, USA) by the potassium bromide (KBr) transmission technique.

2.2.2. Nanocomposites

The great difficulty that exists in the manufacture of nanostructured composite is the dispersion of CNF in the matrix. These materials have basically non-polar surfaces. There is a necessity to make changes on the surface which allows better interaction and dispersion in the polymer matrix of interest. In the present investigation, two different dispersion processes were performed with the aim to study the best process to manufacture the nanocomposites and with the modified CNF. The processes are:

- Mix nanofiber/matrix - Conventional Process
- 3 roll mill dispersion process

2.2.2.1.Mix nanofiber/matrix - Conventional Process

The epoxy system used in the development of this experiment was also Araldite GY 260 and HT 972 curing agent in ratio of 80g of resin and 21.6g of hardener. This amount was sufficient to manufacture samples with 100x14x4mm approximately (Figure 1.1). The resin and hardener were mixed on a hot plate at 100^{o}C until the system becomes homogeneous. 0.508g of CNF was added to the resin system. The compound mixture was placed in a vacuum oven to remove bubbles and then poured into the metal mold which was prior treated with mold release agent. The material was cured in a vacuum oven and a cure ramp according to the schedule shown in Table 2.2. The composition of the composites obtained by the conventional method is described in Table 2.3 and the manufactured composite are presented in Fig. 2.1.

TABLE 2.2. CURING PROCESS OF NANOCOMPOSITES PREPARED BY CONVENTIONAL METHOD

Time	Temperature
30 minutes	110^{o}C
1 hour	120^{o}C
2 hours	140^{o}C
1 hour e 30 minutes	160^{o}C
2 hours	180^{o}C

TABLE 2.3. COMPOSITION OF NANOCOMPOSITES PREPARED BY CONVENTIONAL METHOD

Samples	Composition
BANC1-1	Bisphenol A + curing agent
1NC1-1	Bisphenol A + curing agent + 0,5% de CNF GA1
15NC1-1	Bisphenol A + curing agent + 0,5% de CNF GA15
16NC1-1	Bisphenol A + curing agent + 0,5% de CNF GA16
17NC1-1	Bisphenol A + curing agent + 0,5% de CNF GA17
18NC1-1	Bisphenol A + curing agent + 0,5% de CNF GA18

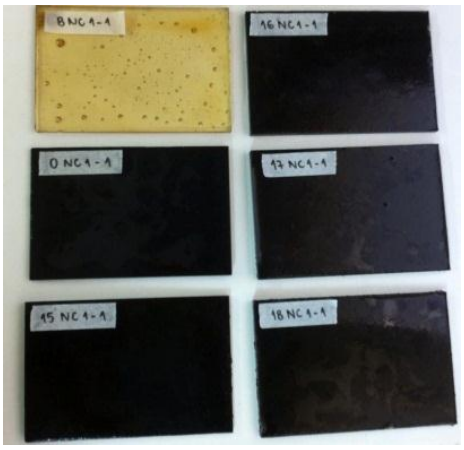

FIG. 2.1. Nanocomposites manufactured via a conventional method.

2.2.2.2. 3 roll mill dispersion

The epoxy system filled with CNF functionalized and non-functionalized were prepared by shear process dispersion using a 3-roll mill adapted for this function. This process was researched and developed at the University of Dayton (Fig. 2.2).

FIG. 2.2. Three roll mill dispersion at composites carried out at University of Dayton Lab.

The epoxy system used consists of Epon 862 (bisphenol F) and curing agent Epikure W (26 wt%). Both kindly provided by the University of Dayton in collaboration with this project. In each composite it was used 160g of resin and curing agent 42.24g. The mold used for composites manufacture is formed by two plates of the following dimensions: 10x10x0.7cm (Fig. 2.3) and the amounts of each mixture were enough prepared to fill the mold. The epoxy resin system was premixed in a vessel containing 0.5% of functionalized and non functionalized CNF. The mixture was then dispersed in a 3 roll mill as it is shown in Figure 2.2. The mixture was processed in the 3 roll mill for 5 times until the CNF was fully dispersed.

FIG. 2.3. Mold used at the University of Dayton for making nanostructured composites.

This mixture was poured in a previously sprayed with mold release agent and the mold was placed in a hot press (Fig. 2.4) under a pressure of 7 tons. The samples were cured according to the curing process shown in Table 2.4 and the compositions of the composites obtained by shear process are presented in Table 2.5.

FIG. 2.4. Hot press used to manufacture nanocomposites at University of Dayton.

TABLE 2.4. CURING PROCESS OF NANOCOMPOSITES PREPARED BY SHEAR METHOD

Time	Temperature
1 hour	120°C
2 hours	180°C

TABLE 2.5. COMPOSITION OF NANOCOMPOSITES PREPARED BY 3 ROLL MILL METHOD

Samples	Composition
BFNC1-2 (M)	Bisphenol F + curing agent
1NC1-2 (M)	Bisphenol F + curing agent + 0,5% de NFC GA1
15NC1-2 (M)	Bisphenol F + curing agent + 0,5% de NFC GA15
16NC1-2 (M)	Bisphenol F + curing agent + 0,5% de NFC GA16
17NC1-2 (M)	Bisfenol F + agente de cura + 0,5% de NFC GA17

2.3. RESULTS AND DISCUSSION

Fig.2.5. shows the results of the dispersion of the samples GA-15 (blank 2), GA-16, GA-17 and GA-18. The samples were dispersed in water under sonication process for an hour. This picture was taken 70 days after the dispersion process.

FIG. 2.5. Illustration of Blank-2, GA-16, GA-17 and GA-18 dispersed after 70 days.

XPS survey spectra (0-1350 eV) were collected for all samples to provide qualitative and semi-quantitative surface analysis information, Table 2.6. The O/C atomic ratios calculated from XPS survey spectra are an important feature in order to compare non irradiated and irradiated samples. The increase of the O/C atomic ratio is an indication of the effectiveness of the grafting process. The surface composition (atomic %) showed a significant increase of oxygen content for the samples irradiated, and for this reason, they offer excellent and very stable dispersion.

TABLE 2.6. SURFACE COMPOSITIONS (ATOMIC %) AND O/C ATOMIC RATIOS CALCULATED FROM BY THE XPS SURVEY SPECTRA (SEE METHODS) FOR CARBON NANOFIBERS AS RECEIVED (GA-1), NON-IRRADIATED SAMPLES (BLANK-1 AND BLANK-2) AND IRRADIATED SAMPLES (GA11, GA12, GA13, GA14, GA16, GA17 AND GA18)

at (%)	GA-1	Blank 1*	Blank 2	GA 11*	GA 12*	GA 13*	GA 14*	GA 16	GA 17	GA 18
C	93.1	90.6	90.2	83.1	79.7	78.4	81.5	80.6	68.3	82.9
O	5.1	7.0	7.6	14.6	18.4	20.3	16.8	18.4	30.7	15.8
N	1.1	1.6	1.4	1.4	0.9	0.9	0.9	0.6	0.5	0.9
Fe	0.1	0.1	0.2	0.1	0.1	0.1	0.2	0.1	0.1	0.1
S	0.5	0.4	0.5	0.4	0.3	0.2	0.4	0.2	0.3	0.2
Si	0.1	0.3	0.1	0.4	0.1	0.1	0.2	0.1	0.1	0.1
O/C	0.04	0.06	0.06	0.13	0.17	0.19	0.15	0.17	0.34	0.14

** Analyzed in K- Alpha XPS equipment from Thermo Fisher Scientific.*

Figure 2.6. shows the effect of the irradiation process on the functionalization of the carbon nanofibers. Non irradiated sample (GA-1) showed mainly C=C, C-H bounds and a shake-up satellite peak ($\pi \rightarrow \pi^*$, 291.3 eV) characteristic of aromatic C structures [2.29-2.31]. A binding energy of 284.3 eV essentially corresponds to non-functionalized sp^2 carbons which would be expected for CNF materials [2.29]. The sample irradiated with 100 kGy of gamma radiation (GA-13) showed more intensity in the peak characteristic of O-C=O bound (~ 289.3 eV) than the sample irradiated with the same dose of e-beam (GA12) which may be an indication that the grafting process was more effective using gamma radiation. These two radiation sources promotes different primary event of interaction with the matter however for both, secondary electron is responsible to initiate the ionization events that produce free radicals. On the other hand, electron beam delivers much higher dose rate leading to heating and contribute to generate various rearrangements of the carbon atoms.

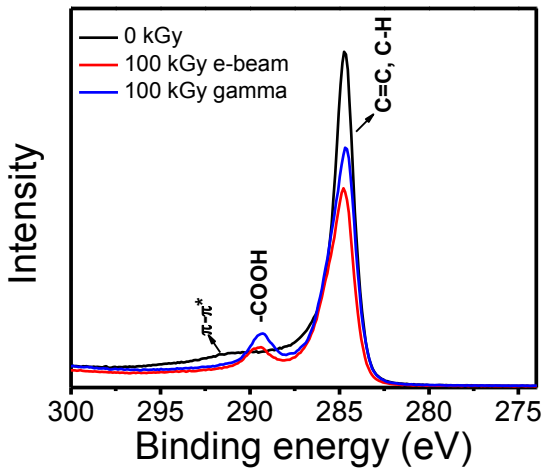

FIG. 2.6. XPS spectra of C1s of PR-25-PS pristine, non irradiated (GA-1) and irradiated with 100 kGy of e-beam (GA-12), and irradiated with 100 kGy of gamma radiation (GA-13). Both samples were analyzed in K- Alpha XPS equipment from ThermoFisher Scientific.

The effect of the irradiation doses on the graphitization level of the carbon nanofibers is showed in Fig. 2.7. In Fig. 2.7a, the samples irradiated with e-beam showed an increase in the intensity of carboxyl peak with the increase of the irradiation dose. For the samples irradiated

with gamma radiation, Fig. 2.7b, the samples irradiated with 90 and 100 kGy showed similar behavior relative to graphitization process evidenced by the carboxyl peak intensities.

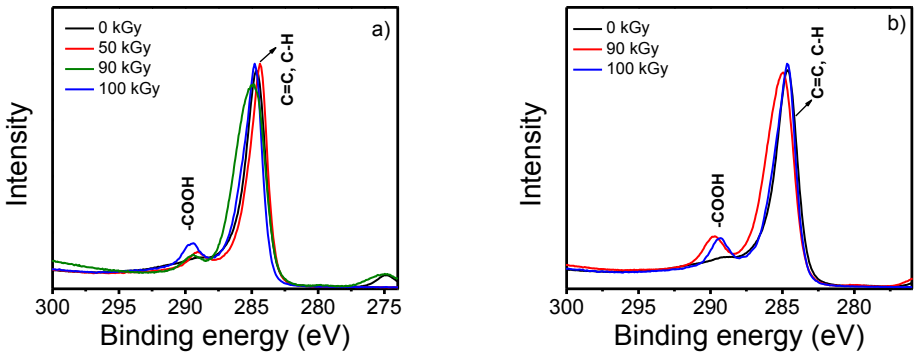

FIG. 2.7. XPS spectra of C1s of PR-25-PS with 6% of inhibitor ($FeSO_4.7H_2O$), where: a) irradiated with different doses of e-beam radiation (0, 50, 90 and 100 kGy). These samples correspond to Blank-2, GA-11, GA-12 and GA-17 in table 2.1; b) irradiated with different doses of gamma radiation (0, 90 and 100 kGy). These samples correspond to Blank-2, GA-16 and GA-13 in Table 2.1.

The X-ray induced CKLL Auger spectra were similar for the six samples (Fig. 2.8a) but did show some minor differences in peak shape and position. It has been shown in the published literature that, after differentiation, C KLL Auger spectra can give important information regarding the relative amount of sp^2 and sp^3 bonding in carbon materials by the so called Auger "D-parameter" [2.32]. The C KLL data were differentiated to give the Auger "D-parameter," which is the energy separation between the primary "hill" and "valley" of the differentiated spectrum. The D-parameter value gives an indirect measure of the % sp^2 character of the material. The measured Auger D-parameter for Sample GA-1 was 21.6 (Fig. 2.8b), similar value to the literature reference for graphite [2.32]. This result indicates a significant amount of sp^2 bonding on the surface of the non-irradiated sample, which is consistent with the $\pi \rightarrow \pi^*$ shake-up peak observed in the XPS C1s peak fit results, and is expected for carbon nanofibers materials.

The Auger D-parameter for the samples irradiated (GA-11, GA-12, GA-13 and GA-14) ranged between 17.0 and 17.7 indicating that these samples had less sp^2 and more sp^3 bonding compared to samples GA-1 and Blank-1 samples. This is an indication of C=C bond breaking, and subsequently formation of new sp^3 carbon atoms on CNT surface with oxygen functional groups.

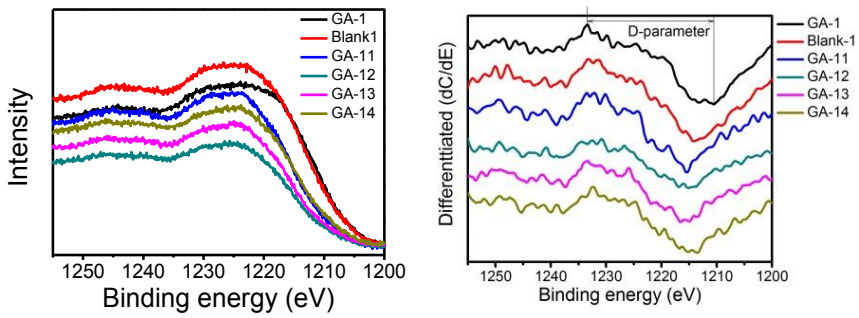

FIG. 2.8. (a) Raw Auger data of carbon nanofibers samples pristine (GA-1, Blank-1) and irradiated samples (GA-11, GA-12, GA-13 and GA-14); (b) Differentiated Auger spectra and Auger D- parameter for PR-25-PS grafted with acrylic acid ^{60}Co γ -rays and industrial electron accelerator.

FTIR spectra of carbon nanofibers are shown in Fig. 2.9. FTIR is a very useful technique to investigate the functional groups attached to the surface of carbon nanofibers. The peaks in the 2805-3010 cm^{-1} region are characteristic of C-H stretching, and their intensities are enhanced after functionalization process (GA-1 and Blank-1 compared with GA-11, GA-13 and GA-14), which can be explained by the attachment of alkyl groups onto the surface of carbon nanofibers and the increase of defects by irradiation [2.33]. Vinyl bounds (C=C) stretching vibrations appear in ~1640 cm^{-1} and are typically from aromatic compounds. The radiation incidence on the carbon nanofibers promotes crosslinking of C=C terminal bounds, transforming Csp^2 in Csp^3 bounds. A peak at ~1090 cm^{-1} in GA-11, GA-13 and GA-14 may be ascribed to the C-O stretching mode, indicating the presence of hydroxyl groups in samples irradiated. The peak around 1740 cm^{-1} can be assigned to the stretching mode of carbonyl groups present in the functionalized samples, indicating the presence of polyacrilate (PAA) chains in carbon nanofibers. In addition, a broad band in the 3100-3600 cm^{-1} region is attributed not only to the presence of hydroxyethyl group and PAA chains containing OH, but also to traces of water in the KBr used for the analysis which is inaccessible to be fully removed.

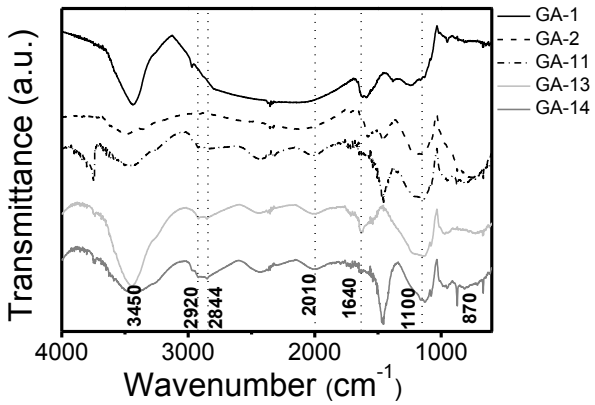

FIG. 2.9. FTIR spectra of GA1, GA2 (blank 1), GA 11, GA 13 and GA 14.

The samples were characterized by Raman spectroscopy and the results are shown in Fig. 2.10. The peaks near 1575 and 1325 cm^{-1} correspond to the G band due to stretching vibrations of the sp^2-hybridized carbon and the disordered D band attributed to defective carbon atoms, respectively. The samples treated with acrylic acid had the D frequency shifted to left 5.5 cm^{-1} and G frequency did not change.

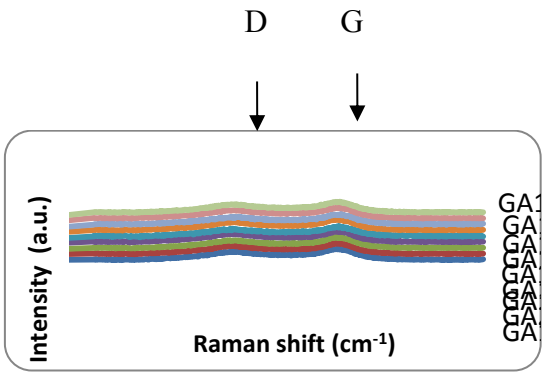

FIG. 2.10. Raman spectroscopy results of PR-25-PS irradiated at 1000 kGy, soaked into monomers solution with water/methanol (50% vol) and washed with deionized water to remove the residual monomers and by products.

The Raman spectra of all carbons showed several common features in the 800-2000 cm^{-1} region, called G and D peaks, which lie around 1560 and 1360 cm^{-1}. The intensity ratio of D band to G band in the Raman spectra has been widely used to evaluate the defects in carbon nanomaterials. The increase of ID/IG ratios may indicate generation of defects on carbon nanofiber surface due to the covalent bonding formation with functional groups grafted on carbon nanofiber surface. The results presented in Figure 2.10. showed that there are no meaningful changes in the carbon nanofiber structure. High radiation dose was not able to damage the bulk CNF structure. It was localized to the surface and did not compromise the core of the carbon nanofiber. Thus, the advantage of this process is that the overall graphitic structure has not been damaged. The radiation grafting reaction is carried out on external layer, which is less organized than the bulk of the wall. Raman spectroscopy is a bulk characterization technique in which the laser penetration (~1 μm) may exceed the thickness of the turbostratic carbon layer deposited on the nanofiber surface where the oxidation takes place. In general, the graphite structure of the nanofiber core did not show any damage.

Generally the Raman spectra of carbon materials are simple, with two most intense bands between 1000 and 2000 cm^{-1}. The dispersion of π electrons in graphene is why Raman spectroscopy is always resonant for carbon. However, Raman has some drawbacks that may lead to misinterpretation of the spectra. Ferrati A. investigated the impact of multiple layers of graphene on the D band of Raman spectrum. For more than five layers, the D band Raman spectrum becomes hardly distinguishable from the bulk graphite. Thus Raman spectroscopy can clearly indentify less than 5 graphene layers [2.34].

The thermogravimetric (TGA) was carried out in a TGA-50 Shimadzu equipment and it is an important tool to investigate the chemical and physical properties of a material. The onset degradation temperature results for functionalized samples are presented in Table 2.7. It showed that the functionalized samples degraded at lower temperature. For instance, the decomposition onset temperatures for GA 13 sample was 108.68 ^{o}C lower than GA1 and 78.54 ^{o}C lower than Blank 1. The reason for the the decrease of onset degradation temperature is that this process introduce oxygen functional groups covalent bonded on CNF surface. These defects on the graphene layers structure may lower the onset degradation temperature of the samples. The thermal stability of non-irradiated CNF (GA1, blank 1 and blank 2) was higher than the irradiated ones. This stability can be attributed to degree of defects and damages (see Table 2.7. and Fig. 2.11a and 2.11b). The non-irradiated sample (GA1, blank 1 and blank 2) began to lose mass between 550 and 622°C, which was attributed to impurities or imperfections in the nanofiber and the functionalized samples, starts to lose weight around 250°C. In addition, the irradiated samples exhibited a more pronounced weight loss from 500-800°C than non- functionalized carbon nanofibers.

TABLE 2.7. ONSET DEGRADATION TEMPERATURE FOR SAMPLE IRRADIATED IN IPEN FACILITIES AT DIFFERENT DOSE

Dose	TGA- Onset Degradation temperature (^{o}C), (10 ^{o} C/min in N2)
GA1	622.40
Blank 1	592.26
GA11	535.57
GA11.1	514.08
GA 13	513.72
GA14	519.68
Blank 2	549.26
GA17	527.83
GA18	527.91

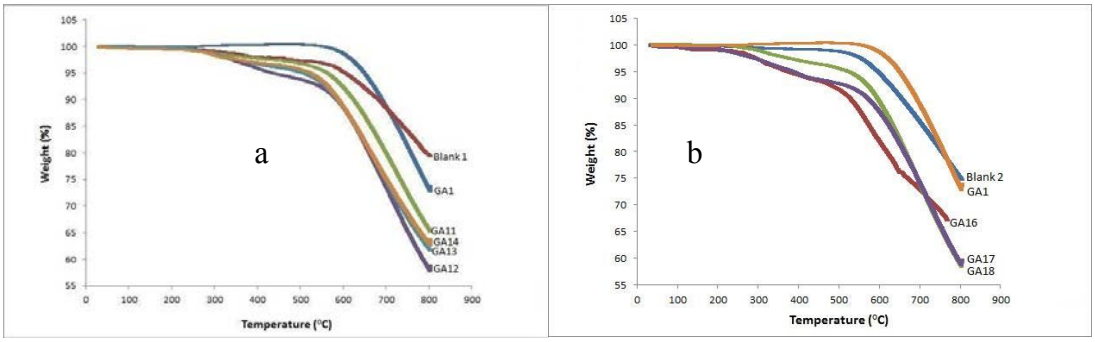

FIG. 2.11. TGA for non funcitionalized and functionalized samples.

The DMA results are very sensitive to changes in structure of materials. The DMA analyses are being carried out in a TA Instruments model DMA 2980, operating at a frequency of 1 Hz in a temperature range from 20 to 200 ^{o}C at a heating rate of 2 ^{o}C/min. The analyses were conducted at the Laboratory of the Division of Materials DCTA. The viscoelastic properties were evaluated mainly by the storage modulus (E'). The E' results at 50 ^{o}C are shown in Tables 2.8. and 2.9. The composites manufactured with functionalized CNF showed an increase in storage modulus in both methods of composites manufacture. The 16NC1-2 (M) sample prepared by 3 roll mill method presented a very high storage modulus when compared to nanocomposites made with non- functionalized samples (see Table 2.9). It may be an indication of rigity of the material however more DMA will be done to verify this result. Overall, there is an increase of stiffness on the nanocomposites manufactured with functionalized CNF. The nanocomposite manufactured with non functionalized CNF (15 CNF -2 NC1 (M)) has a E' lower than E'of the pure resin (NC1 - BF 2 (M)).

TABLE 2.8. ELASTIC MODULUS AT 50 °C OF COMPOSITES MANUFACTURED BY THE CONVENTIONAL METHOD

Samples	E' (MPa)
BANC1-1	1732
1NC1-1	1605
15NC1-1	1600
16NC1-1	1871
17NC1-1	2173
18NC1-1	1823

TABLE 2.9. ELASTIC MODULUS AT 50 °C OF COMPOSITES MANUFACTURED BY THE 3 ROLL MILL METHOD

Samples	E' (MPa)
BFNC1-2 (M)	1714
1NC1-2 (M)	1740
15NC1-2 (M)	1604
16NC1-2 (M)	8993
17NC1-2 (M)	1873

The mechanical properties were investigated so far by flexural test. The flexural test adopted was the three-point bending (ASM 790), conducted by an Instron machine (Fig. 2.12) in the Laboratory of Mechanical Properties (LPM) at Institute of Aeronautics and Space (IAE) / DCTA. Rectangular samples were produced with approximately 100 mm in length, 14 mm width and thickness between 3 and 5 mm. The distance between points 40 mm, a test speed of 1 mm / min and the test was carried out at room temperature. Assays were performed in manufactured composites with functionalized CNF, not functionalized and pure resin according to the information contained in Tables 2.3. and 2.5.

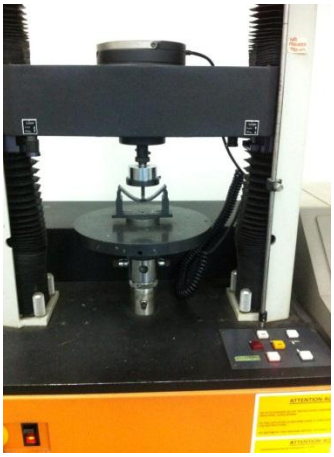

FIG 2.12. – Instron machine - flexural test.

As illustrated in Fig. 2.13. and 2.14., the composites manufactured with functionalized CNF had flexural strength higher than those of composites manufactured non-functionalized CNF. More flexion tests should be performed in order to have good statistic of the results. Comparing the samples 16NC1 -1 and 16NC1-2 (M) it can be observed an increase on flexural strength which can be attributed to the manufacturing process of the composite. 3 roll mill process promotes better interaction CNF/ epoxy. At the same time, the process leads to a shearing wear surface and this can be a disadvantage for samples irradiated by the electron beam that promotes more damages on CNF surface due to electron beam energy and high dose rate compared to gamma radiation. This results is in accordance with DMA, the 17NC1 -2 (M) sample presented lower E' than the 16NC1 -2 (M).

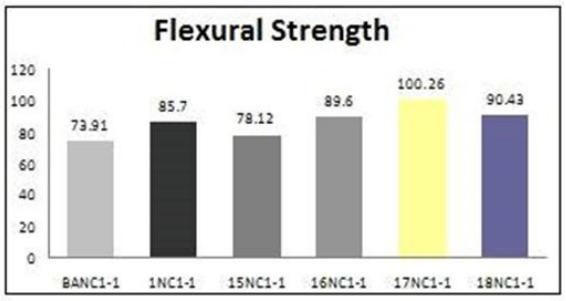

FIG. 2.13. Flexural strength of composites manufactured by convencional method.

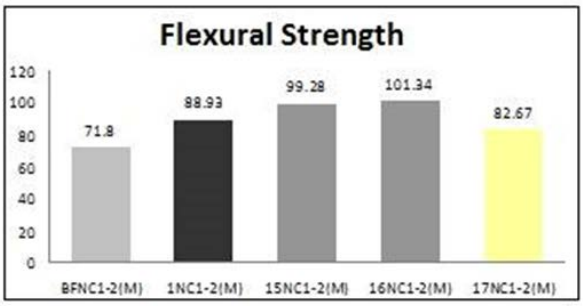

FIG. 2.14. Flexural strength of composites manufactured by 3 roll mill method.

In Fig. 2.15. and 2.16. are shown images of SEM. The morphology of the nanocomposites was analyzed in Magelan model microscope from Federal University of São Carlos in the State of São Paulo. The SEM images of nanocomposites made with GA1 and blank 2 carbon nanofiber are shown in Figure 2.15a and 2.15b. Investigating the morphology of nanocomposites samples, it was observed that the samples presented detachments from the resin system (Fig. 2.15a and 2.15b). The nanocomposites manufactured with functionalized carbon nanofibers presented more molhability and attachment with the resin.

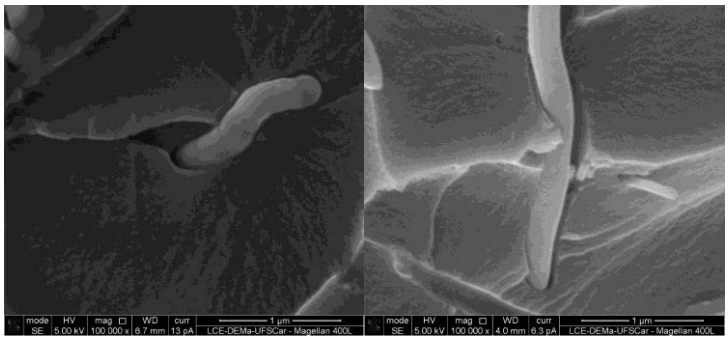

FIG. 2.15. SEM images of non irradiated samples a- nanocomposites manufactered with GA1 and b-. nanocomposites. manufactered with blank2.

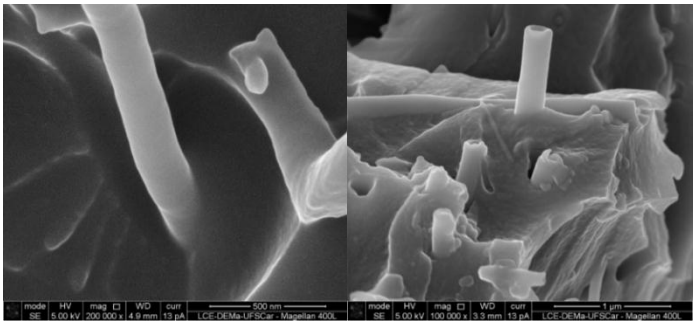

FIG. 2.16. SEM images of irradiated samples a- nanocomposites manufactered with GA16.

2.4. CONCLUSION

The aim of this project is to investigate the use of ionizing radiation to developing a methodology to introduce oxygen functional groups on the CNF surface to improve fiber/matrix dispersion and create better interaction of these two compounds aiming to make composites with better properties.

The changes performed on the surfaces of the carbon nanofibers via ionizing radiation to graft functional groups were successfully performed. The methodology was established and the process was reproducible. We observed that the changes occurred on CNF surface and XPS results showed a significant increase in the percentage of oxygen in the CNF surface.

Two methods investigated to manufacture nanocomposites with functionalized CNF. Overall, the application of these functionalized nanofibers in composites showed promising results. The best results seem to be those that were made by 3 roll mill method. Despite the difficulties that each manufacture methodology, the 3 roll mill process was the most efficient process for providing composites with less bubbles and promoted greater interaction between functionalized nanofiber and the polymer matrix. From the results of DMA and flexural tests, it was observed an increase on the storage modulus and flexural strength on the nanocomposites manufactured with CNF functionalized. The stability of the dispersion of the functionalized CNF in water during months was a good indication that the functionalization via ionizing radiation was successful, it can be suggest that the functionalized nanofiber promoted better interface in the composites analyzed, but different mechanical tests will still be conducted. This interaction could be observed with SEM technique where it was observed that the nanocomposites manufactured with CNF non functionalized presented detachments from the resin system.

ACKNOWLEDGEMENTS

We would like to acknowledge the International Atomic Energy Agency the support to this project as well as we would like to thanks the collaborators such as :

— Dr Luis Claudio de Moura Pardini and Andreza Cardoso Institute of Aeronautics and Space DCTA for the support, technical discussion and collaborations during this project.

— Elizabeth Somessari and Carlos Gaia da Silveira from Institute for Nuclear and Energy Research for the support, technical discussion and availability for the irradiation process which is the main tool for this research project.

— Dr. Tony Saliba and Deborah Daloia from University of Dayton for the technical support on composites manufacturing.

— •Applied Sciences Inc. for the carbon nanofiber.

— Dr. Joyce Araujo and Dr. Martins Erlon from the National Institute of Metrology, Quality and Technology (INMETRO) by important analyzes and investigations conducted during the technical visits.

— Dr Brian Strohmeier Thermo Fisher Scientific by XPS analysis that were important to verify the reproducibility of the method established performed.

— At the Institute for Advanced Studies would like to thank Mr David Neves analysis by X-ray diffraction and the design of the molds for composites. SUTEC colleagues from the implementation of this project and Dr. Raquel Villela of Nuclear Energy Division for technical support. And finally, I thank the student Marina Gorgulho for her work on the project tasks.

REFERENCES TO CHAPTER 2

[2.1] EITAN, A., JIANG, K., DUKES, D., ANDREWS, R., Schadler, L., Surface modification of multiwalled carbon nanotubes: Toward the tailoring of the interface in polymer composite, Chem. Mater. 15 (2003), 3198.

[2.2] LAFDI, K., FOX, W., MATZEK, M., YILDIZ, E., Effect of carbon nanofiber heat treatment on physical properties of polymer nanocomposites, Part I, Journal of Nanomaterials v 2007 (2007), Article ID 53729.

[2.3] LAFDI, K., FOX, W., MATZEK, M., YILDIZ, E., Effect of carbon nanofiber-matrix adhesion on polymer nanocomposite properties- Part II, Journal of Nanomaterials, 2007 (2008) Article ID 53729.

[2.4] YU, H., MO, X. et al., Radiation-induced grafting of multi-walled carbon nanotubes in glycidyl methacrylate-maleic acid binary aqueous solution, J Phys.Chem. 77 (2008) 656.

[2.5] PEDRONI, L. G., ARAUJO, J. R., FELISBERTI, M. I., NOGUEIRA, A.F., Nanocomposites based on MWCNT and styrene-butadiene-styrene block copolymers: Effect of the preparation method on dispersion and polymer-filler interactions, Composites Science and Technology 72 13 (2012) 1487.

[2.6] LONG, D., WU G, ZHU G., Noncovalently modified carbon nanotubes with carboxymethylated chitosan: A controlled donor-acceptor nanohybrid, Int. J. Mol. Sci. 9 (2008) 120.

[2.7] ZHANG X., SREEKUMAR T.V., LIU T., KUMAR S., Properties and Structure of Nitric Acid Oxidized Single Wall Carbon Nanotube Films, J. Phys. Chem. B 108 (2004) 16435.

[2.8] WANG S., LIANG Z., LIU T., WANG B., ZHANG C., Effective amino-functionalization of carbon nanotubes for reinforcing epoxy polymer composite, Nanotech. 17 (2006) 1551.

[2.9] PAREDES J.I., MARTINEZ-ALONSO A., TASCON J.M.D., Oxygen plasma modification of submicron vapor grown carbon fibers as studied by scanning tunneling microscopy, Carbon 40 (2002) 1101.

[2.10] SHIN Y., JEON I., BAEK J., Stability of multi-walled carbon nanotubes in commonly used acidic media, Carbon 50 (2012) 1465.

[2.11] BRUSER V. et al, Surface modification of carbon nanofibers in low temperature plasmas, Diamond Relat. Mater. 13 (2004) 1177.

[2.12] WEI G., SHIRAI K., FUJIKI K., SAITOH H., YAMAUCH T., TSUBOKAWA N., Grafting of vinyl polymers onto VGCF surface and the electric properties of the polymers-grafted VGCF. Carbon 42 (2004) 1923.

[2.13] CHOI S., NHO Y.C., Radiation-Induced Graft Copolymerization of Mixture of Acrylic Acid and Acrylonitrile onto Polypropylene Film, Korea Polym. J. 64 (1998) 287.

[2.14] CHAUDHARI C.V., BHARDWAJ Y.K., SABHARWAL S., Radiation grafting of methyl methacrylate on radiation crosslinked natural rubber film, J. Radioanal. Nucl. Chem. 267 1 (2006) 113.

[2.15] CHEN J., WEI G., MAEKAWA Y., YOSHIDA M., TSOBOKAWA N., Grafting of poly(ethylene-block-ethylene oxide) onto a vapor grown carbon fiber surface by γ-ray radiation grafting, Polymer 44 (2003) 3201.

[2.16] CHEN J., WEI G., MAEKAWA Y., YOSHIDA M., TSOBOKAWA N., Grafting of poly(ethylene-block-ethylene oxide) onto a vapor grown carbon fiber surface by γ-ray radiation grafting, Polymer 44 (2003) 3201.

[2.17] CHEN S. et al., Preparation of Poly(acrylic acid) Grafted Multiwalled Carbon Nanotubes by a Two-Step Irradiation Technique. Macromolecules 39 (2006) 330.
[2.18] JUNG C., KIM D., CHOI J., Surface modification of multi-walled carbon nanotubes by radiation-induced graft polymerization, Curr. Appl. Phys. 9 (2009) 85.
[2.19] MARTÍNEZ-HERNÁNDEZ A., VELASCO-SANTOS C., CASTAÑO V.M., Carbon Nanotubes Composites: Processing, Grafting and Mechanical and Thermal Properties, Curr. Nanosci. 6 (2010) 12.
[2.20] CLOCHARD M.C., BEGUE J., LAFON A., CALDEMAISON D., BITTENCOURT C., PIREAUX J., BETZ N., Tailoring bulk and surface grafting of poly(acrylic acid) in electron-irradiated PVDF, Polymer 45 Issue 25 (2004) 8683.
[2.21] CHEN J., MAEKAW, Y., YOSHIDA M., TSOBOKAWA N., Radiation grafting of polyethylene onto conductive carbon black and application as a novel gas sensor, Polym. J. 34 n 1 (2002), 30.
[2.22] CHEN X. et al. In-Situ X-ray Scattering Studies of a Unique Toughening Mechanism in Surface-Modified Carbon Nanofiber/UHMWPE Nanocomposite Films, Macromolecules 38 (2005) 3883.
[2.23] CHOI S., CHUNG D., KWEN H., Fabrication of Biosensors Using Vinyl Polymer-grafted Carbon Nanotubes. Intech Open Science, 12 (2001) 245.
[2.24] PING X., WANG M., GE X., Surface modification of poly(ethylene terephthalate) (PET) film by gamma-ray induced grafting of poly(acrylic acid) and its application in antibacterial hybrid film, Radiat. Phys. Chem. (2010) 1.
[2.25] SAMMALKORPI M. et al, Irradiation-induced stiffening of carbon nanotube bundles, Nucl. Instrum. Methods B 228 (2005) 142.
[2.26] TSUBOKAWA N. Functionalization of Carbon Material by Surface Grafting of Polymers, Chem. Soc. Jpn. 75 (2002) 2115.
[2.27] EVORA M.C., KLOSTERMAN D., LAFDI K., LI.L., ABOT J.L., Functionalization of carbon nanofiber through electron beam radiation, Carbon 48 (2010) 2937.
[2.28] JUNG C. et al., Surface functionalization of single-walled carbon nanotubes by a radiation grafting, Appl. Chem. 13 1 (2009), 25.
[2.29] FILIK J., MAY P.W., PEARCE S.R.J., WILD R.K., HALLAM H.R, XPS and laser Raman analysis of hydrogenated amorphous carbon films, *Diamond and related materials* 12 (2003) 974.
[2.30] ZHU Y., TANG J., ZHU W., ZHANG M., LIU G., LIU Y., ZHANG W., JIA M, Graphite oxide-supported CaO catalysts for transesterification of soybean oil with methanol Bioresource Technology 102 (2011) 8939.
[2.31] HAN H. S., YOU J., JEONG H., JEON S., Synthesis of graphene oxide grafted poly(lactic acid) with palladium nanoparticles and its application to serotonin sensing, Applied Surface Science 284 1 (2013) 438.
[2.32] TURGEON S., PAYNTER R.W., On the determination of carbon sp^2/sp^3 ratios in polystyrene/polyethylene copolymers by photoelectron spectroscopy, Thin Solid Films 394, (2001) 44.
[2.33] CHEN J., MAEKAW, Y., YOSHIDA M., TSOBOKAWA N., Radiation grafting of polyethylene onto conductive carbon black and application as a novel gas sensor, Polym. J. 34, n 1 (2002) 30.
[2.34] FERRARI, A., Raman spectroscopy of graphene and graphite: Disorder, electron-phononcoupling, doping and nanodiabatic effect, Solid State Commun. 143 (2007) 47.

Chapter 3

USING GAMMA IRRADIATION FOR GRAFTING AND/OR CROSSLINKING OF NATURAL POLYMERS FOR THE FABRICATION OF ACTIVE BEADS AND PACKAGING FILMS BASED ON NANOCELLULOSE

M. LACROIX, S. SALMIERI, A. KHAN, T. HUQ, P. CRIADO, D. BECHER
Canadian Irradiation Centre, Research Laboratories in Sciences Applied to Food,
INRS-Institut Armand-Frappier,
Québec,
Canada

R.A. KHAN,
Bangladesh Atomic Energy Commission,
Ganakbari,
Bangladesh

H. IBRAHIM
Egyptian Atomic Energy Authority, National Centre for Radiation Research and Technology,
Nasr City, Cairo,
Egypt

Abstract

Effect of 2-hydroxylethyl methacrylate (HEMA) monomer grafted on methylcellulose (MC)-based films was characterized. Films were obtained by casting and then exposed to gamma irradiation (5-25 kGy). Results revealed that 1% HEMA-containing films showed the highest puncture strength values (282 N/mm) at 10 kGy. FTIR analysis showed a decrease of the vinyl vibration band from HEMA at 1636 cm^{-1} after grafting, suggesting that graft polymerization occurred via a HEMA reaction from vinylidene into methylene group and via HEMA homopolymerization**.** Moreover, FTIR peaks clearly indicated that MC-g-HEMA copolymer grafting was improved with higher radiation doses. Silane monomer was also grafted on chitosan films by exposition to gamma irradiation (5-25 kGy). The grafting reaction of chitosan based films was able to increase by 34% the tensile strength. When silane was grafted on methylcellulose (MC) based films, a 92% puncture strength increase was observed. Carbone nanotube (CNT) and crystalline nanocellulose (CNC) were added in natural biopolymers as nanomaterial reinforcement. Addition of carbon nanotube has permitted to increase by 131 % the tensile strength of reinforced polycaprolactone based films showing also better moisture and oxygen barrier properties especially for irradiated films at a maximum of 0.5% of carbon nanotube and at a maximal dose of 15 kGy. CNC dispersed in chitosan based film or in alginate based beads using microfluidization increased significantly the tensile strength and have permitted a better protection of the active compounds immobilized in the polymers. An active film was also developed using gallic acid as antioxidant molecule. Gallic acid was grafted on CNC using gamma irradiation and this active polymer was used for the development of antioxidant film and coating for food application. A reaction of gallic acid on CNC surface was carried out under a free radical grafting by using hydrogen peroxide/ascorbic acid (AA) as redox couple initiator. Gallic acid (GA) was incorporated at different ratios with respect to molar ratios CNC/GA (R1=0.66 and R2=8). Gamma radiation was applied from 0 to 20 kGy. Results indicated that increasing radiation doses allowed improving the scavenging radical properties of CNC-*g*-GA from 0.18 to 1.27 TEAC (Trolox Equivalent Scavenging radical Capacity; mM Trolox eq/mg CNC). Higher TEAC value was obtained at 20 kGy (1.27 Trolox eq). Covalent attachment of GA on CNC was characterized by FTIR analysis with typical vibrations of aromatic ester linkage (1730 cm^{-1}). Poly(lactic acid)-nanocrystalline cellulose (PLA-NCC) supramolecular composite films were also prepared from granules of PLA-NCC by compression

molding method. Supramolecular PLA-NCC films were converted to bioactive films using nisin as an antimicrobial agent by an adsorption coating method. Films were then introduced in packages containing sliced cooked ham or ready to eat vegetables as food models and stored for 14 days at 4°C to determine their mechanical, barrier and antimicrobial properties. It was observed that mechanical properties such as tensile strength (TS), tensile modulus (TM), elongation at break (Eb) and water vapor permeability (WVP) values of the bioactive films was stable even after 14 days of storage. Bioactive PLA-NCC films showed a significant reduction of *Listeria monocytogenes* in sliced cooked ham from day 1 and a total inhibition from day 3. For ready to eat vegetable, a quasi-total inhibition of *L. monocytogenes* in vegetables at day 14 was observed. The percentage of nisin release increased continuously from day 0 to day 14, with a release of 21% at day 14.

3.1. INTRODUCTION

Synthetic polymers such as polyethylene, polypropylene are widely used as packaging materials because of their excellent thermo-mechanical properties. But these polymeric materials are not biodegradable. Researchers are investigating alternative packaging materials which are environment-friendly, cheap, light weight and possess good thermo-mechanical properties. Natural biopolymers like chitosan, cellulose derivatives, alginate, poly lactic acid and gellan can be used as alternative of synthetic polymers to prepare biodegradable packaging films and could be used in combination with biodegradable thermoplastic like poly-caprolactone for the development of active packaging films [3.1-3.4]. The use of biodegradable films for food packaging has however, been strongly limited because of the poor barrier properties and weak mechanical properties. Innovative technologies like the use of nanomaterial reinforcement (carbon nanotube, CNT) and irradiation for grafting monomers (ex: silane, HEMA) or crosslinking has the potential to improve the physico-chemical properties of the films and can assure a control release of the active compounds from the film to the surface of the food [3.5]. The dispersion of the nanomaterial in film formulation is also important. To achieve this, a high pressure homogenization technique such as microfluidization can be adopted [3.6]. Finally, nanomaterial can be used for active compound immobilization for the development of active packaging [3.1, 3.5]. The aim of this project is to use gamma irradiation, nanomaterials reinforcement and microfluidization for the development of grafted and active films with higher physico-chemical properties for food applications.

3.2. MATERIALS AND METHODS

3.2.1. Experimental

3.2.1.1.Materials

Preparation of MC based films grafted with trimethylolpropane trimethacrylate (TMPTMA), mechanical and barrier properties were done according to Sharmin et al. [3.7]. Preparation of chitosan films and polycaprolactone (PCL)-based composites grafted with silane and mechanical properties were done according to Sharmin et al. [3.8]. Films preparation (methylcellulose (MC)-g-HEMA films), measurements of mechanical and barrier properties were carried out according to methods by Khan *et al.* [3.9, 3.10]. Irradiated films based on PCL-CNT were prepared and characterized based on Khan et al. [3.3., 3.2]. Film preparation (compression molding of CNC-reinforced PCL films), measurements of mechanical and barrier properties and SEM were carried out according to a method by Khan *et al.* [3.2]. Preparation of chitosan based films grafted with HEMA: measurements of mechanical and barrier properties were carried out according to a method by Khan *et al.* [3.11].

The grafting of antioxidant gallic acid (GA) on CNC for the development of antioxidant films based on gellan gum, the films were prepared as follow: A 2% (w/v) CNC solution was prepared in deionized water and followed reaction with 135 mg ascorbic acid and 567 µl hydrogen peroxide (8M) at 25°C for 2h under stirring. A slow stream of vacuum air and oxygen free nitrogen gas passed on the solution for 30 min each before irradiation treatment. Grafting procedure was followed by the addition of GA at different amount per CNC (R1= 0.66 and R2=8) and reaction was performed for 24h. The obtained grafted CNCs were dialysed in distilled water for 48h in 12-14 kDa membranes in order to eliminate unreacted products. Adding antioxidant properties to CNC is based on reaction of hydroxyl groups contained on the surface of CNC with antioxidant molecules by an oxide-reduction (redox) group. The mechanism is presented by the reaction of Spizzirri et al. [3.12] by which is shown the formation of active places on the polysaccharide by the oxidation of hydrogen peroxide. DPPD scavenging measurement was performed as described by Han et al. [3.13]. Phenolic groups were analyzed by Folin-Ciocalteu procedure and FTIR spectra of freeze dried sample was obtained by using a Spectrum One spectrophometer (Perkin-Elmer, Woodbridge, ON, Canada). Supramolecular PLA-NCC granules (3% w/w NCC concentration) were supplied by Celluforce, 3800 Wesbrook Mall, Vancouver, BC, Canada. The natural antimicrobial agent nisin was procured from Profood International, Inc. (China). PLA-NCC films were treated with nisin by an adsorption/diffusion coating method according to Salmieri et al. [3.14, 3.15].

3.3. RESULTS

3.3.1. MC-based films grafted with TMPTMA by ɣ-radiation, in combination with CNC filling

Combined effects of TMPTMA, CNC and ɣ-radiation led to significant improvements of mechanical and barrier properties of MC-based films. MC-based films containing CNC as a filling agent were prepared and irradiated in presence of TMPTMA as a grafted plasticizer. Optimal mechanical and barrier properties were obtained by using 0.1% monomer (TMPTMA) at 1 kGy (Fig. 3.1). MC-TMPTMA molecular interactions (hydroxyl, carbonyl and vinylidene groups) were supported by FTIR analysis. Grafted films (MC-g-TMPTMA) presented superior mechanical properties with a tensile strength (TS) of 47.9 MPa and a tensile modulus (TM) of 1792 MPa, possibly due to high yield formation of radicals to promote TMPTMA grafting during irradiation. The combined effect of CNC filling enhanced the mechanical properties of grafted

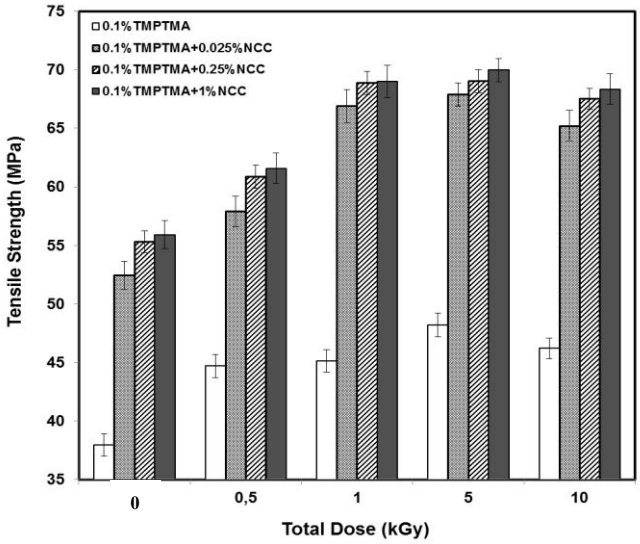

FIG. 3.1. – Effect of CNC concentration combined with ɣ-radiation doses on the TS of MC-g-TMPTMA films.

films (TS = 67 MPa) and optimal treatments were assessed to 4.45% TMPTMA (w/w polymer dry basis), 1 kGy radiation dose and 10% CNC (w/w dry basis) for mechanical improvements. The addition of CNC also led to an additional improvement of the barrier properties, with a significant 25% reduction of water vapor permeability (WVP) of grafted films. SEM analysis provided typical morphological changes due to CNC filling into polymer bulk. These results suggest that incorporation of CNC allowed reducing irradiation dose (5 to 1 kGy) by greatly improving the physicochemical properties of films as compared to grafted films alone.

3.3.2. MC-based films grafted with HEMA by ɣ-radiation

3.3.2.1.Mechanical properties

The puncture PS of MC-based films (1% MC W/V) were found to be 147 N/mm. The MC-g-(1% HEMA) films (solid film containing 30% w/w HEMA, dry basis) performed the highest PS values (282 N/mm) suggesting 1% HEMA as an optimal concentration. In order to investigate the effect of ɣ-radiation, different doses (5-25 kGy) were applied to the films and results showed that the highest PS values (92% improvement) was observed at 10 kGy (Fig. 3.2).

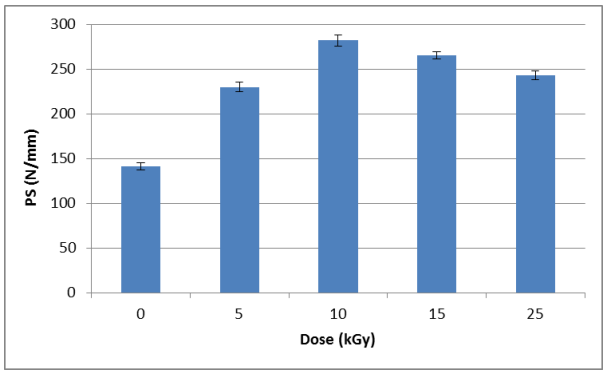

FIG. 3.2. – Effect of gamma radiation on the PS of MC-g-HEMA films.

3.3.2.2.Barrier properties

The values of WVP decreased significantly ($p \leq 0.05$) as the radiation doses increased. The WVP of MC-based films (control without HEMA) was found to be 6.3 g.mm/m^2/day.kPa. For MC-g-HEMA films grafted at 25 kGy, WVP value was measured to 5.5 g.mm/m^2.day.kPa, hence generating a 13% reduction of WVP values as compared to control without HEMA.

3.3.2.3.Grafting copolymerization: FTIR observations

The effect of irradiation dose (10, 25, 50 and 100 kGy) on the structural changes induced by grafting reaction in the polymer blend was also investigated.

Figure 3.3. shows the FTIR spectra of HEMA (a), MC-based films (control; ungrafted) (b) and grafted copolymer MC-g-HEMA films irradiated at 50 kGy (c). The position of peaks of HEMA (a) is mainly assigned to the stretching vibrations of O–H at 3600-3200 cm^{-1}, C=O in ester linkage at 1720 cm^{-1} (with a characteristic shoulder), vinyl groups –CH=CH$_2$ at 1636 cm^{-1}, antisymmetric C–O–C esters at 1297 cm^{-1}, C–C–OH at 1164 cm^{-1}, as previously described Gao et al. [3.16]. The absorption peaks of the MC-based films (b) are mainly assignable to the stretching O–H vibrations at 3600-3200 cm^{-1}, overlapping symmetric and asymmetric C–H at 2950-2850 cm^{-1}, and bound water vibration at 1744 cm^{-1}, as reported by Zaccaron et al.[3.17]. As a result, modifications in characteristic bands were observed after radiation-induced HEMA grafting into MC matrix (c).

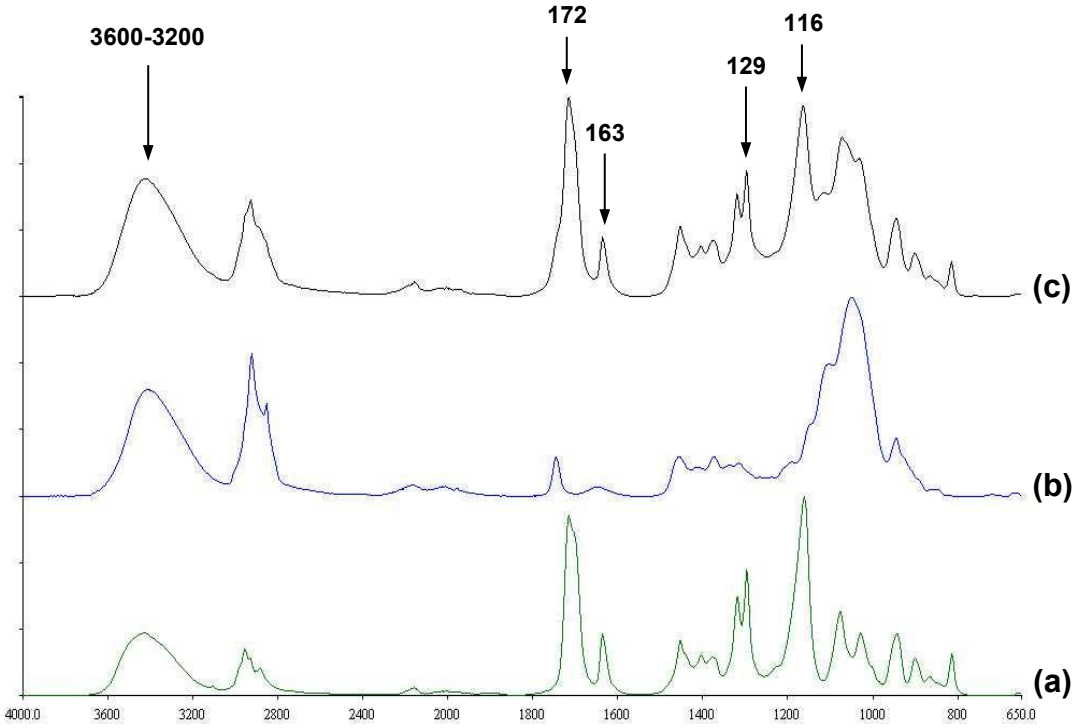

FIG. 3.3. FTIR spectra of HEMA (a), ungrafted MC-based films (b) and grafted copolymer MC-g-HEMA irradiated at 50 kGy (c).

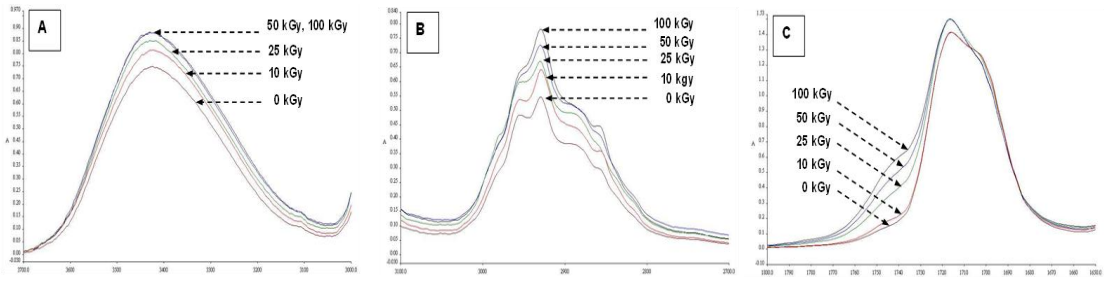

FIG. 3.4. – FTIR spectra of O-H (A), C-H (B) and C=O ester (C) stretching vibrations as related to gamma irradiation doses of 10, 25, 50 and 100 kGy in grafting process.

grafting. Focus on the C=O ester band also indicates an increasing intensity of this band with irradiation doses (with characteristic shoulder at 1250 cm^{-1}). These observations, correlated with a slight decrease of the vinyl band (1636 cm^{-1}), allow supporting that graft copolymerization occurred via a HEMA reaction from vinylidene into methylene group. It was reported that HEMA is a potential grafting agent by using ɣ-radiation [3.9].

3.3.3. Chitosan-based films grafted with silane by ɣ-radiation, in combination with PCL reinforcement

Combined effects of silane grafting, PCL filling and ɣ-radiation led to significant improvements of mechanical properties of chitosan-based films (Fig. 3.5). Final optimal conditions of silane grafting treatment were obtained by using 25% silane (w/w chitosan dry

basis) at 10 kGy irradiation dose (TS = 44 MPa). Silane grafting had also a positive effect on chitosan-PCL insoluble composite films, with significant enhancement of mechanical properties and optimal conditions by using 20% chitosan content in composite film. SEM analysis provided morphological changes induced by silane grafting into chitosan bulk, hence demonstrating chitosan-silane compatibilization by ɣ-radiation and good resulting adhesion between composite components.

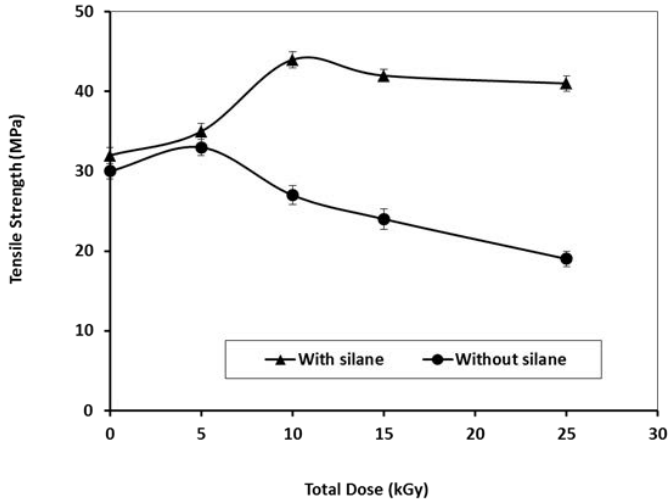

FIG. 3.5. – Effect of ɣ-radiation doses on the TS of chitosan-g-silane films.

3.3.4. PCL-based films reinforced with CNT using ɣ-radiation

The combined effects of CNT filling and ɣ-radiation improved the mechanical and barrier properties of PCL-based films. CNT filling at low concentration (0.2% w/w polymer dry basis) generated high improvements of mechanical and barrier properties of films. Combined effect of ɣ-radiation also led to significant enhancement of film properties and optimal conditions were reached by using 0.2% (w/w polymer dry basis) CNT filling at 10 kGy. SEM analysis of irradiated CNT-PCL composites showed partial homogenization of CNT in PCL matrix with higher density of CNT at the interface structure that possibly conducted to higher mechanical properties of these films (Fig. 3.6).

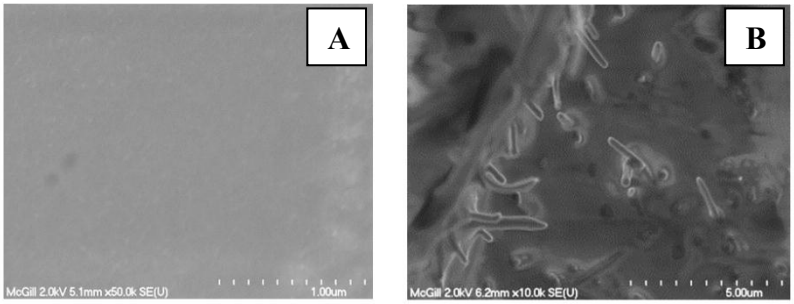

*FIG. 3.6. – SEM images of **(A)** surface and **(B)** interface of PCL films containing 0.2% CNT (w/w dry basis).*

3.3.5. CNC-reinforced PCL nanocomposites: effect of ɣ-radiation

3.3.5.1. Effect of radiation dose on mechanical properties.

PCL films and 5% (w/w) CNC-reinforced PCL nanocomposites were exposed to ɣ-radiation at doses ranging from 2 to 25 kGy. Their TS, TM, and Eb values were then measured. It was found that ɣ-radiation significantly increase the TS of films. At 10 kGy, the PCL films reached an optimal TS value of 28 MPa (75% higher than unirradiated control sample). Similarly, at 10 kGy, the TS of the PCL-NCC composite films reached 41 MPa (58% higher than control composite), also suggesting 10 kGy as an optimal dose. Above 10 kGy, the decrease in film strength can be attributed to radiation degradation of PCL by molecular chain cleavage. The higher improvement of TS value in PCL films might be due to partial hindrance of CNC against radiation-induced molecular crosslinking of PCL. However, the major advantage of CNC incorporation was further improvement of the TS of nanocomposites. Indeed, CNC reinforcement (5%) and ɣ-radiation (10 kGy) altogether significantly increased (156%) the TS of PCL films.

3.3.5.2. Effect of radiation dose on barrier properties

Gamma radiation (10 kGy) improved the WVP of PCL and CNC-PCL nanocomposite films, with a significant decrease of 12% for PCL films (1.32 g.mm/m^2.day.kPa for irradiated films) and 19% for nanocomposite films (0.98 g.mm/m^2.day.kPa for irradiated films). The decrease in WVP of the CNC-PCL films may be due to consumption of -OH groups on the CNC backbone through the formation of crosslinked PCL, resulting in higher hydrophobicity of the material. On the other hand, OTR and CO_2TR measurements indicated that nanocomposite structure allowed decreasing the OTR after 10 kGy radiation. Indeed, the OTR of CNC-PCL films decreased from 146 to 118 cc/m^2.day whereas the OTR of PCL films increased (+ 28%) after ɣ-radiation. Also, the CO_2TR of CNC-PCL films decreased from 960 to 849 cc/m^2.day whereas that of PCL films increased (+23%) after radiation. These observations could be explained by cross-linking process promoted in PCL films that generates amorphous character of the partially crystalline PCL, facilitating the passage of O_2 and CO_2.

3.3.5.3. Surface and interface morphology of nanocomposite films

Figure 3.7A shows spots at the film surface and could be attributed to CNC, suggesting homogenous blend of PCL and CNC after compression molding at 110°C. Figure 7B suggests that CNC was submerged after into PCL matrix, which is a typical observation in thermopalstic polymers.

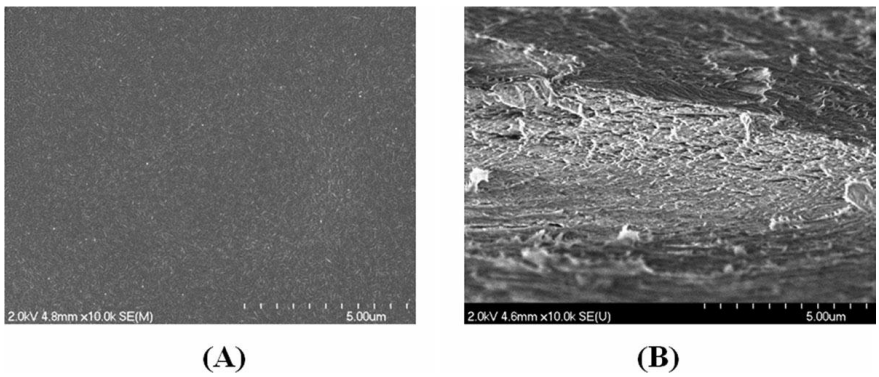

*FIG. 3.7. SEM images of (**A**) surface and (**B**) interface (fracture surface) of CNC(5%)-PCL nanocomposite films.*

In summary, these results showed that CNC is an excellent filling agent for thermoplastic biodegradable PCL. The mechanical properties of PCL were significantly improved by loading low quantities of CNC. The addition of 5% CNC generated a 62% improvement of film strength. The barrier properties of the CNC-PCL nanocomposites were also significantly enhanced compared to PCL. These nanocomposite films could be viable for use in modified atmospheric packaging applications. The effects of ɣ-radiation on PCL films were revealed that irradiated films gained further mechanical and barrier properties over the counterpart control. Thereby, this investigation opens the door to new research for modified atmospheric packaging using nanocomposites.

3.3.6. Effect of ɣ radiation on the mechanical and barrier properties of HEMA-grafted chitosan-based films.

3.3.6.1. Effect of radiation dose and HEMA treatment on mechanical properties

The effect of ɣ radiation on the PS of chitosan and HEMA-grafted chitosan films showed that the PS of irradiated chitosan films increased at low radiation doses (≤ 0.4 kGy) by reaching 597 N/mm at 0.4 kGy, possibly due to chitosan dimerization with acetic acid. At doses > 0.4 kGy, a decrease in PS was observed (-47% at 5 kGy as compared to control), which may be due to the radiation degradation of chitosan. Films containing 0.1% (w/v) HEMA exhibited the highest PS (672 N/mm) at 0.8 kGy (20% higher than control chitosan films). This increase may be attributed to the reaction of acrylic groups from HEMA with amino group of chitosan. A sharp decrease of PS at doses > 0.8 kGy could be due to the formation of poly (HEMA) combined with the degradation of chitosan.

3.3.6.2. Effect of radiation dose and HEMA treatment on barrier properties

The effect of ɣ-radiation on the WVP of chitosan and HEMA-grafted chitosan films showed that at 0.1 kGy, the WVP of chitosan films decreased sharply and reached a value of 3.07 g.mm/m^2.day.kPa (-7% compared to control). However, at radiation doses > 0.1 kGy, the WVP increased with a plateau between 1 and 5 kGy (3.41 g.mm/m^2.day.kPa. Therefore, a very low dose (0.1 kGy) contributed the chitosan films to be more water vapor resistant. On the other hand, the WVP of the HEMA-treated chitosan films decreased along with increasing radiation

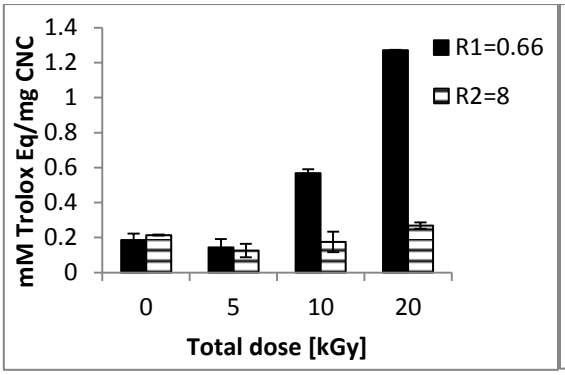

FIG. 3.8. Antiradical properties (mM Trolox Eq) per mg. CNC acid/mg

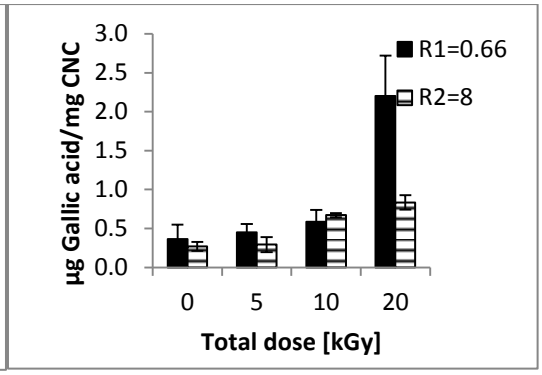

FIG. 3.9. Total phenolic coumpounds (µg gallic different CNC.

doses to reach a plateau at similar dose range of 1-5 kGy, with a minimum WVP of 2.58 g.mm/m^2.day.kPa (-22% reduction).

In summary, this study revealed that low radiation doses (0.2-0.4 kGy) applied on chitosan solution improved the mechanical strength of the cast resulting films. Chitosan-g-HEMA grafted films possessed higher mechanical and barrier properties compared to control chitosan. As a result, ɣ-radiation can be considered as a safe and good source for the preparation of monomer HEMA-grafted films made of polysaccharides such as chitosan.

3.3.7. Antiradical properties and phenolic compounds of modified nanocellulose

The effect of γ-irradiation on gallic acid grafting on CNC at different ratios was observed and presented in Fig. 3.8. Results indicates that increasing from 5 to 20 kGy, an increase on mM Trolox equivalent is increased from 0.14 to 1.27 ($p \leq 0.05$) when R1=0.66 was analyzed. Similar behavior was obtained when 0 and 5 doses were employed ($p \leq 0.05$). Little influence of irradiation dose was suggested after analysis on R2=8, however radical scavenging properties were also observed when higher doses (10, 20 kGy) were carried out on the reaction. Therefore, gallic acid attachment on CNC surface is favoured at higher doses of irradiation and lower ratio of gallic acid respect to CNC amount. Figure 3.9. shows the disposable phenolic compounds attached to CNC. It can be assesed that increasing the irradiation doses from 0 to 20 kGy

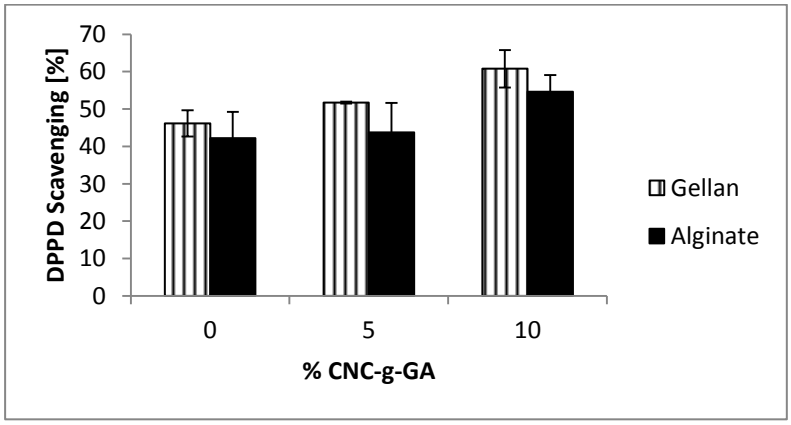

FIG. 3.10. DPPD scavenging of antioxidant gellan and alginate films with addition of different concentration of CNC-g-GA.

increases the grafting of the antioxidant molecule. This phenomenon is correlated to the radical scavenging properties found on CNC. Results also showed highest DPPD radical inhibition was achieved by modified gellan gum films with 60% when 10% (w/w polymer, dry basis) of CNC-g-GA is used compared to ~54% presented in alginate films at the same conditions (Fig. 3.10). The advancement of grafting gallic acid via gamma irradiation at 20 kGy on CNC was followed by FTIR. Fig. 3.11. shows the FTIR spectra of freeze dried (c) CNC-g-GA, (b) CNC and (a) GA in pellet. The position of the peak of GA (a) may be assigned the stretching vibrations of O-H (hydroxyl groups) on the benzene ring at wavelength 3600-3200 cm $^{-1.}$ A sharp O-H band can be

3.3.7.1. FTIR analysis of CNC-g-GA

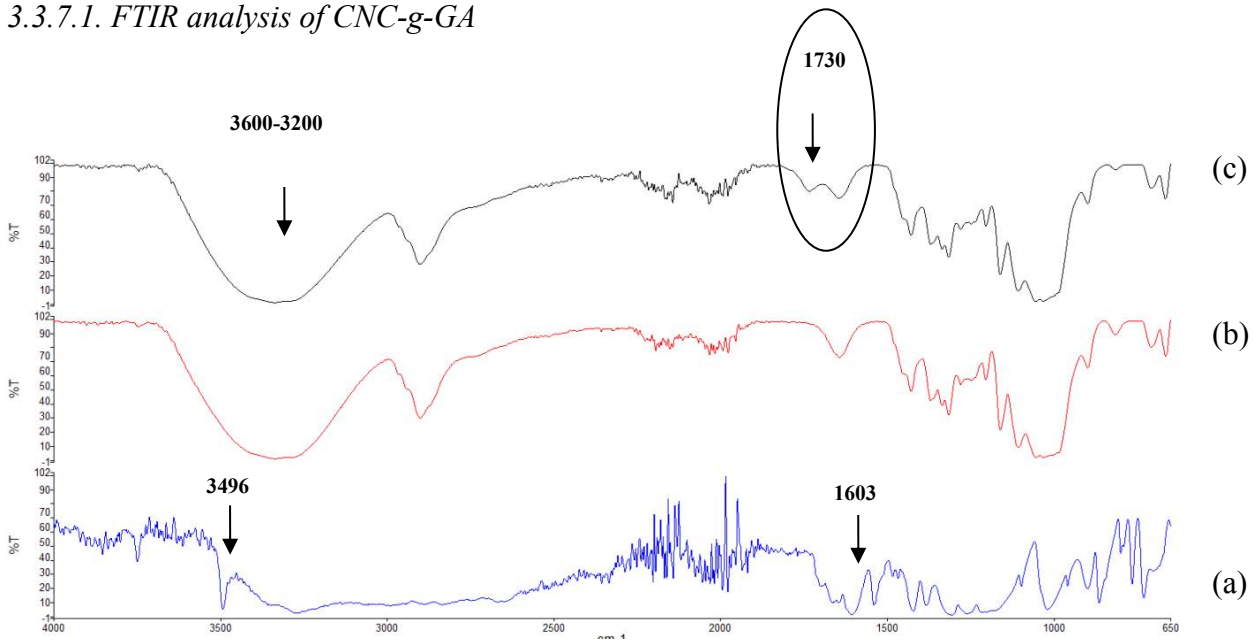

FIG. 3.11. FTIR spectra of GA (a), native CNC (b) and CNC-g-GA modified at R1=0.66 and 20 kGy (c).

observed in GA anhydrous form at the band 3496 cm^{-1}, and position peaks of C=O stretching band was placed at 1603 cm-1, as a result of a grafting of gallic acid on CNC were observed after gamma-irradiation (c). A covalent linkage is demonstrated by a new shifted band at 1730 cm^{-1} indicating a ester linkage of group C=O of gallic acid with CNC.

3.3.7.2. Effect of CNC concentration in gellan gum films

According to the results observed in Fig. 3.12, it can be suggested that increasing the concentration of modified CNC in gellan films, increased significantly their antiradical properties ($P \leq 0.05$). A 20% (w/w polymer, dry basis) of CNC-g-AG increased the radical scavenging from 46 for 0% CNC-g-AG to 68%. It can be suggested that increasing the concentration of native CNC had a slight effect on the DPPD scavenging.

3.3.7.3. Effect of CNC concentration on mechanical properties of gellan gum films

The influence of gallic acid grafting on CNC on the tensile strength and tensile modulus of gellan gum based films showed increases when modified CNC is added to gellan films, however, values were not influenced by gallic acid grafting (data not shown). Applications of antioxidant film is interesting to be applied on food as coatings or packaging in order to prevent browning reaction. Hence, future applications of this formulation will be performed

on mushroom surface to avoid browning and to verify the microbial and the physico-chemical properties of mushrooms.

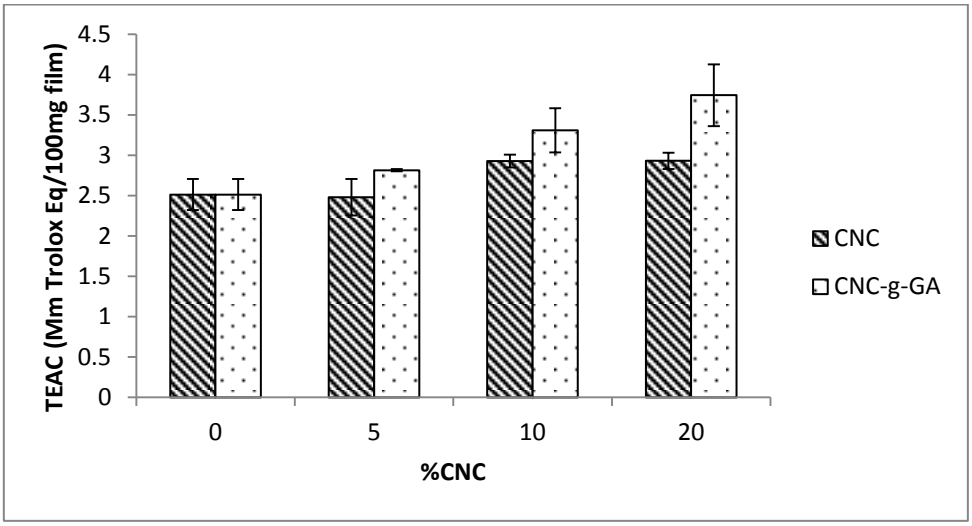

FIG. 3.12. DPPD scanvenging of 1% (w/v) gellan gum films with natif CNC and CNC-g-GA at different concentrations.

3.3.8. Bioactive polylactic acid-nanocrystalline cellulose (PLA-NCC) supramolecular nanocomposite films

The mechanical property of control PLA-NCC films and bioactive PLA-NCC films were measured and a comparative studies were carried out to investigate the efficiency of nisin as the bioactive agent. To investigate the stability of the mechanical properties in food system, one piece of cooked ham sample or pieces of ready to eat vegetables were wrapped using two control and two bioactive supramolecular PLA-NCC films then kept at 4ºC for 14 days. The TS of PLA-NCC-nisin films was significantly lower than control (PLA-NCC without nisin) ($p \leq 0.05$) at day 0 and day 1. Indeed, the adsorption of nisin generated a decrease of TS values from 44.8 to 35.9MPa (reduction of 20%) at day 0 and from 43.6 to 34.3 MPa (reduction of 21%) at day 1. After 14 days in contact with food samples, the TS of PLA-NCC films reached to 39.2 MPa which did not vary significantly ($p > 0.05$) over storage (reduction of 13%) whereas bioactive PLA-NCC-nisin films demonstrated better stability. Bioactive PLA-NCC films showed a significant reduction of *Listeria monocytogenes* in sliced cooked ham from day 1 and a total inhibition from day 3. For ready to eat vegetable, a quasi-total inhibition of *L. monocytogenes* in vegetables at day 14 was observed. The percentage of nisin release increased continuously from day 0 to day 14, with a release of 21% at day 14.

3.4. CONCLUSION

Overall, these reported investigations have emphasized the innovative aspect of polymer compatibilization by radiation grafting and the positive effects of combined treatment of ɣ-radiation with monomer grafting ad nanoparticle reinforcement into polymer bulk. The incorporation of CNC in grafted films significantly improved the mechanical and barrier properties of the films. The incorporation of CNC allowed reducing irradiation dose while greatly improving the physicochemical properties of films (as compared to grafting effect alone). The incorporation of antioxidant molecules to films represents a commercial interest to preserve the food quality during storage. These studies open new issues of preparing

functional, insoluble, biodegradable composite films for “green” packaging applications. Further investigations should be carried out in order to determine specific applications of these new functionalized biomaterials. Bioactive PLA-NCC-nisin films showed very satisfactory mechanical, barrier and antimicrobial properties and could further be explored in food applications to prevent pathogenic contamination during storage of ready-to-eat foods especially in combination with food irradiation to verify the synergistic capacity to inhibit *L. monocytogenes.*

ACKNOWLEDGEMENTS

This research was supported by the National Science and Engineering Research Council of Canada (NSERC) and FPInnovations (Pointe-Claire, Canada) through the RDC program. Authors are grateful to International Atomic Energy Agency (IAEA) for financial support to offer a fellowship IAEA project code: PHI/13002 and for the coordinated Research Project No. F22051 entitled "Radiation Curing of Composites for enhancing their features and utility". Special thanks to Anie Day De Castro Asa, and Dr. Haytham Ibrahim, IAEA scholars, for their valuable research support.

REFERENCES TO CHAPTER 3

[3.1] SALMIERI, S., ISLAM, F., KHAN, R., HOSSAIN, F., IBRAHIM, H., MIAO, C., WADOOD, C.M., HAMAD, Y., LACROIX, M. Antimicrobial nanocomposite films made of poly(lactic acid)-cellulose nanocrystals (PLA-CNC) in food applications: part A—effect of nisin release on the inactivation of *Listeria monocytogenes* in ham, Cellulose **21** (2014) 1837-1850.

[3.2] KHAN, R.A., BECK, S., DUSSAULT, D., SALMIERI, S., BOUCHARD, J., LACROIX, M. Mechanical and barrier properties of nanocrystalline cellulose reinforced poly (caprolactone) composites: effect of gamma radiation, J. Appl. Polymer Sc., **129** (2013a) 3038-3046.

[3.3] KHAN, R. A., BECK, S., DUSSAULT, D., SALMIERI, S., BOUCHARD, J., LACROIX, M. Mechanical and barrier properties of carbon nanotubes-reinforced PCL-based composite films: effect of gamma radiation, J. Appl. Polym. Sci. **127** (2013b) 3962-3969.

[3.4] AZEREDO, H. M. C., MATTOSO, L. H. C., WOOD, D., WILLIAMS, T. G., BUSTILLOS, R. J. A., MCHUGH, T. H. Nanocomposite edible films from mango puree reinforced with cellulose nanofibers, J. Food Sci. **74** (2009) 31–35.

[3.5] HUQ, T., RIEDL, B., BOUCHARD, J., AND LACROIX, M. Microencapsulation of Nisin for Prolonged Efficacy against *Listeria monocytogenes*: *in vitro* and *in situ* studies, Cellulose (2014) (submitted).

[3.6] KHAN, A., VU, K.D., CHAUVE, G., BOUCHARD, J., RIEDL, B., AND LACROIX, M. Optimization of microfluidization for the homogeneous distribution of cellulose nanocrystals (CNCs) in biopolymeric matrix, Cellulose (2014) (submitted).

[3.7] SHARMIN, N., KHAN, R., SALMIERI, S., DUSSAULT, D., BOUCHARD, J., LACROIX, M. Modification and characterization of biodegradable methylcellulose films with trimethylolpropane trimethacrylate (TMPTMA) by γ-radiation: Effect of nanocrystalline cellulose, J. Agric. Food Chem. **60** (2012a) 623-629.

[3.8] SHARMIN, N., KHAN, R.A., SALMIERI, S., DUSSAULT, D., LACROIX, M. Effectiveness of Silane Monomer on Chitosan Films and PCL-Based films, J. Appl. Polym. Sc. **125** (2012b) 224-232.

[3.9] KHAN, R., A., DUSSAULT, D., SALMIERI, S., SAFRANY, A., LACROIX, M., Improvement of the mechanical and barrier properties of methylcellulose-based films by treatment with HEMA and silane monomers under gamma radiation, Rad. Phys. Chem. **81** (2012a) 927-931.

[3.10] KHAN, R. A., SALMIERI, S., DUSSAULT, D., CALDERON, J. U., KAMAL, M. R., SAFRANY, A.; LACROIX, M. Production and properties of nanocellulose-reinforced methylcellulose-based biodegradable films, J. Agric. Food Chem. **58** (2010) 7878-7885.

[3.11] KHAN, A., HUQ, T., KHAN, R.A., DUSSAULT, D., SALMIERI, S., LACROIX, M. Effect of γ-irradiation on the mechanical and barrier properties of HEMA grafted chitosan-based films, Rad. Phys. Chem. **81** (2012b) 941-44.

[3.12] SPIZZIRRI, U.G., IEMMA, F., PUOCI, F., CIRILLO, G., CURCIO, M., PARISI, O.I., PICCI, N. Synthesis of antioxidant polymers by grafting of gallic acid and catechin on gelatin, Biomacromolecules **10** (2009) 1923–1930.

[3.13] HAN, J., BRITTEN, M., ST-GELAIS, D., CHAMPAGNE, C.P., FUSTIER, P., SALMIERI, S., LACROIX, M. Effect of polyphenolic ingredients on physical characteristics of cheese, Food Res. Int. **44** (2011) 494–497.

[3.14] SALMIERI, S., ISLAM, F., HOSSAIN, F.M., HAYTHAM, I., WADOOD, Y. H. LACROIX, M. Preparation and characterization of bioactive poly(lactic acid)-nanocrystalline cellulose (PLA-NCC) supramolecular composite films: Application on ham, **21** (2014) 1837-1850.

[3.15] SALMIERI, S., ISLAM, F., KHAN, R.A., HOSSAIN, F., HAYTHAM, I., MIAO, C., WADOOD, Y.H., LACROIX, M. Antimicrobial nanocomposite films made of poly(lactic acid)-cellulose nanocrystals (PLA-CNC) in food applications – Part B: Effect of oregano essential oil release on the inactivation of *Listeria monocytogenes* in mixed vegetables, (2014) CELS-D-13-00484R2.

[3.16] GAO, B., HU, H., GUO, J.; LI, Y. Preparation of polymethacrylic acid-grafted HEMA/PVP microspheres and preliminary study on basic protein adsorption, Colloid Surface B. **77** (2010) 206-213.

[3.17] ZACCARON, C., OLIVEIRA, R., GUIOTOKU, M., PIRES, A.; SOLDI, V. Blends of hydroxypropyl methylcellulose and poly(1-vinylpyrrolidone-**co**-vinyl acetate): Miscibility and thermal stability, Polym. Degrad. Stabil. **90** (2005) 21-27.

Chapter 4

FABRICATION AND MODIFICATION OF SURFACES AND SCAFFOLDS FROM STARCH BASED POLYMERS FOR TISSUE ENGINEERING USING RADIATION TECHNOLOGY

H. ABD EL-REHIM, S. KORRAA, EL-SAYED HEGAZY
Radiation Research of Polymer Chemistry Department,
National Centre for Radiation Research and Technology (NCRRT),
Atomic Energy Authority,
Cairo,
Egypt

Abstract

Hydrogls from starch/based polymers shave been synthesized by means of gamma radiation- induced graft copolymerization and crosslinking process. The preparation conditions such as irradiation dose andcompositions of the hydrogel component werestudied to obtain reasonable swelling andgelation degree. The obtained hydrogels were characterized using Fourier Transform Infrared spectroscopy. In situ deposition of hydroxyapatite (HAp) inside the hydrogels was achieved via alternate soaking technique. The nano-composites HAp-starch/based polymers were characterized using energy dispersive X-ray spectroscopy, X-ray diffraction, scanning electron and atomic force microscopes. The compressive strength of the composites was also investigated to find out that the (HAp) deposition enhance the compressive strength of the prepared hydrogel. The bioactivity and blood compatibility evaluation of the obtained nano-composites revealed that these nanocomposites were bioactive and biocompatible. Also studies were made to screen the cytotoxicity and evaluate starch scaffolds andtheir blends prepared at different compositions after being sterilized by ionizing radiation. The effect of low level laser energy (LLLI) on enhancing the proliferation of HEPG-2 cells on such scaffolds was also examined. Cytotoxicity and cell adhesion properties were assessed using different techniques as Viability percentage, MTT assay, Lactate dehydrogenase, Apoptosis, D-Cell Phenotypic, Analysis percentage, RT-PCR for albumin, CYP-1 and GATA4 m RNA expression. It was found that the starch based blends exhibited acyto-compatibility that might allow for their use as biomaterials. However, further studies to decrease cytotoxicity are needed. Exposure to 2 J/cm^{2}He: Ne laser greatly enhanced cell proliferation on all of the scaffolds used.

4.1. INTRODUCTION

A commonly applied definition of tissue engineering, is "an interdisciplinary field that applies the principles of engineering and life sciences toward the development of biological substitutes that restore, maintain, or improve tissue function or a whole organ"[4.1]. Cells are often implanted or 'seeded' into an artificial structure capable of supporting three-dimensional tissue formation. These structures, typically called scaffolds, are often critical, both ex vivo as well as in vivo, to recapitulating the in vivo milieu and allowing cells to influence their own microenvironments. Scaffolds usually serve at least one of the following purposes: Allow cell attachment and migration, Deliver and retain cells and biochemical factors, Enable diffusion of vital cell nutrients and expressed products and exert certain mechanical and biological influences to modify the behaviour of the cell phase. To achieve the goal of tissue reconstruction, scaffolds must meet some specific requirements. A high porosity and an adequate pore size are necessary to facilitate cell seeding and diffusion throughout the whole structure of both cells and nutrients [4.2-4.4]. Biodegradability is often an essential factor since scaffolds should preferably be absorbed by the surrounding tissues without the necessity of a surgical removal. The rate at which degradation occurs has to coincide as much as possible with the rate of tissue formation: this means that while cells are fabricating their

own natural matrix structure around themselves, the scaffold is able to provide structural integrity within the body and eventually it will break down leaving the neotissue, newly formed tissue which will take over the mechanical load. Injectability is also important for clinical uses. Recent research on organ printing is showing how crucial a good control of the 3D environment is to ensure reproducibility of experiments and offer better results [4.5-4.7].

4.2. METHODOLOGY

4.2.1. Preparation of (starch/AAc) hydrogels

Starch/AAc hydrogels were obtained by radiation-induced copolymerization of mixtures of different compositions from their aqueous solutions using ^{60}Co γ-irradiation. The mixtures were exposed to different doses up to of 20 kGy. After copolymerization, the tube were broken, the formed polymeric cylinder were removed and cut into discs. The obtained hydrogel discs were washed extensively with distilled water to remove the unreacted component, then air dried at room temperature for further investigations.

4.2.2. Hydroxyapatite deposition on (starch/AAc) hydrogel

(Starch/AAc) hydrogel discs with different compositions were soaked in 50 mL of $CaCl_2$ at 37 ^oC for 24 h. After being removed from $CaCl_2$ solution and rinsed with distilled water, the hydrogels were soaked in 50 mL of Na_2HPO_4 at37 ^oC for 24 h. The hydrogels were removed from Na_2HPO_4 solution and rinsed with distilled water and dried. Repeating these steps (one deposition cycle) results in the deposition of HAp. The mentioned steps were repeated up to nine cycles.

4.3. RESULTS AND DISCUSSION

Studies with biodegradable polymer like starch based polymers have recently demonstrated that these materials have a wide range of properties which make them suitable for use in several biomedical applications ranging from bone plates to carrier drug delivery and tissue engineering scaffolds. In this connection starch based polymers have been synthesized by means of gamma -radiation- induced graft copolymerization and crosslinking process. Different shapes of such polymers were prepared to be used as scaffold surfaces for growing HepG-2 cell line and to form nano-composite scaffolds with hydroxyapatite for bone tissue regeneration.

The effect of irradiation dose on the gel content and swelling behaviour of produced starch based polymers was investigated. It was observed that as the irradiation doses increased the gel content increases to reach its maximum. Thereafter it became decreases again.

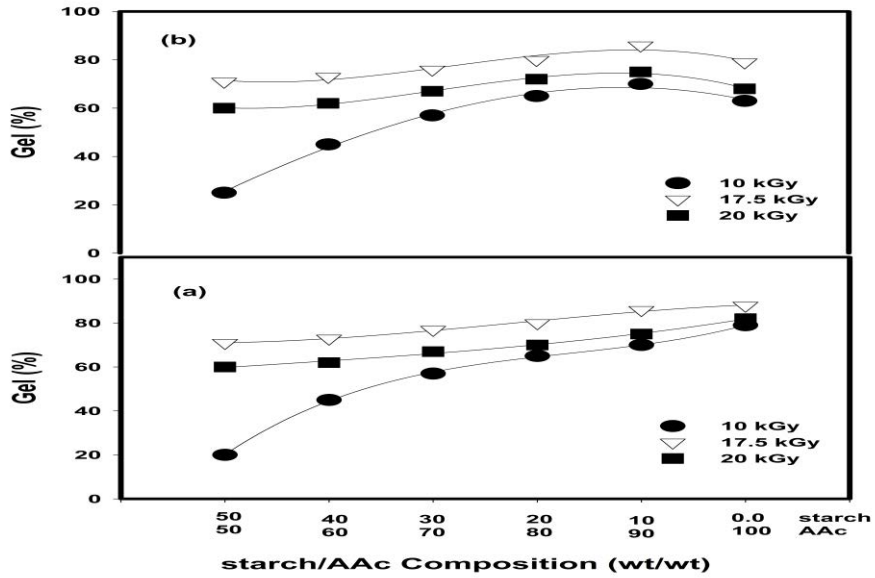

FIG. 4.1. Effect of starch/AAc compositions prepared at different irradiation doses on the gel (%); (a) starch/ AAc and (b) neutralized starch/AAc hydrogels.

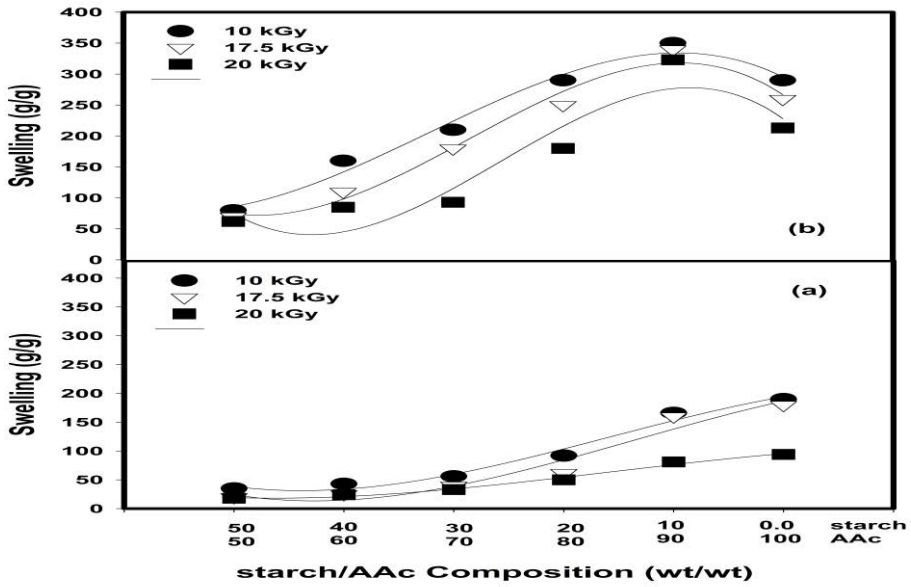

FIG. 4.2. Effect of starch/AAc compositions prepared at different irradiation doses on the gel (%); (a) starch/ AAc and (b) neutralized starch/ AAc hydrogels.

The swelling of starch/AAc and neutralized starch/AAc hydrogels of different compositions in distilled water and in saline solutions was investigated. It is clear that the swelling

increases with increasing AAc content for starch/AAc. Moreover, it was found that as the irradiation dose increases the swelling decreases.

4.3.1. Preparation of starch polymer hyroxyl appatite composite

The polymer – hydroxyapatite (HAp) composite is expected to be useful not only as bone substitute materials and soft tissue adhesive materials. Bone-like apatite could be formed in the desired amount on/in the three-dimensional hydrogel network structure at normal temperature and pressure in vitro using alternatesoaking process. Using this process, hydroxyapatite (HAp) formation can be controlled by changing reaction cycles and the apatite formation not only will be on the surface of the hydrogel but also inside it. The rate of the hydroxyapatite (HAp) formation on/in the hydrogel is affected by the increase in the swelling ratio.

4.3.2. Compressive strengths

The measurements of compression strength values of the prepared composites are very important. Table 4.1. shows the compressive strength of HAp-(starch/AAc) (1:1%) composites after one, three, and seven cycles of alternate soaking compared with that of pure hydrogel. It is noticed that the compressive strength of composites increased initially after the first cycle, and then it decreased with increasing the number of deposition cycles. HAp nanoparticles behave as load carriers leading to good mechanical properties if they are present in small amounts and distributed homogeneously in the hydrogel matrix. If the proportion of the hydroxyapatite (HAp) particles increases, this could lead to nonhomogeneous distribution and, therefore, aggregation of particles may occur. This may cause phase segregation and no homogeneity in the structure and poor adhesion to the matrix leading to a decrease in the compressive strength. The observed compressive behaviour can be explained by the degree of adhesion between the HAp particles and the hydrogel matrix.

TABLE 4.1. THE COMPRESSIVE STRENGTH (MPA) OF NHAP-(STARCH/AAC) (1:1WT%) COMPOSITES AFTER ONE, THREE, FOUR, AND EIGHT CYCLES OF ALTERNATE SOAKING PROCESS COMPARED WITH BLANK HYDROGEL

No. of deposition cycles	Compressive strength (MPa)
0	13
1	31
3	27
7	20

4.3.3. Scanning electron microscopy

Porosity is one of the most important factors affecting the morphological properties of scaffold in bone regeneration process. Higher porosity favours tissue in-growth, bone formation, and forming biological fixation with surrounding tissue. Bone in-growth requires high levels of interconnected porosity. Scanning electron microscopy (SEM) images shown in Figure 4.3. illustrates the topographical properties of starch/NVP copolymer hydrogel of different compositions and its HAp composites afteralternate soaking in $Cacl_2$ and Na_2HPO_4 solution solutions at different deposition cycles.

From Figure 4.3. a) it is observed that (starch/NVP) hydrogels have interconnected irregular porous structure. It is clear that the HAp was deposited on all the possible surfaces of the hydrogel whereas the hydrogel almost kept its surface structure. Also, it can be seen that, the HAp deposited layers increased by increasing NVP content on the prepared hydrogels. On further deposition, the deposited HAp particles grow both in number and in size and the hydrogel surface was completely covered with like HAp as shown in Figure 4.3 c) [4.8].

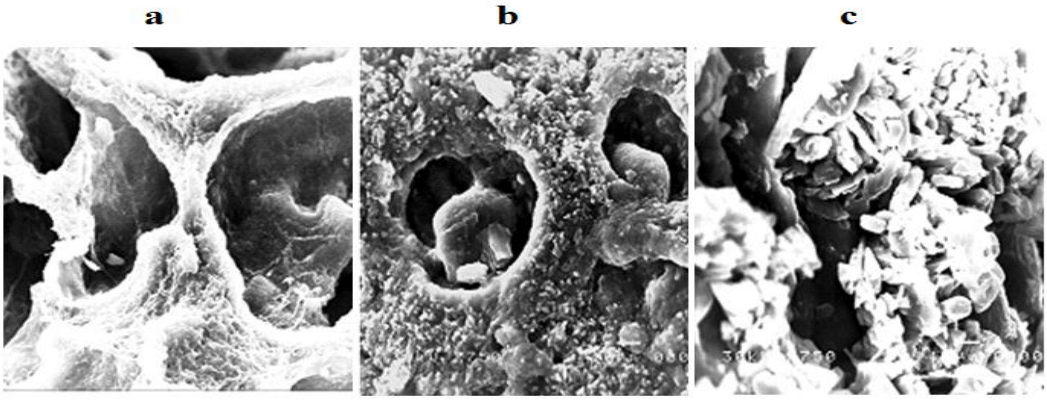

FIG. 4.3. SEM images of starch/NVP hydrogels of different NVP content; (a) starch/NVP, (b) starch/ NVP after single deposition cycle (C) starch/NVP after five deposition.

4.3.4. Biocompatibility

Biocompatibility of starch/ based polymers hydrogel and its composites after different cycles of alternate soaking process was investigated. The obtained results revealed that, hydroxyapatite starch/ based polymers possess the highest biocompatibility if compared with starch/ based polymers hydrogel. The biocompatibility of HAp-(starch/polymers) composites increases by increasing the deposition cycles. The obtained results may be attributed to the improved bio compatible quality of the composites.

4.3.5. Allowance of hepg-2 cell line to grow on the starch based polymer scaffold

The aim of this study was to screen the cytotoxicity and evaluate starch and different starch-based polymer composites after being sterilized by ionizing radiation. Also, the effect of low level laser energy (LLLI) on enhancing the proliferation of HEPG-2 cells on such scaffolds was examined. Cytotoxicity and cell adhesion properties were assessed using different techniques as Viability percentage MTT assay, Lactate dehydrogenase, Apoptosis, D-Cell Phenotypic, Analysis percentage, RT-PCR for albumin, CYP-1 and GATA4 m RNA expression.

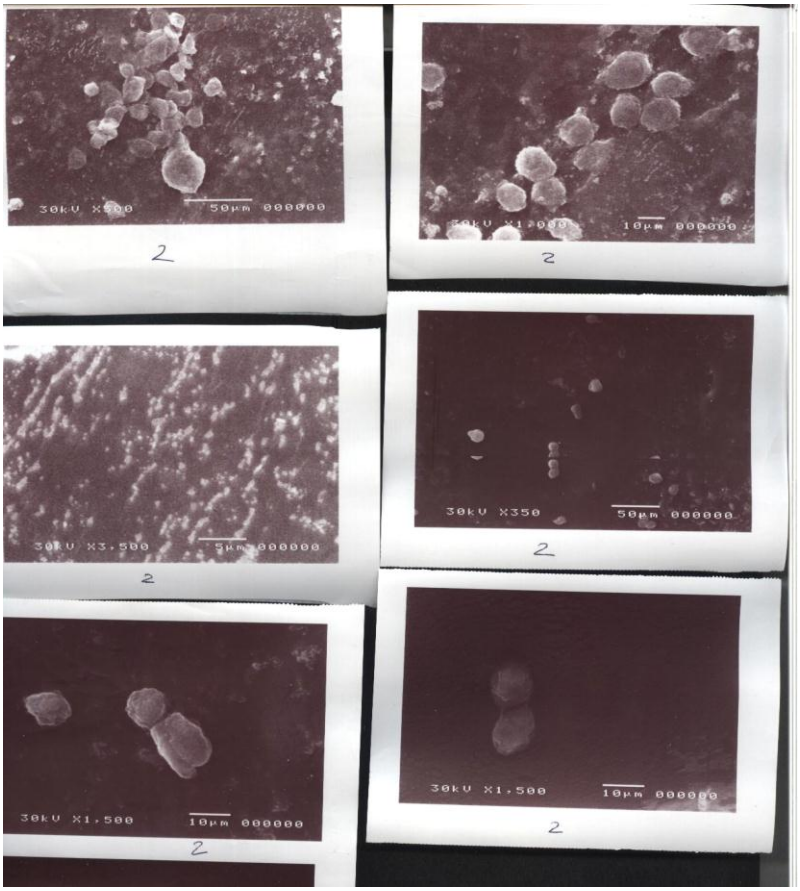

FIG. 4.4. Scanning electron microscope showed the spread of cells on the starch based polymers.

Scanning electron microscope showed the cells were much spread on the starch based polymers and a high number of cells was found to adhere to starch based cellulose acetate composites (Figure 4.4).

The cell morphology of endothelial cell line was also analyzed after direct contact with polymers for 48 hours' time periods and the number of cells adhered to the surfaces of the polymers was determined by quantification of cytosolic lactate dehydrogenase activity. Lactate Dehydrogenase (LDH) release from HEPG-2 cells grown on different polymer composites with and without 2 J/cm^{2}He: Ne laser irradiation was determined and shown in Figure 4.5. It is clear that the release of Lactate Dehydrogenasefrom the cells growth on starch scaffolds is much lower if compared with that for cells growth on starch based polymer composites.

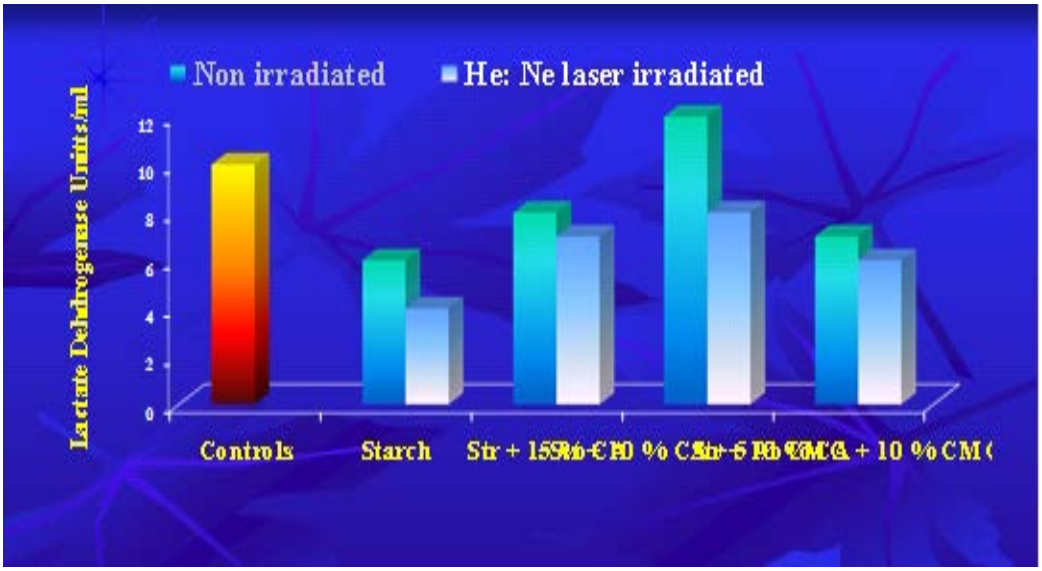

FIG. 4.5. Lactate dehydrogenase (LDH) release from HEPG-2 cells grown on different composites with and without 2 J/cm^{2}He:Ne laser irradiation.

Viability percentage of HEPG-2 cells grown on different composites with and without 2 J/cm2 He:Ne laser Irradiation was investigated as shown in Figure 4.6. Viability testing was carried out using the trypan blue dye exclusion assay. Interference with cell types other than lymphocytes was not suspected, based on the fact that monocytes and grannulocytes adhere to tissue culture walls, while lymphocytes remain suspended in the nutrient media. Viability was estimated at 0, 24, 48, 72 and 96 hours.

It was found that percentage of HEPG-2 cells that allowed to growth on the surface of starch based polymers scaffolds containing CMC is much higher than that of native starch. Also it is clear that the treatment with 2 J/cm^2 He:Ne laser irradiation enhanced the viability of cell.

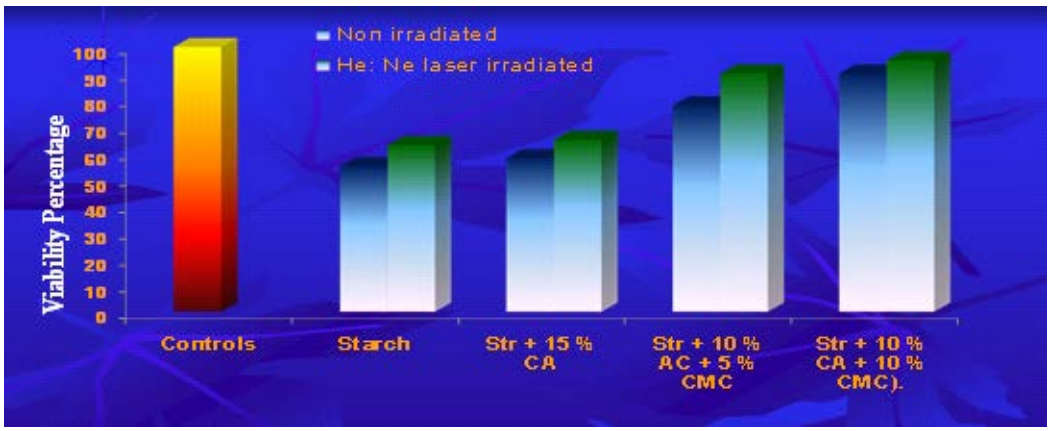

FIG. 4.6. Viability percentage of HEPG-2 cells grown on different composites with and without 2 J/cm^{2}He:Ne laser irradiation.

The MTT assay was performed with the extracts of the materials in order to evaluate the short term effect of degradation products. Figure 4.7. shows absorbance of Micro-culture Tetrazolium Test (MTT assay) from HEPG-2 cells grown on different composites with and without 2 J/cm^{2}He:Ne laser Irradiation. The MTT assay is a colorimetric assay for assessing cell viability. NAD(P)H-dependent cellular oxido-reductase enzymes may, under defined conditions, reflect the number of viable cells present. These enzymes are capable of reducing

the tetrazolium dye MTT 3-(4,5-dimethylthiazol-2-yl)-2,5-diphenyltetrazolium bromide to its insoluble formazan, which has a purple colour.

It is clear from the figure that the surface of starch based polymers scaffolds containing CMC is allowed to growth the cells more better than that of native starch, Also it is clear that the treatment with 2 J/cm^2 He:Ne laser irradiation enhanced the viability of cell .

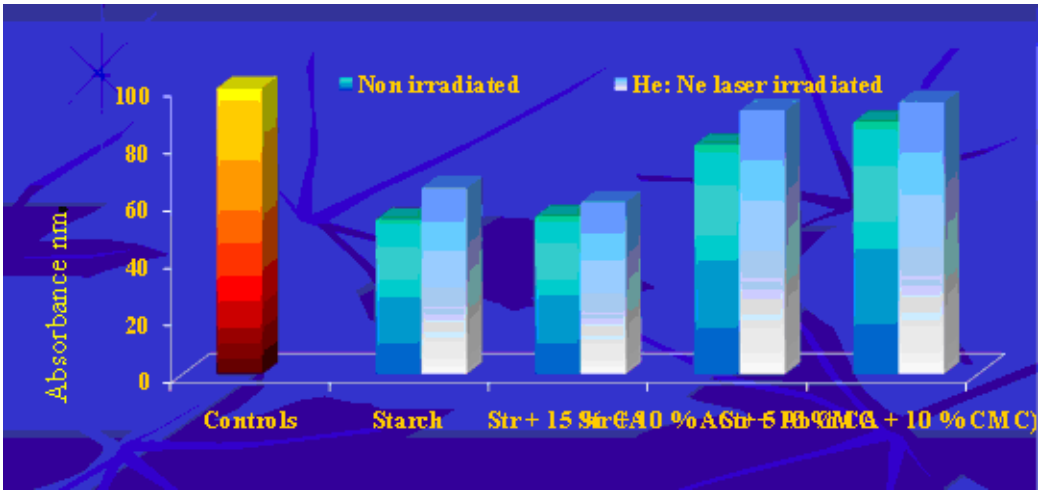

FIG. 4.7. Absorbance of micro-culture tetrazolium test (MTT assay) from HEPG-2 cells grown on different composites with and without 2 J/cm^2 He:Ne laser irradiation.

4.4. CONCLUSIONS

Alternate soaking technique was used to develop a biocompatible bone-like HAp layers within the (starch/polymer) hydrogels. The amount of the deposited HAp within the hydrogels could be increased by increasing the deposition cycles. The prepared composites met the mechanical requirements of these types of materials. In vitro biocompatibility evaluation revealed that, hydroxyl apatite starch/ based polymers composites possess high biocompatibility. However, further studies to decrease cytotoxicity are needed. Exposure to 2 J/cm^{2}He:Ne laser greatly enhanced cell proliferation on all of the scaffolds used.

REFERENCES TO CHAPTER 4

[4.1] LANGER R., VACANTI J.P., Tissue engineering, Science **260** (1993) 920.

[4.2] PATEL H., BONDE M., SRINIVASAN G., Biodegradable Polymer Scaffold for Tissue Engineering, Trends Biomater. Artif. Organs **25** (2011) 20.

[4.3] DHANDAYUTHAPANI B., YOSHIDA Y., MAEKAWA T., KUMAR D.S., Polymeric Scaffolds in Tissue Engineering Application: A Review, Int. J. Polym. Sci. **11** (2011) 19.

[4.4] SMITH I.O., LIU X.H., SMITH L.A., 55MA P.X., Nanostructured polymer scaffolds for tissue engineering and regenerative medicine, Wiley Interdiscip Rev Nanomed Nanobiotechnol. **1** (2009) 226.

[4.5] SELVI G.P., SKYLAB R.S., Identifying and designing a suitable material for scaffold preparation in tissue engineering applications, Int. J. Chem. Tech. Res., **6** (2014) 1890.

[4.6] MALAFAYA P.B., SILVA G.A., REIS R.L., Natural–origin polymers as carriers and scaffolds for biomolecules and cell delivery in tissue engineering applications, Adv. Drug Delivery Rev. **59** (2007) 207.
[4.7] SHOICHET M.S., Polymer Scaffolds for Biomaterials Applications, Macromolecules **43** (2010) 581.
[4.8] RAAFAT A.I., SAAD ELDIN A.A., SALAMA A.A., ALI N.S., Characterization and Bioactivity Evaluation of (Starch/N-vinylpyrrolidone)—Hydroxyapatite Nanocomposite Hydrogels for Bone Tissue Regeneration, J. Appl. Polym. Sci. **128** (2013) 1697.

Chapter 5

RADIATION-CURING OF COMPOSITES: A FOCUS ON THE INTERACTIONS OF CARBON-FIBRES AND OF CELLULOSE NANOCRYSTALS WITH ACRYLATE-BASED MATRICES

PH. PONSAUD, A. MARTIN, C. KOWANDY, M. KRZEMINSKI, P. KOZIK-OSTROWKA, K. FURTAK, K. JADWISZCZAK, G. TATARU, X. COQUERET
Institut de Chimie Moléculaire de Reims,
CNRS UMR 7312,
Université de Reims Champagne Ardenne, Reims
France

D. OŻGA, M. BARCZAK,
Department of Theoretical Chemistry,
Maria Curie Sklodowska University, Lublin
Poland

Ph. PONSAUD, A. MARTIN, M. KRZEMINSKI, B. DEFOORT,
Astrium Space Transportation,
Saint Médard en Jalles
France

J.-E. MAIGRET, V. AGUIÉ-BÉGHIN
Fractionnement des Agroressources et Environnement,
UMR INRA 614, Reims
France

Abstract

The chemical and physico-chemical interactions between the radiation-curable matrix and the reinforcing fibres or fillers are of outmost importance for obtaining beneficial effects in composites with demanding mechanical properties. Our research has been focused on two types of composites based on radiation-curable acrylate-based matrices, one including high modulus carbon fibres, the second one containing cellulose nanocrystals.

- (i) The influence of surface functions present at the surface of carbon fibres was investigated. The inhibiting effect of aromatic hydroxylic and amino groups as well as the sensitizing effect of thiol groups were evaluated by comparing the dose dependence of butyl acrylate samples submitted to EB irradiation in the presence of various additives. We have proposed and evaluated sulfur-based surface modifications and/or sizing application to carbon fibers for inducing the formation of cohesive interfaces. Significant improvements of the transverse strength of unidirectional composites were achieved by implementing this approach.
- (ii) Cellulose nanocrystals prepared from ramie (CNC) were introduced in a radiation-curable polyurethane acrylate emulsion. The influence of the amount of introduced CNC (1 to 10 wt%) on the reactivity under UV or EB-radiation as well as the thermomechanical and tensile properties of the resulting materials was studied. FT-MIR and NIR spectroscopies were used to control the degree of monomers conversion of series of samples. Significant enhancement of the Young's modulus and of the strength at break was observed with 1 wt% of CNC. The profile of the reaction kinetics measured during UV-initiated polymerization was not significantly altered by the presence the nanocrystals in the coalesced material.

Besides this research that was conducted with students, scientists and institutions from Poland, several interactions and other joint projects have been conducted on a cooperative basis, particularly:

— with USA, on new functional copolymers for designing magnetic nanocomposites;
— with Vietnam, on the synthesis of gold nanoparticles by radiation-induced reduction of Au(III) salts in the presence of chitosan, with one PhD defended.

The development of new interactions is in progress with Malaysia (1 PhD application for the grafting of cellulose nanocrystals) and Serbia (characterization of composites including metallic nanoparticles).

5.1. INTRODUCTION

Cross-linking polymerization initiated with UV-visible light or with high energy radiation is a very attractive technology for the fabrication of composite materials with various levels of chemical performance. The method offers many advantages compared to conventional energy- and time-consuming thermal curing processes [5.1]. Free radical and cationic polyaddition chemistries have been investigated in some details by various research groups along the last years. A high degree of control over curing kinetics and material properties can be exerted by adjusting the composition of matrix precursors as well as by acting on process parameters [5.2].

The chemical and physico-chemical interactions between the radiation-curable matrix and the reinforcing fibres or fillers are of outmost importance for obtaining beneficial effects in composites with demanding mechanical properties. Our research has been focused on two types of composites based on radiation-curable acrylate-based matrices, one including high modulus carbon fibres, the second one containing cellulose nanocrystals [5.3].

5.2. RADIATION-CURED CARBON FIBRE REINFORCED COMPOSITES

Radiation-cured composite materials including medium to high modulus carbon fibres generally exhibit lower properties and higher brittleness than that of state-of-the-art thermally cured composites. We have investigated several points related to these issues, and particularly the reduction of the matrix shrinkage on curing, the wettability of carbon fibres, the design of fibre-matrix interface and the use of thermoplastic toughening agents [5.4]. A drastic enhancement of the KIC value exceeding 2 MPa.m1/2 was also obtained for acrylate-based matrices toughened with high glass transition temperature Tg thermoplastics [5.5]. Improving fibre-matrix adhesion and upgrading polymer network toughness are thus two major challenges in this area of performance composites. Particular attention was paid on the functional groups present at the surface of carbon fibres.

5.2.1. Experimental

The aromatic epoxy acrylate resin (Ebecryl 600) was supplied by Cytec. Butyl acrylate (BuA, Aldrich) was purified and rendered free from phenolic stabilizers by elution over a porous organic resin with basic properties. The samples were polymerized by EB-irradiation with an industrial 10 MeV accelerator (CIRCE II, 20 kW). Various types of sized, unsized and acid-oxidized carbon fibres (intermediate modulus grade) were used for preparing unidirectional composites for mechanical testing. The same carbon fibres were analyzed by XPS (R 4000, VG Scienta).

Polymerization was monitored by infrared spectroscopy for multifunctional aromatic monomers (Bruker Alpha FTIR spectrometer in transmission mode) or by size exclusion chromatography chain PL-GPC50 with autosampler PL-ASRT (Polymer Laboratories)

including a set of three PLgel columns 5 μm (2 mixed type-C and 1 type-100) with tetrahydrofuran as the eluent (1 mL.min-1) and with differential refractive index detector. Dynamic mechanical analysis was done on a DMA Rheometrics Analyzer RSA II (operating frequency 1 Hz, heating rate +5°C.min-1). The transverse flexural properties were characterized by 3 point bending tests using an Instron 4400R mechanical testing machine.

5.2.2. Results and discussion

The free radicals generated by a cascade of reactions following the primary ionization processes affecting the matrix precursors initiate quite efficiently the crosslinking polymerization. Typical formulations are based on aromatic diacrylates that enable the formation high Tg networks when monomer conversion is driven to a sufficiently high level (Scheme 5.1.).

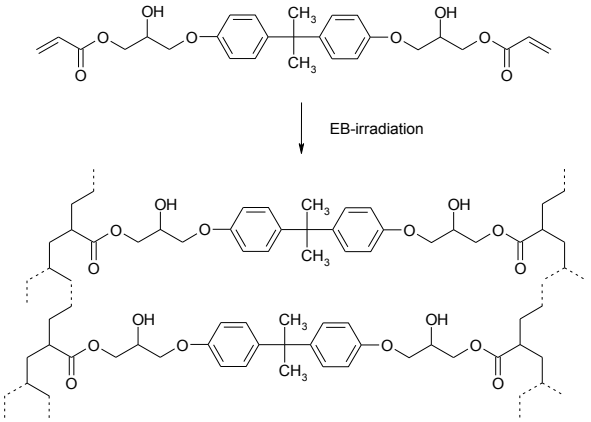

Scheme 5.1. EB-induced formation of high Tg networks by free radical polymerization of epoxydiacrylate prepolymers.

The parameters controlling the progress of the polymerization in the pure matrix have been studied in some details. The spatial distribution of the absorbed dose, the instant dose rate and the fractionation of the dose are influent parameters that need being controlled to ensure the build-up of the network. The temperature profile during irradiation is a key issue since mobility restrictions can early affect the progress of reaction in the material undergoing gradual vitrification [5.6].

The intrinsic properties of a matrix improved by appropriate toughening agents need being relayed by excellent fiber - matrix adhesion for inducing appreciable benefits in terms of transverse properties of a composite structure. The adhesion between carbon fibers and the matrix is generally rather weak in EB-cured composites based on acrylate or on epoxy resins, independently of the type of chemistry and on the presence of commercial sizings may be more compatible with epoxy resins.

A representative SEM picture of fracture profile of an EB-cured (50 kGy) unidirectional carbon-fibre reinforced aromatic epoxy-acrylate composite reveals the presence of regular cylindrical channels from which nude fibers can be extracted with limited mechanical strain, hence producing adhesive failure at the interfaces and brittle failure in the matrix (Fig. 5.1).

Various approaches have been tested during the recent years, including reduction of volume contraction upon curing and surface treatment of fibers.

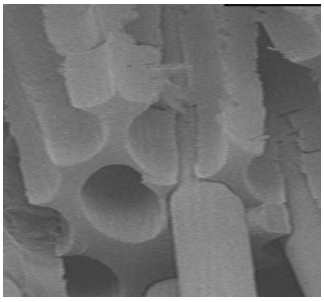

FIG. 5.1. SEM micrograph showing a fractured EB-cured carbon fibre compositewith poorly interacting aromatic diacrylate matrix.

The volume shrinkage associated with polymerization is possibly affecting negatively adhesion between carbon fibres and matrix. EB-curable acrylate formulations have higher cure-induced shrinkage (in the range of 3 to 7% for high performances formulations) compared to thermally cured epoxy amine systems used for similar applications (commonly around 2 to 3 %). The introduction of thermoplastic additives as poly(vinyl acetate) soluble in the prepolymers was tested. This approach allowed to propose formulation with a decrease of the cure-induced shrinkage from 6 to ca 4.5 % of the initial volume. Such an improvement without significant decrease of network's Tg opens an interesting path for upgrading transverse properties, but the first attempts failed to give significant improvements of the fracture properties of standard EB-cured composites [5.7].

Wetting issues have also been considered. The static contact angle of a droplet of resin coated on a glassy carbon plate exhibiting a surface atomic composition similar to the carbon fibres considered for the application was typically θ =20°. The spreading of the prepolymer formulation surface composition was shown to be reduced to some extent by formulating with various types of silicone or fluorinated surfactants (θ < 5°). Though carbon fibre impregnation was somewhat easier when using such resins, the mechanical properties of the resulting EB-cured composites were not significantly enhanced.

The chemistry occurring at the carbon fibre matrix interface during irradiation was also considered. The surface composition of the carbon fibres was analyzed by X-ray photoelectron spectroscopy (XPS). A typical analysis of an unsized commercial fibre allows to determine the atomic composition of the surface and to orient the investigation towards particular functional groups suspected to be present on the basis of the high resolution analysis of the binding energies (Fig. 5.2).

In a representative experiment, we have measured the relative amounts of C, O and N atoms, 83, 15 and 2 % respectively, together with a decomposition into resolved contributions that can be assigned to various aromatic and hetero-atomic functions.

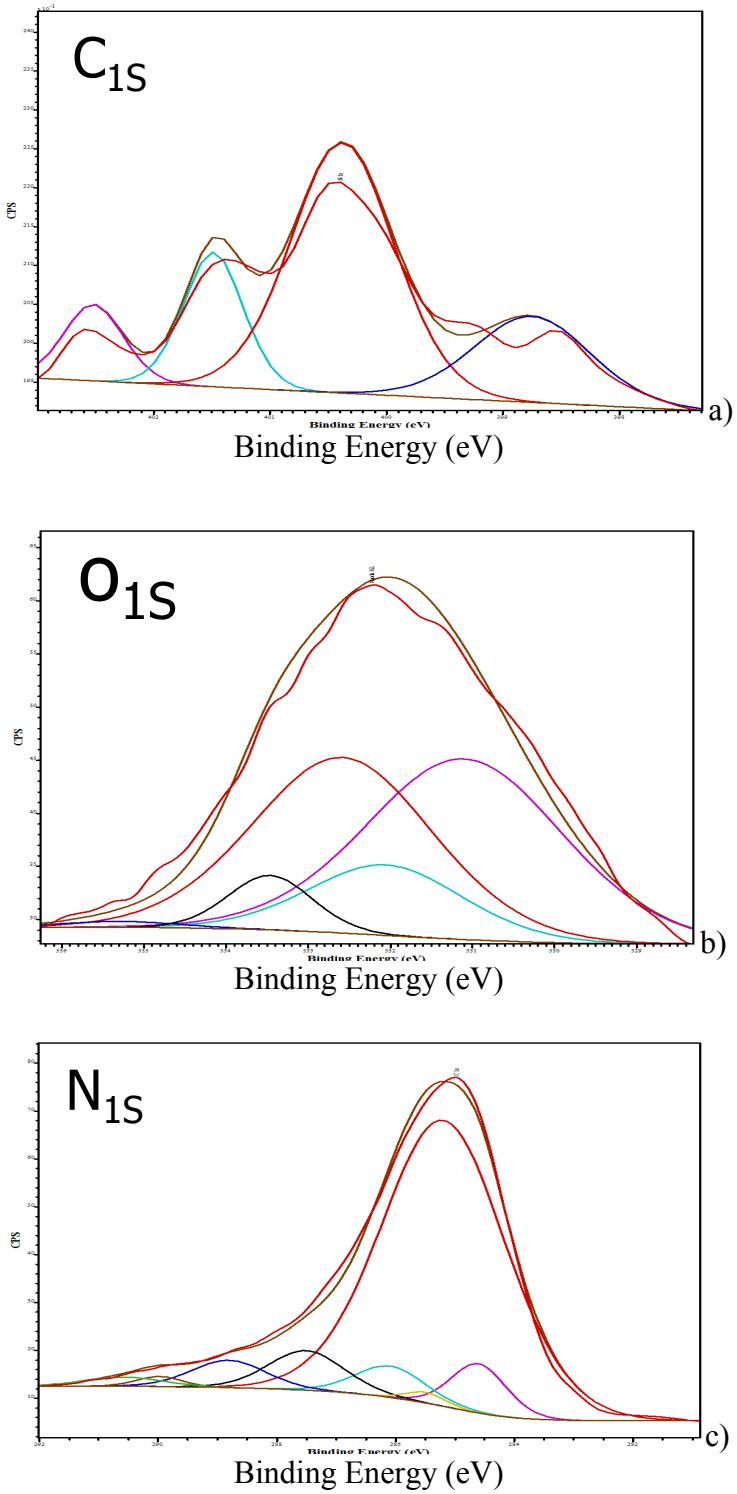

FIG. 5.2. High resolution decomposition of selected domains (C1s, O1s, N1s) of the XPS spectrum of a representative unsized carbon fibre.

Analysis of the data on the basis of current literature allowed to conclude, besides the base graphite aromatics, to the likely presence of the following functional units: phenols, ethers, ketones, carboxylates, amines, amides, imines, nitriles, nitro [5.8].

In order to examine the influence on free radical processes of the presence of these various functional groups at the surface of the carbon fibres, the efficiency of the polymerization of model acrylate monomers under electron beam was assessed and quantified by spectroscopic (FTIR and 1H NMR) as well as by size exclusion chromatography.

A series of aromatic compounds (Scheme 5.2) bearing the reactive functions possibly present at the carbon fibre surface was thus introduced at various concentrations in the purified acrylate (e.g. n-butyl acrylate).

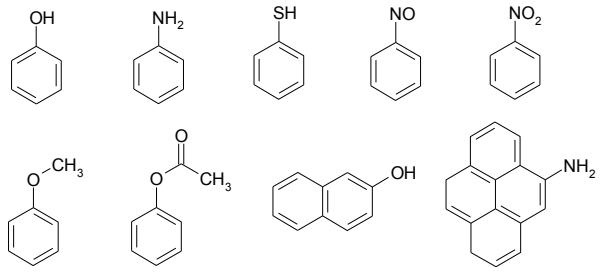

Scheme 5.2. Selected examples of model molecules added to n-butyl acrylate for evaluating the possible inhibiting effects on free radical processes.

Not surprisingly, the results clearly demonstrate the strong inhibiting behavior of the phenolic and amino-aromatic functions [5.9]. A representative example is illustrated by the plots of Fig. 5.2. showing revealing the inhibiting effect of 9-phenanthrol.

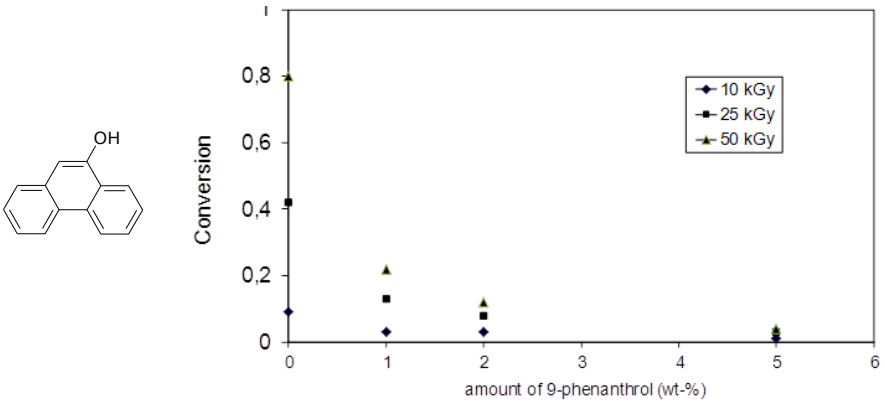

FIG. 5.3. Plots of n-butyl acrylate conversion (SEC quantification) as a function of EB-irradiation dose, revealing the inhibiting effect of 9-phenanthrol at various concentrations.

The absence of adhesion shown by the micrograph of Fig. 5.1. can therefore be explained by the inhibiting effect of such functional groups detected by XPS analysis of the typical commercially available carbon fibres. The complete inhibition or even the retardation of the free radical polymerization could then lead to poorly cohesive interfaces as consequence of the volume contraction in the bulk matrix. The sketch of Scheme 5.3 illustrates the current interpretation of the phenomenon.

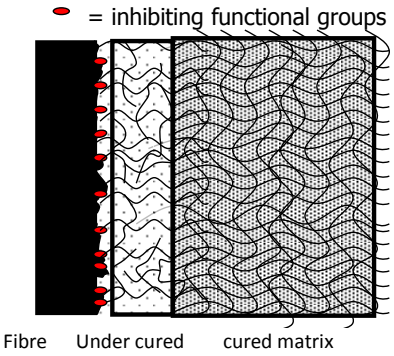

Scheme 5.3. Schematic representation of the influence of inhibiting functional groupsat the carbon fibre surface.

In an attempt to overcome this inhibiting effect, we have used the same experimental approach for selecting functional organic additives possibly acting as sensitizers, by amplifying in a positive manner the formation of active free radicals upon irradiation. Various potentially sensitizing agents were tested among which thiols were found to be good candidates for counteracting the inhibiting effects in the vicinity of the carbon fibres. In addition, the thiol groups are known to undergo transfer reactions that can be exploited for coupling the network under formation to the fiber or to some reactive sizing located around the fibres [5.7].

In one of its variants, the technological process inspired by the approach on model systems involves the treatment of the carbon fibers with thiomalic acid and an epoxy type sizing that yields a reactive coating particularly adapted to matrices curable by EB-initiated free radical mechanism, as depicted in Scheme 5.4 [5.10].

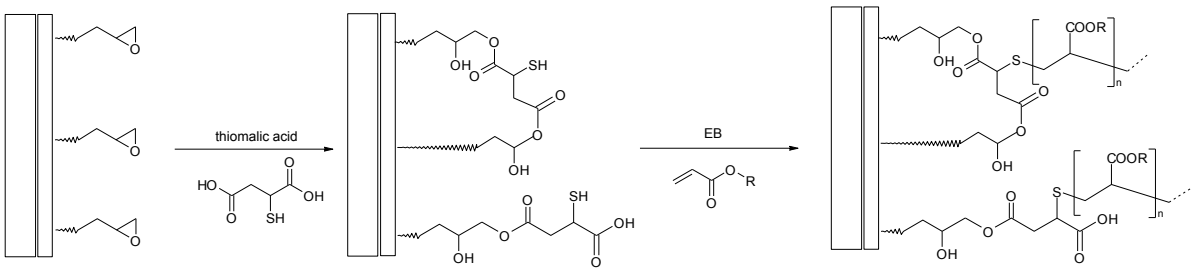

Scheme 5.4. Sketch representing the chemical modification of epoxy functions at the carbon fibre surface by reaction with thiomalic acid.

Significant improvements were achieved on the transverse stress at break, as measured via a three point flexural test, by applying original surface treatments on the fibres so as to induce chemical coupling with the matrix (Scheme 5.5).

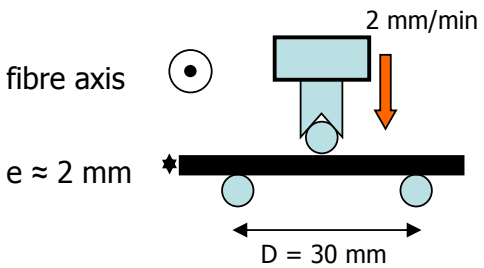

Scheme 5.5. Measurement of the transverse properties of carbon fibre-reinforced composites revealing the degree of interfacial cohesion with the EB-cured aromatic acrylate matrix.

Covalent bonds between carbon fibers sizing and matrix are indeed created with a high efficiency, as a result of chain transfer reactions between grafted thiol groups and growing polymer network. Transverse properties are drastically enhanced and exhibit values over 70 MPa, whereas the same test applied to samples without coupling agents break when submitted to a strain of 29 MPa.

The effect of the presence of thiol functions was further demonstrated by EB-curable adhesives interacting with thiomalic acid treated epoxy materials prepared in the form of blocks and assembled by a radiation cured aromatic acrylate adhesive. The obtained results illustrate the remarkable efficiency of covalent coupling induced by this type of chemistry (Figure 5.3). In the absence of treatment based thiol-containing carboxylic acid, adhesive breaking is observed at low strain (σ = 4.5 MPa), whereas between the epoxy blocks and the EB-cured acrylate adhesive layer, whereas using the thiol-containing coupling agent produces a cohesive break in the acrylate joint at a much higher strain (σ = 9.5 MPa) [5.11].

FIG. 5.4. Optical micrographs showing the fracture surface between two epoxy blocks: a, top) adhesive breaking observed in the absence of a treatment with thiomalic acid; b, bottom) with thiomalic treatment, highly resistant EB-cured joint with cohesive fracture in the underlying epoxy material.

5.3. RADIATION-CURED COMPOSITES INCLUDING CELLULOSE NANOCRYSTALS

The lignocellulosic feedstock offers a vast and renewable source of chemicals and materials with new potentialities to be explored. In particular, cellulose nanocrystals (CNC) obtained by controlled hydrolysis of natural fibres exhibit various structural and mechanical properties that have been recently exploited for obtaining nanocomposites by blending CNC with various thermoplastic materials [5.12-5.14]. A recent article reports on the use of such chemically modified nanofillers in UV-cured formulations used for wood coating [5.15].

We have focused our study on pristine CNCs obtained from ramie as a bio-based reinforcing nanofillers for improving the thermal and mechanical properties of radiation-cured materials. CNC are generally produced and purified as rather diluted aqueous suspensions in which they can be stored in the form of isolated particles. A polyurethane acrylate emulsion also available as a stable aqueous suspension was selected as the matrix precursor. This approach allows for the use of water as a common phase for mixing and casting the curable formulations in molds. Films or bars of thickness as high as 1 or 2 mm can be easily obtained by this method.

Two types radiation commonly used for the processing of paints, coatings, inks and adhesives were used [5.16], (i) high intensity UV-vis LEDs emitting at 395 nm and (ii) low energy EB. A photoinitiator was introduced in the formulations prepared for UV-vis curing. We have used FTIR in the medium and near visible range (NIR) for controlling the conversion of

monomer and adjusting the degree of cure of the samples to be compared at a uniform level. Calorimetric analysis as well as thermo-mechanic and tensile strength measutrements were performed on the obtained series of cured materials.

5.3.1. Experimental

Cellulose nanocrystals were prepared from ramie fibers using the protocol described in previous paper [5.17]. After washing with water until neutrality and dialysis with 6000 cut-off, the aqueous colloidal suspension has a CNC content of 3.6 wt%. It was stored at 4 °C and was sonicated with a Sonics vibra-cell (750W, Fisher-Bioblock) for a few minutes before use. The UV- curing polyurethane dispersion Bayhydrol UV 2282 (39 wt% of dry matter) was obtained from Bayer. The desired amount of CNC suspension was added and submitted to vigorous stirring for 4 hrs. The photoinitiator (Darocur 1173, 1 wt% with respect to the dry content of the polyurethane dispersion) was added to the formulations to be cured under UV-visible light. The uncured films were obtained by evaporation and coalescence of the formulations cast in silicone molds (2 mm thickness). The samples were dried at room temperature during two days, then during next two days on the heating plate at 25°C. The films, obtained as transparent self-standing materials, were irradiated with a 10 MeV Linac accelerator (dose 25 kGy and 2 x 25 kGy, dose rate 15 $kGy.s^{-1}$) or by UV-vis LED (Phoseon Firepower 395 nm, 8 $W.cm^{-2}$).

The samples with appropriate dimensions (width of 5 mm and length of 25mm) were cut from previously prepared films. Dynamic Mechanical Analysis (DMA) was carried out by using a DMA Q800 equipment (TA Instruments) working in the tensile mode. The measurements were performed at a constant frequency of 1 Hz, strain amplitude of 0,05%, in the temperature range from –80°C to 200°C and at a heating rate of 5°C.min-1.

Mechanical microtest with horizontal stretching was carried out with an equipment from the Deben Company. Samples with a length of 25-30 mm and a width of about 5 mm was cut with a scalpel from previously prepared and irradiated films. The elongation speed was 0.4 mm.min-1 on a total displacement of 20 mm.

5.3.2. Results and discussion

We have explored the influence of the presence of CNC over a composition domain ranging from 1 to 10 wt% with respect to the dry polyurethane matrix. Owing to the low content of CNC in the stock suspension, the blended formulations include large amounts of water. Water evaporation has to be achieved carefully for obtaining defect-free materials, without bubbles and of regular thickness. Various drying conditions and various types of molds (aluminium, steel, PTFE, silicone rubber) were tested. In a typical procedure, the blended suspension was cast in a silicone mold and allowed to dry for 2 days at 20°C and then 2 days at 35°C. The weight loss was monitored for controlling extensive elimination of water at the end of the coalescence process. A final thermal treatment at 50°C was applied for achieving the formation of a uniform and transparent material. The conversion level of the samples submitted to EB or to UV-visible irradiation needs being well controlled for allowing a meaningful comparison of the physical and mechanical properties.

Spectroscopic monitoring was performed by MIR spectroscopy for thin films (10-50 μm thickness) and NIR for thicker samples (thickness up to 1 mm). The presence of CNC has

little influence on the reactivity of the blend. Representative temporal profiles of the polymerization kinetics upon 395 nm irradiation are shown on Fig. 5.5.

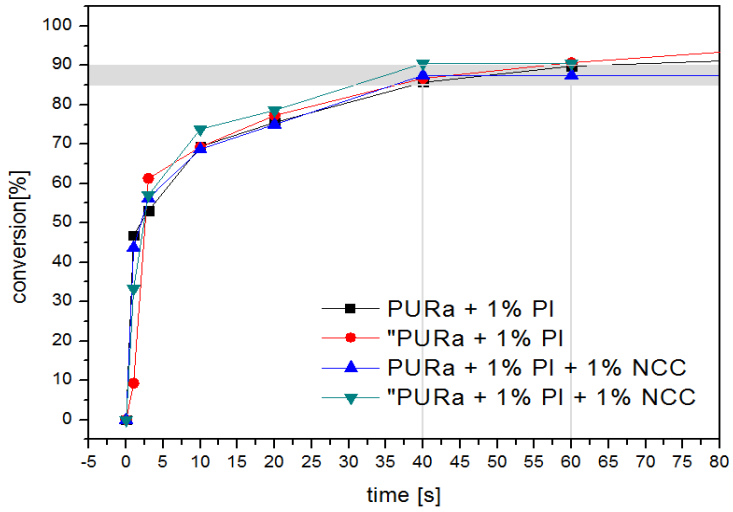

FIG. 5.5. Influence of the presence of 1 wt% CNC on the conversion profiles of PUR acrylate films submitted to 395 nm irradiation.

The target value of acrylate conversion was defined between 85 and 90%, corresponding to the application of EB doses of 25 and 2 x 25 kGy, respectively (Table 5.1)

TABLE 5.1. CONVERSION OF PUR ACRYLATE SAMPLES CONTAINING VARIOUS AMOUNTS OF CNC SUBMITTED TO EB DOSES OF 25 AND 50 KGY, AS DETERMINED BY NIR SPECTROSCOPY

CNC	Dose	Conversion
0	0	0
0	25	85
0	2x25	91
1	0	0
1	25	85
1	2x25	92
2.5	0	0
2.5	25	87
2.5	2x25	89
5	0	0
5	25	85
5	2x25	87
10	0	0
10	25	85
10	2x25	89

The samples cured by photopolymerization were thus prepared with a similar conversion level. The different series of materials were characterized by DSC, DMA and submitted to tensile microtests. The results show that significant improvement of the Young's modulus was achieved by introducing cellulose nanocrystals in amount as low as 1 wt-% in the PUR acrylate materials (Fig. 5.6). Increasing the content of CNC above 1 wt-% was shown not to further increase the modulus at a level of ca. 1500 MPa.

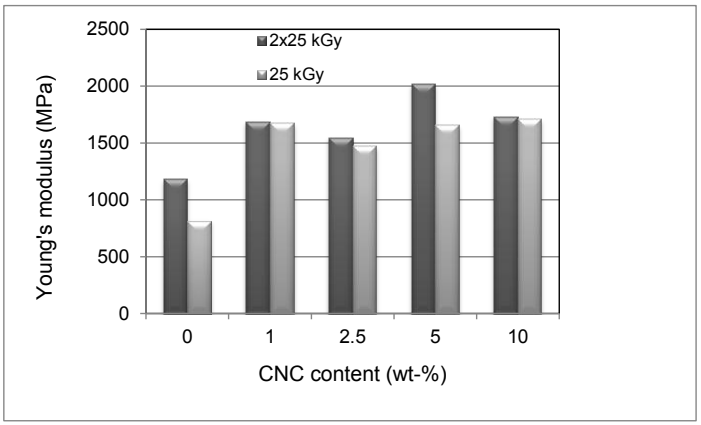

FIG. 5.6. Young's modulus (E) of cured PUR acrylate samples containing various amounts of CNC submitted to EB or to 395 nm (photoinitiator content 1 wt%) irradiation, as determined by mechanical microtests.

The improvement of mechanical properties achieved by introducing 1 wt-% CNC in the matrix is consistent with the general trend expected from simple mixture models. However, the absence of further significant changes at higher values for CNC content raises various questions and needs further investigation. A detailed characterization of the materials morphology would probably provide hints on the distribution of the reinforcing nanofibres. In particular, we have observed that in the absence of sonication of the mixture of latex with added CNC suspension (1 wt-% with respect to dry matter), aggregates are distributed evenly in the cross-section of the samples, with the obvious formation of aggregates (Fig. 5.7).

Sonicated sample

Non sonicated sample

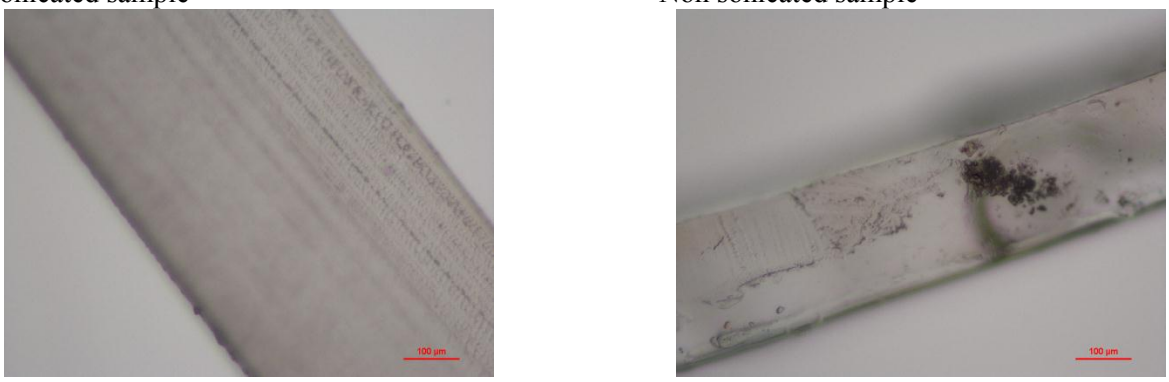

FIG. 5.7. Optical micrographs (polarized light) of the cross-section of EB-cured films prepared from a PUR acrylate formulation containing 1 wt-% of CNC with sonication after mixing (left side) or without sonication (right side).

At CNC levels above 2 wt-%, we suspect the formation of aggregates likely to induce a complex dependence of mechanical properties as function of filler concentration. Moreover, the very limited diffusivity of the individual nanocrystals into the PUR phase suggests that the CNC will be gradually concentrated in the interspace between latex particles during the evaporation and the coalescence steps. Obviously, beneficial interactions are obtained at a limited amount of CNC.

The properties at break were determined for cured samples containing 1 wt-% of CNC and compared to the unfilled PUR acrylate reference materials (Table 5.2).

TABLE 5.2. TENSILE STRENGTH OF CURED PUR ACRYLATE SAMPLES CONTAINING VARIOUS AMOUNTS OF CNC SUBMITTED TO EB OR TO 395 NM (PHOTOINITIATOR PI CONTENT 1 WT%) IRRADIATION, AS DETERMINED BY MECHANICAL MICROTESTS

Sample composition	Dose	Strength □ [MPa]
PUR acryl. + 1 wt-% CNC	25 kGy	38,7 ± 7,8
	2 x 25 kGy	34,6 ± 0,8
PURa	25 kGy	19,9 ± 2,4
	2 x 25 kGy	28,3 ± 10,2
PUR acryl. + 1 wt-% PI + 1 wt-% CNC	200 $J.cm^{-2}$	22,7 ± 4,3
PUR acryl. + 1 wt-% PI	200 $J.cm^{-2}$	24,0 ± 6,8

The obtained results allow concluding to the efficient reinforcing effect of the presence of 1 wt-% CNC in EB-cured samples. The samples cured by photopolymerization do not benefit from the presence of CNC. This observation can be interpreted by the limited radiolysis of the cellulose in EB-treated samples [5.18]. Free radical reaction at the interface with the PUR acrylate would induce covalent coupling between the nanofiller and the matrix. At 25 kGy the degradation of cellulose by chain scission is expected to be moderate. The smaller benefit on mechanical properties that is observed with samples submitted to 2 passes of 25 kGy seems consistent with some degradation of the CNCs. In samples submitted to photopolymerization, the selectivity of the light absorption process and the limited energy of incident photons would not allow such grafting reactions. Further work is in progress for gaining a deeper insight into this interesting phenomenon.

This exploratory study clearly evidences the beneficial effect of the presence of a limited amount of CNC combined with EB irradiation in PUR acrylate materials. The control of composite morphology is a key issue that requires further investigation on the dispersion of CNCs and on the coalescence process. The enhancement of mechanical properties without detrimental impact on the reactivity can be exploited in the fields of coatings, adhesives and structural materials.

5.4. CONCLUSIONS

A variety of technological issues concerning EB-curing have been addressed through a basic approach of radiation physics, radiation chemistry and materials science. Advanced studies aimed at the improvement of matrix toughness, at the reduction of the matrix cure induced shrinkage, and at the design of fiber - matrix interface were addressed. Solutions for matrix toughening with higher processability and compatible with environmental considerations are under development.

A next step will consist in aggregating the technological solutions developed for improving isolated aspects of curing, examined from the viewpoints of processing, of curing kinetics, polymer network performances and fiber-matrix interactions [5.19]. Technological demonstrators with demanding specifications are currently being prepared and further tested. Encouraging results allow envisioning mass production of structural composites as well as

functional materials by means of a reliable, cleaner and more productive out-of-autoclave manufacturing.

ACKNOWLEDGEMENTS

Financial support by Conseil Regional de Champagne Ardenne, MENESR and EU-FEDER Programme (CPER Project PlAneT), by the EADS Foundation, by IAEA (CRP "Radiation processing of (nano)composites for enhancing the features and utility in health care and industry") and by AstriPolska is gratefully acknowledged.

REFERENCES TO CHAPTER 5

[5.1] BÉZIERS, D., Process for the polymerization and/or crosslinking of a resin used in the composition of a composite material part by means of ionizing radiation, Aerospatiale , US Patent 478950 (1984).

[5.2] COQUERET, X., KRZEMINSKI, M., PONSAUD, P., DEFOORT, B. Recent advances in electron-beam curing of carbon fiber-reinforced composites. Radiat. Phys. Chem. 78, 557-561 (2009).

[5.3] KIM J.-K., MAI Y.-W., Engineered Interfaces in Fiber Reinforced Composites, Elsevier (1998).

[5.4] PASCAULT J.-P., SAUTEREAU H., VERDU J., WILLIAMS R. J. J., Thermosetting Polymers, CRC Press (2002).

[5.5] KRZEMINSKI, M., DEFOORT, B., MOLINARI, M., COQUERET, X. Nanoscale toughening for advanced composite matrices cured by electron beam activation. International SAMPE meeting, Seattle-WA, USA, May 17-20 (2010).

[5.6] CHUDA, K., SMOLINSKI, W., DEFOORT, B., RUDZ, W., GAWDZIK, B., RAYSS, J., COQUERET, X. Effects of vitrification on the isothermal polymerization of acrylate blends under radiation. Polimery (Warsaw, Poland), 49, 505-513 (2004).

[5.7] PONSAUD, P. Ph.D. Dissertation, Université des Sciences et Technologies de Lille, France (2005).

[5.8] PROCTOR, A., SHERWOOD, P. M. A., Surface analysis of carbon and carbon fibers for composites, Surf. Interface Anal. 4, 212 (1982).

[5.9] ODIAN G. G., Principles of polymerization, Wiley, New York (2004).

[5.10] DEFOORT, B., PONSAUD, P., COQUERET, X. Method for enhancing adherence of carbon fibers with respect to an organic matrix, Patent WO/2007/031576 (2007).

[5.11] DEFOORT, B., PONSAUD, P., COQUERET, X. Procédé pour améliorer le collage de matériaux divers sur des composites à matrice organique, French Patent n° 06 51700 (2006).

[5.12] DUFRESNE A., Materials Today, 16, 220-227 (2013).

[5.13] SAMIR A., ALLOIN F., DUFRESNE A., Biomacromolecules, 6, 612-626 (2005).

[5.14] SIQUEIRA G., BRAS J., DUFRESNE A., Polymers, 2, 728-765 (2010).

[5.15] POATY B., VARDANYAN, V., WILCZAK, L., CHAUVE, G., RIEDL, B., Progress in Organic Coatings, 77, 813–820 (2014).

[5.16] SCHWALM R., UV Coatings: Basics, Recent Developments and New Applications, Elsevier (2002).

[5.17] HAMBARDZUMYAN, A., FOULON L, CHABBERT B., AGUIÉ-BÉGHIN V. Biomacromolecules 13, 4081-4088 (2012).

[5.18] IVANOV S. V., Radiation chemistry of polymers, VSP (1992).

[5.19] KRZEMINSKI, M., PONSAUD, P., COQUERET, X., DEFOORT, B., LARNAC, G., AVILA, R. Out-of-autoclave technologies for competitive high performance composites. SAMPE 2011, Long Beach, CA (USA), May 23-26 (2011).

Chapter 6

PHOTOINITIATOR-FREE CURING OF ACRYLATE-BASED NANOCOMPOSITES BY MONOCHROMATIC ULTRA VIOLET IRRADIATION

F. BAUER
Institute of Chemical Technology,
Universität Leipzig

U. DECKER, S. NAUMOV
Leibniz-Institut für Oberflächenmodifizierung

CARSTEN RIEDEL
Innovative Oberflächentechnologien GmbH,
Leipzig

Germany

Abstract

Real-time attenuated total reflectance Fourier transfer infra red (ATR-FTIR) studies on radiation curing of acrylate formulations by a monochromatic 172 nm (Xe_2*) excimer lamp and a polychromatic medium pressure mercury arc lamp revealed that under oxygen-free curing conditions photopolymerization reactions take place at high reaction rates even in the absence of a photoinitiator. Due to quantum chemical calculations, the excitation of acrylate molecules by high energy photons (having wavelengths $\lambda<267$ nm) can generate radicals resulting in the self-initiation of acrylic C=C photopolymerization reactions. On a pilot-scale vacuum ultra violet/ultra violet (VUV/UV) lamp set-up, through cure of acrylate-based nanocomposites of about 50 µm thickness has been performed in the absence of any photoinitiator.
Post-curing VUV irradiation of cured acrylate coatings under nitrogen atmosphere resulted in an excitation of C=O groups rather than photodegradation. Radical formation via absorption of high energy photons (having wavelengths $\lambda<219$ nm) by C=O bonds is assumed yielding a higher network density within thin surface layers via radical recombination reactions. FTIR analysis supports the formation of polar C–OH groups generated after H abstraction by·C–O biradicals. Consequently, additional crosslinking reactions within surface-near layers take place via C–C bonds between neighbouring polymer chains rather than via C–O–C bonds. Thus, VUV matted acrylate coatings show enhanced surface hardness, improved chemical resistance, and hydrophilic properties.

6.1. INTRODUCTION

Transparent, scratch and abrasion resistant topcoats are the essential requirements of wood flooring products for some years. To maximize mechanical, optical and chemical performance, a proper selection of lacquer components is very important. Thus, the embedding of inorganic micro- and/or nano-sized particles has drawn increasing attention [6.1-6.3]. For curing such high solid content formulations, photopolymerization is an effective approach owing to its advantages such as high curing speed, low energy consumption, low operation temperature, and less environmental pollution by avoiding volatile organic solvents [6.4]. In addition, acrylate-based resins and reactive diluents are preferred in most photocuring applications because of their superior reactivity [6.5].

To start radical photopolymerization, the generation of primary radicals is necessary. This requires the addition of specific photoinitiator compounds that typically decompose into

radicals by exposure to light of appropriate wavelengths or abstract a hydrogen atom from suitable donors (co-initiators) producing initiating radicals. Because the most common light source in UV curing is the mercury arc lamp, the absorption characteristics of photoinitiators should be tuned to its spectrum. Thus, the efficiency of photoinitiators to convert photons into radicals as well as the quenching of those radicals by inhibitors, such as oxygen molecules dissolved in the acrylate formulation, controls the amount of the photoinitiator for obtaining high polymerization rates.

Unfortunately, unnecessary high amounts of photoinitiator as required for curing in air can lead to some problems, such as unpleasant odour, harmful toxicity and yellowing/weathering of the coatings originated from the presence of unconverted/residual photoinitiator molecules and low-molecular photocleavage fragments trapped in the photocured coatings [6.6]. To minimize the mentioned drawbacks, flushing the UV curing chamber with inert gases such as nitrogen or carbon dioxide, is one of the most efficient methods for obtaining high curing rates at low photoinitiator amounts [6.7, 6.8]. Obviously, any of these UV photopolymerization techniques have to compete with electron beam curing having no requirement of photoinitiators [6.9].

In the absence of any photoinitiator or any other additives, the self-initiation of acrylic and methacylic acids as well as several acrylic monomers has been observed during long-term irradiation with a conventional medium pressure Hg lamp. Depending on the acrylate used, conversions between 50 and 90 % were reached after 30 seconds irradiation [6.10]. Furthermore, the complete conversion of a photoinitiator-free aqueous miniemulsion of acrylate monomers was achieved after 12 min of irradiation with a conventional Hg lamp. However, no acrylate conversion occurred by using a cut-off filter for wavelengths $\lambda <$ 300 nm. These findings point to the short-wavelength portion of the UV emission spectrum of Hg lamps which is essential for acrylate excitation and subsequent self-initiation of photopolymerization [6.11]. Obviously, an efficient generation of starting radicals requires the matching of the absorption spectrum of the initiator molecules with the emission spectrum of the UV source used. But, most photocurable acrylate-based resins and diluting acrylates or monomers do not or only weakly absorb in the spectral region of the mercury arc lamp. Consequently, the emission spectrum of the UV light source used has to be tuned to the typical absorption bands of acrylates at wavelengths $\lambda<220$ nm [6.12-6.14]. Hence, the application of short-wavelength vacuum UV (VUV) irradiation, e.g. emitted by a monochromatic 172 nm (Xe_2*) excimer lamp [6.15], meets two objectives: (i) the photoinitiator-free UV curing and (ii) the manufacture of matt finished coatings.

Gaining popularity not only in wood and parquet flooring in recent times, silk matt and matt clear coats that scatters light, offer an authentic representation of the wood's character by accentuating its natural structure. Two curing procedures have been suggested yielding patterned microstructure surfaces in such a way that the light falling on it is scattered: (i) a single step fabrication of wrinkles by a thin liquid layer of acrylate monomers remaining uncured on the surface due to the quenching of free radicals by oxygen [6.16] and (ii) a combined VUV/UV curing technique by a dual lamp system consisting of a 172 nm excimer lamp and a conventional medium pressure mercury lamp where a VUV-cured top layer floats on the uncured resin [6.17]. The benefits of such little noticeable gloss include masking minor scratches, dust build-up, and footprints. An excellent reproducibility of low gloss coatings by the VUV/UV curing with a gloss level at 60º down to 0.5 units on an industrial scale and resistance to burnishing of such micro-structured surfaces have been shown in furniture, wood panel, and flooring applications [6.13, 6.18, 6.19].

The novelty of the present work of VUV-induced matting of acrylate-based formulations is the photoinitiator-free photopolymerization of acrylates due to the observed radical formation of acrylic C=C bonds by172 nm irradiation. In this study, quantum chemical calculations have been combined with real-time ATR-FTIR spectroscopy and pilot-scale VUV/UV curing experiments to elucidate the effect of the wavelength of UV radiation on the excitation of acrylic C=C and C=O bonds and, thereby, to explain the self initiation of acrylate polymerization by 172 nm irradiation [6.20]. In further studies, two-dimensional infrared (2D IR) correlation spectroscopy [6.21] will be applied for enhancing the spectral resolution and for highlighting subtle cross linking effects due to VUV-induced radical formation of C=O bonds which are responsible for enhanced surface properties such as microhardness, surface energy, and chemical resistance, observed for the photoinitiator-free cured acrylate coatings manufactured by a pilot-scale VUV/UV irradiation equipment.

6.2. EXPERIMENTAL

6.2.1. Materials and preparation of polyacrylate nanocomposites

For the in-situ surface modification of silica nanoparticles within UV curable, acrylate-based formulations, nanosized silica Aerosil 200, Aerosil 380, and Ox 50 (2-15 wt.%, all from Evonik Degussa AG, Germany), various surface modifiers, e.g., methacryloxypropyl-trimethoxysilane and vinyltrimethoxysilane (2-10 wt.%), and aliphatic urethane acrylate resins (20-40 wt.%), e.g., EB 1290 and EB 5129, and 20-60 wt.% tetrahydroxy-ethylpentaerythritol tetraacrylate (SR 494), as well as reactive diluents such as 1,6-hexandiol diacrylate (30-40 wt.%), all purchased from CYTEC Surface Specialties, Germany) were intensively stirred at 60-75 °C using a combination of dissolver and high-performance ball mill (VMA Getzmann, Germany). The detailed composition (parts of oligomers, reactive diluents, and nanofiller) naturally complied with the desired application of the coating such as scratch resistance and/or flexibility as well as with the viscosity of the formulation required for coil coating. No photoinitiator has been added to the nanocomposite formulations and all chemicals were used as received. Details of the nanocomposite preparation can be found elsewhere [6.22]. In addition, commercially available, photoinitiator-free acrylate formulations obtained from Cetelon Nanotechnik GmbH (Germany) have been applied for pilot-scale VUV/UV curing/matting.

6.2.2. Equipment

UV-induced real-time ATR-FTIR measurements were performed on a FTS 6000 spectrometer (Digilab, USA) equipped with a liquid-nitrogen-cooled MCT detector and 2D correlation analysis software. Using the attenuated total reflectance (ATR) technique ("Golden Gate", Graseby Specac, UK), FTIR spectra were obtained in the wavenumber range of 600-4000 cm^{-1} with a spectral resolution of 12 cm^{-1} and a temporal resolution of 18 ms. Using a doctor blade, thin acrylate layers were applied to the (diamond) ATR unit. The IR penetration depth in the ATR experiments was estimated to be 0.8 µm and 2.5 µm at 3000 cm^{-1} and 1000 cm^{-1}, respectively. Acrylate conversion was determined using the C=C band at 810 cm^{-1}. Through-cure of 50 µm thick coatings has been confirmed by ATR-FTIR measurements at front and back side of the films detached from glass substrates. For the determination of the signal intensity of C=O bonds, peak integration between 1650-1800 cm^{-1} has been applied.

For the irradiation set-up attached to the ATR unit, a polychromatic mercury arc lamp (100 $mW \cdot cm^{-2}$, Müller Elektronik-Optik GmbH, Germany) and a monochromatic 172 nm

excimer lamp (15 $mW \cdot cm^{-2}$, Xeradex Radium GmbH, Germany) has been applied. The UV irradiance has been measured direct on the ATR crystal using a VUV radiometer from Gerus mbH (Germany). UV-induced real-time (ATR) FTIR measurements were performed on a Digilab FTS 6000 spectrometer equipped with a liquid-nitrogen-cooled MCT detector. Using the attenuated total reflectance (ATR) technique ("Golden Gate", Graseby Specac), FTIR spectra were obtained in the wavenumber range of 600-4000 cm^{-1} with a spectral resolution of 16 cm^{-1} and a temporal resolution of 21 ms. Using a doctor blade, thin acrylate layers were applied to the (diamond) ATR unit. A rough estimation of the film thickness includes peak integration of CH_x groups between 2700- 3100 cm^{-1} and assuming a thickness of 1.0 μm for the maximum peak area according to the Harrick approximation. For the UV irradiation attached to the ATR unit, a polychromatic mercury arc lamp (100 $mW \cdot cm^{-2}$, Müller Elektronik-Optik GmbH, Germany) and a monochromatic 172 nm excimer lamp (15 $mW \cdot cm^{-2}$, Xeradex Radium GmbH, Germany) has been applied. The UV irradiance has been measured right on the ATR unit using a VUV radiometer from Gerus mbH (Germany). UV spectra of acrylates dissolved in acetonitrile or spin-coated on quartz plates were recorded with a Shimadzu 2101 UV-vis spectrometer.

The microhardness of the composite materials was determined with a Fischerscope H100C hardness tester (Helmut Fischer GmbH, Germany) according to the technical standard ISO 14577. Contact angle measurements of ultra-pure water and diiodomethane were performed using a G2 contact angle meter from Krüss GmbH (Germany). The static contact angles were measured five times for each sample and the method of Owens-Wendt-Rabel and Kälble was used to calculate the surface energy. The gloss (at 60°C) of the coatings was taken using a micro-Tri-glossmeter (Byk-Gardner). Optical images were obtained with an Olympus BX60 light microscope using reflected light.

6.3. RESULTS AND DISCUSSION

For starting and maintaining polymerization reactions, the presence of reactive radicals is a compulsory requirement irrespective of their particular generation. Besides the addition of various external initiators, polymerization reactions of (alkyl) acrylates can be initiated thermally via a triplet diradical formation of dimeric acrylate species [6.23] and by absorption of appropriate high energy VUV photons yielding excited molecules as indicated by absorption bands of acrylates in the VUV region [6.13, 6.24].

6.3.1. Quantum chemical calculations on radical formation of acrylates

Quantum chemical calculations have been demonstrated to be extremely beneficial for the elucidation of photochemical processes such as the radiation induced crosslinking of surface modified silica nanoparticles with acrylate resins [6.25], the self-initiation of UV photopolymerization of brominated acrylates [6.26], and the VUV photodegradation of organosilanes [6.27]. The excitation of acrylates by the absorption of high energy UV photons (having a minimum energy of 4.7 eV, i.e. wavelengths λ <267 nm) converts the ground state S_0 to the S_1 singlet state as shown in Fig. 6.1. This includes significant changes in the electron distribution of the conjugated C=C–C=O system of acrylate molecules from the highest occupied molecular orbital (HOMO) into the lowest unoccupied molecular orbital (LUMO). Please note that in the excited S_1 state the ester C–O–C bond is also involved in the electron distribution of the acrylic C=C–C=O system. By intersystem crossing to the excited $^*T_1$ triplet state, a C–C· biradical localized at the vinyl double bond is finally formed. The high energy ·C–C·biradical in the $^*T_1$ state can undergo different reactions [6.28] like inter-

and intramolecular hydrogen transfer, the addition to a ground-state acrylate molecule, and predominately the relaxation from the $^*T_1$ state into the T_1 state by a three-dimensional rearrangement of the excited molecules. Nevertheless, from an energetic point of view all radicals formed are able to start the polymeric chain growth. Thus, the absorption of 172 nm photons (which approximates 7.2 eV) will result in the self-initiation of acrylic C=C photopolymerization reactions. It should be furthermore noted that the quantum chemical calculations convincingly explains why even the weak short wavelength portion of the UV emission spectrum of typical medium-pressure mercury lamps (e.g. wavelengths λ at 205, 226, and 254 nm) initiates the self-photopolymerization of conventional acrylate formulations without using a photoinitiator [6.10, 6.11, 6.29].

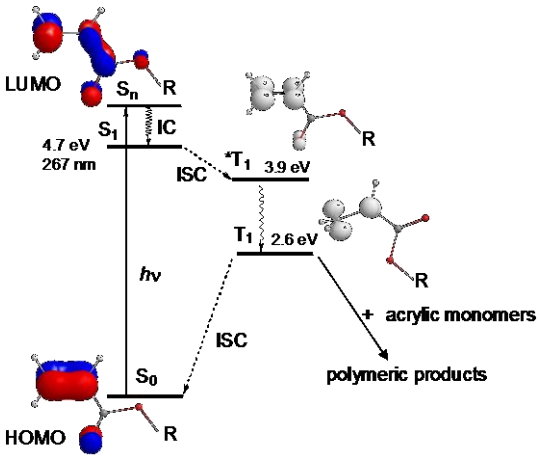

FIG. 6.1. Energy diagram of photochemical activation of acrylic C=C bonds and electron distribution in the HOMO und LUMO of acrylates.

6.3.2. Self-initiation of acrylic C=C photopolymerization by 172 nm irradiation

While photoinitiator-free, nanoparticle-containing acrylate formulations were used for all of the VUV/UV-cured application studies, for the majority of real-time ATR-FTIR measurements tripropyleneglycol diacracrylate (TPGDA) has been employed as representative acrylate. Particularly with regard to the VUV-induced post-curing effects on the surface of polyacrylate coatings, such FTIR studies of complex nanocomposite formulations in the region of C–O–C vibrations at 1000-1250 cm^{-1} proved to be difficult because of the strong Si-O vibrations of silica nanoparticles at about 1100 cm^{-1} (Fig. 6.2).

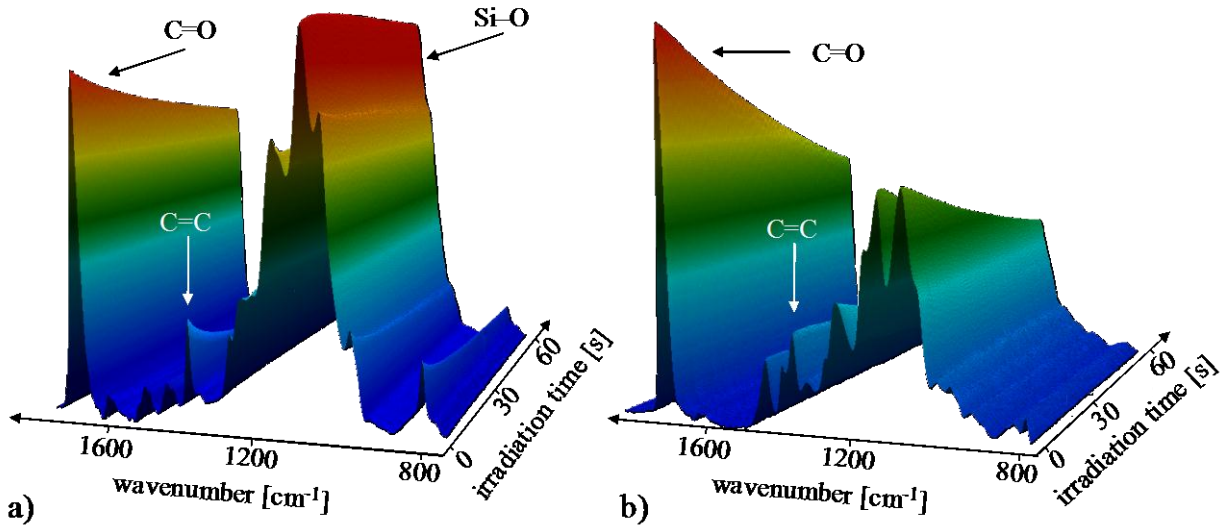

Fig.6.2. 3D images of phototinitiator-free, VUV induced curing of acrylates (a) with an (b) without silica nanoparticles.

Typical acrylates such as TPGDA show strong absorption bands at wavelengths shorter than 220 nm. Therefore, photons emitted by the traditional medium pressure mercury arc lamps (having wavelengths 400>λ>250 nm) are typically considered to be inefficient for the direct photopolymerization of acrylate molecules and the addition of a photoinitiator for the generation of radicals is recommended. In contrast, the short-wavelength emission of the monochromatic 172 nm excimer lamp is in accordance with the absorption spectrum of acrylates [6.13, 6.24]. Hence, self-initiation and photoinitiator-free polymerisation of acrylates (comparable to the polymerization by electron-beam irradiation [6.30]) will take place when acrylate-based formulations are exposed to an intense radiation of a Xe_2* excimer lamp.

For example, Fig. 6.3. shows the ATR-FTIR spectra of neat TPGDA before and after 60 sec of 172 nm irradiation. Significant changes in the typical regions of C=C bands (1636, 1408, and 810 cm^{-1}) and CH_2 bands (2934 and 1453 cm^{-1}) indicate to the onset of the photoinitiator-free photopolymerization by 172 nm irradiation. Thus, the C=C double bond conversion vs. irradiation time profile of TPGDA (Fig. 6.4) demonstrates that an irradiance of 15 $mW \cdot cm^{-2}$ by the monochromatic 172 nm excimer lamp is sufficient to generate enough free radicals for high acrylate conversion (>85 %) during an exposure time of <10s. In common with the decrease of the C=C double bonds due to photopolymerization reactions, a corresponding increase of the CH_2 groups (ν_{as} at 2934 cm^{-1} and ν_s at 1453 cm^{-1}) can be observed. Moreover, the different photochemical reactivity of several acrylates under 172 nm irradiation has been recently revealed by real-time ATR-FTIR spectroscopy [6.14]. It should be mentioned at this point that the radical formation is inextricably linked to the excitation of acrylic C=C bonds by 172 nm irradiation and that the type of acrylate (e.g. acrylate monomers, aliphatic and aromatic urethane acrylate oligomers) is therefore less important.

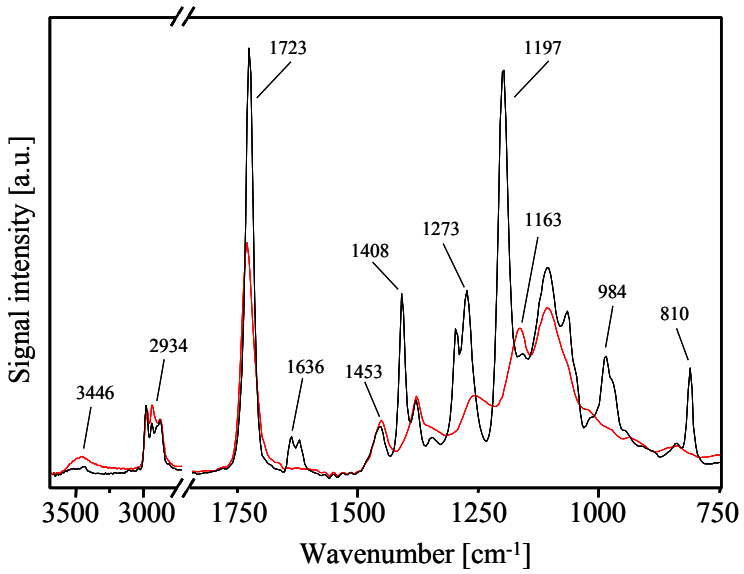

FIG. 6.3. ATR-FTIR spectrum of TPGDA before (—) and after (—) photoinitiator-free curing by a 172 nm excimer lamp.

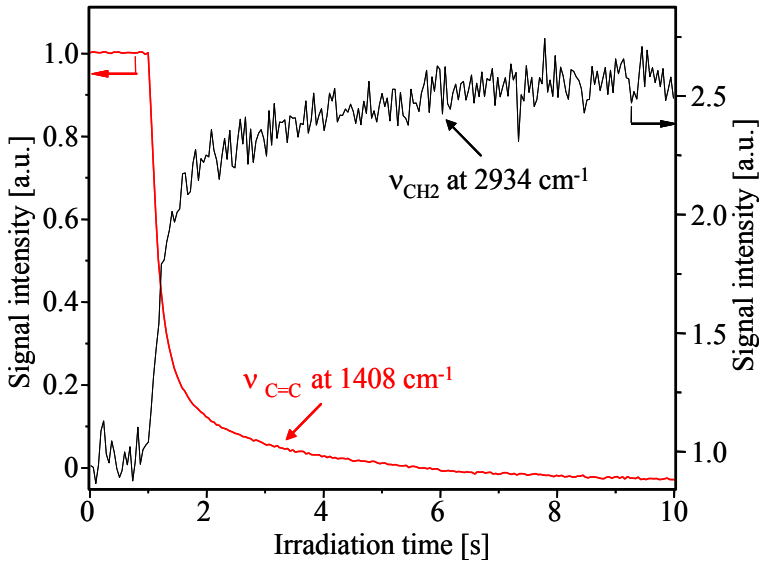

FIG. 6.4. Kinetic profiles of the ν(C=C) and ν(CH_2) bands during photoinitiator-free photopolymerization of TPGDA upon VUV irradiation.

Irrespective of the high efficiency of photoinitiator-free radical formation by monochromatic 172 nm excimer lamps [6.13], the thickness of through-cure of acrylate-based nanocomposite films is limited to some microns due to the penetration depth of 172 nm photons. Hence, a wide application of polychromatic low-pressure mercury lamps having characteristic short-wavelength emissions at 185 and 254 nm, and thereby suited even for thicker coatings, may be expected for photoinitiator-free curing in the near future.

6.3.3. Monomer-Polymer transformation during photopolymerization

Obviously, the conjugated C=C–C=O electron system of acrylates will be lost during photopolymerization reactions. For that reason, the C=O stretching band at 1723 cm^{-1} (Fig. 6.3) as well as the O=C–O–C antisymmetric stretching band at 1197 cm^{-1} (Fig. 6.5) will change in intensity and peak position. To be more precise, C=O and C–O–C bands of acrylic mono- and oligomers will disappear during radiation curing whereas the analogous bands that are assigned to the acrylate polymers will emerge.

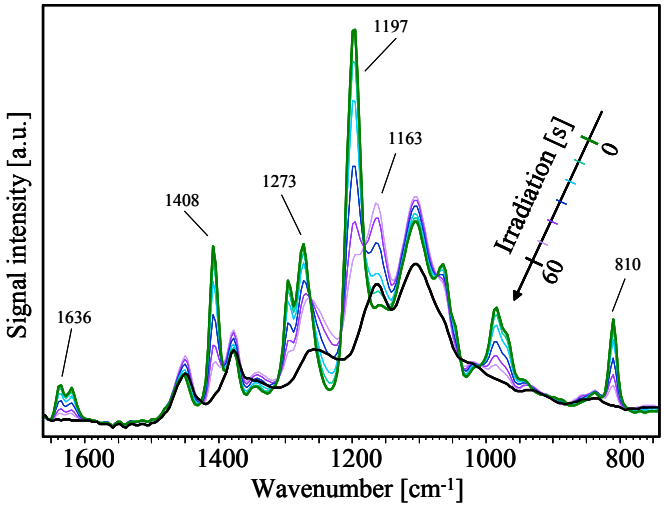

FIG. 6.5. FTIR spectra of TPGDA during photoinitiator-free curing at various VUV exposure times within the region ν(C=C) and ν(C–O–C) of 1650-750 cm^{-1}.

For example, photopolymerization results in the appearance of a band at 1163 cm^{-1} (as shown in Fig. 6.5) which has to be assigned to O=C–O–C antisymmetric stretching vibrations of the acrylate polymers formed [6.31]. But then again, the intensity of this band decreases at longer VUV irradiation times. Hence, the time profiles of selected IR band intensities reported in Fig. 6.6. indicate a two-stage VUV irradiation process: (i) a photoinitiator-free curing period with high polymerization rates and (ii) comparatively slow post-curing reactions of surface modification and/or degradation. Moreover, the concurrent decrease of the C=C band at 1410 cm^{-1} and the C–O–C band at 1197 cm^{-1} indicates their close mechanistic relationship, i.e. breaking the extended C=C–(O)C–O–C electronic system of acrylates during polymerization reactions. Similary, the rapid increase of the C–O–C band at 1163 cm^{-1} and the CH_x bands in the region 2800-3000 cm^{-1} is due to polymer formation.

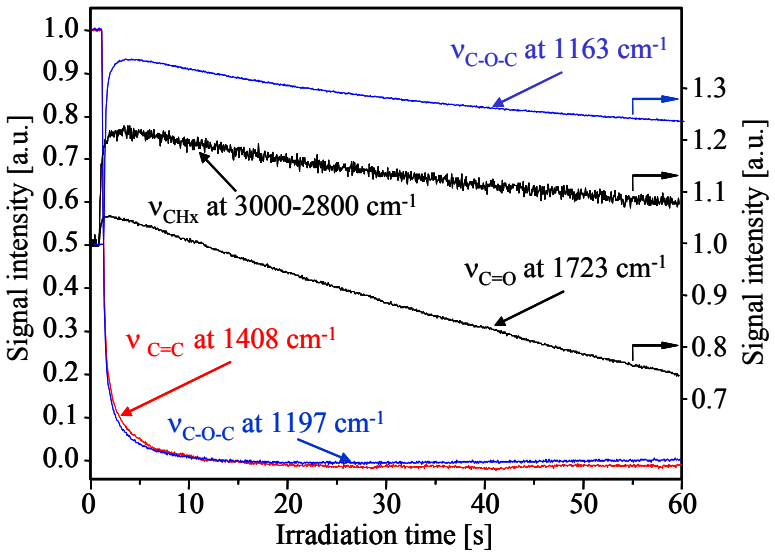

FIG.6.6. Kinetic profiles of the ν(C=C), ν(C=O) and ν(C–O–C) bands during photoinitiator-free photopolymerization of TPGDA upon VUV irradiation.

After the photoinitiator-free VUV curing process, further 172 nm irradiation yields a steady decline of the C=O, C–O–C and CH_x bands indicating some photodegradation (even under an inert atmosphere) of the polyacrylate formed. But, a more pronounced reduction of the C=O band at 1723 cm^{-1} (Fig. 6.6) gives a hint to a specific activation of C=O groups by 172 nm photons.

6.3.4. Post-curing VUV irradiation and excitation of C=O bonds

Extending the 172 nm irradiation (under an inert atmosphere to suppress oxygen inhibition) longer than required for the complete conversion of acrylic C=C double bonds, a continuous decrease of the C=O band at 1723 cm^{-1} and the O=C–O–C band at 1163 cm^{-1} becomes evident (Fig. 6.6). For irradiation with highly energetic photons in air, the reduction of IR signal intensities can be convincingly explained by the transformation and degradation of the organic polymer [6.32]. Such photodegradation in air can even be observed using polychromatic (Hg) UV lamps but at irradiation times that are far beyond typical curing times. For example, Lee et al. [6.33] observed a decrease of the intensity of the C=O band in poly(ethylene terephthalate) films with increasing irradiation time up to 90 min.

As wettability studies of different polymeric biomaterials after VUV irradiation [6.34] revealed, a specific excitation of C=O groups by 172 nm photons can be expected. Fig. 6.7. convincingly shows that the emission spectrum of the 172 nm (Xe_2*) excimer lamp matches well with the calculated absorption spectrum of polyacrylates. While the conjugated C=C–C=O electron system of acrylates show a broad absorption band around 200 nm, the photosensitive groups of the cured polymer matrix were mainly characterized by C=O absorption bands with a maximum around 180 nm. It can be expected that the absorption of high energy VUV photons (having a minimum energy of 5.7 eV, i.e. wavelengths λ <219 nm) finally yields ·C–O· biradicals (Fig. 6.8). As quantum chemical calculations of the polymer excitation have shown, the triplet state (T_1) can abstract hydrogen from the polymer substrate via two reaction pathways differing energetically only a little. Such radical transfer reactions and the subsequent recombination of neighbouring radicals yielding additional crosslinks between polymer chains can explain both (i) the increased chemical resistance of VUV irradiated polyacrylate surfaces and (ii) their change from a hydrophobic to a more hydrophilic character.

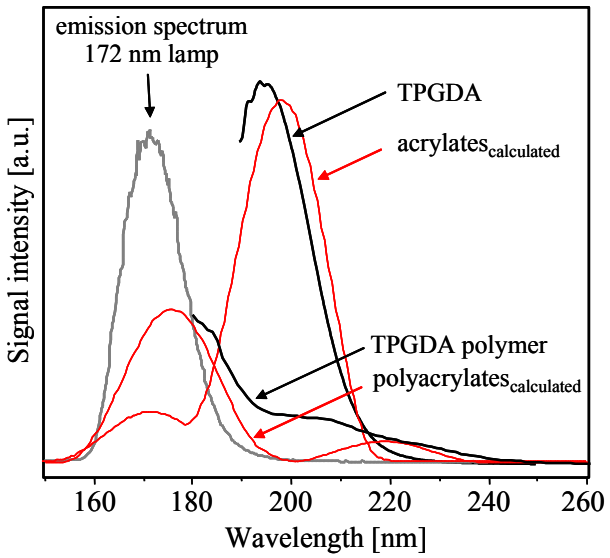

FIG. 6.7. UV spectra of TPGDA (before and after curing) and calculated spectra of acrylates (before and after curing) with the emission spectrum of the monochromatic 172 nm excimer lamp.

Hydrogen abstraction by the·C–O·biradicals will mainly result in the formation of OH groups (of a hemiacetal) as indicated by the appearance of a broad IR band at 3450 cm^{-1}. This change of surface composition is also manifested in an increase of surface energy and a decrease of the water contact angle of acrylate polymers irradiated with 172 nm excimer lamps (Table 6.1). In the case of VUV irradiation studies under nitrogen atmosphere, however, photooxidation and photodegradation are of minor importance [6.35]. Finally, the conversion curves clearly show that the direct generation of acrylate radicals by VUV irradiation takes place with very high efficiency and the subsequent polymerization rate can keep up with reaction rates of photoinitiator-induced polymerization of acrylate formulations [6.13].

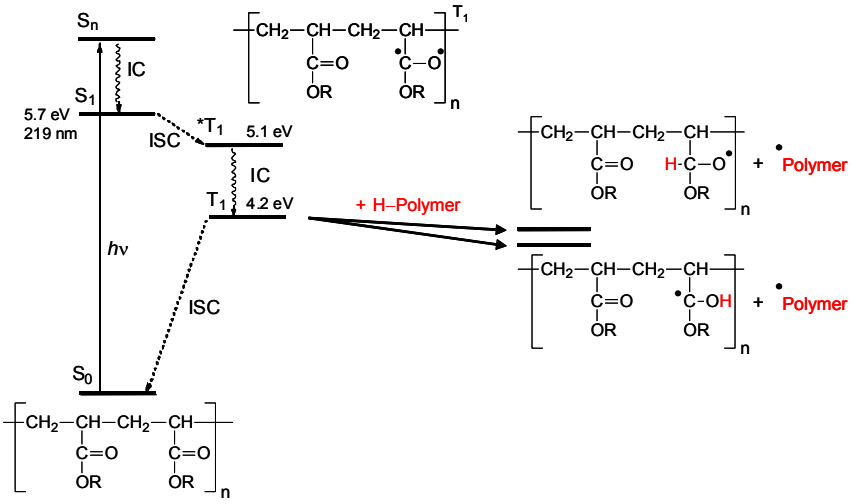

FIG. 6.8. Energy diagram of photochemical activation of C=O bonds in polyacrylates and proposed pathway of hydrogen abstraction from nearby polymer chains finally resulting in additional cross-linking reactions. (IC= internal conversion, ISC = intersystem crossing)

While the formation of OH groups can easily be verified, the corresponding proof of the other, energetically less likely reaction pathway of the ·C–O· biradical, i.e. yielding the

formation of CH groups and C–O–C bonds, is more difficult and requires IR band deconvolution.

6.3.5. Photoinitiator-free VUV/UV matting and curing of acrylate nanocomposites

Without adding so-called matting agents (organic and inorganic microparticles), acrylate-based coatings with sheen levels of low gloss can be achieved by a combination of a 172 nm (Xe_2*) excimer lamp with a conventional medium pressure Hg lamp [6.19, 6.36]. Although offering a more elegant appearance, high gloss coatings tend to highlight imperfections including dust build-up and greasy contaminations such as finger prints. Therefore, matt finishes are more and more chosen primarily because of an authentic representation of a wood floor look, minor scratches are less noticeable and the ease of for high-fidelity patterning. This VUV/UV matting technique has been scaled-up to web widths up to 2300 mm and web speeds between 10 and 120 m/min and successfully applied to clear coats on laminate/parquet floorings, automotive interior components, and finish/plastic foils [6.17].

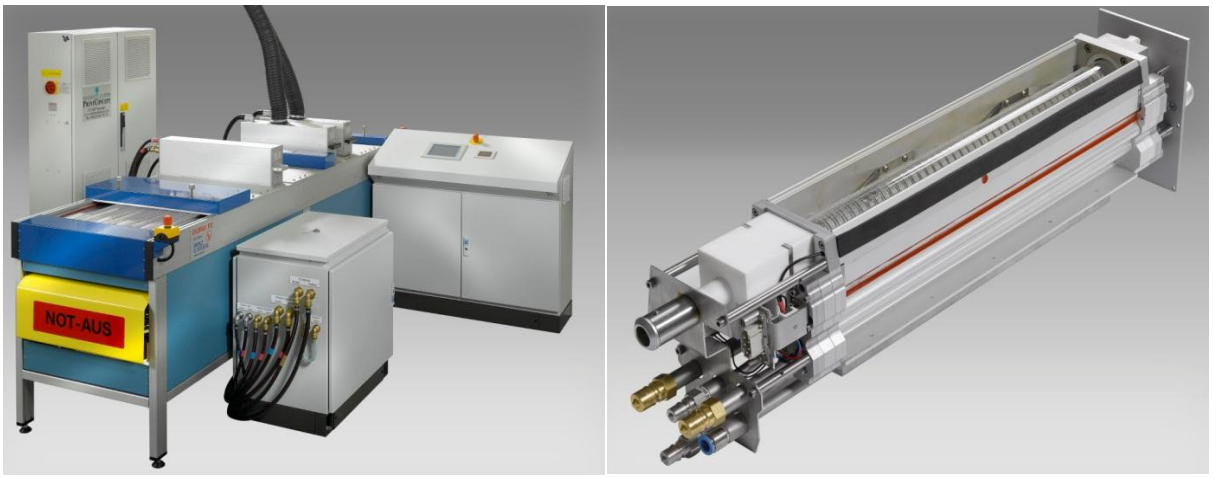

FIG. 6.9. VUV/UV lamp set-up manufactured by Innovative Oberflächentechnologien GmbH (Leipzig, Germany) for curing/matting of acrylate-based nanocomposites. Details of 172 nm excimer lamp (right).

Figure 6.10. illustrates the sheen levels to be expected for high gloss and matt finishes. The left portion of Fig. 6.10. with a higher gloss floor shows the typical reflections of light sources whereas the natural optical appearance of wood without any interfering reflections is displayed on the right. Such matted finishes do not only fascinate by their optical appearance but also by their pleasant haptic sensation ("soft-touch" coatings).

FIG. 6.10. Reflectance behavior of acrylate-based nanocomposite clear coats on laminate cured by a (Hg) UV lamp (left) and the dual VUV/UV lamp system (right, with microscopic enlargement of the surface pattern). The gloss levels at 60° are 87 and 4 units, respectively.

Using the described dual VUV/UV lamp set-up, through cure of photoinitiator-free acrylate formulations of about 50 µm thickness has been performed. To test the photoinitiator-free VUV/UV curing/matting technique for their suitability in industrial applications, an acrylate formulation containing 2 wt.% surface-modified silica nanoparticles was cured by different radiation sources (Table 6.1). Although the C=C conversions by electron beam and VUV/UV of the photoinitiator-free formulation are slightly lower than those of the photoinitiator-containing ones, microhardness measurements and swelling studies (using iodine dissolved in ethanol) revealed that VUV matted surfaces are typically harder and more resistant against chemicals or solvents than glossy ones, respectively. Surely, an optimization of the EB dose will provide better surface and bulk properties for this coating formulation. However, the comparison of the microhardness at the same degree of conversion (Table 6.1) obtained by electron beam and VUV/UV curing enables an effective evaluation of the VUV/UV curing/matting technique to be a really alternative opportunity for photoinitiator-free photo-polymerization. Nevertheless, electron beam curing will continue having certain advantages over UV curing for thick and pigmented coatings [6.9].

TABLE 6.1. SURFACE PROPERTIES OF VUV/UV-MATTED ACRYLATE-BASED NANOCOMPOSITE COMPARED WITH CURING BY A MERCURY UV LAMP AND AN ELECTRON BEAM

	matted and cured by dual VUV/UV lamp set-up[a]	matted and cured by dual VUV/UV lamp set-up[b]	cured by (Hg) UV lamp[b]	cured by electron beam (50 kGy)[a]
C=C Conversion (%)	77	84	84	76
Gloss (at 60°)	3 ± 1	5 ± 1	65 ± 3	70 ± 3
Microhardness (N/mm^2)	210 ± 30	215 ± 20	195 ± 10	175 ± 10
Surface energy (mN/m)	46 ± 1	47 ± 2	42 ± 1	50 ± 1
Water contact angle (°)	64 ± 1	66 ± 1	72 ± 1	63 ± 1
Chemical resistance (iodine in ethanol, 1 h)	☺	☺	😐	☹

[a] photoinitiator-free
[b] 2 wt.% photoinitiator (Darocure 1173)

6.4. CONCLUSIONS

Fundamentals of VUV induced matting of photoinitiator-containing, acrylate-based formulations (i.e. without the addition of commonly used matting agents) have been addressed in the last Research Coordination Meeting on Radiation Curing of Composites for Enhancing their Features and Utility in Health Care and Industry. In this work, the application of the dual VUV/UV lamp set-up and nitrogen flushing on a pilot scale has been extended to the photoinitiator-free curing and matting of acrylate-based nanocomposites of about 50 µm thickness. The effect of VUV irradiation (using a 172 nm excimer lamp) on acrylic C=C bonds for radical formation and self-initiation of the photopolymerization was investigated by real-time ATR-FTIR spectroscopy. Quantum chemical calculations prove that the absorption of high energy photons (having wavelengths $\lambda<267$ nm) can immediately generate radicals from typical acrylates, i.e. radical formation is not limited to special acrylate such as brominated aromatic acrylates. Moreover, this theoretical result convincingly explains why even the weak short wavelength portion of the UV emission spectrum of typical medium-pressure mercury lamps initiates the self-photopolymerization of conventional acrylate formulations without using a photoinitiator.

Furthermore, 172 nm excimer irradiation additionally results in a specific excitation of C=O bonds with subsequent radical formation, transfer and recombination reactions. 2D correlation analysis of time-resolved ATR-FTIR spectra supports the formation of ·C–O· biradicals followed by H abstraction and the generation of polar C-OH groups as well as additional crosslinking reactions between neighbouring polymer segments via new C–C bonds. Hence, VUV irradiation of cured acrylate coatings under nitrogen atmosphere yields a higher network density within surface-near layers rather than photodegradation of the coating. As a consequence, acrylate coatings cured and matted by a dual VUV/UV lamp set-up do not only fascinate by their optical appearance but also show enhanced surface hardness and improved chemical resistance. Finally, these outstanding properties of photoinitiator-free nanocomposite coatings obtained by curing/matting with a dual VUV/UV lamp set-up are

expected to be achieved by single low-pressure mercury lamps offering appropriate wavelengths for both surface and through-cure.

REFERENCES TO CHAPTER 6

[6.1] H. ZOU, S.S. WU, J. SHEn, Chem. Rev. 108 (2008) 3893.
[6.2] V. LANDRY, P. BLANCHET, B. RIEDL, Prog. Org. Coat. 67 (2009) 381.
[6.3] M. SANGERMANO, M. MESSORI, Macromol. Mat. Eng. 295 (2010) 603.
[6.4] R. MEHNERT, A. PINCUS, I. JANOVSKY, UV & EB Curing Technology & Equipment, Wiley-SITA, London, 1998.
[6.5] C. DECKER, Prog. Polym. Sci. 21 (1996) 593.
[6.6] M.H. KIM, J.B. LEE, K.Y. CHOI, J. Ind. Eng. Chem. 19 (2012) 292.
[6.7] B. DE RUITER, R.M. MEERTENS, Macromol. Symp. 187 (2002) 407.
[6.8] K. STUDER, C. DECKER, E. BECK, R. SCHWALM, Prog. Org. Coat. 48 (2003) 101.
[6.9] V. KUMAR, N.M.J. PAUL, Y.K. BHARDWAJ, N.K. GOEL, S. FRANCIS, K.S.S. SARMA, L. VARSHNEY, Prog. Org. Coat. 76 (2013) 1119.
[6.10] H.L. WANG, H.R. BROWN, Macromol. Rapic Comm. 25 (2004) 1095.
[6.11] P.A. HOIJEMBERG, A. CHEMTOB, C. CROUTXE-BARGHORN, Macromol. Chem. Phys. 212 (2011) 2417.
[6.12] T. SCHERZER, J. Polym. Sci. A: Polym. Chem. 42 (2004) 894.
[6.13] F. BAUER, U. DECKER, S. NAUMOV, C. RIEDEL, Prog. Org. Coat. 69 (2010) 287.
[6.14] T. SCHERZER, Macromol. Chem. Phys. 213 (2012) 324.
[6.15] U. KOGELSCHATZ, H. ESROM, J.Y. ZHANG, I.W. BOYD, Appl. Surf. Sci. 168 (2000) 29.
[6.16] D. CHANDRA, A.J. CROSBY, Adv. Mater. 23 (2011) 3441.
[6.17] C. RIEDEL, Technical bulletin "ExciRad 172" of IOT GmbH (2007).
[6.18] R. SCHUBERT, F. FROST, M. HINKEFUSS, R. KONIECZNY, B. MARQUARDT, R. MEHNERT, M.R. BUCHMEISER, Surf. Coat. Technol. 203 (2009) 3734.
[6.19] F. BAUER, U. DECKER, K. CZIHAL, R. MEHNERT, C. RIEDEL, M. RIEMSCHNEIDER, R. SCHUBERT, M.R. BUCHMEISER, Progr. Org. Coat. 64 (2009) 474.
[6.20] C. RIEDEL, R. MEHNERT, F. BAUER, R. SCHUBERT, EP 10 2008 061 244.8 (2008), assigned to Innovative Oberflächentechnologien GmbH.
[6.21] I. NODA, Appl. Spectrosc. 47 (1993) 1329.
[6.22] F. BAUER, R. FLYUNT, K. CZIHAL, M.R. BUCHMEISER, H. LANGGUTH, R. MEHNERT, Macromol. Mater. Eng. 291 (2006) 493.
[6.23] S. SRINIVASAN, M.W. LEE, M.C. GRADY, M. SOROUSH, A.M. RAPPE, J. Phys. Chem. A 115 (2011) 1125.
[6.24] L. PRAGER, L. WENNRICH, W. KNOLLE, S. NAUMOV, A. PRAGER, Mater. Chem. Phys. 134 (2012) 235.
[6.25] F. BAUER, R. FLYUNT, K. CZIHAL, H. ERNST, S. NAUMOV, M.R. BUCHMEISER, Nucl. Instr. Meth. Phys. Res. B 265 (2007) 87.
[6.26] T. SCHERZER, W. KNOLLE, S. NAUMOV, C. ELSNER, M.R. BUCHMEISER, J. Polym. Sci. A - Polym. Chem. 46 (2008) 4905.
[6.27] L. PRAGER, L. WENNRICH, R. HELLER, W. KNOLLE, S. NAUMOVLL, A. PRAGER, D. DECKER, H. LIEBE, M.R. BUCHMEISER, Chem. Europ. J. 15 (2009) 675.

[6.28] W. KNOLLE, T. SCHERZER, S. NAUMOV, R. MEHNERT, Radiat. Phys. Chem. 67 (2003) 341.
[6.29] L. HUANG, Y.M. LI, J.W. YANG, Z.H. ZENG, Y.L. CHEN, Polymer 50 (2009) 4325.
[6.30] R. MEHNERT, S. NAUMOV, W. KNOLLE, I. JANOVSKY, Macromol. Chem. Phys. 201 (2000) 2447.
[6.31] T. NAKANO, S. SHIMADA, R. SAITOH, I. NODA, Appl. Spectrosc. 47 (1993) 1337.
[6.32] A.C. FOZZA, J. ROCH, J.E. KLEMBERGSAPIEHA, A. KRUSE, A. HOLLANDER, M.R. WERTHEIMER, Nucl. Instr. Meth. Phys. Res. B 131 (1997) 205.
[6.33] C.O. LEE, B. CHAE, S.B. KIM, Y.M. JUNG, S.W. LEE, Vibr. Spectr. 60 (2012) 142.
[6.34] C. O'CONNELL, R. SHERLOCK, M.D. BALL, B. ASZALOS-KISS, U. PRENDERGAST, T.J. GLYNN, Appl. Surf. Sci. 255 (2009) 4405.
[6.35] T. BAHNERS, L. PRAGER, S. KRIEHN, J.S. GUTMANN, Appl. Surf. Sci. 259 (2012) 847.
[6.36] R. SCHUBERT, T. SCHERZER, M. HINKEFUSS, B. MARQUARDT, J. VOGEL, M.R. BUCHMEISER, Surf. Coat. Technol. 203 (2009) 1844.

Chapter 7

DEVELOPMENT OF RADIATION PROCESSED CONDUCTING NANO-COMPOSITES FOR SENSING APPLICATIONS

AND

USE OF RADIATION DEGRADED POLY(TETRAFLUORO ETHYLENE) POWDER AS A REINFORCING FILLER IN ELASTOMERS AND THERMOPLASTICS

K.A. DUBEY, Y.K. BHARDWAJ, C.V. CHAUDHARI, V. KUMAR, K.S.S. SARMA, S.A. KHADER, S. ACHARYA
Bhabha Atomic Research Centre,
Trombay, Mumbai,
India

Abstract

High-energy radiation was used for the property enhancement of conducting polymer nanocomposites. It was demonstrated that high-energy radiation can improve conducting, physical and mechanical properties of such composites, enabling their applications as strain sensors, chemiresistive sensors, over current protection devices, electromagnetic interference (EMI) shielding and high dielectric constant materials. Innovative strategies such as selective percolation, hybrid fillers and percolation in percolation were used to develop highly conducting nanocomposites at relatively lower loading of conducting fillers. In addition, the use of radiation processed polytetrafluoroethylene (RPTFE) powder as reinforcing filler was explored for developing high-modulus-light-weight composites. Extensive studies on radiation processing of polymer blends and coatings containing nanoparticulate fillers were also carried. In this report however, strain sensors and RPTFE reinforced composites are specifically discussed. Radiation dose was found to have a profound effect on the sensing and sensitivity (gauge factor) of the strain sensors. Effect of graphene on the strain sensing characteristics of a radiation crosslinked thermoplastic-elastomeric blend/conducting nano carbon black (NCB) nanocomposites was also investigated. The graphene content was found to have significant effect on the electromechanical response; the sensitivity of the sensor was highest for 0.02 weight fraction of graphene and was ~3 times that of observed for nanocomposites without graphene. RPTFE was found to act as reinforcing filler for polydimethylsiloxane (PDMS), improving not only the elastic modulus but also coefficient of friction. The exceptional improvement in mechanical properties of ethylene vinyl acetate (EVA)/organoclay composites on introduction of RPTFE indicated exceptional synergy between two fillers. X-ray diffraction studies revealed ~10% intergallery expansion in organoclay on higher RPTFE loading. These results prove that the radiation degraded PTFE can be effectively used for the development of high modulus composites.

7.1. INTRODUCTION

Conducting polymer nanocomposites are promising materials for many applications such as chemiresistive and electromechanical sensors, EMI shields, super capacitor, energy storage and actuators. These materials are low cost, flexible and lightweight. Several strategies namely selective percolation and hybrid fillers are frequently used to achieve high electrical conductivity at a lower concentration of conducting phase [7.1, 7.2]. In addition to higher electrical conductivity, hybrid fillers have also been reported to impart synergistic enhancement in the mechanical properties of polymer composites [7.3, 7.4].

Strain sensors are used in applications ranging from electronic-skin devices to damage detection and fatigue studies [7.5]. Different materials and different techniques are used to develop strain sensors [7.6-7.12]. Electromechanical response of a conducting polymer composite depends on the disaggregation dynamics of the percolated conducting phase within the insulating polymer phase [7.12-7.15].The main factor affecting disaggregation-reaggregation dynamics is the percolation threshold [7.5, 7.9, 7.16-7.18]. In conventionally percolated composites, optimal strain sensing response can be achieved; however, due to high filler loading the processing of nanocomposites and the physico-mechanical properties of polymer are comprised [7.19]. Innovative strategies are therefore needed to develop reversible electromechanical sensors with good flexibility, elongation at break and low hysteresis [7.6, 7.10, 7.12, 7.20-7.22]. To obtain desirable percolation behaviour as well as physico-mechanical properties, polymer alloying or blending is a useful approach [7.1, 7.23]. Percolation in percolation, selective percolation and multiple percolations of conducting fillers has been reported in several polymer blends and alloys [7.2, 7.24-7.25]. Recently, Yan et al reported development of graphene-nanocellulose nano paper based strain sensor that has applicability up to 100% strain [7.14]. In another study, Li et al have shown PDMS/graphene based strain sensor having exceptionally high gauge factor [7.18].

PTFE, a fluropolymer undergoes degradation on irradiation and turns into high quality free flowing PTFE powder after mechanical milling [7.18]. PTFE powder because of its very low coefficient of friction (COF) can act as solid internal lubricant and can be easily produced by using high-energy radiation [7.18]. There have been several investigations on improving mechanical and tribological properties of polymer through several approaches; however, the use of RPTFE has not been explored in such applications [7.14, 7.26]. Moreover, radiation crosslinking behaviour of PTFE filled crosslinking-type polymers is not yet investigated.

There has been considerable work on strain sensors; however, the use of high-energy radiation for the development of strain sensors is not explored. Likewise, the use of radiolytically degraded PTFE as reinforcing filler has not been yet investigated. This report presents some of the interesting results on radiation processed conducting nanocomposites, electromechanical sensors and RPTFE reinforced polymer composites.

7.2. MATERIALS AND METHODS

7.2.1. MATERIALS

Nano carbon nano black (NCB) (size 50 nm, surface area 70 m^2/g, density 1.8 g/cc) used in the present study was procured from TA Corporation, MUMBAI, India. Polydimethylsiloxane (Hardness=40±3 and density=1.13±0.05 g/cc) containing vulcanizator 2,5-dimethyl-2,5-bis(tert-butyl peroxy) hexane (0.65%), and no sensitizer or crosslinking agent procured from DJ Silicone, China was used as such. Xylene used for swelling and crosslinking density determination was of AnalaR grade (Purity > 99%). Teflon scrap (PTFE) in ribbon form generated during machining of Teflon rods was procured from local supplier M/s Max Tools Co. Mumbai. The scrap was washed with toluene followed by strong soap solution and finally dried prior to irradiation. The cleaned PTFE had a bulk density = 2.1 g/cc, Melting point=330°C and surface energy=22 mJ/m^2. Flurocarbon elastomer used was Viton® [66% fluorine; copolymer of vinylidene fluoride (VF2) and hexafluoropropylene (HFP)]. Graphene powder (graphene purity 95%, sheet thickness: 3-6 nm, average surface area: >200 m^2/gm, aspect ratio: 70, specific gravity: 2 gm/cc) was purchased from Otto Chemie Pvt Ltd, Mumbai India.

7.2.2. METHODS

7.2.3. Sample preparation and characterization

A series of composites were prepared by mixing the components homogeneously in Brabender plasticordar at desired temperatures, rpm and time. Weight of the components was carefully chosen by considering the bulk density of the components to get volume contribution with respect to the constituents, assuring proper filling of the mixing chamber. The homogeneous mix was cut to small pieces and compressed into sheets of size 12x12 cm of different thicknesses in range 1-4 mm using compression-moulding machine at 150 kg/cm^2 pressure for desired time and temperature.

7.2.4. Physico-mechanical properties

For tensile strength measurements, at least five dumbbell shaped specimens were cut from composite sheets using a steel die. The thickness of the samples was determined to the nearest of 0.1 mm. The tensile strength and elongation at break were measured by Hemetek universal testing machine using crosshead speed of 10 mm/min at room temperature.

7.2.5. X-ray diffraction (XRD) studies

XRD patterns were recorded using a Philips X-ray diffractometer PW 1710 (Almelo, Netherlands) using monochromatized CuK_α radiation from an X-ray generator operated at 30 kV & 20 mA.

7.2.6. Small angle x-ray scattering

The structural morphology of the composites has been investigated by SAXS using small angle goniometer mounted on Rigaku rotating anode x-ray generator. X-ray intensities I(Q) were recorded using a scintillation counter with pulse height analyzer by varying the scattering angle 2θ where Q (= 4.sin (θ) /λ) is the scattering vector, λ is the wavelength of incident x-rays of CuKα. The intensities were corrected for sample absorption and smearing effects of collimating slits [7.19].

7.2.7. DC Electrical conductivity

For DC conductivity measurement samples were punched out from composite sheets using stainless steel punch to get samples with aspect ratio (Diameter/Thickness)>10. The conductivity of the samples was measured by recording the resistance of the samples by a two-probe arrangement. For the samples having resistance higher than 10^6 ohms, a mega ohm meter was used. For ensuring good electrical contact, the surfaces of the specimens were polished with 800-grit sandpaper and conductive silver paste was placed between the electrodes and the specimens. For each composition, at least three specimens were tested. All measurements were performed at ~24°C and relative humidity of 55%.

7.2.8. AC Electrical conductivity

For AC conductivity measurement samples of cylindrical shape with circular area of 1.0 cm^2 were cut from compression moulded sheet of 1 mm thickness. Both sides of the samples were coated with conducting Ag paste. The dielectric measurements were performed on an Agilent 4294A Impedance Analyzer (USA) over the frequency range of 10^2-10^6 Hz at 25^{o}C.

7.2.9. Electromechanical measurements

Uniaxial stretching mechanical strain was applied to the nanocomposites and electrical resistance of the nanocomposites was measured via a computer-coupled multimeter having data acquisition rate of 0.5 sec^{-1} [7.11]. The contacts were made by applying conducting pastes on both sides of the samples. Different strain and strain rates were used for different experiments. Utmost care was taken to confirm that prior to measurements the samples were neither deformed nor under any preload stress. To overcome experimental constraints, the cyclic experiments were conducted between 3 and 8% (effective strain 5%) and 3 and 13% (10%) strain limits. The base line resistance used in the calculation corresponded to 3% strain. The gauge factor (GF) which reflects the sensitivity of a strain sensor was calculated using following relation.

$$GF = (\Delta R / R_0) / \varepsilon \qquad (7.1)$$

Where $\Delta R / R_0$ is relative change in the resistance; R_o reflects baseline strain resistance. and is the applied strain ($\Delta l/l_0$). It may be noted that GF depends on both intrinsic piezoelectric effect and geometric factors. The relationship between these factors and GF can be described as

$$GF = (\frac{\Delta R / R}{\varepsilon}) = \frac{\Delta \rho / \rho_0}{\varepsilon} + 1 + 2\upsilon \qquad (7.2)$$

Where ν is Poisson's ratio & ρ_0 the baseline electrical resistivity [7.28]. For elastomers, the Poisson ratio is generally close to 0.5, which suggests that GF >2 reflects contributions from electromechanical factors [7.1, 7.23].

7.3. RESULTS AND DISCUSSION

7.3.1. Development of high performance composites for PTC/NTC applications using selective percolation in thermoplastic alloys

A multiphase polymer composite consisting of two incompatible polymers polycaprolactam/EVA) and a conducting filler (NCB) having preferential percolation in one of the polymers was synthesized (figure 7.1). Figure 7.2 represents the variation in the conductivity with the variation of EVA/polycaprolactam blend composition for different carbon black (CB) loading. The observed U-shape resistivity behaviour of incompatible polymer blends has been reported for other systems as well. There are however not many studies reporting the variation in the compositional dependent U-shape conductivity behaviour. It can be seen from the figure that at 10 wt% CB loading, the conductivity could be observed for the composites having polycaprolactam volume fraction 50% or more, whereas at 25 wt% CB loading substantial conductivity over the entire composition range was observed. The conductivity of the blends with 30 wt% CB loading was higher than that of 25 wt% loading at all compositions; however the difference was not as high as was observed between 10 wt% and 25 wt% loading. This observation suggests that the selective localization of CB in incompatible blends, strongly depends on the blend composition, and percolation can be achieved at low CB loading by carefully architecting the blend morphology. The analysis of interfacial tension by Wu's equation predicted the localization of CB at the interface.

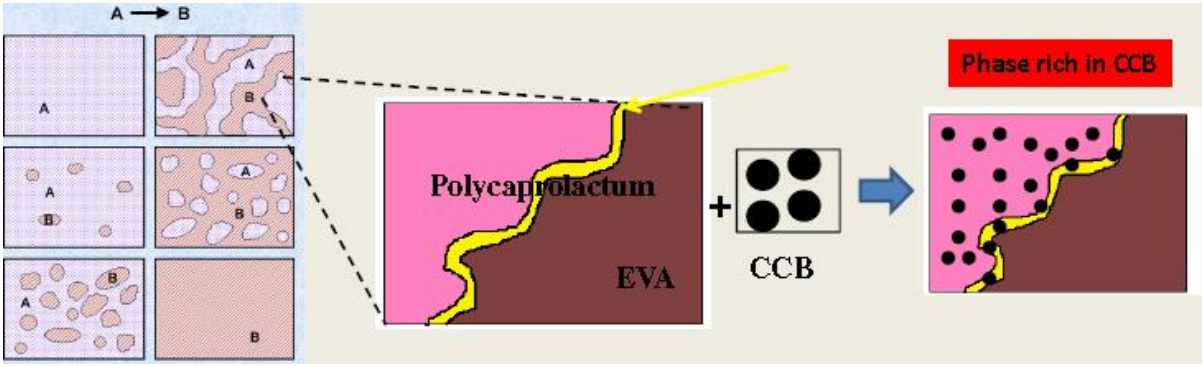

FIG.7.1. Schematic representation of selective percolation

Though it does not predict the percolation in the matrix, it can be safely concluded that even in the system where CB is expected to localise at the interface; anomalous behaviour of conductivity is observed as percolation is a function of both, the interfacial length/structure and filler volume fraction. It may be noted that by incorporating interfacial length and other morphological parameters into experimental design, better physico-mechanical properties along with the targeted conductivity behaviour can be achieved, e.g. the properties of EVA/polycaprolactam blends having pre-dominantly one component are much better than those in the intermediate composition range, both in terms of mechanical and electrical properties.

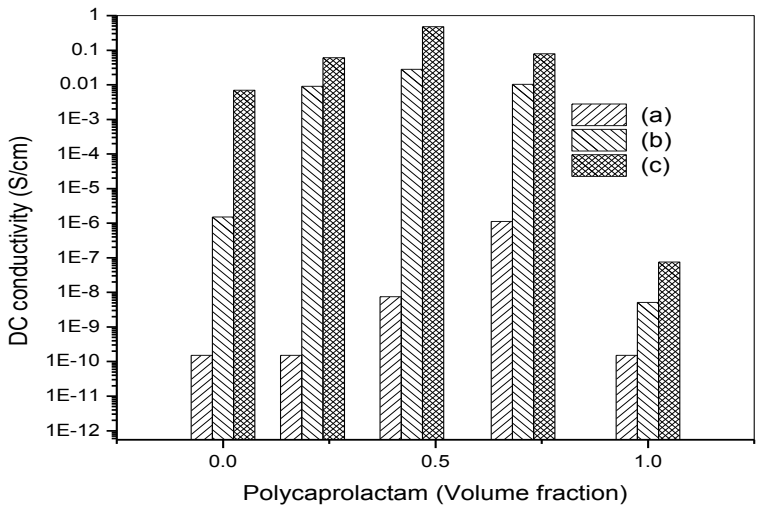

FIG.7.2. Variation of DC conductivity with blend composition (a) 10wt% CB (b) 25wt% CB (c) 30wt% CB

Figure 7.3 shows SAXS curves of binary and ternary composites. It can be seen from the profiles that polycaprolactam/CB composites have the highest scattering intensity, whereas the ternary composites having 3:1 polycaprolactam/EVA composition has the lowest scattering intensity. Since the variation between the densities ($\Delta\rho$) of amorphous and crystalline fraction of EVA and polycaprolactam is significant (0.082 g/cc and 0.146 respectively), the interface region in the blends may play a crucial role in the overall small angle x-ray scattering. As polycaprolactam/EVA system is expected to be highly immiscible and therefore the SAXS profiles in the high-Q region will be governed by the following relation

$$\log_{q\to\infty} q^4 I_q = k \qquad (7.3)$$

However, if there is any miscibility between the components at some composition, or if CB is modifying the interaction between polycaprolactam and EVA, an interface layer is expected to exist and the SAXS pattern is expected to follow following relation

$$\log_{q\to\infty} q^4 I_q = k \exp(-{\sigma_{int}}^2 q^2) \qquad (7.4)$$

The variation of ln $(q^4 I_q)$ with q^2 is shown in figure 7.3. In all composites, flattening of the curve was observed as q increases, suggesting these composites can be approximated as ideal binary system and there is no signature of interface layer (σ_{int}) between polycaprolactam and EVA phases.

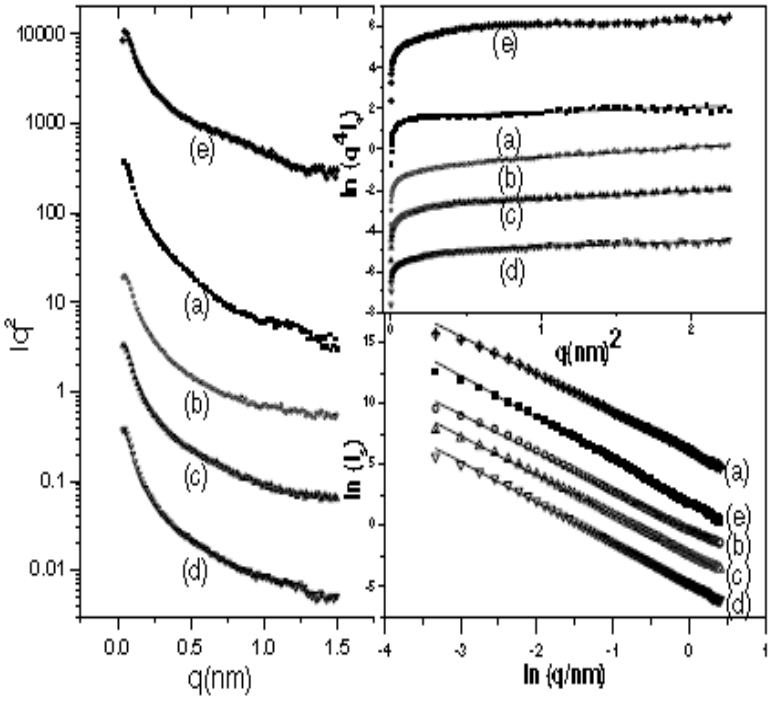

FIG.7.3. Small angle X-ray profiles of polymer composites (1) Variation of $q^2 I_q$ with q (2) Variation of ln $(q^4 I_q)$ with q^2 (a) EVA/CB 30 wt% (b) EVA/polycaprolactam (3:1)/CB 30 wt% (c) EVA /polycaprolactam (1:1)/CB 30 wt% (d) EVA /polycaprolactam (1:3)/CB 30 wt% (e) Polycaprolactam/CB 30 wt%

The scattering pattern was therefore attributed to the carbon black aggregates, as CB is known to demonstrate surface fractal decay with the increase in scattering vector. The polycaprolactam/EVA/CB composites have the lowest value of k whereas the polycaprolactam/CB and EVA/CB systems have much higher values of k, indicating significant variation in the phase structure of the composites during blend formation; more importantly, all the composites had positive slopes . This finding suggests that the equation is not applicable in this system, and the composites have sharp interfaces and do not contain diffuse boundaries.

The SAXS profiles displayed on log-log scale show linear variation indicating a power-law behaviour for the intensity $I(Q) \sim Q^{-\alpha}$. The magnitude of the exponent (or Porod index) α

provides the information about the morphology of the system as well as about the fractal dimension D_s was estimated by fitting the SAXS data . For the composites of this study, the values of α were found to be in the range of 3.5-3.1, suggesting morphology of the agglomerates can be approximated between flaky and spherical. The linear behaviour of the profiles as plotted on log-log scale spanning more than a decade of Q-range also suggests a surface fractal nature of the domains signifying rough surfaces [7.29-7.30]. The fractal dimension Ds (6-α) represents the extent of roughness. Thus, the value of 2 for Ds (that is $\alpha = 4$) indicates perfectly smooth surface for the scattering domains. In order to obtained the structural parameters, the data has been fitted to modified Debye type function [7.31]

$$I_q = \frac{I_0}{[1 + \frac{1+\alpha}{3}(Rq)^2]^{-\alpha/2}} \tag{7.5}$$

Where R is the average size of the domains and α is Porod index. R was found to be the in range 47-60 nm for the EVA/polycaprolactam/CB composites and this order of magnitude is higher than the values predicted from the additive rule; clearly pointing out that the CB distribution in blends is very different from that in individual polymers.

The EVA /polycaprolactam (3:1)/NCB 30 wt% nanocomposites were crosslinked at 200 kGy. Figure 7.4 shows the effect of temperature on the relative change in resistance for crosslinked and un-crosslinked composites. It can be seen from the figure that for un-crosslinked samples positive temperature coefficient (PTC) was observed up to 120^{o}C followed by negative temperature coefficient (NTC). On the other hand, there was no NTC effect in the crosslinked nanocomposites, reflecting the suitability of the composites for PTC devices.

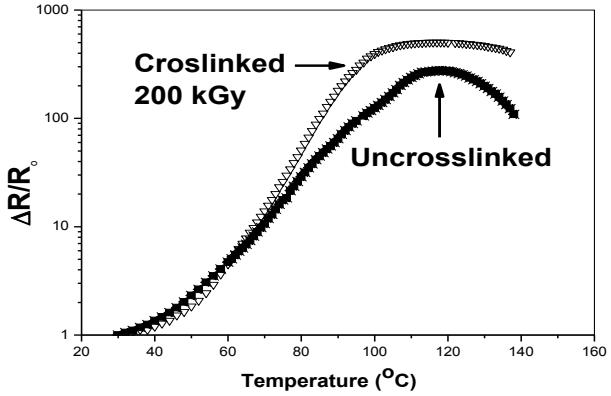

FIG.7.4. PTC transition in crosslinked (200 kGy) and pristine polycaprolactam/EVA nanocomposites (EVA /polycaprolactam (3:1)/CB 30 wt%)

Preferential percolation is a promising strategy to develop conducting composites at lower loading of conducting filler; however little information is available on temperature dependence of conductivity of such composites. This study reports synthesis and positive temperature coefficient (PTC) behaviour of a novel multiphase polymer composite in which conducting filler preferentially percolates in a composite containing two incompatible polymers, both having glass transition in the temperature range of study. High electrical conductivity and good mechanical behaviour was demonstrated by acrylonitrile butadiene styrene (ABS)/polycaprolactam (PCL)/nano carbon black (NCB) composites, which was dependent on blend composition as well as on the extent of NCB loading (figure 7.5). The ternary composites showed inverted U shape conductivity curves at 30 wt% NCB which relatively flattened at 50 wt% loading. Glass transition of PCL phase largely remained unaffected though slight compositional dependence in glass transition temperature of ABS was observed. PTC intensity was considerably less for ternary composites than for binary ABS/NCB or PCL/NCB composites. Theoretical analysis of the dispersion state of NCB in this phase-separated system revealed preferential distribution of NCB in ABS domain. PTC effect was also found to decrease significantly with increase in NCB content. ABS/PCL/NCB (1:1:2) composites showed no significant temperature dependence (zero positive coefficients) up to 413K while ABS/NCB 30 wt% NCB composites showed highest PTC. A sudden rise was observed in the glass transition region of polymers for all composites; however, the effect was less pronounced for ternary composites (figure 7.6).

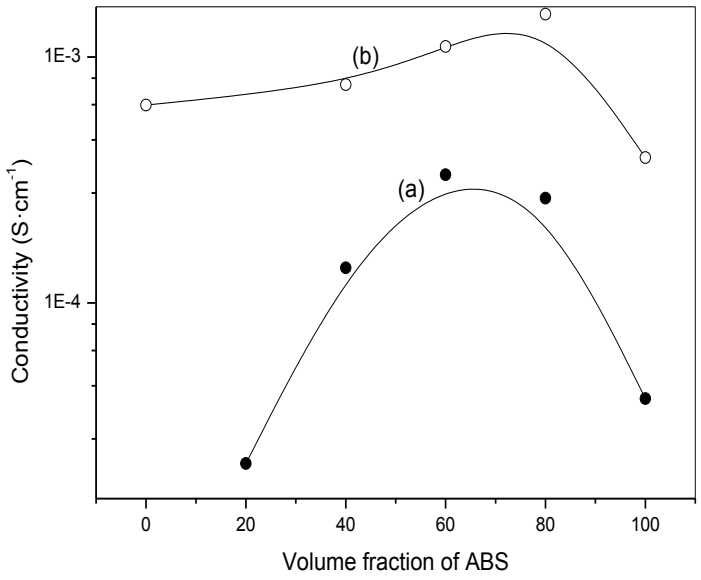

FIG.7.5. Variation of DC conductivity with blend composition for (a) 30% NCB (b) 50% NCB

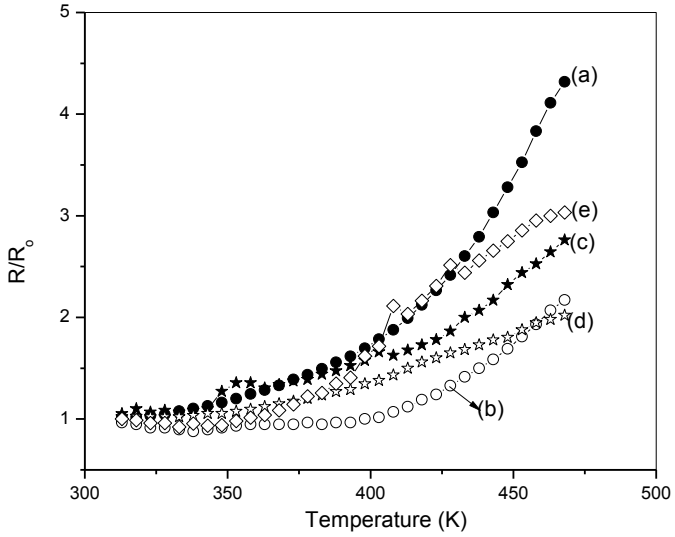

FIG.7.6. Temperature dependence of electrical conductivity for the composites containing 50wt% NCB (a) ABS 0% (b) ABS40% (c) ABS 60% (d) ABS 80% (e) ABS 100%.

7.3.2. Filler-matrix and inter-filler interactions in EVA/RPTFE/organoclay nanocomposites

Ethylene vinyl acetate (EVA) has many commercial applications; and has been reported to be crosslinked easily, using high-energy radiation. High energy, 10 MeV electron beam accelerator was used for the crosslinking of EVA and its composites. The composites of EVA, poly(tetrafluoroethylene) micro-particles (PTFEMP) and organoclay were prepared in different proportions by melt compounding and their structural morphology, mechanical hysteresis, surface wetting and thermal behaviour were studied. Incorporation of PTFEMP and organoclay in EVA led to increase in mechanical hysteresis. SAXS results showed that interfacial interactions were minimal between EVA and PTFEMP which were observed to be quite strong in EVA/organoclay composites. Further experiments are in progress to understand the effect of radiation on polymer-nanofiller interaction. Mechanical properties of ternary composites demonstrated high synergy between fillers, leading to manifold increase in the modulus of dual filler filled composites in comparison to single filler systems (figure 7.7). Melt viscosity of EVA increased substantially on the addition of either of the fillers. X-ray diffraction studies revealed around 10% intergallery expansion in organoclay (figure 7.8). For composites with high loading of PTFEMP; the crystallinity of EVA was not affected [7.4].

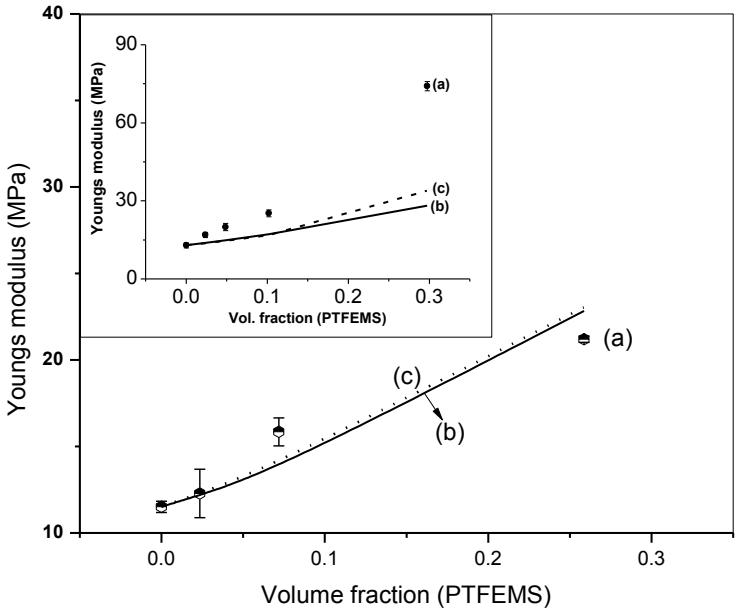

FIG.7.7. Stress-strain profiles for EVA/Organoclay (5%) composites having different loading of PTFEMP (a) 5% (b) 10% (c) 20% (d) 50% Inset: Effect of organoclay loading on modulus (a) EVA (b) EVA/PTFEMP (15%) composites

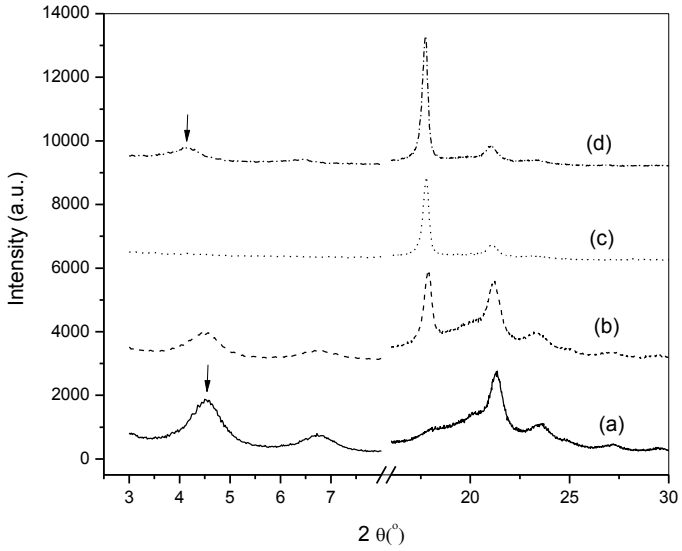

FIG.7.8.WAXRD profiles of composites (a) $EV_{0.10}^{0.00}$ *(b)* $EV_{0.10}^{0.15}$ *(c)* $EV_{0.00}^{0.50}$ *(d)* $EV_{0.05}^{0.50}$ *(subscript denotes organoclay weight fraction; superscript denotes RPTFE weight fraction)*

7.3.3. Development of electron beam crosslinked PDMS/PTFEMP composites with low coefficient of friction and high elastic modulus

Crosslinked composites were synthesized via internal compounding of Polydimethylsiloxane and Polytetrafluoroethylene micro-powder (PTFEMP) in various proportions and subsequently crosslinking to different extent by electron beam irradiation. The PTFE micro-powder was generated by degrading PTFE ribbons using gamma radiation in presence of

CCl_4. Elastic modulus is one of the most important properties of crosslinked polymers; it has been reported to have direct correlation with crosslinking density and provides an estimate of the resistance to elastic deformation [7.32]. Elastic modulus of PDMS/PTFEMP composites increased significantly with the increase in the radiation dose as well as with increase in PTFEMP fraction (figure 7.9) as reported earlier for other filled elastomeric and polymeric systems [7.33-7.35]. The composites showed greater increase in elastic modulus than pure PDMS. Polymer-filler interaction, XRD and FTIR investigations reflected complex changes in composites during compounding and radiation crosslinking. PTFEMP loading didn't affect contact angle much but significantly reduced coefficient of friction for composites.

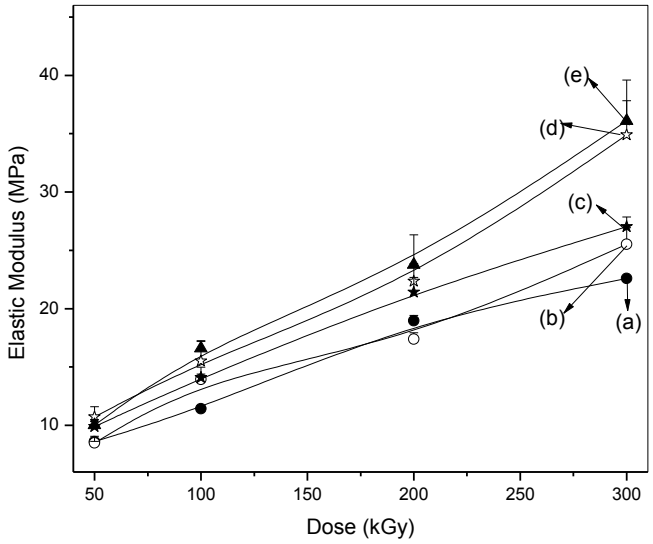

FIG.7.9. Variation in elastic modulus of un-irradiated PDMS/PTFEMP composites loaded to different extent of PTFEMP (a) 0% (b) 5% (c) 10% (d) 15% (e) 20%

Interestingly, with increase in radiation dose, filled composites showed greater increase in the elastic modulus than unfilled PDMS. Relative increase was about three times for unfilled PDMS whereas PDMS containing 20 wt % PTFEMP showed increase of about 3.6 times, when radiation dose increased from 50 to 300 kGy. Such synergistic effect might be attributed to the positive interaction through chemical bonding between PTFEMP and PDMS chains. PTFEMP has very low surface energy [7.36] and therefore their interactions with PDMS matrix are expected to be weaker; however, as reflected from polymer filler interaction studies (presented in the next section), PTFEMP was found to significantly reinforce the PDMS matrix.

7.3.3.1.Polymer-filler interaction and density

One of the most plausible explanations for the increase in the elastic modulus of PDMS/PTFEMP composites with PTFEMP loading might be good interactions between PTFEMP and PDMS interfaces. Therefore, interactions between PTFEMP and PDMS were assessed using Kraus equation:

$$\frac{V_{ro}}{V_{rf}} = 1 - m\left(\frac{\phi_f}{1-\phi_f}\right) \tag{7.6}$$

Where V_{ro} is the volume fraction of the polymer in the swollen rubber, V_{rf}, volume fraction of polymer in the swollen filled system and ϕ_f is the volume fraction of the filler in the filled composite [7.34]. To access the polymer filler interaction, V_{ro}/V_{rf} was plotted against $\phi_f/(1-\phi_f)$. A linear profile with negative slope obtained suggested high reinforcement by filler. The polymer-filler interaction parameter C (Kraus constant) was calculated using the Kraus equation (equation 7.7) by putting "m" value obtained from plotting suitable parameters of equation (7.6)

$$C = \frac{m - V_{r0} + 1}{3(1 - V_{r0}^{1/3})} \tag{7.7}$$

The negative slope for composites implied positive polymer filler interaction. The C value for the system was found to be 1.1± 0.2. This suggests that in the weight fraction range of present study PTFEMP is reinforcing the PDMS matrix.

7.3.3.2.Development of radiation processed strain sensors

For polymer nanocomposite based strain sensors, selection of suitable polymer matrix is a very critical aspect which determines the performance and application range of the strain sensor. Fluorocarbon elastomers (FCE) have excellent resistance to extreme temperatures and chemical environment and therefore can be used in several higher end applications [7.37-7.39]. A fluorocarbon elastomer (FCE)/nanocarbon black (NCB) nanocomposites based strain sensor was developed and the effect of network density on the AC and DC conductivity as well as on the electromechanical performance of the sensor was investigated. Nanocomposite matrices with different network densities were achieved by irradiating with high energy radiation from Co-60 gamma source for different doses. No change in conductivity was observed up to 0.20 weight fraction of the NCB and there was a sharp rise in the electrical conductivity thereafter. The conductivity behaviour of the composites is often governed by a power law given by following equation [7.40]

$$\sigma = \sigma_f (V_f - V_c)^t \tag{7.8}$$

Where V_f is the volume fraction of the filler, V_c is the percolation threshold, σ_f is the filler conductivity and t is the critical exponent. Resistance of the composites increased almost linearly with strain till elongation at break, however, the rise in the region close to EB was much steeper (figure 7.10). The highest range during which change in resistance varied linearly with applied strain was observed for the composites irradiated to 25 kGy (before gel point), though the relative change in resistance (slope) was significantly less in comparisons to composites having higher network density.

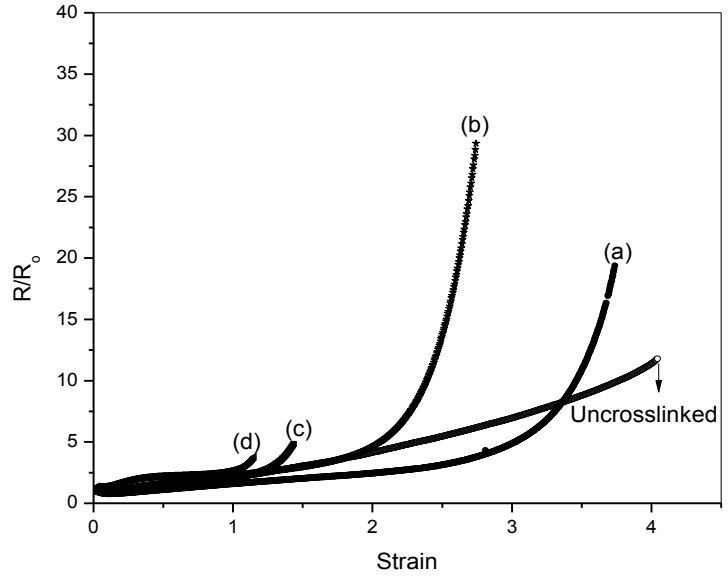

FIG.7.10. Variation in relative resistance of nanocomposite with 0.35 weight fraction of NCB crosslinked to different extent with strain (a) 73 μmol/g (b) 290 μmol/g (c) 415 μmol/g (d) 440 μmol/g

As the response for at all network density was linear in 10-50% strain range and since all samples have EB>50%, the gauge factor in this range was calculated for different samples to understand the effect of network density on the strain sensing response. It can be seen from the figure 7.11 that gauge factor (GF) is low for FCE irradiated to 25 kGy and is high for samples irradiated to 100 kGy (290 μmol/g) and decreased slightly thereafter. This trend can be attributed to three factors (i) change in conductivity with increase in network density and the percolation threshold for the filler (ii) elongation at break of the composite i.e. maximum strain that it can sustain without failing (iii) Change in filler aggregation-disaggregation dynamics due to increase in network density. Bautista-Quijano et. al. have recently reported GF in the range 0.48-0.73 for MWCNT-polysulfone films, depending on the MWNT fraction [7.20]. On the other hand Ferrreira et. al. has investigated strain sensing response of poly(vinylidene fluoride)/carbon nanotubes based sensor where GF of ~4 has been reported though the strain range is relatively small [7.21]. For strain sensing application, the reversibility of resistance change is a desirable attribute [7.5, 7.22, 7.25]. To check the variations in the strain change under cyclic load; the composites with different network densities were exposed to 10% cyclic strain. The resistance was normalized with respect to the baseline strain resistance. It can be seen from figure 7.11 that for 5% strain, the composite irradiated to 50 kGy (73.2 μmol/g) showed perfectly reproducible response and there was no change in residual resistance and peak resistance. The change in resistance during this range was ~50% and gauge factor was ~10. For 10%, strain in the same composites again the response was highly stable and again there was no significant difference in residual and peak strain. The resistance change was around 102% and gauge factor was around 10.2. For composite irradiated to a dose of 200 kGy (415 μmol/g) for 5% strain, a different strain sensing response was observed. For every strain cycle, two peaks were observed and the peak and residual resistance changed every next cycle. Relative change in resistance was ~44 % and the gauge factor ~ 8.8. For 10% strains also two peaks were observed with the resistance change ~112 % and gauge factor of ~11.2. These results indicate 50 kGy is the optimal radiation dose for cyclic strain sensing applications.

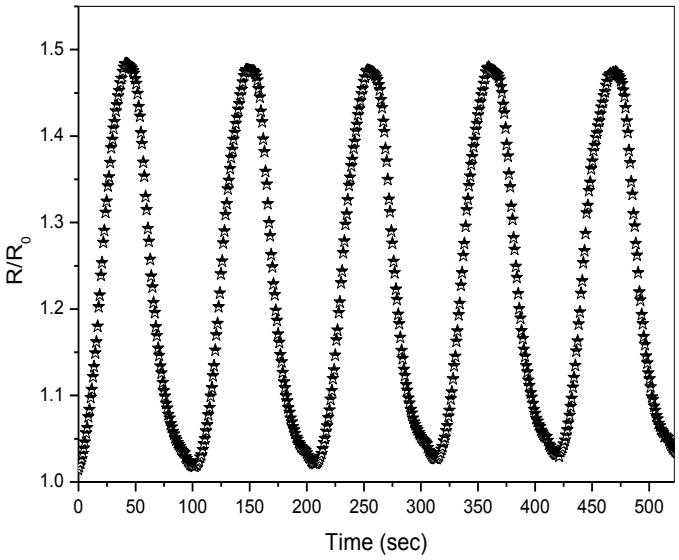

FIG.7.11. Sensing response of nanocomposite with 0.35 weight fraction of NCB irradiated to 50kGy at 5% strain at strain rate of 1mm/min

7.4. CONCLUSIONS

A FCE/NCB nanocomposites based strain sensor was developed. Nanocomposites of different network densities were obtained using high energy gamma radiation. The density of crosslinked networks was found to have a profound effect on the sensing range as well as on the gauge factor. Cyclic strain sensing response was also found to be affected by network density and best results were observed for the network density of 73.2 μmol/g. Ethylene vinyl acetate/polycaprolactam /carbon black composites showed excellent conducting behaviour and the percolation threshold of NCB in blends was found to be much lower than the percolation thresholds of NCB in the constituent polymers. Crystallographic parameters of the components did not significantly change on composite formation; however increase in the crystallinity of the polycaprolactam phase with increase in its content in the blend was observed, contributing to the increased conductivity of the ternary composites. The results from EVA and PDMS matrix suggest that radiation degraded PTFE can act as reinforcing filler. These results indicate that high energy radiation can be an effective tool for the property enhancement of conducting nanocomposites and to develop high modulus nanocomposites for various sensing, electrical and structural applications.

REFERENCES TO CHAPTER 7

[7.1] DUBEY, K.A., BHARDWAJ, Y.K., CHAUDHARI, C.V., GOEL, N.K., SABHARWAL, S., RAJKUMAR, K., CHAKRABORTY, S.K., Radiation effects on Styrene-butadiene-Ethylene propylene diene monomer-multiple walled carbon nanotube nano-composites: Vulcanization and characterization. Polym Adv Technol. 22 (2011) 1888.

[7.2] SINHA, S.K., DUBEY, K.A., GROVER, V.G., SASTRY, P., BHARDWAJ, Y.K., PANICKER, L., TYAGI, A.K., MAHANWAR, P.A., BAMBOLE, V.A.,. Selective

interfacial localization in conducting polycaprolactam/ethylene vinyl acetate/carbon black composites, Polym Composites **34** 6 (2013) 912.
[7.3] PRASAD, K.E., DAS, B., MAITRA, U., RAMAMURTY, U., RAO, C.N.R., Extraordinary synergy in the mechanical properties of polymer matrix composites reinforced with 2 nanocarbons, Proc Natl Acad Sci U S A. **106** 32 (2009) 13186.
[7.4] DUBEY, K.A., MAJJI, S., SINHA, S.K., BHARDWAJ, Y.K., ACHARYA, S., CHAUDHARI, C.V., VARSHNEY, L., Synergetic effects of radiolytically degraded PTFE microparticles and organoclay in PTFE-reinforced ethylene vinyl acetate composites, Mater Chem Phys **143** (2013) 149.
[7.5] SHYR, T.W., SHIE, J.W., JIANG, C.H., Li, J.J., A Textile-based wearable sensing device designed for monitoring the flexion angle of elbow and knee movements, Sensors **14** 3 (2014) 4050.
[7.6] NOH, T.K., RYU, U.C., LEE, Y.W., Compact and wide range polarimetric strain sensor based on polarization-maintaining photonic crystal fiber, Actuat A-Phys. **213** (2014) 89.
[7.7] RORIZ, P., CARVALHO, L., FRAZAO, O., SANTOS, J.L., SIMOES, J.L., From conventional sensors to fibre optic sensors for strain and force measurements in biomechanics applications: A review, J Biomech **47** 6 (2014) 1251.
[7.8] FERNBERG, P., NILSSON, G., JOFFE, R., Piezoresistive performance of long-fiber composites with carbon nanotube doped matrix, J Intel Mat Syst Str. **20** 9 (2009) 1017.
[7.9] ALAMAUSI, HU, N., FUKUNAGA, H., ATOBE, S., LIU, Y., LI, J., Piezoresistive strain sensors made from carbon nanotubes based polymer nanocomposites, Sensors **11** 11 (2011) 10691.
[7.10] WANG, Y., WANG, A.X., WANG, Y., CHYU, M.K., WANG, Q.M., Fabrication and characterization of carbon nanotube–polyimide composite based high temperature flexible thin film piezoresistive strain sensor, Sensor Actuat A-Phys. **199** (2013) 265.
[7.11] COSTA, P., SILVA, J., ANSON-CASAS, A., MARTINEZ, M.J., ABAD, M.J., VIANA, S., LANCEROS-MENDEZ, S., Effect of carbon nanotube type and functionalization on the electrical, thermal, mechanical and electromechanical properties of carbon nanotube/styrene-butadiene-styrene composites for large strain sensor applications, Compos Part B Eng. **61** (2014) 136.
[7.12] FESTIN, N., PLESSE, C., PIRIM, P., CHEVROT, C., VIDAL, F., Electro-active Interpenetrating Polymer Networks actuators and strain sensors: Fabrication, position control and sensing properties, Sensor Actuat B-Chem. **193** (2014) 82.
[7.13] SAFDARI, M. AL-HAIK, M., Electrical conductivity of synergistically hybridized nanocomposites based on graphite nanoplatelets and carbon nanotubes, Nanotechnology **23** 40 (2012) 405202.
[7.14] YAN, C., WANG, J., KANG, W., CUI, M., WANG, X., FOO, C.Y., CHEE, K.J., LEE, P.S., Highly stretchable piezoresistive graphene-nanocellulose nanopaper for strain sensors, Adv Mater. **26** 13 (2014) 2022.
[7.15] ZHAO, X., ZHAO, J., CAO, J.P., WANG, D., HU, G.H., CHAN, F., DANG, Z.H., Effect of the selective localization of carbon nanotubes in polystyrene/poly(vinylidene fluoride) blends on their dielectric, thermal, and mechanical properties, Mater Des. **56** (2014) 807.
[7.16] STOYANOV, H., Mc CARTHY, D., KOLLOSCHE, M., KOFOD, G., Dielectric properties and electric breakdown strength of a subpercolative composite of carbon black in thermoplastic copolymer, Appl Phys Lett. **94** 23 (2009) 232905.

[7.17] HINDERMANN-BISCHOFF, M., EHRBURGER-DOLLE, F., Electrical conductivity of carbon black–polyethylene composites: Experimental evidence of the change of cluster connectivity in the PTC effect, Carbon **39** 3 (2001) 375.
[7.18] LI, X., ZHANG, R., YU, W., WANG, K., WEI, J., WU, D., CAO, A., LI, Z., CHENG, Y., ZHENG, Q., RUOFF, R.S., ZHU, H., Stretchable and highly sensitive graphene-on-polymer strain sensors, Sci Rep. **2** (2012) 870.
[7.19] TERASAWA, N., TAKEUCHI, I., Electrochemical and electromechanical properties of carbon black/carbon fiber composite polymer actuator with higher performance than single-walled carbon nanotube polymer actuator, Electrochimica Acta. **123** (2014) 340.
[7.20] BAUTISTA-QUIJANO, B.R., AVILES, F., AGUILAR, J.O., TAPIA, A., Strain sensing capabilities of a piezoresistive MWCNT-polysulfone film, Sensor Actuat A-Phys. **159** 2 (2010) 135.
[7.21] FERREIRA, A., ROCHA, J.G., ANSON-CASOS, A., MARTINEZ, M.T., VAZ, F., LANCEROS-MENDEZ, S., Electromechanical performance of poly(vinylidene fluoride)/carbon nanotube composites for strain sensor applications. Sensor Actuat A-Phys. **178** (2012) 10.
[7.22] COSTA, P., FERREIRA, A., SENCADAS, V., VIANA, J.C., LANCEROS-MENDEZ, S., Electro-mechanical properties of triblock copolymer styrene butadiene–styrene/carbon nanotube composites for large deformation sensor application, Sensor Actuat A-Phys. **201** (2013) 135.
[7.23] DUBEY, K.A., BHARDWAJ, Y.K., CHAUDHARI, C.V., SABHARWAL, S., LDPE/EVA/PCR/MWNT nanocomposites: Radiation crosslinking and physicomechanical characteristics, Polym Composite. **32** 5 (2011) 737.
[7.24] NAIR, A.B., KURIAN, P, RANI, J., Effect of expanded graphite on thermal, mechanical and dielectric properties of ethylene–propylene–diene terpolymer/hexa fluoropropylene–vinylidinefluoride dipolymer rubber blends, Eur Polym J. **49** 1 (2013) 247.
[7.25] JI, M., DENG, H., YAN, D., LI, X, DUAN, L., FU, Q., Selective localization of multi-walled carbon nanotubes in thermoplastic elastomer blends: An effective method for tunable resistivity–strain sensing behaviour, Compos Sci Technol. **92** (2014) 16.
[7.26] MAJJI, S., DUBEY, K.A., MONDAL, R.K., BHARDWAJ, Y.K., ACHARYA, S., VARSHNEY, L., Development of electron beam cross-linked PDMS/PTFEM composites with low coefficient of friction and high elastic modulus. Polym-Plast Technol, **53** 5 (20140 435.
[7.27] SCHMIDT, P.W., HEIGHT, R., Acta Cryst **13** (1960) 480.
[7.28] WINDOW, A.L., HOLISTER, G.S., (Eds.), Strain Gauge Technology, Elsevier Applied Science, London, (1992).
[7.29] MARTIN, J.E., HURD, A.J., Scattering from fractals, J Appl Crystallogr. **20** 2 (1987) 61.
[7.30] TEIXEIRA, J., Small-angle scattering by fractal systems, J Appl Crystallogr. **21** 6 (1988) 781.
[7.31] DEDYE, P., ANDERSON, H.R., BRUMBERGER, H., Scattering by an inhomogeneous solid 2: The correlation function and its application, J Appl Phys. 28 6 (1957) 679.
[7.32] MAKUCCHI, K., CHENG, S., (Eds.), Radiation Processing of Polymer Materials and its Industrial Applications, John Wiley & Sons, Inc., New Jersey (2012) 201 pp.
[7.33] NIELSEN, L.E., Generalized equation for the elastic moduli of composite materials, J Appl Phys. **41** 11 (1970) 4626.

[7.34] PERRAUD, S., VALLAT, M.F., DAVID, M.O., KUCZYNSKI, J., Network characteristics of hydrogenated nitrile butadiene rubber networks obtained by radiation crosslinking by electron beam, Polym Degrad Stabil. **95** 9 (2010) 1495.
[7.35] SABET, M., HASSAN, A., RATNAM, C.T., Electron beam irradiation of low density polyethylene/ethylene vinyl acetate filled with metal hydroxides for wire and cable applications, Polym Degrad Stabil. **97** 8 (2012) 1432.
[7.36] BRADY, R.F. Jr., Fluoropolymers, Chem Brit. **26** (1990) 427.
[7.37] BALACHANDRAN, A., PHILIP, N.K., RANI, J., Effect of expanded graphite on thermal, mechanical and dielectric properties of ethylene–propylene–diene terpolymer/hexa fluoropropylene–vinylidinefluoride dipolymer rubber blends, Eur Polym J. **49** 1 (2013) 247.
[7.38] DROBNY, J.G., (Ed.), Technology of Fluoropolymers, 2nd Edition, William Andrew Publishing, (2013) 149 pp.
[7.39] SINHA, N.K., MUKHOPADHYAY, R., RAJ, B., Mechanical behaviour of fluoroelastomer considering long term ageing, Nucl Eng Des. **254** (2013) 89.
[7.40] LUX, F., Models proposed to explain the electrical conductivity of mixtures made of conductive and insulating materials, J Mater Sc. **28** 2 (1993) 285.

Chapter 8

RADIATION-ENGINEERING OF ALL PLASTIC NANOCOMPOSITE FILMS

C. DISPENZA, M.A. SABATINO, S. TODARO, S. ALESSI, G. SPADARO
Dipartimento di Ingegneria Chimica,
Gestionale, Informatica, Meccanica,
Università degli Studi di Palermo,
Palermo

C. DISPENZA
CNR - Istituto di Biofisica (Palermo unit),
Palermo

Italy

Abstract

In recent years, polymer nanocomposites have fascinated scientists, engineers and industrialists on the premise that the creation of new and more performing polymeric materials is possible by the combination of different building blocks with controlled dimensions at the nanoscale. Unfortunately, uniform dispersion of the hetero-phase domains within the plastic matrix or on its surface often fails due to the unfavorable thermodynamics, thus resulting in migration and irreversible aggregation phenomena. *In-situ* generation of a dispersed hetero-phase within the same polymer matrix or in its precursors increases the chances of achieving a better control of morphology by eliminating the often critical harvesting and re-dispersion steps in the manufacturing process. Strong interaction at the interface must be also provided to avoid aggregation and coarse phase-separation in usage.
With this purpose, radiation grafting of a functional monomer onto polypropylene film has been applied to modify the molecular structure and properties of the otherwise chemically inert film. The radiation-grafted film has become permeable to the precursors of polymerization of a conducting polymer, namely polyaniline that can grow as a thin skin from its surface as well as an interpenetrated network into the film. Chemical attachment of the conducting polymer to the polyolefin has been demonstrated. The nanocomposite film shows an increase of electrical conductivity of several orders of magnitudes and amenability to be used as flexible electrode. In consideration of the well-known possibility of controlling the extent and depth of chemical modification of a substrate by radiation grafting, by tuning both system composition and irradiation conditions, this approach can enable a good degree of control of the morphology of the heterophase that forms on or within the substrate and thereby of the nanocomposite film.
The recourse to suitable carriers, as chaperones of active molecules or nanoparticles into structurally different polymer matrices, is another possible strategy to obtain more uniform and stable dispersions. For this purpose, the possibility of obtaining colloidally stable micro-/nanoparticles from a partially degalactosylated xyloglucan (Deg-XG) has been investigated. ^{60}Co γ-irradiation was applied to reduce the size of polymeric clusters in water. Irradiation was performed on the solid powder in air, up to a maximum dose of 60 kGy. FTIR and GPC analyses do not evidence any significant change of functional groups of the polymer and its average molecular weight, respectively. Deconvolution of GPC curves point to a change in the proportion between two main fractions of different molecular weight clusters, with a prevailing contribution of the lower over the higher MW clusters at the increase of the absorbed dose. Aqueous dispersions of the irradiated materials at low concentrations were characterized by dynamic light scattering measurements as function of the time and at different temperatures. For all systems an increase of scattered light intensity as function of the time at 37°C was observed. The fastest kinetics and the highest pseudo-plateau were shown by the 20 kGy irradiated system. Globular particles with 300-400 nm hydrodynamic diameters are formed. Their propensity to incorporate hydrophobic small guest molecules or high molecular weight biomolecules

was assessed. The possibility of preparing optically transparent films from native xyloglucan incorporating these particles by solvent casting was demonstrated.

8.1. INTRODUCTION

In recent years, nanocomposites have fascinated scientists, engineers and industrialists on the premise that the creation of new and more performing materials is possible by the combination of very different building blocks with controlled dimensions in the nanosize region. For example, metal or metal-oxide nanoparticles or thin coatings have been combined with organic polymers as matrices or substrates in order to exploit the electrical, optical, catalytic or mechanical properties (hardness, high elastic modulus, etc.) of the inorganic component with the low specific weight, good processability, flexibility and toughness of the polymer. All-plastic hybrids have been conceived to exploit the different properties of structurally different polymers in a single construct. However, there are still technical limitations and challenges for polymer nanocomposites production on a commercial scale, since it requests material composition consistency and reliability.

Unfortunately, uniform dispersion of nanoparticles within a plastic matrix or on a plastic surface often fails and for a number of reasons. Nanoparticles, after synthesis in a solvent medium, are harvested as larger structures of conjoined aggregates in the dry form or, if transported and stored in the dispersed state, they may undergo flocculation and sedimentation with time. Once formed, these agglomerated particles are very difficult to break up during the compounding process, with the result that the properties of the final material are well below their potential. Even if colloidal stability is achieved or re-dispersion proves to be successful in compounding, the problem remains that a plastic nanocomposite in which nano-scale hetero-phases are dispersed in the polymer matrix generating a huge amount of interfacial area is far away from its preferred state of thermodynamic equilibrium for the polymer. Polymeric chains at the interface experience conformational restraints that can be freed by phase separation during processing, with the help of the shear forces that occur in the flow (e.g in extrusion or injection molding), or during the product life-time if the polymer chains gain sufficient mobility upon heating, by solvent uptake, or by molecular degradation.

In-situ generation of the dispersed phase within the same polymer matrix or its precursors increases the chances of achieving a uniform distribution of nanoparticles, by eliminating the often critical harvesting and re-dispersion phases of the process. Strong interaction at the interface are required to avoid migration and leakage or undesired aggregation in use.

Reducing the interfacial tension and the interfacial area of the dispersed phase in the matrix by recourse of suitable carriers, as chaperones of active molecules or nanoparticles into structurally similar polymer matrices, is another possible strategy to achieve the same goal.

In the framework of this CRP, radiation grafting of a functional monomer onto polyolefin film has been applied to modify the molecular structure and properties of the otherwise incompatible and chemically inert film. The film has become permeable to the precursors of polymerization of conducting polymer that formed in situ.
Radiation processing has been shown to be a viable methodology to tailor the supramolecular structure of a polysaccharide here evaluated as a carrier of additives or active ingredients into polysaccharide-based films.

8.1.1. In situ formation of conductive polyaniline thin skins onto radiation grafted polypropylene films

Traditional polyolefins are still unparalleled for chemical resistance and mechanical properties, in terms of strength, flexibility, deformation at break and tear resistance. Other properties, such as electrical conductivity or semi-conductivity, are required to open up opportunities in more remunerative application fields, which span from intrinsic antistatic films to electromagnetic shielding materials, flexible electronics, active and intelligent food packaging films or flexible electrodes for sensing biologically relevant parameters in vivo [8.1].

In order to retain most of the advantageous properties of polyolefins, composite nanostructures with other functional materials can be pursued. Metals or metal oxides are often blended or cast onto polymers to confer electrical conductivity and modified optical properties [8.2]. They require significant weight fractions of very fine powders to be added in the presence of multi-functional 'cocktail' of additives, comprising different organic promoters. Often, chemical-functionalization of the polyolefin is also necessary. All plastic hybrids made by a polyolefin matrix and a conducting polymer nanofiller holds the promise of superior flexibility and better compatibility, if a strong interface between components is achieved, e.g. through chemical bonding between the two components.

Polyaniline is a well-known conducting polymer, discovered in the late 19th century and still under investigation due to the excellent compromise between performance and costs. In particular, electrical conductivity induced by Brønsted acids doping, chemical and solvent resistance makes it an interesting material for a variety of electrical and electronic devices, and particularly for chemical sensors and biosensors and energy storage devices [8.3]. Difficult processability of the inherently conductive, emeraldine-salt (PANI-ES) form has always been a serious limitation for its use, since PANI-ES is insoluble and infusible. In-situ polymerisation methods of PANI-ES offer a possibility of overcoming these limitations.
In a previous work of some of the Authors, polyaniline was chemically grown onto the surface of ethylene-acrylic acid copolymer (EAA) film [8.4], with the aim of inducing electrical conductivity and electronic control of a range of physical and chemical properties of the film surface. The all polymeric *conductive-insulating hybrid* material was prepared by a typical wet-chemistry approach. Other reserachers report on PANI growth onto microporous PP films have been also used as a substrate but the obtained composite films showed a highly heterogeneous structure and anisotropic conductivity [8.5]. However, high-quality well defined thin films are essential for the exploitation of the electronic, magnetic and optical properties of these materials.

Here, a commercially available polypropylene (PP), in form of films has been functionalised by radiation-induced grafting of acrylic acid. Radiation-induced grafting of monomers into polymers is a praticularly an interesting approach towards the modification of polymeric substrates, because the resultant material retains most of its original characteristics and acquires additional properties from the grafted monomer. Another advantage of the process is that the grafting may be accomplished in any physical form irrespective of the polymer shape and size [8.6-8.15].

The acrylic acid-grafted film has been then acylated to facilitate the conversion of carboxyl groups into primary amino groups by reaction with a variety of diamines.

This first part of the research has been carried out at the National Center for Radiation Research and Technology Atomic Energy Authority, Cairo Egypt, by Ms Noha Deghiedi under the supervision of Dr. Hassan El Rheim. The films have been used as substrates for in-situ polymerization of polyaniline and characterized for their optical, electrochemical, morphological and electrical characterization at the University of Palermo.

8.1.2. Radiation engineering of polysaccharide chaperones

This research aims to develop biodegradable polymer micro/nanoparticles as carriers of "active" molecules, biomolecules or nanoparticles to be used as additives in biodegradable plastics. Biodegradable polymers derived from renewable resources are attracting a lot of interest, but this enthusiasm is counterbalanced by persistent questions of availability, cost, performance, and processability. All these issues are inter-related. Biopolymers that are dominating the scene are polylactic acid (PLA), polyhydroxyalkanoates (PHAs), polyhydroxy butyrate (PHB) and polyhydroxy butyrate-valerate (PHBV), and polyglycolic acid (PGA). There is another whole class of biomaterials, that is *polysaccharide-based*, that can be processed to form films and coatings, biomedical devices for drug delivery and tissue engineering [8.16, 8.17].

Polysaccharide films are much like other plastics, in that they need help from additives to address inherent weaknesses in processability, improved physical and barrier properties. They need to be colored or to be transparent. They need to be stabilized against degradation or the rate of their degradation needs to be enhanced, depending on the circumstances. They have to incorporate and retain, or release active ingredients.

Xyloglucan, an abundant and rather inexpensive polysaccharide, has been here selected as potential carrier for additives in polysaccharides films. By increasing the degree of degalactosylation, variants with increased hydrophobicity and aggregation propensity in water are obtained. The native xyloglucan, in turn, is fairly hydrophilic and film forming.

Degalactosylated xyloglucans are commercialized as dry powders. Complete disaggregation of degalactosylated xyloglucan clusters in water is difficult to achieve, even with recourse to high energy mechanical stirring, ultrasounds, increasing the temperature (autoclaving) or increasing the pH.

High energy irradiation with ^{60}Co photons of the dry powder will be proved to be effective in reducing the size of clusters when the polymer is dispersed in water. Irradiation has been performed at the Centre for Radiation Research and Technology, Institute of Nuclear Chemistry and Technology, Warsaw, Poland in collaboration with Prof. G. Przybytniak and Dr Marta Walo, on dry solid powders in air. Dynamic light scattering measurements as function of the time and the temperature was carried out to study the supramolecular organization of the irradiated polymer at the increase of the temperature, as function of the irradiation dose. FTIR spectroscopy, GPC and SEM analyses were also carried out on the irradiated polymers. Incorporation of various model molecules, characterized by different polarity and molecular weight, was attempted. Finally, fluorescein-loaded Deg-XG nanoparticles were dispersed into xyloglucan films to check on their dispersion ability in the films.

8.2. EXPERIMENTAL

8.2.1. Preparation and characterization of conductive constructs

8.2.1.1.Preparation of radiation-grafted polyacrilic acid-polypropylene films

Isotactic polypropylene (PP) films (65% degree of crystalinity, biaxially oriented, El-Nasr Company for Intermediate Chemicals, Egypt) with an average thickness of 30 μm were washed, dried in an oven until they attained a constant weight and then immersed in an acrylic acid (AA) (Acros Chemical Company, USA) aqueous solution at 30:70 (vol%) within glass tubes in the presence of ferrous ammonium sulphate ($Fe(NH_4)_2SO_4.6H_2O$, Sigma-Aldrich) at 2.5 wt%. Samples were then subjected to ^{60}Co γ-irradiation at a dose rate 3.2 kGy/h and total absorbed dose of 20 kGy.

Polyacrylic acid-grafted (PP-g-PAA) films were removed from the aqueous solution. Eventual AA homopolymer formed was extracted with boiled water for 4 hours. PAA-grafted films were dried at room temperature to constant weight. A grafting degree of about 40 % was estimated gravimetrically, according to the equation:

$$\text{Degree of grafting (\%)} = \frac{W_g - W_o}{W_o} \times 100$$

where, W_0 and W_g are the weight of the film before and after irradiation, respectively.

Water uptake was also measured on PP-g-PAA films by drying them in a vacuum oven at 60°C overnight and. keeping them immersed in bi-distilled water to constant weight. The swelling degree was measured as:

$$SW(\%) = \frac{Weq - W0}{W0} x100 = 8$$

where, Weq and W0 are the weight of the film before and after immersion in water, respectively.

8.2.1.2.Conversion of polyacrylic acid-polypropylene films into amino groups surface functionalized derivatives

In order to convert the carboxyl groups present on the radiation-grafted PP into primary amino groups, using selected diamines, they were first transformed into acyl chloride groups using thionyl chloride. Conversion of acyl chloride groups into primary amino groups was carried out in water, in the presence of the diamine (0.2 M) at room temperature and under stirred conditions. Six different diamines (all reagent grade from Sigma-Aldrich) were evaluated, namely hydrazine (hydr), ethylene diamine (ETDA) and 1,6 diaminohexane (1,6 DAH) and the ortho (o-), metha (m-) and para (m-) substituted phenylene (PDA) diamines. Films will be named as PP-g-PAA(X)/PANI with the acronym of the diamine reported in brackets and collectively as PP-g-PAA(Am)/PANI.

8.2.1.3.In situ polymerization of polyaniline skins onto carboxyl and amino-functionalised PP-g-PAA films

Films destined to PANI modification were placed into the polymerization reactor in the presence of water, aniline (0.1 M) and hydrochloric acid (37%, A.C.S. reagent, Sigma-Aldrich). The films were immersed in this solution and kept in a vertical position during

polymerization, in order to avoid gross PANI deposition and curling that would impede uniform coating of the substrate. Polymerization was initiated by dropwise addition of ammonium persulphate (APS) ($(NH4)_2S_2O_8$, 98% Sigma-Aldrich) at 1:1 molar ratio with respect to aniline. Temperature was maintained at 2-4 °C for the first 5 hours while constant nitrogen reflux and stirring were also provided. Then, stirring was continued and the reactor discharged after 24 h. The films turned out dark green and some PANI was also found as precipitate at the bottom of the reactor. Films were then repeatedly washed with distilled water and acidified water before drying. Selected films were treated with sodium hydroxide to convert the emeradine salt in emeraldine base and thoroughly washed with NMP, in order to remove the PANI that did not strongly adhere to the substrate, then characterized before and after re-acidification with HCl. The amount of incorporated PANI on PP-g-PAA films was estimated gravimetrically before and after NMP extraction and it was always in the 2-4 wt%.

8.2.1.4.Electropolymerisation of PANI on PP-g-PAA(Am)/PANI films

The electrochemical polymerization of aniline (aniline 0.1 M in HCl 0.1 M) has been carried out by cyclic voltammetry or chronoamperometric methods. The experiments were carried out using a A Princeton Applied Research (mod.PARSTAT 2273) potentiostat with a standard three electrodes cell equipped with a platinum counter electrode and a SCE as reference. The cyclic voltammetric deposition was performed using a sweep rate of 100 mV/s in the potential range from -0.6 V to 0.8 V (SCE), for 50 or 90 cycles. The chronoamperometric deposition was performed at a constant potential of 1 V for 1000 s. The working electrode is any of the PP-g-PAA(Am)/PANI films (surface area 2.6 cm^2) that has been electrically connected to a copper wire by a copper adhesive. The experiments were carried out at room temperature under nitrogen.

8.2.1.5.Structural, thermal and morphological characterization

FT-IR spectroscopy was used to characterize the films after each functionalisation step. Spectra were recorded at 30 scans per spectrum, 1 cm^{-1} resolution and normalized with respect to methylene symmetric bending vibration band at 1337 cm^{-1}.

Surface chemical composition of the samples was investigated by *XPS* in an ultra-high vacuum (UHV) chamber with a base pressure in the range of 10^{-8} Torr during data collection. Photoemission spectra were collected by a VG Microtech ESCA 3000 Multilab spectrometer, equipped with a standard Al K_α excitation source (hv = 1486.6 eV) and a nine-channeltrons detection system. The hemispherical analyser operated in the CAE mode, at a constant pass energy of 20 eV. The binding energy (BE) scale was calibrated by measuring C 1s peak (BE = 285.1 eV) from the surface contamination and the accuracy of the measurement was ± 0.1eV. Photoemission data were collected and processed by using the VGX900 software. Data analysis was performed by a nonlinear least square curve-fitting program using a properly weighted sum of Lorentzian and Gaussian component curves, after background subtraction according to Shirley and Sherwood [8.18]. Surface relative atomic concentrations were calculated by a standard quantification routine, including Wagner's energy dependence of attenuation length [8.19] and standard set of VG Escalab sensitivity factors. The uncertainty on the atomic concentration is of the order of 10%.
UV–Vis absorption spectra were measured by Shimadzu 2401-PC spectrophotometer (scan speed 40 nm/min, integration time 2 sec, bandwidth 1 nm) at room temperature in the wavelength range 200-900 nm.

Thermogravimetric analysis (TGA) was performed with a STA6000 Simultaneous Thermal Analyzer, Perkin Elmer USA, in gaseous nitrogen flux on approx. 10–20 mg samples of the films. A temperature ramp from 30 C to 900 °C was programmed with a heating rate of 10 °C/min.

Morphological characterization of both film surfaces and cross-sections was carried out by *a field emission scanning electron microscopy* (FESEM) system (JEOL) at an accelerating voltage of 10 kV. Samples were generally observed before and after sputtering a graphite layer (Sputtering Scancoat Six - Edwards), in order to improve images quality at high magnification.

8.2.1.6.Impedance spectroscopy

Impedance frequency dispersions for films were measured in the frequency range 10^{-1}–10^{5} Hz and at room temperature by means of a *Frequency Response Analyzer* (Schlumberger, mod.1255), applying an ac signal of 0.02 V peak-to-peak, using a two electrode cell, having two circular gold plated electrodes (working and counter). Circular films of 20.5 mm diameter were gently pressed between the electrodes in order to ensure the electrical contact. Measuring cell and apparatus were placed into a Faraday cage for shielding electromagnetic interference. The electrical impedance was generally plotted in the complex plane as Z" as function of Z', known as Cole–Cole plot, and as impedance modulus, |Z|, and phase angle, log η, as function of frequency, that are the Nyquist and Bode diagrams, respectively.

8.2.2 Preparation and characterization of polysaccharide chaperones

8.2.2.1. Materials and irradiation experiments

Degalactosylated xyloglucan (Deg-XG), with a galactose removal ratio of 44%, was a kind gift of DSP Gokyo Food and Chemicals (Japan).

Irradiation of Deg-XG powder was carried out in air, at room temperature, using a ^{60}Co source (Gamma Chamber 5000, Institute of Nuclear Chemistry and Technology, Warsaw, Poland) at 8 kGy/h and irradiation doses of 10, 20, 40 and 60 kGy. The polymer was dispersed in water at 0.1, 0.25 and 0.5 wt % by homogenization at 5°C for 3 hours at 13500 rpm. Centrifugation at 8000 rpm for 45 minutes was performed to remove large aggregates and residual debris. The influence of centrifugation on the average hydrodynamic diameter and polydispersity index of this xyloglucan in water was studied by dynamic light scattering measurements; results are reported elsewhere [8.20]. Dispersions are stored at 5°C prior to use. Polymer nanoparticles were produced by temperature-induced aggregation of aqueous dispersions at 37°C.

8.2.2.2.Incorporation of actives

Low molecular weight model molecules with different solubility in water, i.e. theophylline (TH) and camptothecin (CPT) were encapsulated in the polymer nanoparticles.

Concentrated TH aqueous solution (to a final nominal concentration of $2{,}5*10^{-3}$ M) was added to a Deg-XG aqueous dispersion (0.1 wt%) following three different procedures: a) by mixing with the "as prepared" Deg-XG dispersion at 5°C; b) by incubation at 37°C together with the "as prepared" Deg-XG dispersion; c) by incubation at 37°C together with a Deg-XG

dispersion previously incubated at 37°C for 24 hours. After 24 hours each system was centrifuged to remove the TH in excess and UV-vis absorption measurements were performed to evaluate residual theophylline concentration in the uptake solution.

For CPT incorporation, Deg-XG aqueous dispersion (polymer concentration: 0.1 wt%) was loaded with CPT ($2*10^{-5}$ M) previously solubilized in DMSO (10^{-3} M). The maximum DMSO concentration in the final formulation was 5 wt%. Solutions were prepared by magnetic stirring for 24 hours in the dark. Then, liquid-liquid extraction with diethyl-ether was performed to remove the drug that was not adsorbed by the polymer. The extracted CPT was re-dispersed in DMSO and CPT concentration was evaluated by UV-Vis absorption measurements.

8.2.2.3.Film preparation by solvent casting

Xyloglucan films were prepared both with and without degalactosylated xyloglucan nanoparticles incorporating fluorescein as colorant. Xyloglucan solutions at 4 wt% were prepared in water by magnetic stirring for 24 hours. Films were obtained by casting of a thin layer of polymer solution on a horizontal plate. Then, glycerol in 4:1 volumetric ratio with the aqueous polymer solution was sprayed on this layer. Films were let dry out in air.

8.2.2.4.Characterizations

Dynamic light scattering (DLS) analysis was performed using a Brookhaven Instruments BI200-SM goniometer. The influence of temperature in the range 15-37°C was investigated. Intensity autocorrelation function at the scattering angle of 90° and time autocorrelation function were measured by using a Brookhaven BI-9000 correlator and a 100mW solid-state laser (Quantum-Ventus MPC 6000) tuned at λ = 532 nm. All samples were analyzed after filtration with 5 μm cellulose acetate (Millipore) syringe filters to remove gross contaminants. When samples showed a monomodal distribution, DLS data were analyzed by the method of cumulants, which provides information on the mean value and standard deviation of the distribution of hydrodynamic size of nanoparticles [8.21].

Gel Permeation Chromatography (GPC) was performed using two Shodex SB HQ columns in series (806 and 804) thermostated at 15 °C with a Knauer oven, connected to a HPLC device (LC-2010 AT Prominence, Shimadzu, Kyoto, Japan) equipped with a 50 □l sample loop. All samples were eluted with 0.02% sodium azide solution at 0.5 ml/min; the refractive index was recorded with a Smartline RI detector 2300 Knauer.

FTIR analysis was carried out with Perkin Elmer-Spectrum 400 apparatus by dispersing freeze dried polymers in potassium bromide and compressing into pellets. Spectra were recorded at 30 scans per spectrum and 1 cm^{-1} resolution in the 4000-400 cm^{-1} range.

Surface morphology was imaged by a field emission scanning electron microscopy (FESEM) system (JEOL) at an accelerating voltage of 10 kV. Samples for FESEM were coated with a gold layer by JFC-1300 gold coater (JEOL) for 50 s at 30 mA before scanning.

8.3. RESULTS AND DISCUSSION

8.3.1. Preparation and optical characterisation of skin–core poly(propylene)-g-poly(acrylicacid)/polyaniline hybrids.

Polyaniline-polypropylene nanocomposites were generated in three steps: first, PP films were chemically modified by radiation grafting of acrylic acid, following the typical "direct irradiation" approach (*Step I*). Then, carboxyl groups of grafted AA were transformed into amino groups via a conventional chemical derivatisation route (*Step II*). Finally, the amino groups on the substrate were oxidised to become a potential anchoring site for the *in-situ* polymerisation of aniline ("grafting from" approach). (*Step III*).

Irradiation of PP films in aqueous AA generates, simultaneously, monomer radicals in the aqueous medium and polymer radicals in the solid substrate. Grafting can be the result of propagation reactions of PP radicals by addition of monomer and, to a less extent, of combination reactions of polymeric radicals with monomer radicals. Competitive reactions between polymer radicals and dissolved oxygen (with formation of peroxides and hydroperoxides), and molecular degradation due to chain scission reactions cannot be ruled out. Upon irradiation, the grafting front of acrylic acid into the PP films is expected to progress from the surface to the interior of the film, alongside with the swelling front of the monomer aqueous solution, due to the progressive chemical modification of the substrate. Average degree of grafting of about 40% and water uptake of about 8 % were measured for the irradiated films. Water uptake for the pristine PP is negligible.

In figure 8.1. (a-d), surfaces (a, c) and cross-sections (b, d) of untreated (a, b) and PP-g-PAA (c, d) films are shown. The surface of irradiated films is coated by dense layer of small nanoparticles and larger dome-shaped aggregates. The modification of surface topography can be due to both the modification of polypropylene under gamma-irradiation (preferential degradation of the amorphous/low molecular weight fractions) and poly acrylic acid chains grafting and segregation due to their poor compatibility with PP. A similar modification of surface topology was observed in PP films exposed to corona discharge treatment both in air and in the presence of acrylic acid [8.22]. From a close look to the cross-section is evident that the compact surface layer is a few hundred of nanometers thickness while the underneath material is more porous, with spherical nanoparticles (20-50 nm) more sparingly, yet uniformly distributed to a depth of about 10 μm from the surface.

FTIR spectra (Figure 8.2a) of PP-g-PAA show new bands at 1716 cm^{-1} (-COOH), 1645 cm^{-1} (-C=CH-C=O-) and in the 1300-1100 cm^{-1} region (carboxylate anions - also evident for a band at 1400 cm^{-1} - and C-O-C groups). XPS analysis confirms an increased level of surface oxidation, with oxygen content rising from 9.2 to 21.6 % and with a slight prevalence of O-C (532.0 eV) with respect to O=C (533.5 eV). The degree of grafting of PAA on the surface, estimated from the surface carboxyl content, is of about 35.5 %, which does not differ very much with the average bulk value measured gravimetrically.

Chemical functionality shift from carboxyl to primary amino groups was achieved via the acyl intermediate route. The conversion of carboxyl groups into acyl chloride (ACl) groups was quantitative: the FTIR spectrum (Figure 8.2b) of PP-g-PACl shows the two characteristic peaks of acyl chloride at 1790 cm^{-1} and 1736 cm^{-1}.

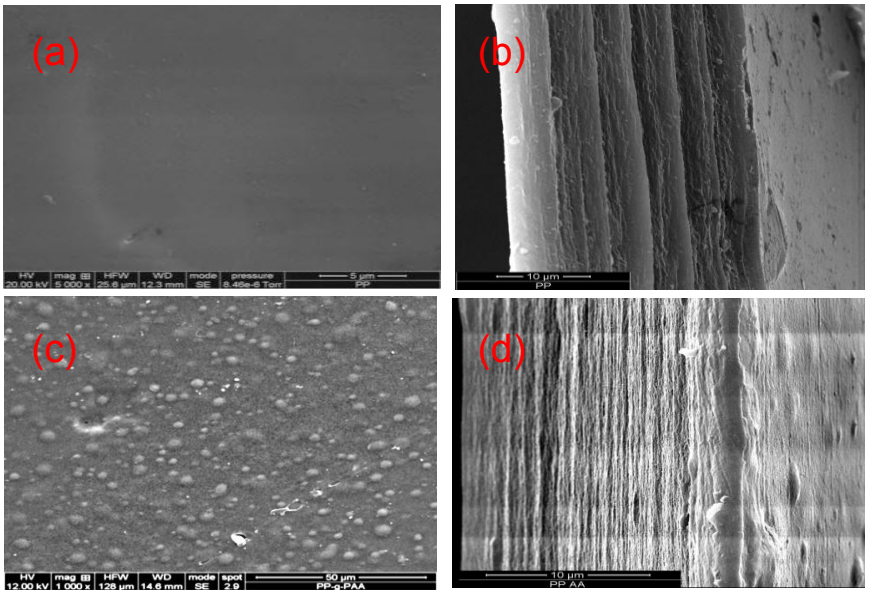

FIG. 8.1. SEM micrographs of surfaces (a, c) and cross-sections (b, d) of pristine PP (a, b) and PP-g-PAA (c, d) films.

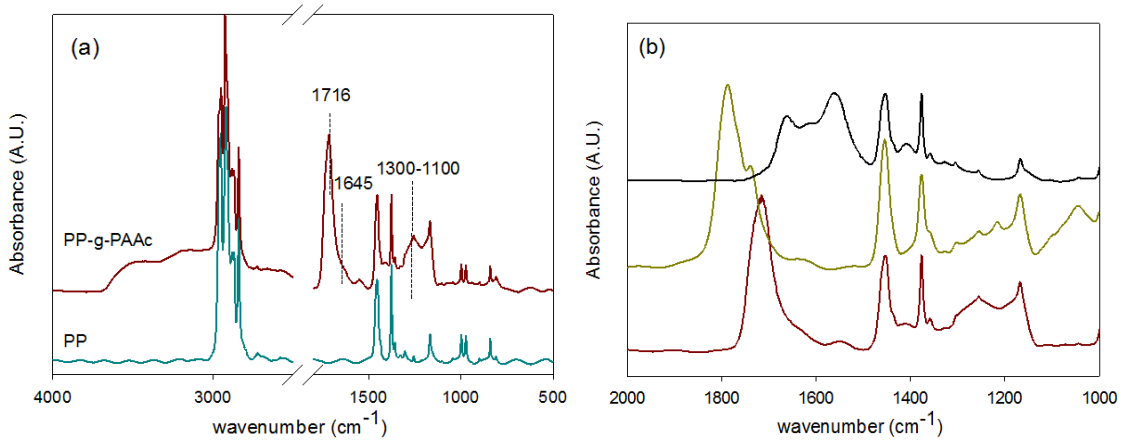

FIG 8.2. FTIR spectra of pristine PP and PP-g-PAA films(a); spectra of PP-g-PAA before (red)and after acylation (green) and after reaction with hydrazine (black) (b).

Derivatisation with any of the aliphatic diamines (see figure 8.2b, for hydrazine) causes the disappearance of the band at 1790 cm^{-1} and the appearance of two new strong bands at about 1670–1650 cm^{-1}, and 1575–1565 cm^{-1} owing to N-H bending absorptions of the amide linkages and primary amine groups, respectively. A small but distinct component from protonated carboxyl groups in the carbonyl envelope appears. In particular, when derivatisation is performed with any of the di-substituted phenylenes, the disappearance of the acyl chloride band is accompanied by a partial restoration of the carboxyl carbonyl absorption at 1716 cm^{-1}. It can be argued that water compete with the primary amines in the nucleophile substitution of chlorine atoms, the aromatic diamines being less efficient with respect to the aliphatic owing to their lower nucleophilicity and higher steric hindrance. The first of the two N-H bands for the aromatic diamines, as well as for hydrazine, are significantly shifted to higher frequencies with respect to aliphatic ones (1668 cm^{-1} vs. 1652 cm^{-1}), probably due to resonance effects.

In-situ PANI polymerisation was performed by immersing the various amino-functionalised films in an aqueous solution of aniline (0.1 M) and HCl in the presence of an equimolar amount of $(NH4)_2S_2O_8$ as initiator. The locus of aniline polymerisation can be the aqueous phase, which contains both the anilinium ions and the redox initiator, where also the quinoidal dimers and trimers are soluble. The amino groups of aniline oligomers have lower oxidation potential than the monomer, therefore they add more favourably the monomer, mainly in "para" position (para-directed electrophilic attack). Chain-growth polymerisation of aniline takes place with a head-to-tail configuration. Every addition step consumes one molecule of oxidant. The oxidant can be either the redox initiator or a pernigraniline sequence that turns into an emeraldine sequence by accepting an electron. The final oxidation state of the polymer is dependent by these rearrangements and it is generally the semi-oxidated, most stable, emeraldine form. At the increase of molecular weight, oligomers become more and more hydrophobic and either nucleate a second phase, that eventually precipitates, or adsorb at the film surface. In principle, also the amino groups present on the PP film can be oxidized (transformed into the radical cation intermediate) and promote formation of aniline grafts. Different diamines would have a different nucleophilicity, oxidation potential and offer different steric hindrance to the attack of aniline and its oligomers.

Polypropylene films were visually inspected after each reactive step. While grafting PAA onto PP, as well as derivatisation reactions with hydrazine, the aliphatic diamines and the aromatic para-substituted diamine left films colorless and transparent, both ortho- and meta-substituted aromatic diamines imparted a distinct yellow colour to PP films, yet preserving their transparency. After PANI polymerization, all the amino-functionalized films presented an uniform, dark green colour, characteristic of polyaniline in the form of protonated emeraldine (PANI-ES). Substrates treated with the aromatic diamines showed higher reflectance. Since we are interested in evaluating if PANI is irreversibly attached on the amino-functionalised PP films, the insoluble PANI salt was converted into its base form and films were extensively extracted with NMP, which is known to be a good solvent for emeraldine base. All films retained a uniform blue color (characteristic of emeraldine base) and partially recovered their transparency. This would suggest that, underneath a top layer, a finely dispersed and strongly covalently attached amount of PANI, which cannot be extracted and removed by NMP, is present.

UV-vis absorption spectra (here not reported) on PP films after PAA grafting and derivatisation with the various diamines confirm the optical transparency and colorless appearance of all the substrates, with the already discussed exception of ortho- and meta-substituted phenylenediamines, which show an absorption band in the 430-480 nm range. The effect of the presence of a polyaniline on all substrates, as prepared, after treatment with a strong alkali, after extraction with NMP, and reacidification on films optical density and wavenumbers at the maximum of absorption (at λ_{peak}) in the visible range is shown in table 8.2. PP and PP-g-PAA films have an OD of about 0.3. After PANI polymerization, we observe: (a) for all systems the typical broad absorption band in the visible range, peaking at 800-850 nm, with a long tail extending toward the near-IR region, attributable to the polarone structure characteristic of PANI-ES; (b) red-shift of the polarone band for films that were previously modified with the aromatic diamines (although it is hydrazine that gives highest bathochromic shift with λ_{peak}=846 nm); (c) higher optical density at λ_{peak} for substrates treated with aliphatic diamines; (d) the lowest OD value at peak for the PP-g-PAA/PANI-ES film, likely due to its non-uniform coverage; (e) after treatment with a strong alkali,

extraction with NMP and reacidification with HCl, the polarone band is at at ~900 nm for all systems.

TABLE 8.1. OPTICAL DENSITY AND WAVENUMBERS AT THE MAXIMUM OF ABSORPTION (AT λ_{PEAK}) IN THE VISIBLE RANGE FOR PP-G-PAA/PANI NANOCOMPOSITES WITH DIFFERENT PRIMING TREATMENTS: AS PREPARED, AFTER TREATMENT WITH A STRONG ALKALI, AFTER EXTRACTION WITH NMP, AND REACIDIFICATION

Systems	λ_{PEAK}	OD	λ_{PEAK}	OD	λ_{PEAK}	OD	λ_{PEAK}	OD
	As prepared		Treated NaOH		Washed with NMP		HCl	
PP-g-PAA/PANI	811	1.084	548	1.122	615	0.731	900	0.629
PP-g-PAA(Hydr)/PANI	846	1.292	570	1.712	627	1.135	900	0.735
PP-g-PAA(ETDA)/PANI	811	2.081	560	2.254	610	1.372	900	0.932
PP-g-PAA(1,6 DAH)/PANI	800	2.732	570	2.373	600	1.442	900	0.988
PP-g-PAA(o-PDA)/PANI	825	1.973	538	1.872	595	1.164	900	0.613
PP-g-PAA(m-PDA)/PANI	825	1.852	560	2.008	595	0.932	900	0.612
PP-g-PAA(p-PDA)/PANI	825	1.663	543	2.615	595	0.901	900	0.603

FTIR spectra of PP-g-PAA films covered by PANI-ES (as prepared films) show only little spectroscopic evidence of PANI (see Figure 8.3). When films are treated with NaOH and extracted with NMP a new prominent absorption appears at 1572 cm^{-1}. This multi-band envelope can see contributions from quinoids (~1565 cm^{-1}) and benzenoids (~1500 cm^{-1}) but also from carboxylate ions (~1560 cm^{-1}) and from the amide II band (1660 cm^{-1}). The presence of carboxylate ions is also confirmed by the 1400 cm^{-1} peak, whereas the band at 1380-1350 cm^{-1} corresponds to C-N stretching, higher in position due to an increase in double bond character. Residual carboxyl groups are also evident from the absorption band at 1713 cm^{-1}. These groups may establish both electrostatic and/or hydrogen bonding interactions with polyaniline chains, acting both as templating agent and secondary dopant, i.e. contributing to stabilise the polarone (polycation) form of PANI. A comparison among the FTIR spectra of the different systems after NMP treatment (spectra not shown) shows many similarities and some subtle differences. All spectra have their main absorption band at 1570-1560 cm^{-1}, but spectra of films reacted with EDTA and hydrazine do not show the shoulder at 1720 cm^{-1}, that is present on all other systems and, particularly, on PP-g-PAA/PANI. Both the main peak at 1570-1560 cm^{-1} and its component at 1647-1660 cm^{-1} are shifted to lower frequencies for substrates modified with the aliphatic EDTA and 1,6 DAH, which would suggest a lower degree of interaction between the substrate and the conducting polymer.

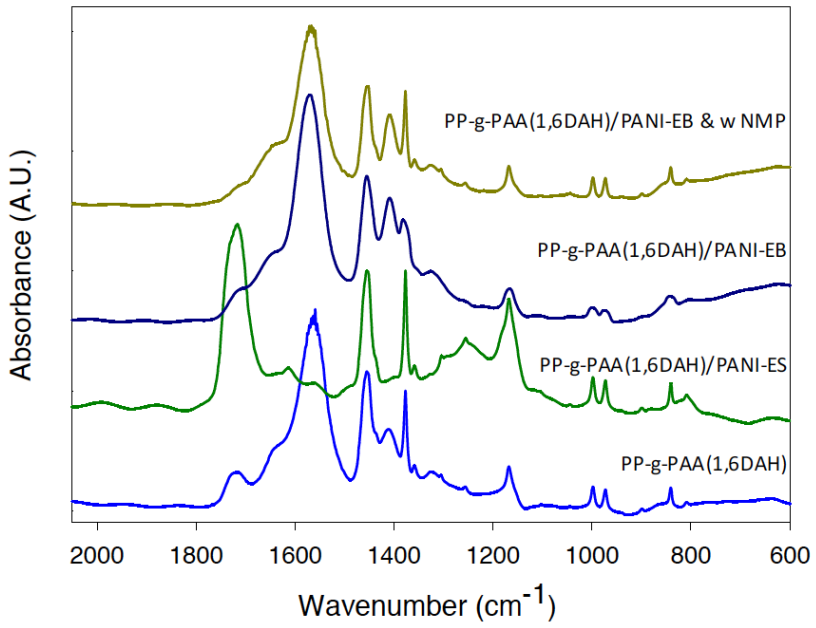

FIG. 8.3. FTIR spectra of the amino functionalised PP-g-PAA/PANI film (PP-g-PAA(1,6DAH)) and corresponding PANI nanocomposite film: as prepared (PP-g-PAA(1,6DAH)/PANI-ES), after treatment with a strong alkali (PP-g-PAA(1,6DAH)/PANI-EB), after extraction with NMP (PP-g-PAA(1,6DAH)/PANI-EB & wNMP).

Scanning electron microscopy (SEM) was used to analyse both the topographical features of the films surface and the morphology of their cross-sections, as obtained by shearing the films in liquid nitrogen after cutting a small pre-crack opening. In general, all poly(propylene)-g-poly(acrylicacid)/polyaniline composites show a characteristic skin-core morphology with 200-500 nm thick, compact outer layers and a porous core. In particular, surfaces of PP-gPAA(Hydr)/PANI and of films obtained with the three aromatic diamines modified substrates were covered by a fairly compact surface layer of PANI nanoparticles with a globular morphology (see Figure 8.4c for PP-gPAA(m-PDA)/PANI)**.** Contrarywise, surfaces of substrates pre-treated with the aliphatic amines were more heterogeneous both in terms of quality of the coverage and morphology of PANI (see Figure 8.4a for PP-gPAA(EDTA)/PANI)**.** The core morphology is typical of an interpenetrated network (Figures 8.4b,d).

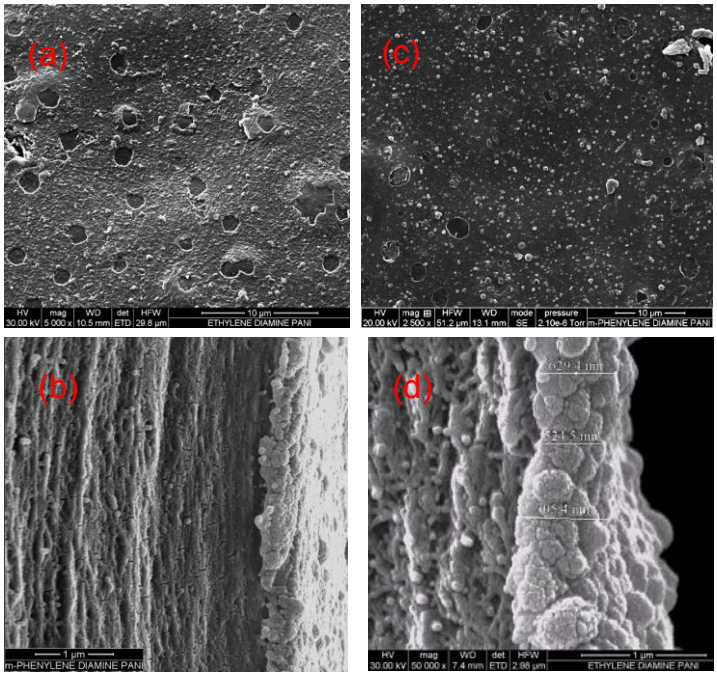

FIG. 8.4. Morphology of PP-gPAA(EDTA)/PANI film surface (a), cross-section (b); and of PP-gPAA(m-PDA)/PANI film surface (c) and (d).

8.3.1.1.Impedance spectroscopy of skin-core functional hybrids

All PANI-grafted films display increased conductivity with respect to the PP-g-PAA substrate, which in turn shows an almost ideal capacitive behaviour with phase angle close to 90° at all the investigated frequencies and bulk resistance above $10^{12}\Omega$. Figure 8.5. reports the Nyquist plots for the different films obtained by grafting PANI on PP-g-PAA.

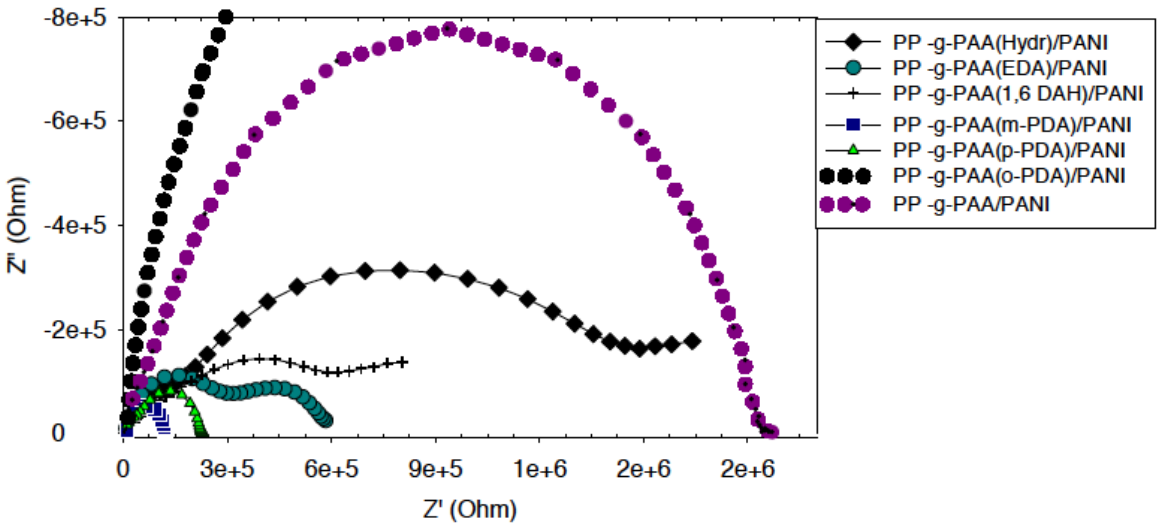

FIG. 8.5. Nyquist plots for the different films obtained by grafting PANI on PP-g-PAA after modification with the different diamines.

The electrical properties of the composite films strongly change depending on the amine group used for the functionalization. The overall film resistance, roughly represented by the right-hand intercept in the real axis of the circles in the figure, is many orders of magnitude

lower with respect to the PP-g-PAA and it varies of more then a factor of 10 by changing the amine group. Different shapes of the Nyquist plots are observed for different films, e.g. with single or double circles. Also for the phenylenediamines, a sensible influence on film properties is observed depending on the position of the amine groups. In order to get more quantitative information on film properties, a fitting (Electrochemical Impedance Modeling Software Z SimpWin of Princeton Applied Research) of the different complex impedance curves was performed. Starting from the most conductive one, which shows a single circle in the Nyquist plots, namely the PP-g-PAA(m-PDA) film, an excellent fitting of the frequency dispersion was obtained using a R(CR)(CR) equivalent circuit, which simulates a two-layer structure for the film.

TABLE 8.2. VALUES OF THE FITTING PARAMETERS FOR PP-G-PAA/PANI AND PP-G-PAA(M-PDA)/PANI FILMS, DESCRIBED WITH A R(QR)(QR)

Systems	R_0	Q_1 (C, n)	R_1	Q_2 (C, n)	R_2
PP-g-PAA/PANI	119	$1.88*10^{-10}$ 0.9213	$1.75*10^{6}$	$3.56*10^{-10}$ 0.8604	$8.21*10^{4}$
PP-g-PAA(m-PDA)/PANI	4187	$5.75*10^{-10}$ 1	$1.07*10^{5}$	$1.045*10^{-10}$ 1	$9.129*10^{3}$

Values of the fitting parameters for PP-g-PAA/PANI and PP-g-PAA(m-PDA)/PANI films are reported in Table 8.1. The values for PP-g-PAA(m-PDA)/PANI indicate for both layers an ideal capacitive behaviour. Fitting of impedance measurements suggests in this case an effective penetration of PANI particles throughout the whole film. Furthermore, values of capacity of both layers reported in Table 8.1. point to a different relative thickness of the two layers, even if their precise estimation is not possible due to uncertainty on the real dielectric constant. It is interesting to compare this frequency dispersion with that recorded for the film without derivatisation of carboxyl groups into ammine groups (PP-g-PAA/PANI); again, an excellent fitting was obtained using a two-layer model (fig. 8.2b), with some significant differences in the calculated parameters (see Table 8.1): a) resistance values are more than one order of magnitude higher than the corresponding ones for the PP-g-PAA(m-PDA) film, as expected from the comparison of the relative Nyquist plots of Fig. 8.1; b) fitting requires the use of *constant phase elements*, in spite of capacitive ones, whose exponents (n in Table 8.1) differ sensibly from unity. This last fact indicates a non-ideal capacitive behaviour of the layers; the origin of non-ideality is not yet clear, but we are prone to exclude geometrical factors (fractal effects) considering that film structure and morphology is rather similar to the one of other film and think that it is more related to electronic properties of the film. Finally, the modulus of the Q elements is of the same order of magnitude for both films. Thus, addition of a further functionalizing group, namely the m-phenilendiamine group, greatly favours PANI polimerization and its penetration into the bulk of the film.

More complex impedance dispersions are shown by the other films, often requiring to consider a Warburg element, related to slow diffusion phenomena inside films, or even assumption of a three-layer model in order to obtain a satisfying fitting. This likely means a less uniform penetration of PANI within the polymeric matrix.

As a proof of a concept, one of the PANI-grafted films was used as electrode to elctropolymerise PANI. Figure 8.6 shows the difference in the Nyquist plots for PP-g-

PAA(EDTA) film before and after PANI electropolymersation, carried out in different conditions. A significant increase of conductivity is evident.

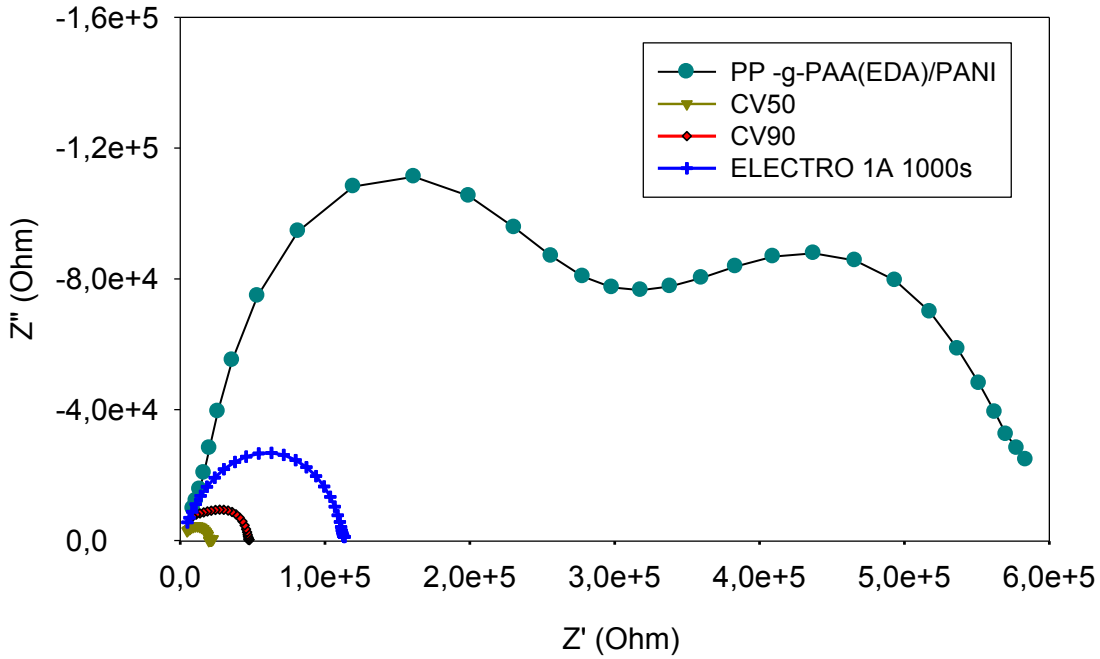

FIG. 8.6. Nyquist plots for the films obtained on PP-g-PAA(EDTA)/PANI before and after electropolymerisation.

8.3.2. Gamma irradiation effects on Deg-XG

8.3.2.1. Effects on molecular weight distribution

GFC measurements were performed at 15°C to gather information on the molecular weight distributions of irradiated Deg-XG at various doses (see Fig. 8.7). Modification of the curves can be better appreciated through the deconvolution of the raw data in different families. The non-irradiated polymer molecular weight distribution has been satisfactorily fitted with four families, among which two are the most representative. The proportion among the two main populations as function of the dose is summarized in the last panel of Fig. 8.7, as area percentage under each curve. At the increase of irradiation dose, a relative increase of the area under the curve referring to the lower molecular weights at the expenses of the higher molecular weight fractions can be observed. Chemical analyses conducted by FT-IR measurements do not evidence significant chemical modifications after gamma-irradiation (data not shown).

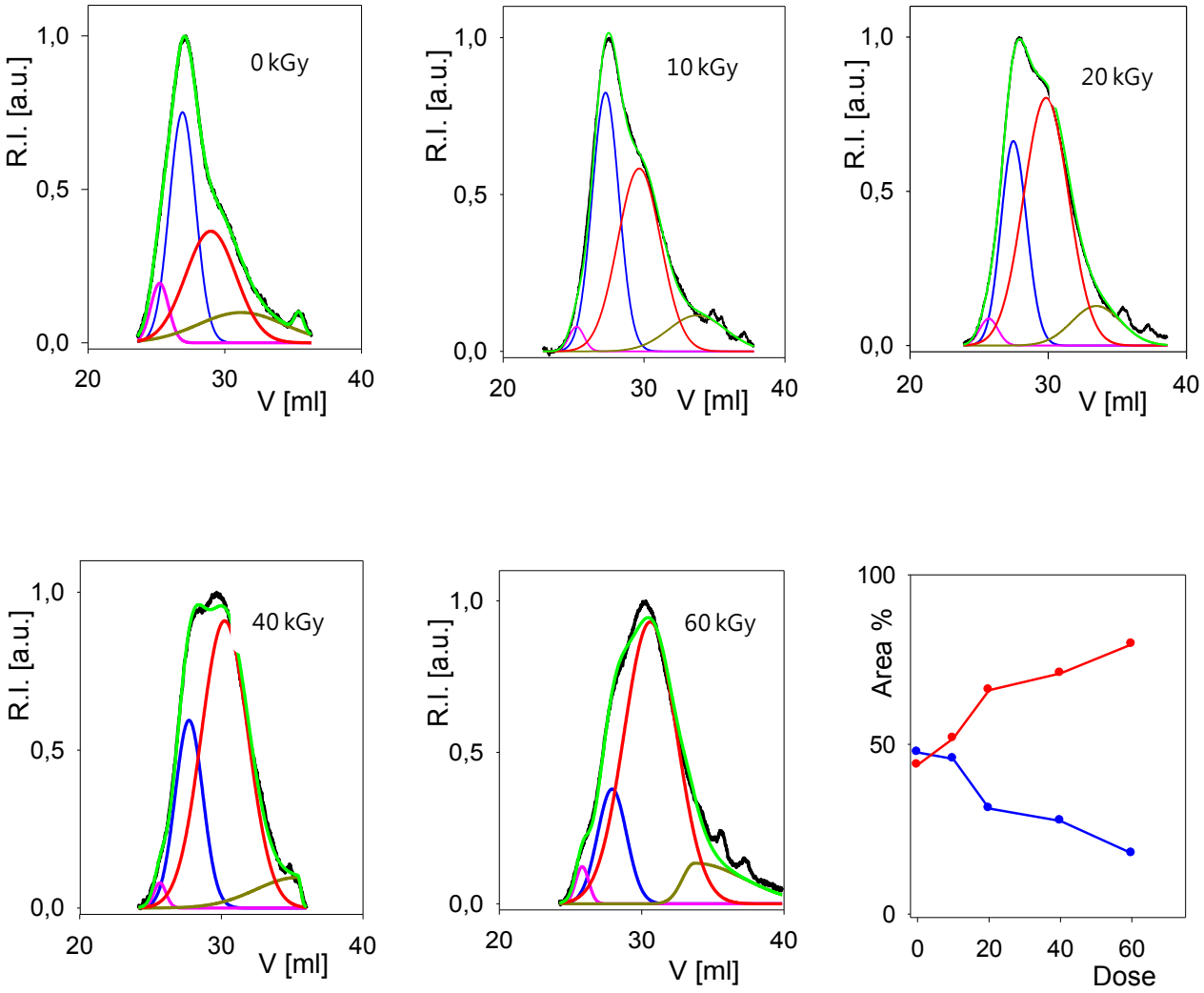

FIG. 8.7. HPLC results for the polymer dispersed in water at 0.1 wt% irradiated with 0 kGy (non irradiated), 10 kGy, 20 kGy, 40 kGy and 60 kGy. The chromatographic profile (black line) was deconvoluted using four different families Last panel reports area % under each curve as function of the dose for the two more significant families (red and blue).

8.3.2.2.Kinetics studies performed by DLS measurements

In principle, chain-scission reactions may involve either the backbone or the lateral grafts. In the latter case, changes in water solubility and temperature-responsiveness are expected. Deg-XG dispersions prepared with the non-irradiated and the irradiated polymers were subjected to repeated DLS measurements runs at 15°C and 37°C to study the aggregation behavior as function of the time. Fig. 8.8. shows the time courses of the scattered light intensity for non-irradiated Deg-XG at 15°C and 37°C (Fig. 8.8a) and for Deg-XG irradiated at the various doses (Fig. 8.8b), after dispersion in water at low concentration. When observed at 15°C for up to about 20 hours, all samples do not shown aggregation and the scattered light intensity does not show variations over time. When incubated at 37°C the scattered light intensity increases with time. This increase can be related to an increase of particle size and/or density of the clusters. Irradiation affects the rate of the observed kinetics with a maximum of aggregation rate for the 20 kGy-irradiated system, which probably shows the best

compromise between size of initial clusters and mobility. Tab. 3 reports the average hydrodynamic diameters and widths of distributions at both at 15°C and at 37°C. These values were calculated according to the cumulant method [8.21].

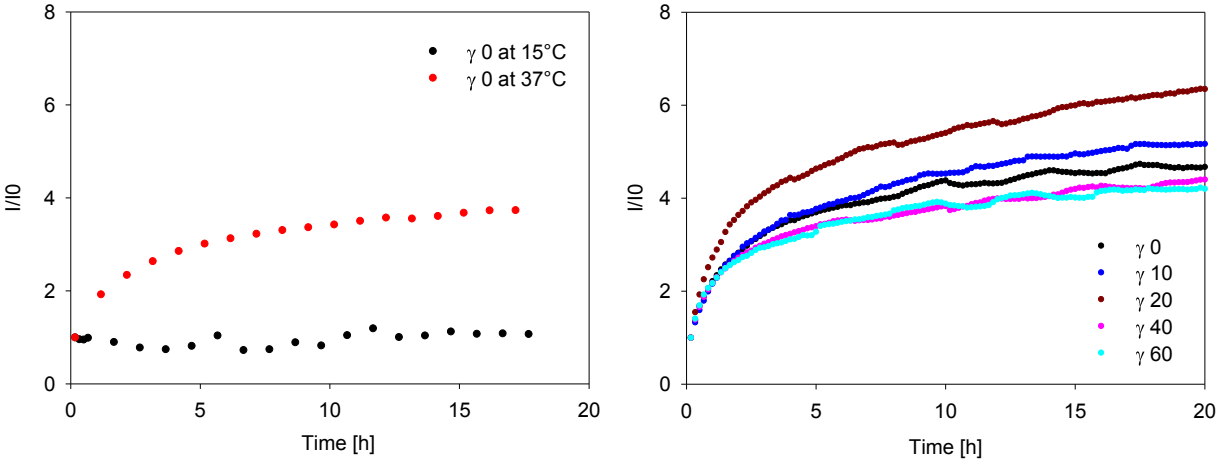

FIG. 8.8. Time courses of scattered light intensity for(a) non-irradiated and (b) irradiated Deg-XG dispersed in water.

TABLE 8.3. AVERAGE HYDRODYNAMIC DIAMETERS AND WIDTHS OF DISTRIBUTIONS AT BOTH 15°C AND 37°C

Sample	Dh [nm]		
	15°C	*37°C*	
	t_0-20h	*t_0h*	*t_20h*
γ 0	205 ± 65	313 ± 117	353 ± 112
γ 10	254 ± 85	218 ± 79	299 ± 90
γ 20	260 ± 80	253 ± 76	364 ± 115
γ 40	215 ± 65	217 ± 75	268 ± 74
γ 60	208 ± 58	198 ± 56	257 ± 62

Deg-XG nanoparticles morphology was investigated by scanning electron microscopy. Fig. 8.9. shows that the temperature-triggered self-assembly leads to the formation of spherical aggregates.

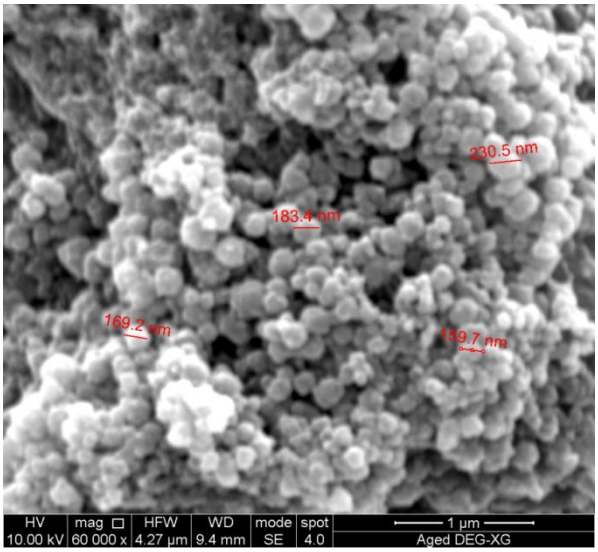

FIG. 8.9. SEM image of Deg-XG nanoparticles

8.3.2.3.Model molecules incorporation

Theophylline-loaded Deg-XG dispersions were prepared according to three different protocols described in par. 2.2.2. All dispersions were centrifuged to remove the drug not incorporated in the nanoparticles. For the three protocols the entrapment efficiency was always ~ 14%, while the drug load content was ~ 7%.

CPT-loaded Deg-XG dispersions prepared incubating the polymer with drug solutions at low concentration ($2*10^{-5}$ M) were prepared at 20°C and then, subjected to liquid-liquid extraction to remove the drug that was not incorporated in the nanoparticles. CPT concentration for each extraction was evaluated through UV-Vis absorption measurements and the entrapment efficiency was found to be ~ 40%. Camptothecin (CPT) is a more hydrophobic than theophylline. The very low solubility in water and considerable self-aggregation phenomenon exhibited by this molecule forced to work with a very low CPT concentration in water, in the absence of surfactants. For this reason, the drug load content was very low.

Future developments of this research are in the direction of incorporating large hydrophobic biomolecules, such as growth factors or enzymes in the nanoparticles and dispersing the loaded particles into polysaccharide-based films. XG-based film incorporating 2 wt% of fluorescein-loaded Deg-XG nanoparticles have been prepared. The film preserves its transparency and retains the pigment, showing the typical yellow color from fluorescein even under compressive stress, whereas if the colored molecule is dispersed directly in XG, it is easily released under pressure.

8.4. CONCLUDING REMARKS

Two established approaches to radiation-induced modifications of polymers, and precisely radiation-grafting and radiation-induced degradation, have been here applied to achieve an uniform dispersion of hetero-phase domains within a plastic matrix or on its surface and to promote strong interaction at the interphase, thus preventing migration and irreversible aggregation phenomena.

High energy radiation processing has been applied to polypropylene films in order to graft functional groups on the otherwise chemically inert material that can promote the formation of a chemically bonded polyaniline heterophase on the surface of the films, as well as interpenetrated into the core of the films, by *in-situ* polymerisation.

Decreases of resistivity up to nine order of magnitude are observed. The flexible PP-g-PAA(Am)/PANI films can be used as electrodes to promote the growth of polyaniline or other conducting polymers by electropolymerisation, with further improvements of conductivity.

Since radiation grafting of functional monomers into polymers, and to polyolefines in particular, is a well-established technique, that allows a good control over the depth and extent of substrate modification, we consider this approach very appealing for the generation of nanocomposite functional films with controlled chemical structure, morfology and properties.

The recourse to suitable carriers, as chaperones of active molecules or nanoparticles into structurally different polymer matrices, is another possible strategy to obtain more uniform and stable dispersions. For this purpose, we have selected a natural biopolymer, xyloglucan, as elective material to produce polymer nanoparticles to incorporate, in the development of the project, additives to control the durability of bioplastics or to introduce specific functionality into polysaccharide-based films and coatings. This approach preserves the full biodegradability of the nanocomposite material and reduces the chemical mismatch between the additive and the polymer matrix. The possibility of tailoring the size of clusters formed in water by a temperature-responsive partially degalactosilated xyloglucan variant through gamma-irradiation offer an interesting manipulative tool to control aggregation propensity and particle size.

COLLABORATIVE RESEARCH ACTIVITY

Gamma irradiation has been performed at in collaboration with Prof. G. Przybytniak at the Centre for Radiation Research and Technology, Institute of Nuclear Chemistry and Technology, Dorodna 16, 03-195 Warsaw, Poland.

A training programme for Ms. Noha Deghiedy from 04/03/2012 to 04/03/2012 has been provided, aimed to the synthesis and characterization of polyaniline-coated polyolefin films with induced surface electrical conductivity. In particular polyolefin films, produced, radiation grafted with acrylic acid and primed with a variety of difunctional coupling agents at the National Center for Radiation Research and Technology Atomic energy authority, Cairo Egypt, have been fully characterized at the University of Palermo through FTIR, UV and XPS spectroscopies, then used as substrates for in-situ polymerization of polyaniline. The surface coated films were subjected to spectroscopic, morphological (SEM), electrochemical (CV) and electric (Impedance Spectroscopy) characterizations.

REFERENCES TO CHAPTER 8

[8.1] MECERREYES, D., MARCILLA, R., OCHOTECO, E., GRANDE, H., POMPOSO, J.A., VERGAZ, R., SÁNCHEZ PENA J.M., A simplified all-polymer flexible electrochromic device, Electrochim. Acta, 49 (2004) 3555–3559.

[8.2] MADARIA, A.R., KUMAR, A., ISHIKAWA, F.N., ZHOU, C., Uniform, highly conductive, and patterned transparent films of a percolating silver nanowire network on rigid and flexible substrates using a dry transfer technique, Nano Res., 3 (2010) 564–573.

[8.3] MASSARI, A.M., STEVENSON, K.J., HUPP, J.T., Development and application of patterned conducting polymer thin films as chemoresponsive and electrochemically responsive optical diffraction gratings, J. Electroanal. Chem. 500 (2001) 185-191.

[8.4] SCAFFARO, R., LO RE, G., DISPENZA, C., SABATINO, M.A., ARMELAO, L., A new route for the preparation offlexible skin-core poly(ethylene-coacrylic acid)/polyaniline functional hybrids, React. Funct. Polym., 71 (2012) 1177-1186.

[8.5] YANG, J., HOU, J., ZHU, W., XU, M., WAN, M., Substituted polyaniline-polypropylene film composites: preparation and properties Synth. Met., 80 (1996) 283-289.

[8.6] CHAPIRO, A., Radiation Chemistry of Polymeric Systems; Wiley-Interscience: New York, (1962).

[8.7] KAJ, K., Radiation- Induced Grafting of Acrylic Acid onto Polyester Fiber, *Ind.* Eng. Chem. Prod. Res. Dev., 24 (1) (1985) 95–102.

[8.8] GUPTA, B., BŰCHI, F.N., SCHERER, G.G.. Cation exchange membranes by pre-irradiation grafting of styrene into FEP films. I. Influence of synthesis conditions, *J.* Polym. Sci. Part A: Polym. Chem., 2 (1994) 1931-1938

[8.9] PLESSIER, C.; GUPTA, B.; CHAPIRO, A., Modification of polypropylene fiber by radiation-induced graft copolymerization of acrylonitrile monomer, J. Appl. Polym. Sci., 69 (1998) 1343-1348.

[8.10] KWON, O.H., NHO, Y.C., CHEN, J., Surface modification of polypropylene film by radiation-induced grafting and its blood compatibility, J. Appl. Polym. Sci., 88 (2003) 1726-1736.

[8.11] BOZZI, A., CHAPIRO, A., Synthesis of perm-selective membranes by grafting acrylic acid into air-irradiated Teflon-FEP films, Radiat. Phys. Chem, 32 (1988) 193-196

[8.12] GUPTA, B., ANJUM, N., GUPTA, A.P., Influence of solvents on radiation-induced graft copolymerization of acrylamide into polyethylene films J. Appl. Polym. Sci., 77 (2000) 1401-1404.

[8.13] MINGHONG, W., BAO, B., CHEN, J., XU, Y., ZHOU, S., MA, Z.T., Preparation of thermosensitive hydrogel (PP-g-NIPAAm) with one-off switching for controlled release of drugs, Radiat. Phys. Chem, 56 (1999) 341-346.

[8.13] EL-SALMAWI, K.M., EL-NAGGAR, A.M.,. SAID, H.M., ZAHRAN, A.H., Graft Copolymers of Polypropylene Films.1. Radiation-induced Grafting of Mixed Monomers. Polym. Intern. 42 (1997) 225-234.

[8.14] BUCIO, E., CEDILLO, G., BURILLO, G., OGAWA, T., Radiation-induced grafting of functional acrylic monomers onto polyethylene and polypropylene films using acryloyl chloride, Polym. Bull., 46 (2001) 115–121.

[8.15] ZONGHUA, L., YANPENG, J., YIFEI, W., CHANGREN, Z., ZIYONG, Z., Polysaccharides-based nanoparticles as drug delivery systems, Adv. Drug. Deliver *Rev*. 60 (2008) 1650-1662

[8.16] VAN VLIEBERGHE, S., DUBRUEL, P., SCHACHT, E., Biopolymer-based hydrogels as scaffolds for tissue engineering applications: a review, Biomacromol. 12 (2011) 1387-1408
[8.17] SHERWOOD, P.M.A., BRIGGS, D., SEAH, M.P., (Eds.), Practical Surface Analysis, Wiley, New York, 1990, p. 181
[8.18] WAGNER, C.D., DAVIS, L.E., RIGGS, W.M., Surf. Interface Anal., 2 (1986) 53-55.
[8.19] TODARO, S., SABATINO M.A., WALO M., MANGIONE M.R., BULONE D., DISPENZA C., Influence of gamma-irradiation on thermally-induced mesoscopic gelation of degalactosylated xyloglucans, Rad. Phys. Chem. 94 (2014) 245-248.
[8.20] KOPPEL D.E. Analysis of Macromolecular Polydispersity in Intensity Correlation Spectroscopy: The Method of Cumulants, J. Chem. Phys., 57 (1972) 4814.
[8.21] KALAPAT, N., AMORNSAKCHAI, T., Surface modification of biaxially oriented polypropylene (BOPP) film using acrylic acid-corona treatment: Part I. Properties and characterization of treated films, Surf. Coat. Technol., 207 (2012) 594–601.

Chapter 9

DEVELOPMENT OF PARTIALLY BIO-BASED THERMOPLASTIC PACKAGING MATERIALS SUITABLE FOR RADIATION STERILIZABLE PRODUCTS

T. YASIN, A.B. SAQIB, M. NISAR, M. SHAFIQ
Department of Metallurgy and Materials Engineering,
Pakistan Institute of Engineering and Applied Sciences,
Islamabad,
Pakistan

K. HEMVICHIAN
Nuclear Research & Development Group,
Thailand Institute of Nuclear Technology,
Chatuchak, Bangkok,
Thailand

Y.C. NHO
Radiation Research Division of Industry and Environment,
Korea Atomic Energy Research Institute,
Jeongeup-si, Jeollabuk-do,
Republic of Korea

Abstract

This work aimed to develop a polysaccharide based biodegradable packaging material for radiation sterilizable products in order to mitigate the environmental pollution resulted by biostable polymers. Mostly, these biostable polymers are petroleum based which are becoming expensive and their reserves are also depleting with time. The blend of polyethylene and starch were prepared with different amount of functionalized sepiolite using melt mixing technique. Both the electron beam and Co-60 were used to irradiate the composites in air at different doses up to maximum of 100 kGy. The effect of different amount of functionalized sepiolite and ionizing radiation on thermo-mechanical properties of high density polyethylene (HDPE)/starch was investigated. Scanning electron microscopy revealed good dispersion and interfacial adhesion of the additives in the polymer matrix. Both the addition of sepiolite and the radiation dose improved the tensile strength and thermal stability of the composites. The sample irradiated at high gamma dose as well as electron beam showed comparable properties. The obtained results are quite encouraging and will have promising potential as packaging materials for food, drug and other disposable items etc.

9.1. INTRODUCTION

The long term stability and visible appearance of the biostable polymer waste generated environmental concerns. The improper disposal of the polymer waste also faced lot of objections which include complete ban on its commercial use [9.1]. In Pakistan, Environmental Protection Council conducted a national study on plastic bags in 2004. This revealed that about 55 billion bags were being manufactured and consumed annually in the country with an annual growth rate of 15%. The annual average consumption of plastic bags was estimated at 397 bags per person nearly 1 bag/person/day. Based on this trend, nearly 112 billion plastic bags will be consumed by year 2015 [9.2]. The government is trying to address this issue by introducing photo-degradable plastic bags; hydro-soluble plastic bags; and oxo-biodegradable bags, say no plastic bag slogans etc.

The researchers are also trying to find out some green solutions which include: use of completely biodegradable natural or synthetic polymer, use of oxo-biodegradable or biodegradable additives into polymers [9.3-9.8]. The viability of these solutions generates further issues such as: shelf -life of the materials/product, cost, regulations, acceptability of the converters etc. The addition of biopolymers derived from biomass into biostable polymers addresses most of the issues. In addition, the green nature, renewability and biodegradability further increase their acceptance. Different bio-polymer such as: starch, cellulose, chitosan, poly(3-hydroxybutyrate) were added and studied in polymers [9.9-9.11].

A large number of gamma and electron beam irradiation facilities are being used for the sterilization of agricultural and healthcare products [9.12-9.13]. These products are usually packed in plastic bags, vials, tubes, etc which are mostly made from thermoplastic materials. These materials become crosslinked upon irradiation and enhanced its resistance against weathering and biodegradation.

Polyethylene is widely used in packaging industry in various forms [9.14]. It is very stable against biodegradation and its complete degradation needs many years. Efforts have been made to enhance its biodegradation by adding biopolymer [9.15-9.17]. Starch, a natural biopolymer has been selected as biodegradable additive. It is renewable, low cost material with good oxygen barrier properties in dry state [9.28]. Its addition in polyethylene not only reduces the amount of biostable polymer but after biodegradation of starch, the remaining polymer structure become weak, brittle, and degrade more easily [9.19-9.21].

Many researchers have developed polyethylene/starch blend and only few have studied the effect of ionizing radiation on these blend [9.22-9.24]. Our group is trying to develop polysaccharide based biodegradable packaging materials. A comprehensive study has been started in order to enhance the applications of these packaging material in radiation sterilizable products. The effect of ionizing radiation is different for each polymeric material; therefore, it is very important to determine the effect of radiation on these materials. Recently, the influence of functionalized sepiolite and electron beam irradiation on the properties of high-density polyethylene/starch blend was studied [9.23]. This study further elaborates and includes the effect of gamma radiation, its dose rate effect on these polyethylene/starch blends containing functionalized nanoclay.

9.2. MATERIALS AND METHODS

The high-density polyethylene (HDP 547999; mfi= 2.2 g/10 min, 190 °C/2.16 kg), maleic anhydride grafted polyethylene (MA-g-PE), sepiolite, stearic acid and vinyl triethoxy silane were obtained from Sigma-Aldrich Chemie (Steinheim, Germany). The maize starch (Gelose 80, amylose content 80 %) was obtained from Penford (Lane Cove, NSW, Penford Australia). the antioxidants, Irganox-1010 (AO-1) and Irgafos-168 (AO-2) were purchased from Ciba Specialty Chemicals (Basel, Switzerland). Sepiolite is functionalized with vinyl triethoxy silane using published methods [9.25]. The remaining chemicals were used without any further purification.

9.2.1. Preparation of composites

The starch, sepiolite and MA-g-PE are dried in vacuum oven for 8 hour at 60 ^{o}C. The PE/starch blend and its composites are prepared by melt compounding method using Thermo Haake Rheomix-600 (Thermo Electron Corp, Karlsruhe, Germany). HDPE (90 wt%) and MA-g-PE (10 wt%) are melted at 170 °C under the constant rotors speed of 60 rpm. After 3

min, the other additives; starch (10 phr), sepiolite (0-6 phr), stearic acid (1 phr), AO-1 (0.2 phr) and AO-2 (0.1 phr) are added and mixed for another 15 min. The heat pressed sheets are prepared at 170 ^{o}C under the pressure of 200 bar. The PE0, PE2, PE4 and PE6 identification codes are used to represent composites containing 0, 2, 4 and 6 phr of sepiolite.

9.2.2. Gamma radiation of composites

Gamma irradiation of composites was carried at two different dose rates. One batch of samples was irradiated in air at room temperature at dose rate of 5.6 kGy/h at the Thailand Institute of Nuclear Technology using Co-60 gamma irradiator (Gamma Chamber 5000, BRIT). Second batch of samples was irradiated at dose rate of 0.9 kGy/h using Co-60 gamma irradiator (Model JS-7900, IR-148) at Pakistan Radiation Services at Lahore.

9.2.3. Fourier transform infrared spectroscopy

The structural analysis is performed using a Nicolet 6700 Fourier transform infrared (FT-IR) Spectrometer (Thermo Scientific, Waltham, USA). The spectra are obtained using attenuated total reflectance mode in the range of 4000 to 400 cm^{-1} at a resolution of 6 cm^{-1}. Average of 116 scans is reported.

9.2.4. X-ray Diffraction

X-ray diffraction patterns of the composites are obtained on STOE X-ray diffractometer (Darmstadt, Germany) using CuKα radiation (1.541 ºA). The samples are scanned from 2º to 45º at 20 kV.

9.2.5. Morphological analysis

The morphology of composites is examined using a scanning electron microscope, JSM 6490LA (JEOL, Japan) at 20 kV. The cryo-fractured samples are coated with gold prior to analysis. Energy dispersive spectroscopy is also performed to investigate the elemental composition.

9.2.6. Thermogravimetric analysis

The thermal stability of samples is investigated using thermogravimetric analyzer (Mettler-Toledo TGA/SDTA851^{e}, Switzerland). The analysis is performed under nitrogen (40 mL/min) at heating rate of 20 ^{o}C/min from 50 to 600 ^{o}C.

9.2.7. Gel content determination

The gel content of irradiated composites were calculated according to ASTM 2765 using Soxhlet apparatus. The samples are extracted in boiling xylene for 8 h and the gel content is calculated using following formula:

Gel content (%) = $(W_1/W_0) \times 100$

Where, W_0 and W_1 are weight of sample before and after extraction respectively.

9.2.8. Tensile properties

Tensile tests are carried out at room temperature using a universal tensile testing machine, SANS BSS-500 kg (SANS group, China) according to ASTM D-638 at a crosshead speed of 50 mm/min and 10 kN load cell. Five specimens are tested for each formulation and the average results are reported.

9.2.9. Solvent uptake measurement

The solvent uptake of samples is measured in various solvents. Three pieces of sample with uniform size and weight (~ 0.5 g) are immersed in solvent (20 mL) at room temperature (~ 25 °C). After certain time period the sample is removed and wiped out the excess solvent with lint free filter paper and weighed again. The solvent uptake is measured as:

Solvent uptake (%) = $[(W_2 - W_1)/W_1] \times 100$

Where, W_1 and W_2 are weight of sample before and after swelling respectively

9.3. RESULTS AND DISCUSSION

9.3.1. Structural analysis

Figure 9.1. presents the FTIR spectra unirradiated and irradiated composites are given in Fig. 9.1. IR peaks appeared in the region of 3000-2850 cm^{-1} and 1460-1470 cm^{-1} correspond to streching and bending vibrations of C-H bonds present in polyethylene respectively. Charectaristic peaks of starch are appeared at 990, 1024 and 1078 cm^{-1}. Bands appeared at 990 and 1024 cm^{-1} correspond to the C-O streching present in anhydroglucose ring and 1078 cm^{-1} correspond to streching of C-O in C-O-H group.

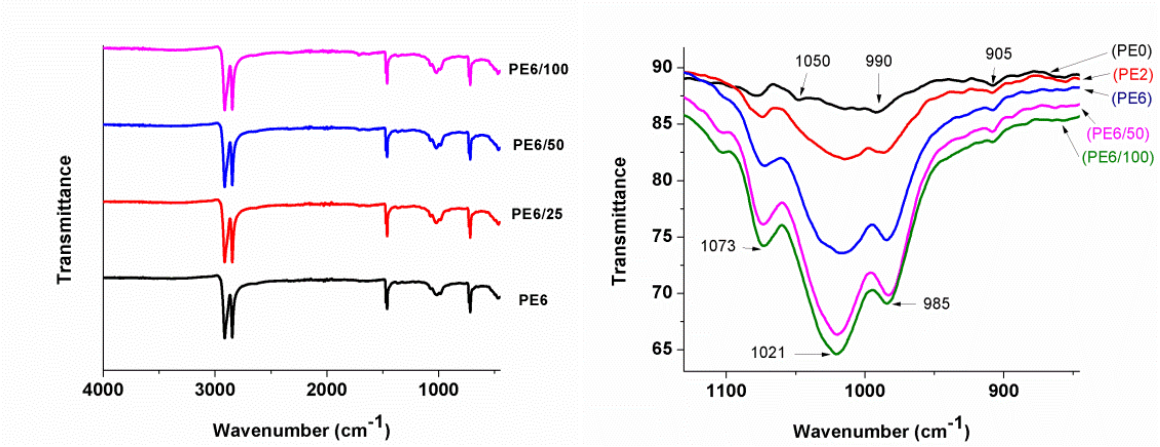

FIG. 9.1. Infrared spectra of unirradiated and irradiated composites in the range of 4000-450 cm^{-1} (left) and 1150-850 cm^{-1} (right)

Characteristic peaks of sepiolite are observed at 1021 and 470 cm^{-1} corresponding to streching and bending vibration of Si-O respectively. Increased intensity of bands at 1020 cm^{-}

[1] from PE2 and PE6 indicates the increased amount of sepiolite. Similarly gamma irradiation of PE6 at absorbed dose of 50 and 100 kGy had further increased the intensity of these bands. Bands appeared at 1078 and 990cm^{-1} has been shifted to lower wave number at 1073 and 985 cm^{-1} respectively as well as their intensity is increased with increase with sepiolite and dose. This behaviour is attributed to the formation of hydrogen bonding between C-O-H group present in starch and polar group of PE-g-MA as reported by Shujan et al. Spectra of gamma irradiated samples are similar to unirradiated samples which shows that polyethylene and other additive retained their structural integrity during gamma irradiation.

9.3.2. X-ray diffraction

The effect of ionizing radiation on crystallinity and crystal structure of composites is carried out using X-ray diffraction (XRD) technique. The XRD patterns of PE0, PE2, PE6 and PE6/100 are shown in Figure 9.2. The spectrum of PE0 shows the peaks at 21.6°, 24.0° and 36.4° which are characteristics peaks of polyethylene corresponding to (110), (200) and (020) planes respectively. The main peak of sepiolite corresponding to its (110) plane is appeared at 7.2° and the intensity of this peak is increase from PE2 to PE6 indicates the presence of higher amount of sepiolite in PE6. It is also observed that intensities of polyethylene peaks appeared at 21.6° and 24° are decreased with increasing amount of sepiolite from PE2 to PE6. The addition of 2% clay increases the crystallinity of PE from 53.75 % to 65.00 %. This increase is basically due to the presence of clay crystals within the PE matrix and its crystals further summing up the results to enhance the % crystallinity to 65 %. On increasing the percentage of clay from 2% to 6%, the percent crystallinity is further increased to 69%. However, irradiation of PE containing 6% clay with a dose of 50 kGy and 100 kGy interestingly reduced the % crystallinity. The plausible explanation of this is the PE crystallite lamella rearrangements formation of network structure by gamma radiation has also reduced the crystallinity of polyethylene.

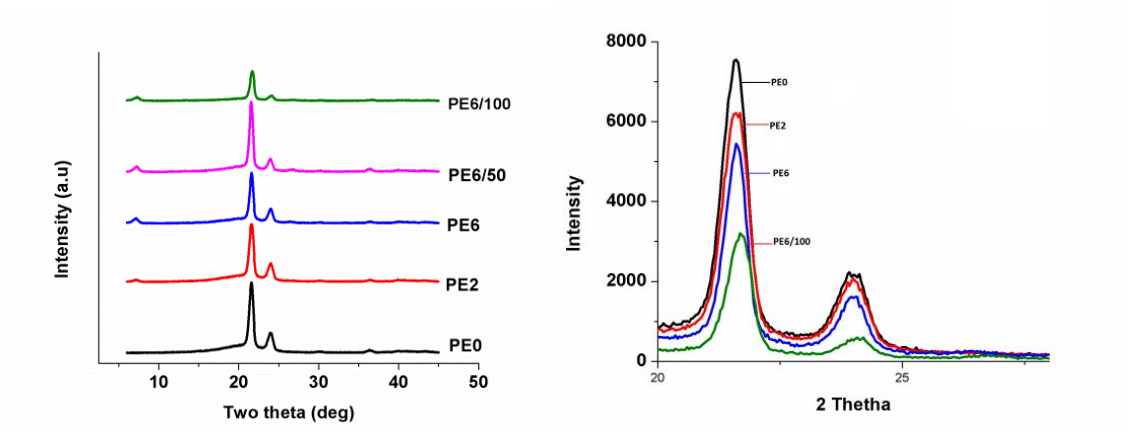

FIG. 9.2. XRD pattern of unirradiated and irradiated composites in range of 5°-50° (left), 20°-25° (right).

9.3.3. Morphological analysis

The scanning electron micrographs of the fractured surfaces of unirradiated and irradiated PE6 composites are shown in Figure 9.3. The micrographs of unirradiated composite showed good compatibility and dispersion of the additives in the polymer matrix. Both the addition of

MA-g-PE and the functionalization of sepiolite improved the dispersion and interfacial adhesion of the additives. In their absence, voids and gaps were observed in LDPE/starch/sepiolite composites [9.10]. The micrographs of irradiated composite showed ductile nature of the samples which confirm the interfacial adhesion and compatibility of the additives with the matrix. This improvement is resulted by radiation-induced reactions such as: crosslinking of polymer chains, grafting of sepiolite in the matrix.

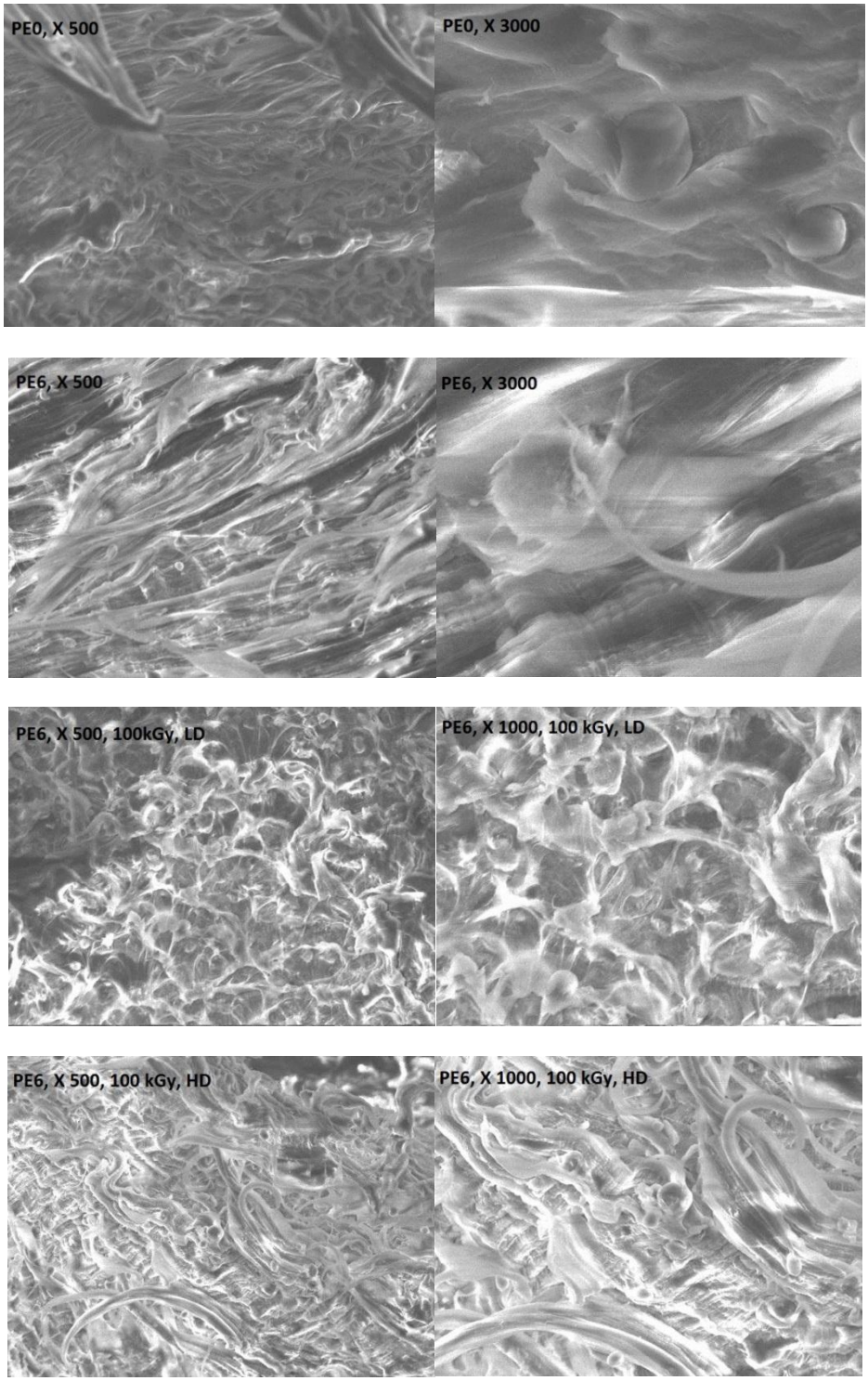

FIG. 9.3. Sem micrographs of unirradiated and irradiated composites at different maginification.

9.3.4. Gel content analysis

The amount of crosslinking induced by gamma irradiation in the polyethylene/starch blend and its composites was determined by gel content measurements. Gel content of composites at different dose rates and at various doses is depicted in Figure 9.4. This figure shows that the gel content of composites is increased with increase in absorbed dose. In addition, the increase in amount of sepiolite from 0 to 6 phr had reduced the gel content. This might be attributed to the formation of H^o and OH^o due to radiolysis of water molecules present in sepiolite which stabilized the polyethylene macro-radicles and reduced its gel content.

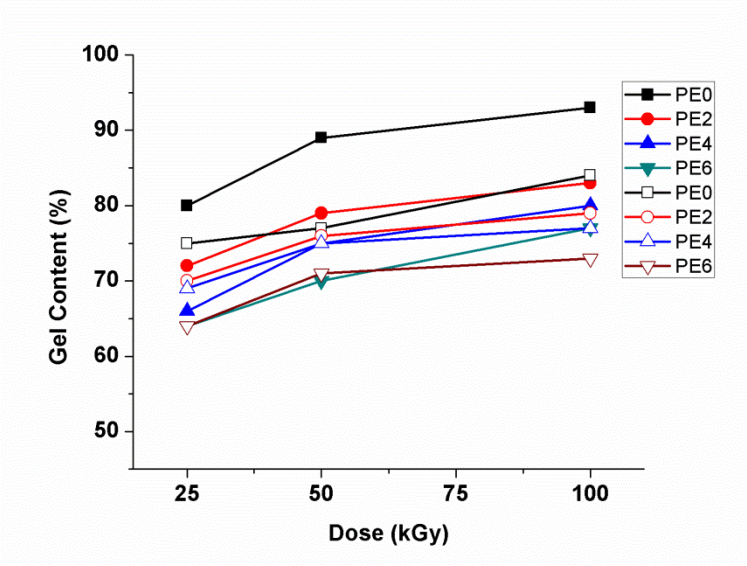

FIG. 9.5. Gel content of the composites at high dose rate (solid) and low dose rate (hollow)

9.3.5. Thermogravimeric analysis

Thermal stability of the composites is studied by using thermogrametric analysis. The thermograms of unirradiated and irradiated composites are given in Figure 9.5.

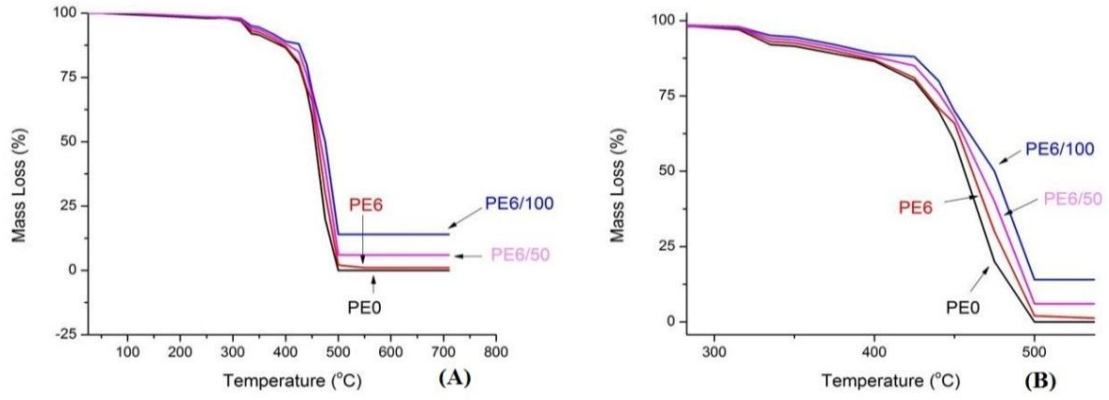

FIG. 9.5. Thermograms of PE0.PE6, PE6/50 and PE6/100 in the range of 25-550 °C (A) and 300-550 °C (B).

This figure shows that all samples had undergone two steps degradation. The first mass loss occurred around 310 °C which is almost identical for all samples. This mass loss is associated with the degradation of starch. The second mass loss occurred at higher temperature and is

mainly due to the degradation of polyethylene. It is also observed that the degradation temperature of PE6 is shifted towards higher temperature as compared to PE0. This indicates that incorporation of sepiolite in polyethylene/starch blend has improved its thermal stability. Similarly, high thermal stability of irradiated PE6 indicates that gamma irradiation has further improved its thermal stability. This improvement is attributed to formation of crosslinked network due to gamma radiation.

9.3.6. Mechanical Properties

The tensile strength (Tb) and elongation at break (Eb) of pristine HDPE are 18.7 MPa and 932% respectively. The Tb of unirradiated and irradiated composites is given in Table 9.1. This table shows that Tb of the samples is increased with increase in amount of sepiolite. This behavior is due to the reinforcing effect of filler particles which increase the resistance against chain movement. The Tb of irradiated composites is also increased with increase in absorbed dose. This trend is attributed to the formation of crosslinked network structure induced by gamma radiation as indicated by gel content analysis. At a given dose, Tb is increased with increase in sepiolite, indicating the reaction of the vinyl group of functionized sepiolite with polymer matrix upon irradiation.

TABLE 9.1. TENSILE STRENGTH (MPa) OF UNIRRADIATED AND IRRADIATED COMPOSITES AT DIFFERENT DOSES

	Modified Sepiolite	Dose rate (5.6 kGy/h)			Dose rate (0.9 kGy/h)		
Dose (kGy)	0	25	50	100	25	50	100
PE0	20.8	23.6	24.8	26.7	23.1	24.0	25.7
PE2	21.6	25.9	26.0	26.9	24.4	25.6	26.0
PE4	22.6	26.0	27.7	27.9	24.8	25.9	26.9
PE6	23.3	27.3	27.8	29.6	25.5	26.9	28.7

Table 9.2. shows the Eb of the unirradiated and irradiated composites. The Eb is decreased with increasing amount of sepiolite and dose. It is also clear from these tables that both Tb and Eb of the composites samples subjected to higher dose rate are higher than that of the samples irradiated at lower dose rate.

TABLE 9.2. ELONGATION AT BREAK (%) OF UNIRRADIATED AND IRRADIATED COMPOSITES AT DIFFERENT DOSES

	Modified Sepiolite	Dose rate (5.6 kGy/h)			Dose rate (0.9 kGy/h)		
Dose (kGy)	0	25	50	100	25	50	100
PE0	546	518	467	313	107	83	24
PE2	472	420	175	168	45	31	21
PE4	253	195	126	63	33	23	15
PE6	112	97	59	49	20	13	9

9.3.7. Solvent uptake measurements

The solvent uptake study of the composites was carried out in different solvents having different polarity and results were presented in Table III and IV. This table showed the following trend in the solvent uptake of composites in descending order: chloroform > xylene > kerosene oil > acetone > water > methanol > NaOH > H_2SO_4. The higher solvent uptake in chloroform was due to its optimum polarity as well as its interaction with the additives present in the composites. The increased uptake with increase in time is due to the more absorption of solvents by composites. The solvent uptake of PE6 is slightly higher than PE_0, and the values were lowered with increase in the absorbed dose. The reduction in solvent uptake in radiation crosslinked samples was attributed to the formation of network structure which hinders the solvent absorption.

TABLE 9.3. SOLVENT UPTAKE VALUES (%) OF UNIRRADIATED AND IRRADIATED COMPOSITES (PE6) IN DIFFERENT SOLVENT (25 kGy)

Solvent	Unirradiated		PE_6 EB [23]		PE_6 γ HD		PE_6 γ LD	
	24 hr	48 hr	24 hr	48 hr	24 hr	48 hr	24 hr	48 hr
Xylene	8.65	8.50	7.18	7.51	7.62	7.18	8.22	7.66
Kerosene oil	7.04	6.88	5.62	5.96	6.36	6.70	6.57	6.70
Chloroform	13.99	13.62	12.78	13.02	12.69	13.21	14.59	13.88
Acetone	1.32	1.27	1.19	1.35	0.89	1.55	1.13	1.85
Methanol	0.87	0.98	0.53	0.80	0.66	0.86	0.82	1.50
NaOH	1.01	0.38	0.44	0.67	0.90	1.25	0.66	0.66
H_2SO_4	0.50	0.46	0.31	0.63	0.32	0.26	0.20	0.34
H_2O	0.48	0.59	0.28	0.32	0.46	0.40	0.44	0.38

TABLE 9.4. SOLVENT UPTAKE VALUES (%) OF UNIRRADIATED AND IRRADIATED COMPOSITES (PE6) IN DIFFERENT SOLVENT (100 kGy)

Solvent	PE_6 EB [23]		PE_6 γ HD		PE_6 γ LD	
	24 hr	48 hr	24 hr	48 hr	24 hr	48 hr
Xylene	6.78	6.80	7.25	6.96	6.96	7.03
Kerosene oil	5.30	5.71	5.67	6.22	5.20	6.33
Chloroform	12.77	12.77	12.69	12.22	12.94	12.73
Acetone	1.63	1.42	0.61	1.28	0.56	1.04
Methanol	0.09	0.19	0.72	1.38	0.49	1.24
NaOH	0.33	0.08	0.64	1.11	1.24	0.43
H_2SO_4	0.12	0.25	1.59	1.18	0.62	0.69
H_2O	0.28	0.65	0.69	1.09	0.74	0.88

9.4. CONCLUSIONS

Polyethylene based biodegradable packaging material for radiation sterilizable products were prepared using melt mixing technique. These composites contain different amount of functionalized sepiolite. The influence of electron beam and Co-60 radiation on thermo-mechanical properties was investigated. The gel content of developed composites is increased with the increase in dose. The intensities of XRD peaks of polyethylene appeared at 21.6^o and 24^o are decreased with increasing amount of sepiolite. Scanning electron microscopy revealed good dispersion and interfacial adhesion of the additives in the polymer matrix. Both the addition of sepiolite and the radiation dose improved the tensile strength and thermal stability of the composites. The comparison of dose rate revealed that Tb and Eb of the composites samples subjected to higher gamma dose rate is higher than that of the samples irradiated at lower gamma dose rate. The obtained results are quite encouraging and will have promising potential as packaging materials for food, drug and other disposable items etc.

REFERENCES TO CHAPTER 9

[9.1] MIR, S., YASIN, T., HALLEY, P.J SIDDIQI, HM., NICHOLSON, T., Thermal, rheological, mechanical and morphological behavior of HDPE/chitosan blend, Carbohydrate Polymers, 83, 414–421, 2011

[9.2] ARVANITOYANNISA, I., BILIADERIS C. G., OGAWAB, H., KAWASAKIB, N., "Biodegradable films made from low-density polyethylene (LDPE), rice starch and potato starch for food packaging applications: Part 1", Carbohy. Polym., **36** (1998) 89- 104

[9.3] BUCCI, D.Z., TAVARES, L.B.B., SELL, I."PHB packaging for the storage of food products", Polym. Test., 24 (2005) 564-571

[9.4] RAY, S.S., OKAMOTO, M. "Biodegradable polylactide and its composites: opening a new dimension for plastics and composites", Macromol. Rapid. Comm., **24** (2003) 815-840

[9.5] WITT, U., EINIG, T., YAMAMOTO, K.M.I., DECKWER, W.D., MÜLLER, R.J. "Biodegradation of aliphatic–aromatic co-polyesters: evaluation of the final biodegradability and ecotoxicological impact of degradation intermediates", Chemosphere, **44** (2001) 289-299

[9.6] BRIASSOULIS, D. "Mechanical behavior of biodegradable agricultural films under real field conditions", Polym. Degrad. Stabil., **91**/16 (2006) 1256-1272

[9.7] ABRUSC, C., PABLOS, J.L., MARÍN, I., ESPÍ, E., CORRALES, T., CATALINA, F., "Comparative effect of metal stearates as pro-oxidant additives on bacterial biodegradation of thermal- and photo-degraded low densitypolyethylene mulchingfilms", Int. Biodeter. Biodegrad., **83** (2013) 25-32

[9.8] YASHCHUK, O., PORTILLO, F. S., HERMIDA, E. B., "Degradation of polyethylene film samples containing oxodegradable additives", Procedia Mater. Sc.**1**(2012) 439 – 445

[9.9] MOHANTY, A.K., MISRA, M., DRZAL, L.T., "Sustainable bio-Composites from renewable resources: opportunities and challenges in the green materials world", J. Polym. Environ., **10** (2002) 19-26

[9.10] MIR. S., YASIN, T., HALLEY, P.J., SIDDIQI, H.M., OZDEMIR, O., NGUYEN, A., "Thermal and rheological effects of sepiolite in linear low-density polyethylene/starch blend", J. Appl. Polym. Sci., **127/2** (2013) 1330–1337;

[9.11] MASOOD, F., YASIN, T., HAMEED, A., Comparative oxo-biodegradation study of poly-3-hydroxybutyrate-co-3-hydroxyvalerate/polypropylene blend in controlled environments, int. Biodeter. Biodegrad, **87** (2013) 1-8,

[9.12] HAJI-SAEID, M., SAMPA, M.H., RAMAMOORTH, N.Y., GUVEN, O., CHMIELEWSKI, A.G., "The role of IAEA in coordinating research and transferring technology in radiation chemistry and processing of polymers", Nucl. Instrum. Methods Phys. Res. Sect. B,**51** (2007) 265

[9.13] IAEA TECDOC Emerging applications of Radiation processing for the 21st century, Vienna 28-30 April 2003.

[9.14] PIRINGER, O. G.; BANER, A. L., "Plastic packaging: interactions with food and pharmaceuticals". Wiley-VCH: Weinheim, 2008

[9.15] CERCLÉ, C., SARAZIN, P., FAVIS, B.D., "High performance polyethylene/thermoplastic starch blends through controlledemulsification phenomena", Carbohyd. Polym., **92** (2013) 138– 148

[9.16] BYUNG, C. J., SOO, Y.H., JEONG, G.J., YOUNG, C.B., "Mechanical properties and morphology of the modified HDPE/starch reactive blend", J. Appl.Polym.Sci.,**82** (2001) 3313-3320

[9.17] GUPTA, A.T., KUMAR, V., SHARMA, M., SHUKLA, S.K., "Physicochemical studies on the interaction behaviour of potato starch filled low density polyethylene grafted maleic anhydride and low density polyethylene biodegradable composite sheets", Polym. Plast. Technol. Eng., **48** (2009) 587-594

[9.18] WALKER, A.M., TAO, Y., TORKELSON, J.M., "Polyethylene/starch blends with enhanced oxygen barrier and mechanical properties: Effect of granule morphology damage by solid-state shear pulverization", Polymer, **48** (2007) 1066-1074

[9.19] SHUJUN, W., JIUGAO, Y., JINGLIN, Y., "Preparation and characterization of compatible and degradable thermoplastic starch/polyethylene film", J. Polym.Environ.,**14** (2006) 65-70

[9.20] CHANDRA, R., RUSTGI, R., "Biodegradation of maleatedlinear low-density polyethylene and starch blends", Polym. Degrad. Stabil., **56** (1997) 185-202
[9.21] LIAO, H., WU, C."Synthesis and characterization of polyethylene-octene elastomer/clay/biodegradable starch composites", J. Appl. Polym. Sci., **97** (2005) 397-404
[9.22] SENNA, M.M., HOSSAM, F.M., WAHAB, A., EL-NAGGAR M., "Compatibilization of low-density polyethylene/plasticized starch blends by reactive compounds and electron beam irradiation", Polym. Compos.,**29** (2008) 1137-1141
[9.23] YASIN, T., NISAR, M., SHAFIQ, M., NHO, Y.C., AHMAD, R., "Influence of Sepiolite and Electron Beam Irradiation on the Structural and Physicochemical Properties of Polyethylene/Starch Nanocomposites". Polym. Composites, **34/3** (2013) 408–416.
[9.24] EL-REHIM, H.A., EL-SAYED, A.H., ALI, A.M., RABIE, A.M., "Synergistic effect of combining UV-sunlight-soil burial treatment on the biodegradation rate of LDPE/starch blends", J. Photo. Chem. Photo. Boil. A: Chem., **163** (2004) 547-556
[9.25] SHAFIQ, M., YASIN, T., SAEED, S., "Synthesis and characterization of linear low-density polyethylene/sepiolite nanocomposites". J. Appl. Polym. Sci., **123** (2012) 1718-1723.

Chapter 10

RADIATION SYNTHESIS AND CURING OF NANOCOMPOSITES SUITABLE FOR PRACTICAL APPLICATIONS

G. PRZYBYTNIAK, K. CIEŚLA, E. KORNACKA, J. SADŁO, M. BUCZKOWSKI, A. NOWICKI
Institute of Nuclear Chemistry and Technology
Warsaw,
Poland

Abstract

Under the CRP the studies on micro- and nanostructures incorporated into synthetic and natural polymers were conducted. The metal agglomerates and metal haloids synthesis was supported by ionizing radiation and the products were then stabilized in various matrices. The effect of Ag^{+} and Cu^{2+} coordination by the functional groups of the copolymer constructed from acrylic acid and acrylamide was investigated by EPR spectroscopy and by swelling with aqueous solutions at various pH. Molecular sieve were applied as a matrix stabilizing metal clusters produced by gamma-irradiation. It was confirmed that dimension and charge of the products depend on the geometry of sodalite cages as well as the presence of water molecules and/or anions in the porous structure. It was also proved that track-etched membranes produced by heavy ion beam can be applied as templates for obtaining silver halides in the form of nano/micro rods and grains. In the second stage of the project the influence of nanocarbon particles on radiation cured epoxy resin was investigated. By EPR spectroscopy it was found that ionizing radiation generates at least two types of paramagnetic defects in graphene oxide. They are probably located in the pre-existing crystal damages as a total population of defects remains almost constant. It was confirmed that epoxy resins might be cured by ionizing radiation in the presence of selected cationic initiators. The thermal effect and induction time of the process strongly depends on dose rate. Induction time increases at smaller concentrations of initiator and lower dose rates as well as in the presence of graphene oxide. It was confirmed that a new type of cumarine based initiator is an attractive alternative for the commercial product (Rhodosil). Our work on the polysaccharide based multicomponent systems has shown that irradiation causes changes in interaction of starch with the naturally occurring or admixed lipids/surfactants. The subject of research were three surfactants: cetyltrimethylammonium bromide (CTAB, cationic), sodium laurate (Na-Lau, anionic) and mono-lauroyl glycerol (MLG, non-ionic), and two lipids: lauric acid (Lau) and palmitic acid (Pam). The specific changes in the thermal properties of the systems constructed from irradiated starch and Na-Lau and Na-Pam were found. Additionally, the meaningful differences between the processes occurring in the systems containing lauric and palmitic acids were discovered, suggesting formation of the Lau inclusion complexes and surface complexes in the case of Pam. It was also found that irradiation of the films formed in the starch-NaLau-nanocellulose system might decrease their hydrophilicity. The starch particles with reduced dimensions were detected after radiation treatment.

10.1. OBJECTIVE OF THE RESEARCH

Very fast development of nanotechnology in material science and engineering stimulates progress in the production and stabilization of nanostructures. The assembly of nanoparticles by “bottom-up” approach supported by ionizing radiation leads to the creation of functional materials that might be applied in various branches of industry. The radiation methods are suitable not only for the generation of metallic particles but also for designing their dimension, controlling the geometry, modification of the environment followed by the strengthening nanoparticle stabilization. Therefore, research in this area might result in significant scientific and practical benefits.

Studies of reinforced epoxy resins are now receiving great attention as recently many industrial applications of such products have been successfully implemented in several areas, e.g. aerospace, automobile, marine, construction, etc. However, when thermally cured, toxic low molecular components are emitted during the process and the final product is brittle with low crack resistance what limits its utility for structural applications. Environmentally friendly radiation treatment as an alternative method to thermal curing of nanocomposites has been proposed.

The third part of the investigations was focused on the applicability of selected polysaccharides in food packaging and pharmacy. The main goal of the studies was to improve their properties as a potential barrier or carrier for active components [10.1-10.6]. This might be achieved by the modification of composition and by adjustment of the interaction between particular components in the multicomposite system using physical and chemical methods. Therefore, the introduction of the hydrophobic compounds (such as lipids or surfactants [10.3, 10.4] or nanoparticles i.e. nanopolysaccharides [10.5, 10.6]) is expected to improve barrier properties against water and to modify microstructure of the resulting films, coatings or particles. Application of ionizing radiation seems to be the perspective possibility for modification of their structure by degradation, crosslinking or grafting in the systems containing polysaccharides.

10.2. RESEARCH CONDUCTED AT THE INSTITUTE OF NUCLEAR SCIENCE AND TECHNOLOGY

10.2.1. Metal/metal halides nanostructures sythetized with support of ionising radiation

Three issues related to radiation processing of the products containing metals or their compounds were investigated in order to expand knowledge on the systems which might find applications in medicine and selected braches of industry.

1. Organic-inorganic hybrid materials show attractive features because they might combine the properties of both kinds of phases. Among them silver and copper fillers are widely studied due to many potential applications, e.g. in catalysis. The size of metal particles formed in polymer matrix using gamma-rays depends on radiation conditions, concentration and chemical nature of stabilizing surrounding. On the basis of the studies performed it was concluded that metal cations (Ag^{+}, Cu^{2+}) introduced into polymeric matrices synthesized with support of ionizing radiation influence macroscopic properties of the final product. Films constructed from the copolymer of acrylic acid and acrylamide exhibit pH responsive properties – at acidity environment diffusion of aqueous solutions is slowed down whereas in ionic state (at higher pH) diffusion increases even threefold. It was confirmed that the features and susceptibility on water penetration might be controlled by crosslinking density resulting from applied doses. The structure determines diffusion of metal ions and their coordination by the functional groups of polymeric macromolecules. Low temperature EPR spectra revealed that Cu^{2+} is coordinated by only one or two carboxylic acid groups and the number of ligands is increasing at ambient temperatures when amine group of acrylamide mer is incorporated into metallic centre surrounding. Thus, the penetration of water molecules is influenced by intra- and intermolecular hydrogen bonding system, radiation crosslinking and metal complexes that play a role of additional network nodes.

2. Silver in the form of aggregates has attracted great interest due to its unique properties as a catalyst. In this respect size of the particles and their distribution play a crucial role. Sodalites are very convenient matrices for the stabilization of various metallic clusters. Generated by gamma rays silver atoms form agglomerates that have a tendency to produce stable structures with silver cations present in the cages. The paramagnetic products were characterized by EPR spectroscopy. Fig. 10.1. shows an example of the spectrum recorded under cryogenic conditions for the clusters constructed from six atoms.

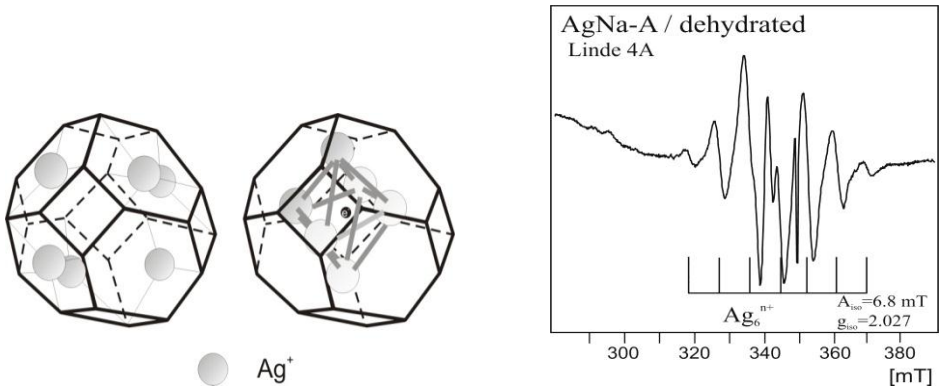

FIG. 10.1. Hexamer spaced in the cage and its EPR spectrum recorded at 110 K for dehydrated Ag-sodalite gamma-irradiated at 77 K.

Two mechanisms of the silver cluster formation are proposed (i) agglomeration process is initiated by radiolytic formation of silver atoms Ag^0 and involves the reaction between silver atom and Ag^+ leading to the formation of silver dimmers Ag_2^+, trimmers Ag_3^{2+}, tetramers Ag_4^{3+}, etc., (ii) pre-arrangement of silver cations in the cages (Fig. 10.1). The nuclearity of clusters stabilized in sodalites depends also on the size of sodalite crystallites, hydration, temperature and presence of additional functional groups.

3. Membranes produced by the exposure of polymer films (polyesters) to heavy ion beam can be applied for the template synthesis of silver haloids (AgCl, AgBr) microstructures. Silver haloids in the form of nano and microrods have been embedded in track-etched membrane (TM) of a pore size from 0.2 μm up to 2.3 μm, Fig. 10.2. The size of the deposited structures corresponds to the diameter of membrane pores. Additionally, on membrane surfaces micrograins have been deposited. The phenomenon was confirmed only on the surface remaining in contact with NaCl solution, whereas $AgNO_3$ solution separated by the membrane does not induce such an effect.

   Light having a wavelength of 366 nm and 10 MeV electron beam influence silver haloids microstructures inducing darkening which might be measured by a photometric method. Additionally, changes in morphology of micrograins were found. It seems that the nano and microstructures of silver haloids might be used as indicators of UV or ionizing radiation.

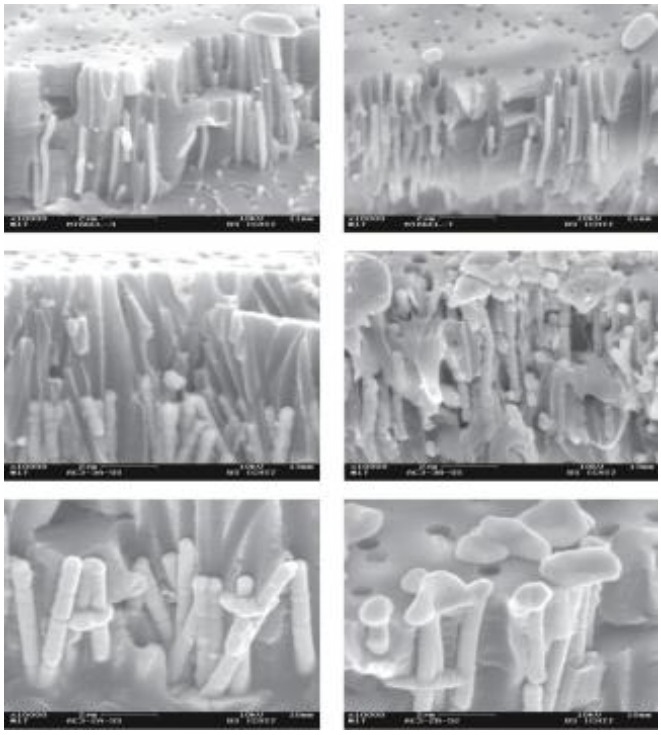

FIG. 10.2. Fractures of TMs with deposited AgCl microstructures (SEM photographs – magnification 10000x). Upper row – pore size: 0.2 μm; middle row - pore size: 0.4 μm; lower row - pore size: 0.7 μm. Left column – membranes surface at the side of $AgNO_3$ solution; right column - membranes surface at the side of NaCl solution

10.2.2. Radiation cured epoxy resin nanocomposites containing carbon nanoparticles

Graphene is a promising material that potentially might replace some of the currently used substances in many applications. Features such as outstanding flexibility, transparency, conductivity, elasticity, impermeability, chemical inertness are characteristic only for good quality graphene thus its applicability is determined by the type and number of defects which usually deteriorate the performance of graphene-based devices [10.7]. From this point of view graphene oxide is less attractive material than graphene used for electronic and optical applications but for production of nanocomposites the structural imperfections do not diminish its value as an important and desirable filler. The influence of irradiation on the graphene properties is of fundamental science interest since the theoretical and practical significance [10.8-10.10]. In the past the irradiation effects in bulk graphite were recognized extensively due to its wide applications in nuclear reactors. At the same time, no analogous data are available for graphene and graphene oxide.

In the course of our work graphene oxide (GO) was irradiated to various doses in the range of 0-1200 kGy with accelerated electrons (10 MeV). At room temperature the EPR spectrum of graphene oxide shows almost symmetric narrow singlet of g=2.0029 and line width Hpp=0.50 mT, Fig.10.3a, b. It was found that at high values of microwave power additionally a broader low intensity signal emerges attributed to the other type of paramagnetic centre. The value of g-factor is lower (2.0027) what suggests delocalization over at least several carbon atoms. Intensity of the signals increases when the absorbed dose grows, Fig. 10.3c. The effect is particularly apparent in the range of 0-200 kGy. The origin of the detected peaks has not been discovered yet. Usually it is assumed that they are related to dangling bonds of paramagnetic defects or conduction electrons [10.11].

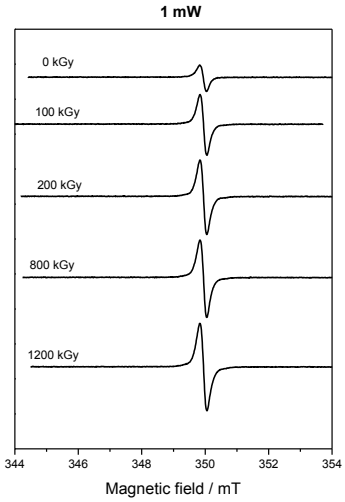

A

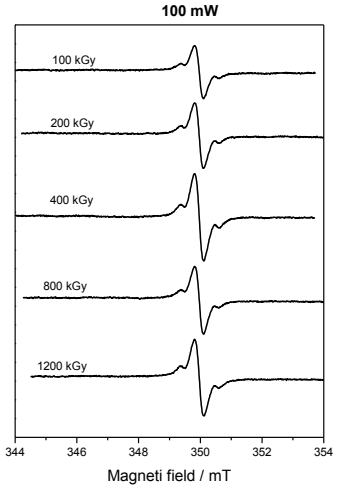

B

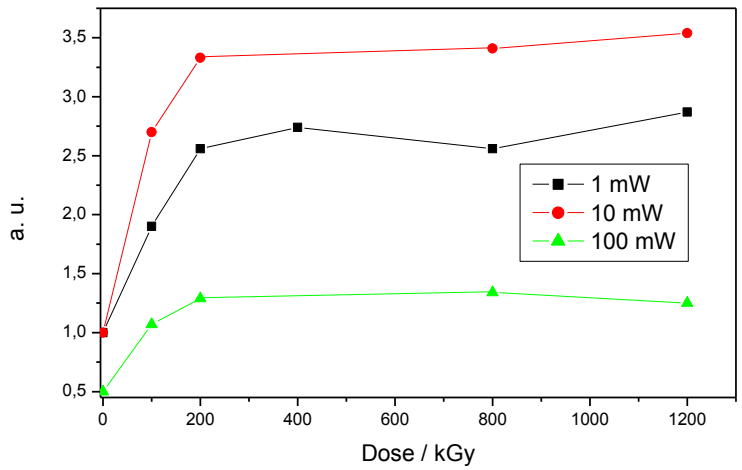

C

FIG. 10.3. EPR spectra of GO irradiated with an electron beam, recorded at various microwave powers (A and B). Profiles of the increase of paramagnetic centre population determined on the basis of double integration of the EPR signals (C).

The data were confronted with Raman spectroscopy results, Fig. 10.4. It was found that area of G and D mode corresponded to sp^2 and sp^3 hybridization respectively, slightly decreased for the low doses and increased for higher ones. The results showed that an increase in total number of lattice defects was followed by the annealing process for higher doses.

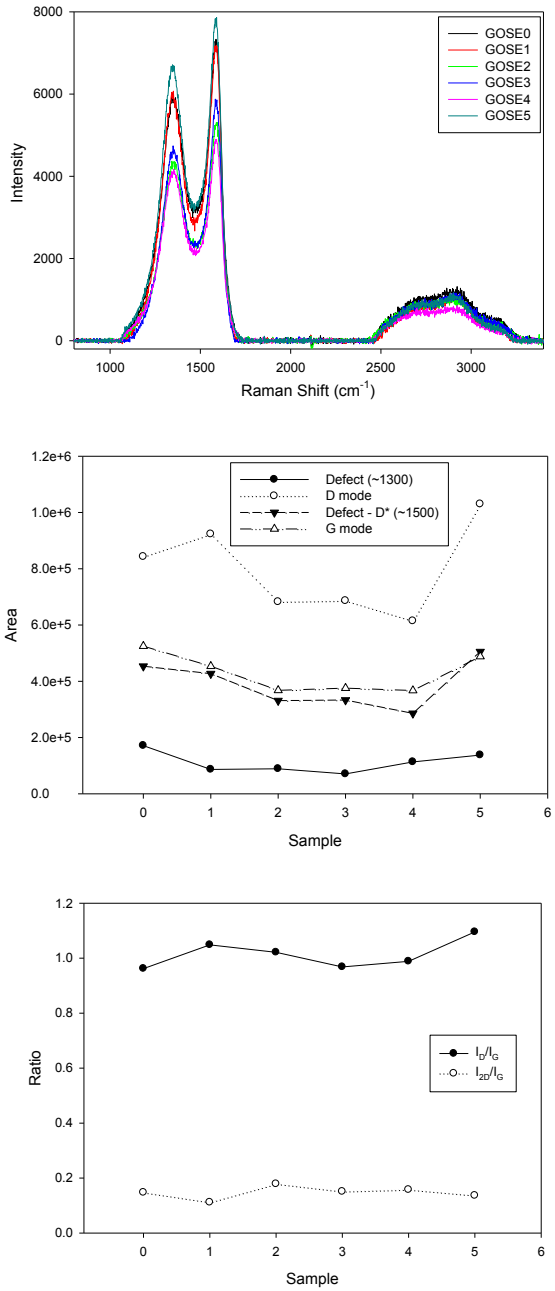

FIG. 10.4. Comparison of Raman spectra of GO irradiated with various doses of gamma-rays (A). Fluctuations of various modes determined by Raman spectroscopy (B and C). 0-0 kGy, 1-100 kGy, 2-200 kGy, 3-400 kGy, 4-800 kGy, 5-1200 kGy.

The EPR studies confirmed that there are at least two types of paramagnetic centers in the studied graphene-based product. Upon radiation treatment the concentration of such defects increases up to 200 kGy and then remains almost constant to 1200 kGy. The changes are inconsistent with the total population of defects (diamagnetic and paramagnetic ones) determined on the basis of G and D peaks of Raman spectra. Increase of paramagnetic centers

followed by irradiation probably results from conversion of non-paramagnetic defects to paramagnetic defects due to localization of electrons in pre-existing crystal imperfections. Irradiation with electron beam does not reduce the population of functional groups in GO in spite of well known electron mobility within the plane of graphene sheets. It seems that the process just convert them into other substituents.

In the next stage of the research graphene oxide and nanocarbon tubes were introduced into the epoxy resin. Previous papers reported successful radiation curing of non-filled thermosets [10.12-10.14]. The work was focused on the studies related to radiation-induced curing of epoxy resin based on diglycidyl ether of bisphenol A (DGEBA) and its commercial analogue Epidian. Carbon nanotubes (CNT and MWCNT) in the form of suspension in epoxy resin were provided by Nanomaterials Co, Warsaw, Poland. Graphene oxide was synthesized by Hummer's method at the Institute of Electronic Materials and Technology, Warsaw [10.15], whereas the reduced form of the material (RGO) was prepared at the Institute of Nuclear Chemistry and Technology as a suspension in dichloromethane.

A cationic initiator [4(1-methylethyl)phenyl][4-methylphenyl]iodonium tetrakis-(pentafluoro-phenyl)borate salt (IPB, Scheme 1A) was purchased in Secant Chemicals Inc., USA. In order to compare quality of the resins synthesized using various initiators other derivatives of iodonium salts containing coumarine substituent and SbF_6(1-) or PF_6(1-) anions were also applied (prepared at the Technical University in Cracow, Poland) [10.16].

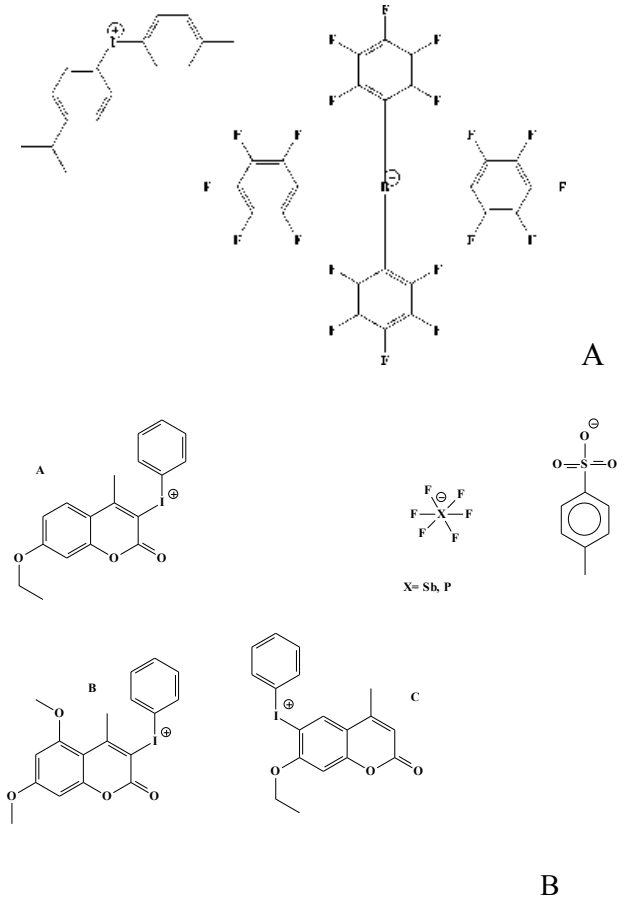

Scheme 10.1. Formulae of cationic initiators used for radiation induced polymerization of epoxy resins (A) Rhodorsil 2074 (IPB) and (B) iodonium salt based on cumarine substituents.

An cationic initiators were dissolved in epoxy resin at 60-65 ^{o}C in an ultrasonic bath. In the same way carbon nanofilers were dispersed in the resins.

For irradiation an Elektronika accelerator generating 10 MeV electron beam was applied at an average dose rate of approximately 3 kGy/min. Gamma irradiation was performed in a Gamma Cell 5000 at dose rates of 6.4 kGy/h or 3.2 kGy using appropriate shields. In order to estimate conversion of radiation energy into heat by the chamber walls, the temperature was recorded with a thermocouple for the chamber unloaded and loaded with water or epoxy resin free from initiator. Progress in the thermal effects is shown in Fig. 10.5a. The diagrams indicate that even after 6 h the temperature in the loaded chamber is lower than 50 ^{o}C and has not reached equilibrium yet. On the basis of these results it was assumed that under applied conditions ionizing radiation can not initiate intensive thermal curing in the absence of the initiator. The temperature profiles related to the radiation-induced curing of several specimens carefully insulated by styrene foams are presented in Fig. 10.5b. For comparison, the progress of thermal effect for the epoxy resin free from the initiator is also demonstrated.

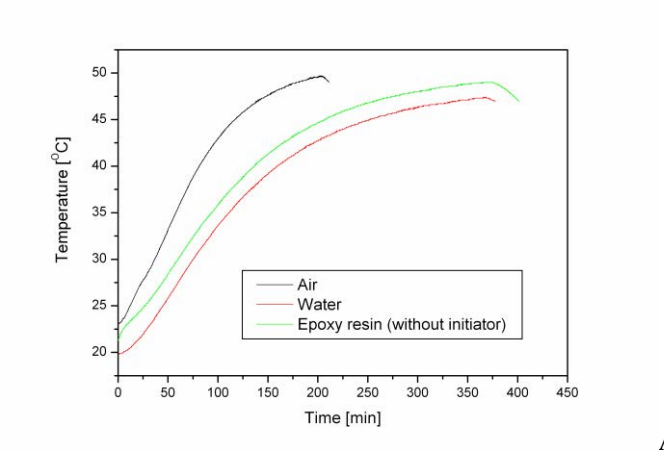

A

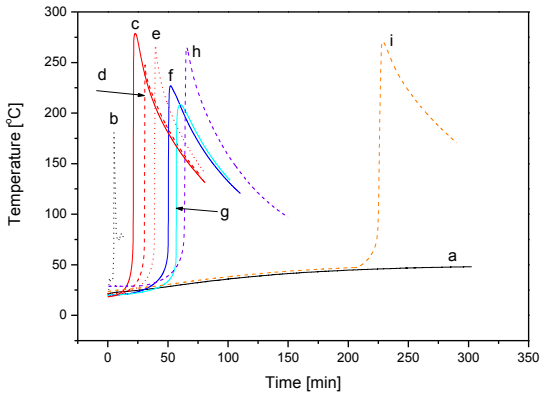

B

FIG. 10.*5. Thermal effects for the selected materials placed in GammaChamber 5000 (A). Temperature changes in the DGEBA based resin during radiation-induced curing: a – without IPB, b – 1% IPB, EB, c, d – 1% IPB, e – 0.5% IPB, f – 0.25% IPB, g – 0.25% IPB, 0.1% CNT, h – 0.25% IPB, 0.1% GO, i – 0,5% RGO, 1% IPB; a,c – irradiation at 6.4 kGy/h; d, e, f, g, h, i – irradiation at 3.2 kGy/h. Except (b) all samples were irradiated in GC5000 (B).*

For all samples, except this one containing RGO ("i" peak), the rapid temperature increase has been confirmed for the irradiation lasting less than 60 min, i.e. for the period in which the temperature in the chamber loaded with the materials free from initiator does not reach 35 ^{o}C.

During induction stage no substantial thermal effect was found. Nevertheless, radiation induced processes of DGEBA associated with the epoxy ring-opening are possible. The effects cumulate until the beginning of violent polymerization which is accompanied by heat release. The processes involve fast cationic initiator depletion.

Worth noting that in spite of various dose rates and initiator concentrations maximum temperature of the exothermic curing reaches over 200 ^{o}C for all comprising IPB systems irradiated in a gamma chamber. High temperature of polymerization results in significant thermal stress of the cured product. For the bulk specimens the effects can result in cracking and subsequently destruction of the material.

For the same concentration of the initiator (1% - b, c, and d profiles) the thermal changes depend predominantly on the method of irradiation. Induction time is very short for an electron beam treatment (a few minutes) and much longer for gamma radiation. In the second case, the maximum temperature is achieved just after 30 min and 45 min at 6.4 kGy/h (3.2 kGy) and 3.2 kGy (2.4 kGy), respectively. These discrepancies arise from various phenomena standing behind electron beam and gamma-rays irradiations. In the former case, the processes result from generation in situ the sufficient population of intermediates due to high dose rate what causes fast exhaustion of the initiator combined with decay of radicals and other active centres. Therefore, in this system intensity of the peak is smaller in comparison with gamma initiated processes.

The presence of graphene derivatives the induction time of curing increases, particularly in the case of RGO, what can results from adsorption of the initiator by the developed surface of the fillers. On the other hand, nanotubes that have not oxygen containing functional groups do not reveal such phenomena. Therefore, is seems that access to polar substituents in GO and RGO facilitates binding of the initiator to the carbon nanostructures what delays curing of the resin.

Due to strong thermal effects of curing in the presence of IPB, several other initiators based on cumarine derivatives and synthesized at the Technical University in Cracow, Poland were tested. In Fig. 10.6. the temperature profiles of radiation initiated curing are collected for the following samples irradiated with a dose rate of 3.2 kGy/h and various initiators:

1st series; photoinitiators containing the same cumarine cation and various anions: A1 C1 - SbF_6 ; A2 C1 - TsOH ; A3 C1 - PF_6

2nd series; photoinitiators constructed from differently substituted cumarine cation and the same PF_6 anion: A3 C1 - PF_6 ; A3 C2 - PF_6; A3 C3 - PF_6 (see Scheme 1)

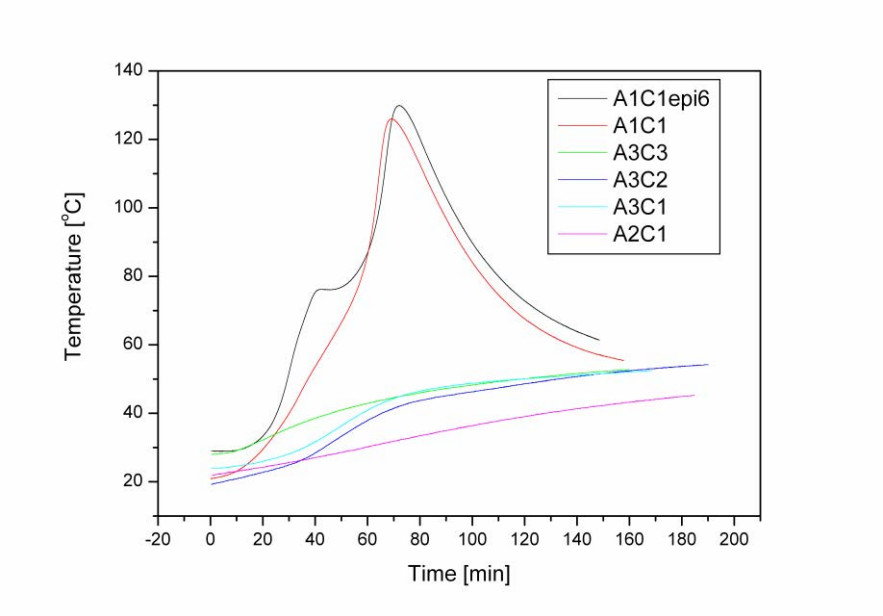

FIG. 10.6. Thermal effects of DGEBA and Epidian cured in the presence of 1wt % of cumarine initiators, dose rate 3.2 kGy/h. Except specimen A1C1epi6, all other samples were synthesized basing on DGEBA.

It was found that only one of the cumarine initiators is very efficient whereas for three others thermal effects of polymerization are small and A2C1 is completely inactive. Interestingly, the efficiency depends not only on the initiating curing cations but also on the structure of anion which participate in the process as strong Lewis acid. Thermal studies revealed significant differences in the intensities and shapes of the peaks recorded during irradiation. The method might be regarded as a screening test of new catalysts applied for the curing processes of epoxy resins and their composites.

In order to determine utility of the products obtained, the mechanical tests have been conducted. The stress-strain studies of radiation cured Epidian free from additives or doped with nanocarbon fillers in the presence of 1% IPB showed tensile strength at breaks in the range of 15-56 MPa, Tab. 10.1.

TABLE 10.1. TENSILE STRENGTH AT BREAK FOR EPOXY RESIN BASED ON EPIDIAN AND ITS COMPOSITES COMPRISING RGO, GRAPHITE AND CNT

Epoxy resin	Filler	Strength at break [MPa]
Epidian + 1% IPB	-	34.7
Epidian + 1% IPB	RGO; 1%	15.0
Epidian + 1% IPB	Graphite; 15 μm; 1%	36.5
Epidian + 1% IPB	CNT; 0.1%	39.2
Epidian +plast.+ 1% IPB	CNT; 0.1%	41,9
Epidian + 1% IPB	MWCNT; 0,1%	56,4

The highest increase of tensile strength at break showed nanocomposite containing MWCNT whereas for the same concentration of CNT the increase was smaller but also significant. Additionally, for the specimens listed in Table 10.1. the stiffness tests were carried out in the temperature range from 80 to 150 ^{0}C. The resin bars were inserted into the thermal chamber, heated to the selected temperature and after reaching thermal equilibrium the force required for deflection of the specimen by a constant value (0.8 mm) was measured. The results are shown in Fig. 10.7.

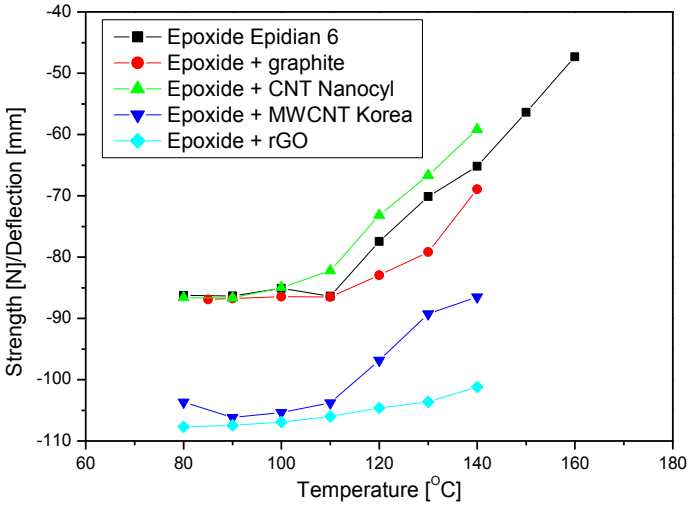

FIG. 10.7. Stiffness of nanocarbon composites based on epoxy resin at elevated temperatures.

For the epoxy resin and its composite with some fillers, such as graphite and CNT, the differences are negligible. The products remain rigid to about 110 ^{o}C (onset of glass transition) and then the force necessary for bar bending decreases gradually with increasing temperature. The cured composites containing MWNCT or RGO fillers are more rigid at elevated temperatures. Additionally, for RGO no sharp change of applied force versus temperature is observed, in contrast to the resin reinforced with MWCNT.

The differences reveal beneficial changes in the mechanical properties at elevated temperatures what for some engineering materials applied in automotive or aerospace industry is essential. The results confirmed that ionizing radiation initiates epoxy resin curing efficiently and that mechanical and thermal properties of its composites, particularly in the presence of MWCNT and RGO, are significantly improved. The evidences for radiation induced epoxy ring-opening of GO and RGO were not found.

10.2.3. Application of ionizing radiation for preparation of biodegradable packaging materials based on polysaccharide nanocomposites.

10.2.3.1. Ionizing radiation influence on interaction of starch with lipids and surfactants

With reference to the modification of hydrophilic/hydrophobic properties of the starch based systems the special attention was focused on radiation induced modification of interaction between potato starch and lipid/surfactant. This concerns starch capability of formation the complexes and the structural properties of the resulting products [10.17, 10.18]. The following ligands were investigated: cationic surfactant (cetyltrimethylammonium bromide;

CTAB), two anionic surfactants: sodium laurate (NaLau) and sodium palmitate (NaPam) as well as two lipids: lauric acid (Lau) and palmitic acid (Pam). Moreover, the effect of starch irradiation on the microstructure of the starch/ligand films was studied. Native solid starch was irradiated with ^{60}Co gamma-rays in a gamma cell "Issledovatel". The structural properties of the systems containing starch and lipid/surfactant were studied by means of differential scanning calorimetry (DSC), wide-angle X-ray diffraction (WAXS), FTIR spectroscopy and scanning electron microscopy (SEM).

DSC measurements were carried out for the starch suspensions during several heating – cooling – heating cycles at heating and cooling rates of 10 or 5 $^{o}Cmin^{-1}$. During the first heating formation of the surfactants and lipids micelles took place simultaneously with the starch gelatinization. Formation of the complex (exothermic) occurs during gelatinisation (endothermic). Melting of the resulting amylose-lipid complex occurs if heating is continued at the higher temperatures (above 60 ^{o}C). During the further cooling and heating cycles, the processes of crystallization and melting of amylose-lipid complexes and lipid-rich phase were confirmed.

In the first stage of the experiments the effect of gamma radiation with doses of 30 and 20 kGy on the interaction between starch and selected lipids/surfactants was studied. In this preliminary step the suspensions at surfactant (or lipid): polysaccharide: water ratio of 1:10 : 11 or 1:10:10 were investigated. This corresponds to 0.274, 0.458, 0.359, 0.498, 0.390 mmol, of CTAB, NaLau, NaPam, Lau or Pam per 1 g of starch, respectively. Free lipids were not detected by DSC for all applied compositions, except this one comprising CTAB. The complementary studies were carried out for the suspensions/gels of the smaller surfactant/lipid to starch ratios (corresponding to 0.274 mmol of NaLau, 0.269, 0.136 mmol of NaPam, 0.274 and 0.68 mmol of Pam per 1 g of starch.

The differences were noticed between thermal effects recorded for all systems containing non-irradiated and irradiated starch (30 and/or 20 kGy) during the first cooling and the subsequent heating and cooling cycles.

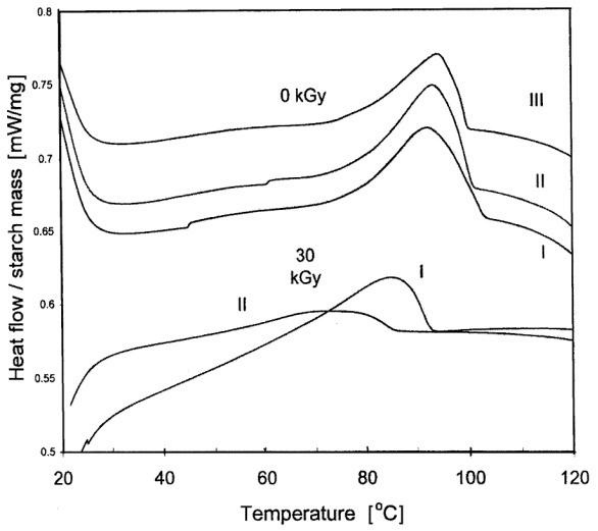

FIG. 10.8 (a). DSC curves recorded during the first and subsequent cooling cycles carried out at a cooling rate of 10 $^{o}Cmin^{-1}$ for the systems containing starch non-irradiated and irradiated to a dose of 30 kGy.

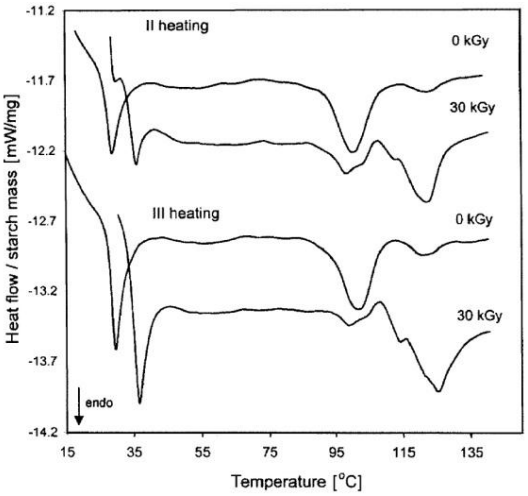

FIG. 10.8 (b). Thermal effects attributed to the melting of amylose-lipid inclusion complexes recorded during the second and third heating of the system containing sodium laurate admixed to the non-irradiated and irradiated starch (at weight ratio 1:10).

Transformations of the starch-lipid inclusion complexes occur at lower temperature for the irradiated than for non-irradiated starch doped with CTAB or Lau. Additionally, heating and cooling thermograms revealed in this case smaller enthalpy (Fig. 10.8), similarly as in the previously examined systems [10.19]. Moreover, thermal treatment (melting and crystallization during thermal analysis) also influences initial and irradiated starch complexes. In particular, well recognized ordering of the complex structure occurs in the composition formed by non-irradiated starch and both ligands. It was found that the differences between the complexes formed between CTAB and non-irradiated or irradiated starch were significant already after irradiation with a dose of 2 kGy.

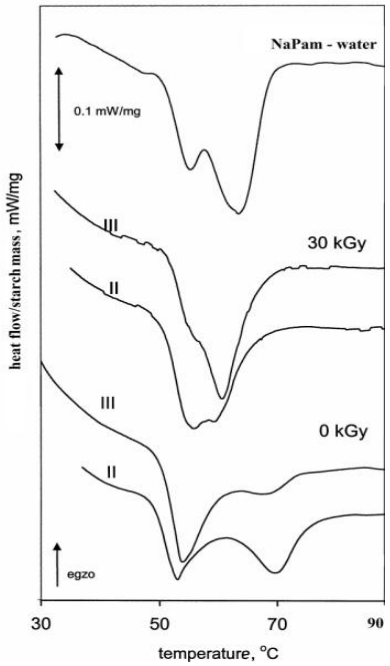

FIG. 10.9 (a). Low temperature thermal effects recorded during the first, second and third heating of the system containing sodium palmitate admixed to the non-irradiated and irradiated starch (at weight ratio 1:10) in comparison with NaPam : water system.

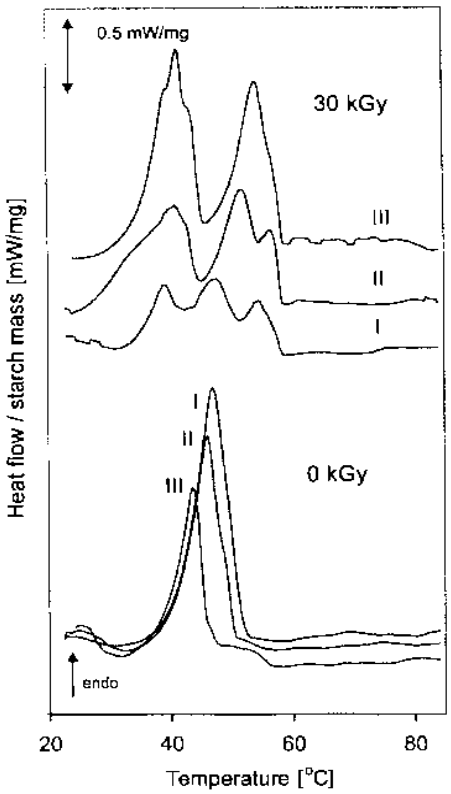

FIG. 10.9 (b). Low temperature thermal effects recorded during the first, second and third cooling of the system containing sodium palmitate admixed to the non-irradiated and irradiated starch (at weight ratio 1:10).

Thermal effect attributed to melting of amylose-lipid complex for irradiated starch containing both anionic surfactants (NaLau and NaPam) occurs at higher temperature than for the system comprising non-irradiated starch. In both cases the exothermal process (probably crystallization) accompanies melting of the irradiated starch complex contrary to non-irradiated one, Fig. 10.8 (b).

The significant differences were noticed between melting and crystallization of free lipid phase, Fig. 10.9. Melting temperature of these domains is lower for non-irradiated than for irradiated starch. The effect can be attributed to the structural differences of the intermediate phase (so called surface complexes) containing lipids and non-irradiated or irradiated starch. It seems that the interaction between the lipids and non-irradiated starch is weaker as compared to irradiated starch.

Typical diffractogramms for V – type starch gels were recorded in the case of the standard products prepared with the addition of CTAB, Na-Lau and Na-Pam, Fig. 10.10a [10.17, 10.18]. For the products containing irradiated starch and the lipids, the broaden reflections and the higher background level were observed. The sample formed from Na-Pam and starch in a ratio of 0.061 was additionally heated at 140 ^{o}C before casting, Fig. 10.10b. In this case the B-type structure was formed in the films containing irradiated starch. There was no peak related to the presence of free surfactant, contrary to the sample comprising non-irradiated starch that still revealed the V-type pattern. Diffractograms of the products formed from irradiated starch and lauric or palmitic acids suggest the presence of two phase systems, probably B and V or A and V, with a dominant content of V phase, Fig. 10.10c. Apparent contribution of the crystalline fraction for the larger lipid amount introduced into the sample (0.016 or 0.056 lipid per 1 g starch) rises from the facilitated crystallization possible in the

system containing irradiated starch and can be related to the reduced binding capacity of the irradiated starch.

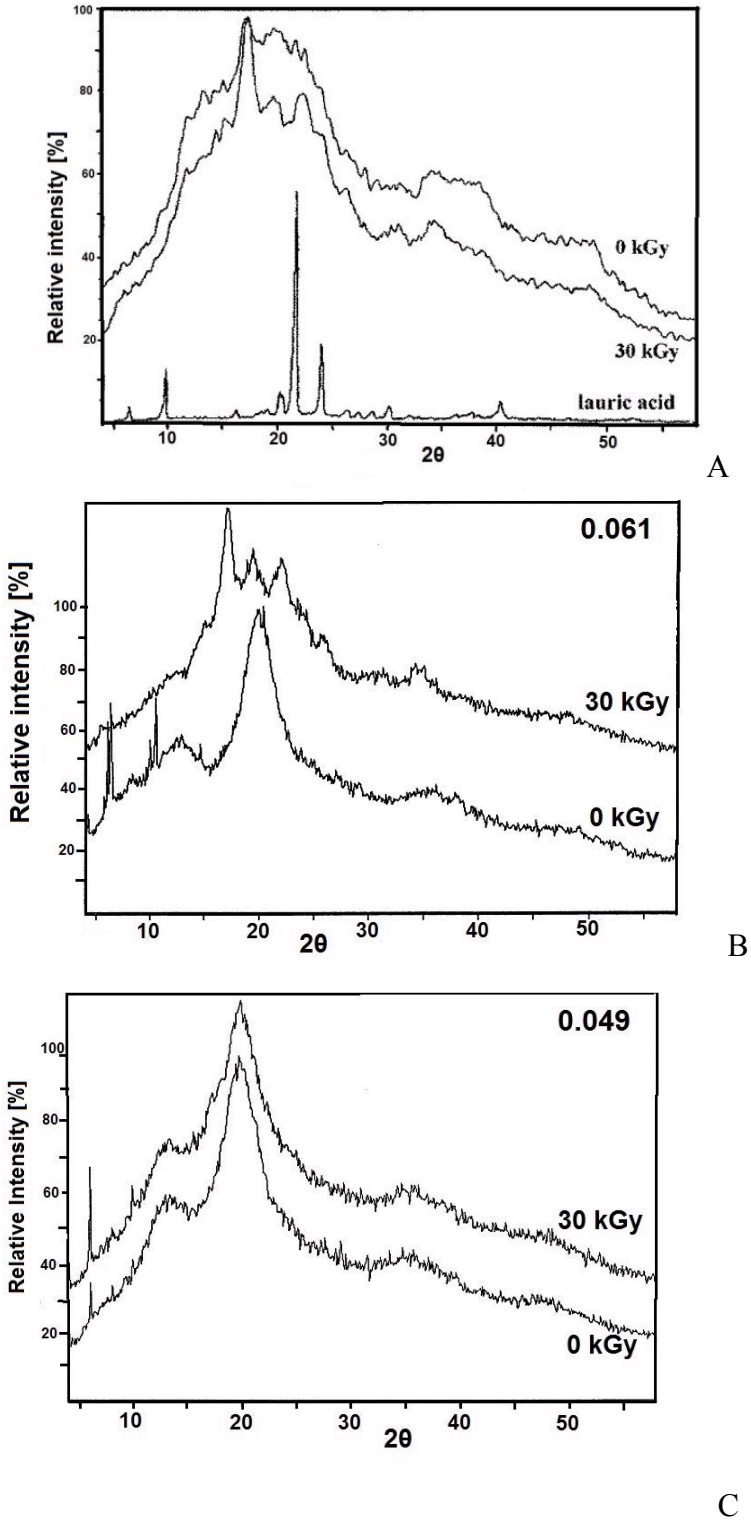

FIG. 10.10. Diffractograms of the products containing non-irradiated or irradiated starch and: (A) lauric acid (Lau: starch ratio 0,016) confronted with diffractograms of lauric acid. (B) Na-Pam (Na-Pam to starch ratio 0.049) recorded for complexes formed at 70-90 °C. (C) Na-Pam (Na-Pam to starch ratio 0.061) recorded for the complexes heated at 140 °C.

For the systems containing CTAB, Lau or Pam the FTIR bands of maximum at ca. 1643 cm^{-1} originating from the stretching vibrations of the C=O groups were observed, e.g. Fig. 10.11A. In the carbonyl regions there are no separate bands that might be attributed to free lipids. Band intensities were lower for the systems containing non-irradiated starch. On the other hand, products containing NaLau (or NaPam) showed two bands having the maximum at approximately 1644 and 1556 cm^{-1}, Fig. 10.11B. Decrease in the intensities of the additional bands observed for the product containing irradiated starch irradiation results from homogenization of the system.

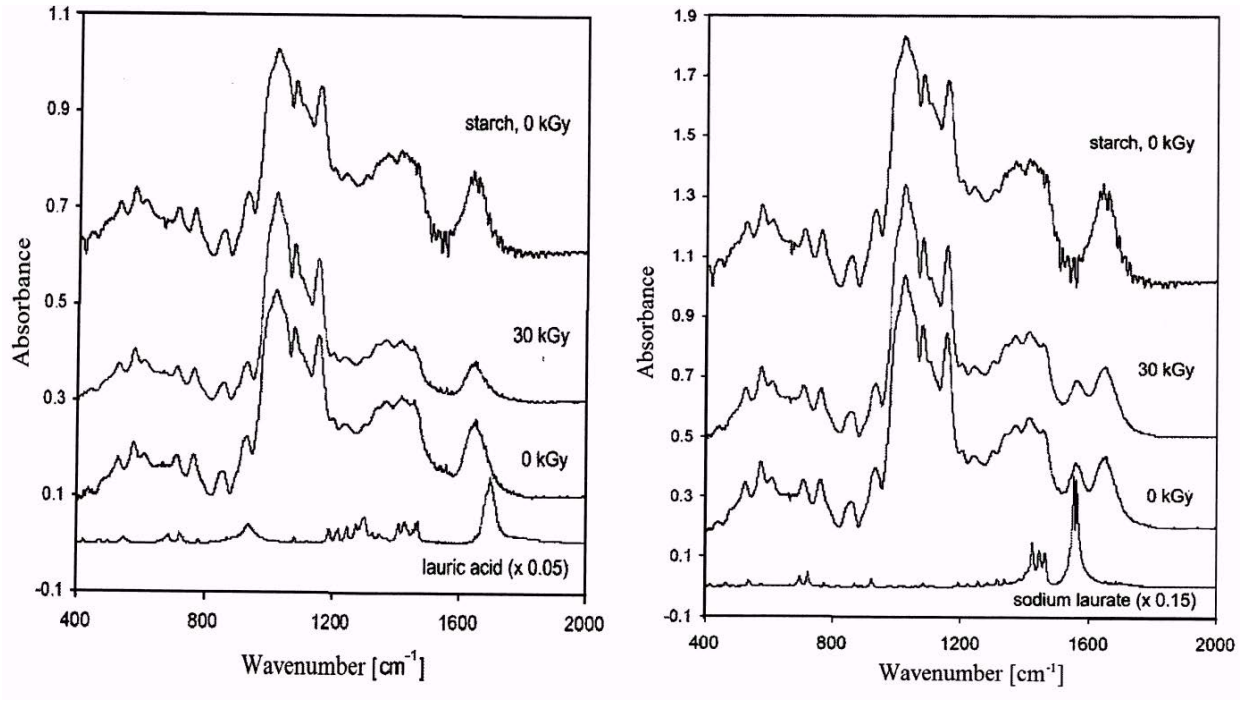

FIG. 10.11. FTIR spectra recorded for the products containing non-irradiated or irradiated starch and:

(A) lauric acid (Lau to starch ratio 0.016), confronted with the spectra of starch and lauric acid.
(B) NaLau (NaLau to starch ratio 0.038), confronted with the spectra of starch and NaLau.

All films prepared on the basis of irradiated starch seem to be more smooth and homogeneous as compared to these ones containing non-irradiated starch (SEM, Fig. 10.12). Their structure is characterized by better ordering and lack of orientation of the structural elements.

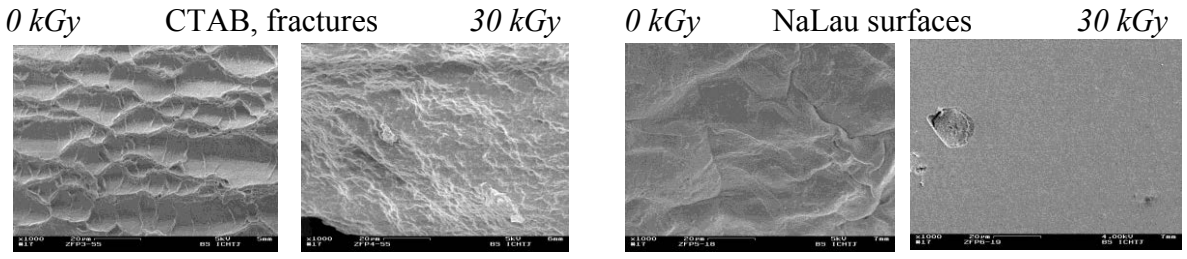

FIG. 10.12. The examples of SEM images recorded for chemically stained potato starch - CTAB films (fractures) and potato starch - NaLau films (surfaces) (1000x)

10.2.3.2.Application of ionizing radiation for modification of the system containing polysaccharide nanoparticles.

Cellulose fibers are widely applied as a reinforcing agents in polymers. Recently cellulose nanocrystals (NCC) and nanofibres (NFC) were found to be the effective agents that might improve the properties of polymer films. Beneficial properties of polysaccharide nanoparticles trigger high interest in searching the new methods for preparation and modification of such material. Simultaneously, radiation was found to be an appropriate factor improving properties of the polysaccharide films containing nanocellulose.

Our present studies concern preparation of the starch-NaLau-nanocellulose films (with addition of 30 % glycerol) and modification their surface properties by irradiation (Table 10.1). The results show that the appropriate introduction of NCC or NFC enables to obtain films of decreased hydrophilicity as compared to the pure starch-NaLau films and that irradiation enables further reduction of hydrophilicity (Table 10.2).

In the next step the trials were carried out for preparation of the starch particles with a reduced dimension. The gel solutions of starch were then prepared and irradiated with a dose of 290-300 kGy. The particles dimensions in gels, in precipitates and in solutions were analyzed. It was found that the size of particles (determined using of Zetasizer) was always smaller in the case of the irradiated samples as compared to the non-irradiated ones. For example, Mean value equal to 450.9 nm (with peaks at 409 and 5214 showing of intensity 93% and 6.9% respectively) was determined in the case of the precipitate of the initial starch, while the appropriate value found for the irradiated starch (gamma, 290 kGy) was equal to 174,4 (peaks at 200.4 and 51.9 nm with intensity of 96.1 and 3.9 %).

TABLE 10.2. THE AVERAGE VALUES OF CONTACT ANGLE DETERMINED FOR THE NON-IRRADIATED AND THE IRRADIATED STARCH-NALAU-NANOCELLULOSE FILMS (0.036 G NALAU PER 1 G OF STARCH). A, B – TWO VARIOUS PROCEDURES APPLIED FOR THE NANOCELLULOSE INTRODUCTION

composition		Irradiated films		
	0 kGy	5 kGy (γ)	25 kGy (γ)	25 kGy (e)
Starch/NaLau	70.9	74.5	80.7	82.5
Starch/NaLau+ NCC[a]	81.8	82.7	75.3	88.6
Starch/NaLau+ NCC[b]	73.7	79.2	83.7	72.3
Starch/NaLau+ NFC[b]	78.8	89.9	91.3	87.0

10.3. KEY RESULTS AND CONCLUSION

The thermal effects recorded during radiation curing of epoxy resins in the presence of cationic photoinitiators and selected carbon nanofillers were influenced predominantly by the type of radiation and dose rates, the concentration of initiator and the nature of nanofillers. The induction time of curing was even twice longer for graphene composites than for non-filled matrix due to limited availability of the initiator absorbed on the developed surface of dispersed phase. Under adiabatic conditions gamma radiation induced polymerization resulted in the completely cured products.

Cheap and easy to synthesize cumarine based initiators might be used instead of IPB. The maximum thermal effect is then achieved after longer time but its intensity is over 100 ^{o}C lower what is a desirable phenomenon reducing resin shrinkage and diminishing internal stress occurring in the case of high temperature polymerization.

The differences between interaction of all examined ligands and irradiated and non-irradiated starch were confirmed by DSC, FTIR and WAXS methods. Irradiated starch is able to bind less surfactant both in the form of inclusion complexes and in the form of the surface complexes. However, the effects of irradiation differ depending on the ligands. Moreover, the differences between the influence of thermal treatment on the ability to form these complexes have been identified.

Decrease in the inclusion complex symmetry was confirmed for irradiated starch and CTAB or Lau. Moreover, improvement of the complex ordering might be concluded after further thermal treatment of the complex formed with the participation of non-irradiated starch, while rather opposite effect was observed in the case of irradiated one.

For starch-NaLau, starch-NaPam and starch-Pam the similar phenomena result from irradiation. The better ordering of the inclusion complexes formed by irradiated starch and NaLau or NaPam were found as compared to those formed by non-irradiated starch. Interaction of starch with free surfactant phase seems to be weaker after irradiation and strengthened after thermal treatment in the case of the initial starch but weaker in the case of the non-irradiated starch.

The WAXD and FTIR results indicate the facilitated crystallization in the system containing irradiated starch as compared to non-irradiated starch and the formation of more homogeneous complexes in the first case.
Films prepared form irradiated starch and lipid or surfactants reveal smoother and more homogeneous structure as compared to these ones formed using non-irradiated starch.

The appropriate introduction of nanocellulose into the starch-NaLau films might lead to the decrease of their hydrophilicity, which can still be further reduced by irradiation with gamma-rays or electron beam (5 or 25 kGy).

ACKNOWLEDGEMENTS

This research was supported by the Polish Ministry of Science and Higher Education (Agreement No 2863/IAEA/2013) and by International Atomic Energy Agency (Coordinated Research Project No F22051, Research Contract 16666).

REFERENCES TO CHAPTER 10

[10.1] CAMPOS A., GERSHENSON L.N., FLORES S.K., “Developmnentt of edible films and coatings with antimicrobial activity. Review paper”, Food Bioprocess Technol. **4** (2011) 849 – 875.

[10.2] JIMENEZ, A., FABRA, M.J., TALENS P., CHIRALT A., “Edible and biodegradable starch films: A review”, Food Bioprocess Technol. **5 (**2012) 2058 – 2076.

[10.3] GENNADIOS, A., HANNA, M.A., KURTH, L.B. "Application of edible coating on meats, poultry and seafoods: A review", Lebensm-Wiss Technol. **30** (1997) 337 – 350.
[10.4] CIEŚLA, K.A., NOWICKI, A., BUCZKOWSKI, M. J., „Radiation modification of the functional properties of the edible films prepared using starch and starch – lipid system", NUKLEONIKA **55** (2) (2010) 233 - 242.
[10.5] KALIA, S., DUFRESNE, A., CHERIAN, B.M., KAITH, B. S., AVEROUS, L., NJUGUNA, J., NASSIOPOULOS, E., "Cellulose-Based Bio- and Nanocomposites: A Review", Int. J.Polym. Sci. **2011** (2011) 35.
[10.6] KHAN, R.A., SALMIERI, S., DUSSAULT, D., URIBE-CALDERON, J., KHAMAL, M.R., SAFRANY, A., LACROIX, M., "Production of nanocellulose-reinforced methylcellulose –based biodegradable films", J. Agric. Food Chem. **58** (2010) 7878-7885.
[10.7] ZHU, Y., MURALI, S., CAI, W., LI, W., SUK, W., POTTS, J.R., RUOFF, R.S., "Graphene and Graphene Oxide: Synthesis, Properties and Applications", Adv. Mater **22** (2010) 3906-3924.
[10.8] BANHART, F., "Irradiation effects in carbon nanostructures"Rep. Prog. Phys. **62** (1999) 1181-1221.
[10.9] KRASHENINNIKOV, A., BANHART, F., "Engineering of nanostructured carbon materials with electron or ion beam", Nat. Mater. **6** (2007) 723-733.
[10.10] KRASHENINNIKOV, A.V., NORDLUND, K., "Ion and electron irradiation-induced effects in nanostructured materials", J. Appl. Phys. **107** (2010) 071301.
[10.11] BANHART, F., KOTAKOSKI, J., KRASHENINNIKOV, A.V., "Structural defects in graphene", Acsnano **5** (2011) 26-41
[10.12] DISPENZA, C., SCRO, S., VALENZA, A., SPADARO, G., "High energy radiation cure of resin systems for structural adhesives and composite applications", Radiat. Phys. Chem. **63** (2002) 69–73.
[10.13] SPADARO, G., CALDERARO, E., TOMARCHIO, E., DISPENZA C., "Novel epoxy formulations for high energy radiation curable composites", Radiat. Phys. Chem. **72** (2005) 465–473.
[10.14] ALESSIA, S., PARLATOB, A., DISPENZA, C., DE MARIA, M., G. SPADARO, G., "The influence of the processing temperature on gamma curing of epoxy resins for the production of advanced composites", Radiat. Phys. Chem. **76** (2007) 1347–1350.
[10.15] SOBON, G., SOTOR, J., JAGIELLO, J., KOZINSKI, R., ZDROJEK, M., HOLDYNSKI, M., PALETKO, P., BOGUSLAWSKI, J., LIPINSKA, L., "Graphene oxide vs. reduced graphene oxide as saturable absorbers for Er-doped passively mode-locked fiber laser", Optics Express **20** (2012) 19463-19473.
[10.16] ORTYL J., R. POPIELARZ R., "The new photoinitiators for cationic photopolymerization", Polimery **7/8** (2012) 510-514.
[10.17] CZUCHAJOWSKA, Z., SIEVERT, D., POMERANZ, Y., „Enzyme resistant starch. IV. Effect of complexing lipids", Cereal Chem. **68** (5) (1991) 537- 542.
[10.18] TANG, M.C., COPELAND, L., "Analysis of complexes between lipids and wheat starch", Carbohydr. Polym. **67** (2007) 80 – 85.
[10.19] CIEŚLA, K., ELIASSON, A.C., Nucl. Instr. Met. Phys Res., "DSC studies of retrogradation and amylose-lipid complex transition taking place in gamma irradiated wheat starch", Nim B **265** (2007) 399-405.

Chapter 11

RADIOLYTIC SYNTHESIS OF NANOCOMPOSITES BASED ON NOBLE METAL NANOPARTICLES AND NATURAL POLYMER, AND THEIR APPLICATION AS BIOMATERIAL

A. RADOSAVLJEVIĆ, J. KRSTIĆ, J. SPASOJEVIĆ, Z. KAČAREVIĆ-POPOVIĆ
VINČA Institute of Nuclear Sciences,
University of Belgrade,
Laboratory for Radiation Chemistry and Physics,
Belgrade,
Serbia

11.1. INTRODUCTION

The objective of this project was to develop simple, one-step radiolytic methodology to obtain noble metal/natural polymer based hybrid composite nanosystems with the goal of exploring favorable characteristics of radiation technology for nanoscale engineering of materials, especially for biomedical application. The crosslinking of polymers and reduction of metal ions were performed by means of radiation chemistry method due to its advantage over chemical methods.

To achieve project goals the research activities were focused on developing synthesis strategies of formation of silver nanoparticles (Ag NPs) and crosslinking of polymer matrix consisting of poly(vinyl alcohol)/chitosan (PVA/CS) blend system, or only chitosan (CS). Noble metal NPs are generally considered as environmentally friendly antibacterial materials. The CS is used because of its biodegradability, unique cationic and antibacterial properties, while the PVA was chosen due to biodegradability, bioinertness, cell and blood compatibility and excellent mechanical properties. PVA and CS are good protectants or dispersants for preparing NPs, and play an important part in the controllable production and stabilization of NPs with definite size. Moreover, they both can reduce metal ions to some extent, and promote the nucleation of NPs. These two polymers have been used successfully in many biomedical applications including scaffolds for wound healing applications. Namely, hydrogels facilitate autolysis and may be beneficial in managing ulcers containing necrotic tissue. For example, debridement using hydrogel is more effective than standard wound care for healing diabetic foot ulcers [11.1]. Potential problem for biomedical application of hydrogels is that microorganisms may grow in hydrogel materials due to their natural biocompatible properties. Therefore incorporation of antibacterial agents is required.

Silver nanoparticles are rampantly used in many medical procedures and devices in biomedical fields, but they have their drawbacks due to nanotoxicity. These challenges have led to restrictions in the availability or complete withdrawal. The antibacterial efficacy and reducing toxic effect can be improved by introduction of CS and CS derivatives, as a nontoxic, biodegradable, biocompatible and antibacterial polysaccharide. Therefore the development and optimization of silver delivery systems through therapeutic window (achieve antibacterial efficacy and be below the toxicity) is very important field in applied polymer science and it can be expected to significantly increase an accuracy and easiness of applications. Moreover, preliminary results showed that CS/PVA scaffolds could integrate with the damaged tissue to promote consistent functional recovery of peripheral nerve tissue,

but additional investigation is required for this to be confirmed. In addition, investigations indicate that noble metal NPs such as Ag or Au had a stimulatory effect on nerve cell proliferation. Therefore investigated hydrogel nanosystems, beside the use as an antibacterial scaffold, have the option of applying as tissue-engineering platform for the treatment of peripheral nerve injury.

To achieve the project outputs, research activities were divided in several sections:

1) The investigation of *in vitro* silver release by the simple nano-Ag/PVA hydrogel device as a model system. Namely, the recent studies suggest that Ag NPs exert toxicity to bacteria and other organisms not by direct particle-specific effect but by released Ag^+ ions [11.2]. In that case, Ag NPs behaves in analogy to a drug delivery system, in which the particle contains a concentrated inventory of active species, the ions [11.3]. Moreover, for the use of nano-Ag loaded hydrogels in biomedicine it should be possible to modulate the release of Ag^+ ions that would be delivered to the patient at a controlled rate. This would allow achieving adequate concentrations and prolonged effectiveness. Thus the study was aimed to quantify the amount of Ag^+ ions released in an *in vitro* medium and to use, for the first time, the elements of pharmacokinetic drug delivery paradigm to the nano-Ag/PVA hydrogel as a model system for the evaluation of the release kinetics and the release mechanism. In general, it is known that the release of soluble drug entrapped in a hydrogels should be closely related to the swelling characteristics of the hydrogels. That's because the release occurs only after fluid penetrates into the polymeric networks and dissolve the drug, which is followed by diffusion along the aqueous pathways to the surface of the device [11.4]. Therefore, the swelling characteristics of nano-Ag/PVA hydrogel device and diffusion parameters of simulated body fluid (SBF) (at 37^oC) were investigated.

2) We introduce CS in the system, first by blending with PVA. Namely, CS/PVA blending allows investigating the possibility of *in situ* radiolytic method to control the size of Ag NPs by changing the composition of CS/PVA matrix.

3) Investigation of the radiation chemical pathways for the synthesis of hydrogel nanocomposites containing CS. The synthesis of noble metal/polymer hybrid nanosystems was performed by two radiation chemistry pathways: first, we developed synthetic strategies for radiolitically incorporation of Ag NPs in previously crosslinked matrix consisting of PVA and water soluble CS (previously obtained by γ-irradiation), using liquid filled cavities in polymer matrix as nanoreactors (template synthesis); second, we explored the possibility of simultaneously crosslinking of polymers and *in situ* synthesis of Ag NPs by γ-irradiation.

11.2. EXPERIMENTAL PART

11.2.1. Materials

Poly(vinyl alcohol) (PVA) with M_w=72 kDa and 99% of minimal degree of hydrolysis, silver nitrate ($AgNO_3$) and 2-propanol ($(CH_3)_2CHOH$) were supplied from Merck (Germany); acetic acid (CH_3COOH) from Zorka Pharma (Serbia) and low molecular weight chitosan (CS) with 75-85% degree of deacetylation from Sigma-Aldrich (USA). All chemicals were used without additional purification. Water from Millipore Milli-Q system was used in all experiments. Prior to γ-irradiation, in order to remove oxygen, all solutions are saturated with argon gas (Ar) (Messer Tehnogas, Serbia) for 20 min. Systems were exposed to γ-rays (^{60}Co source) in closed cells, under the ambient condition.

11.2.2. Preparation of Ag-PVA hydrogel nanocomposites.

PVA solution (5 wt%) was exposed to γ-irradiation up to the absorbed dose of 25 kGy (dose rate 0.33 kGy/h) to induce crosslinking. The samples of PVA xerogel (dried gel) were left to swell (for 48 h) in solutions containing different concentrations of $AgNO_3$ (4, 8, 16, 30, 75 and 100 mM) and 0.2 M 2-propanol, and then were exposed to γ-irradiation (dose rate 10 kGy/h) up to 7, 14, 28, 53, 133 and 177 kGy, respectively, in order to perform a reduction of Ag^+ ions in hydrogels. The obtained hydrogel nanocomposites are labeled as S1, S2, S3, S4, S5 and S6, respectively, whereby pure PVA hydrogel is labeled as S7.

11.2.3. Preparation of uncrosslinked Ag-CS/PVA nanocomposites.

Solutions of CS (2.5 wt%) and PVA (5 wt%) were used to prepare solutions in which the mass ratios of CS/PVA were 100/0, 80/20, 60/40, 40/60, 20/80 and 0/100. In all prepared solutions, $AgNO_3$ and $(CH_3)_2CHOH$ were added up to the concentration of 5 mM and 0.2 M, respectively. Solutions were exposed to γ-irradiation in order to reduce the silver (absorbed dose 8.5 kGy, dose rate 6 kGy/h). After solvent evaporation from colloids, the uncrosslinked Ag-CS/PVA nanocomposite films (10-30 μm thick) were formed.

11.2.4. Preparation of water soluble chitosan.

CS solution (5 wt%) was prepared by dissolving low molecular CS (M_w=94.8±8.74 kDa) in 1M acetic acid for 3 h with constant mixing. This solution then exposed to γ-irradiation up to 100 kGy (dose rate 20 kGy/h) to perform reducing of molecular weight down to M_w=31.3±4.73 kDa. After neutralization of polymer acetic solution with 1M aqueous solution of NaOH, supernatant (wsCS solution) was 1.43 wt%, with mass yield of 28.56%. Thus obtained wsCS was used for the further preparation of the PVA/wsCS hydrogels.

11.2.5. Preparation of Ag-PVA/wsCS hydrogel nanocomposites.

Solutions of PVA and wsCS were mixed, and to form homogeneous mixture. PVA in the final solution was 8 wt%, while the content of wsCS was 2 wt% and 4 wt%. The polymer solutions were exposed to γ-irradiation at a dose rate of 0.33 kGy/h, up to the different absorbed dose: 8 wt% PVA up to 25 kGy (labeled as S8), 8 wt% PVA/2 wt% wsCS up to 75 kGy (labeled as S9), and 8 wt% PVA/4 wt% wsCS up to 50 kGy and 75 kGy (labeled as S10 and S11, respectively). γ-irradiation of samples was followed by four freeze-thawing cycles (2 h at −20°C and 1 h at 25°C). The obtained hydrogels were left to swell in solutions containing of 8 mM $AgNO_3$ and 0.2 M 2-propanol, and then were subjected to γ-irradiation up to 14 kGy (dose rate 14.6 kGy/h) in order to reduce Ag^+ ions. The hydrogel nanocomposites are labeled as Ag-S8, Ag-S9, Ag-S10 and Ag-S11, respectively. Simultaneous curing of polymers and formation of Ag NPs was investigated by exposing $AgNO_3$/PVA (8 mM/8 wt%, labeled as Ag-S12) and $AgNO_3$/PVA/wsCs mixtures (8mM/8 wt%/2 wt% and 8mM/8 wt%/4 wt%, labeled as Ag-S13 and Ag-S14, respectively) to γ-irradiation up to 200 kGy (dose rate 12.2 kGy/h), divided in several portions (50+40+40+40+30).

11.2.6. Methods of characterization.

Molecular weight of chitosan was determined using a Zetasizer Nano ZS applying Static Light Scattering (SLS) method. Toluene was used as a standard. For obtaining Debye plots, 3-5 different concentrations in the range of 0.25-2.0 g/L of each sample were made with 1M acetic acid as a solvent. The results were corrected by using size parameter (Z-Average) for each sample, previously provided by Dynamic Light Scattering (DLS) measurements, and also assuming coil shape of polymers. The UV-Vis absorption spectra were recorded using Thermo Fisher Scientific Evolution 600 UV-Vis Spectrophotometer, while the theoretical calculations of Ag NPs size were made using software "MiePlot V.3.4". The XRD and FTIR measurements were performed on Bruker D8 Advance Diffractometer and Thermo Electron Corporation Nicolet 380 Spectrophotometer (working in ATR mode), respectively. SEM analysis of nanocomposites was performed on JEOL JSM-6610LV instrument, operated at an accelerating voltage of 20 kV. Prior to the analysis, the samples were coated with thin layer of gold (around 15 nm). Swelling behavior of Ag-PVA and Ag-PVA/wsCS hydrogels was investigated in excess of simulated body fluid (SBF) at 37±1^{o}C and deionized water at 25±1^{o}C, respectively. The SBF (pH=7.4) was prepared according to the procedure for Kokubo's solution. The release of Ag^{+} ions from Ag/PVA hydrogel device was examined at 37±1^{o}C in phosphate buffer (pH=7). The release media were replaced periodically with an equal volume of fresh solution to create infinite sink conditions. In addition, the total content of silver within the nano-Ag/hydrogel device was determined upon treatment in HNO3 (1:1 v/v) to induce the oxidation of all of the Ag NPs into Ag^{+} ions. Philips PYU UNICAM SP9 atomic absorption spectrometer was used to determine the released Ag^{+} ions concentration. X-ray photoelectron spectroscopy (XPS) analysis was carried out using SPECS Systems with XP50M X-ray source for Focus 500 and PHOIBOS 100/150 analyzer. Moreover, the antibacterial properties of the Ag/PVA and Ag-PVA/wsCS hydrogel devices against *Escherichia coli* and *Staphylococcus aureus* were assessed by using the agar diffusion test at 37^{o}C for 24 h.

11.3. RESULTS AND DISCUSSION

The UV-Vis absorption spectra of Ag/PVA hydrogel nanocomposites (Fig. 11.1) showed the surface plasmon bands peaking in the range from 392−406 nm, due to formation of Ag NPs [11.5-11.7].

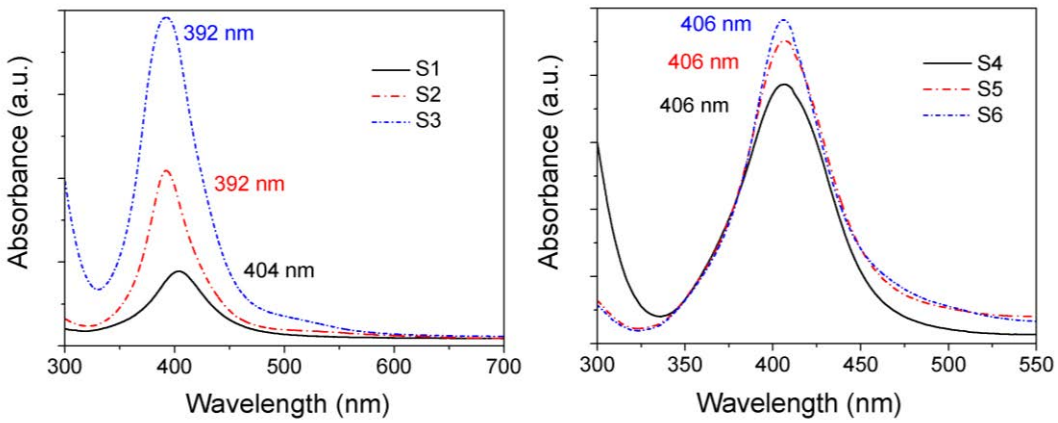

FIG. 11.1. UV-Vis absorption spectra of Ag/PVA hydrogel nanocomposites.

TABLE 11.1. VALUES OF RADIUS (r), MOLAR CONCENTRATION (C_{AAS}), SURFACE AREA ($S.A.$) AND SOLUBILITY (S_r) OF Ag NPs

Sample	$C_{AAS}\times10^6$ (g/cm^3)	r (nm)	S.A. (m^2/g)	S_r (mg/L)
S1	117.2	4.12	69.3	0.067
S2	97.2	3.30	86.7	0.111
S3	201.1	4.00	71.4	0.071
S4	2169.4	4.20	67.9	0.065
S5	5409.7	4.20	67.9	0.065
S6	5524.5	3.68	77.6	0.086

These NPs are spherical in shape, with the face centered cubic (*fcc*) crystal structure and diameter in the range of 6.5−8.5 nm. This confirms that the NPs span intrinsic size ranges (r ranges from 1−10 nm), therefore quasy-static approximation of Mie's theory can be applied, and UV-Vis spectroscopy can be used as a sizing technique [11.8-11.10]. The radius (r) of AgNPs is given in Table 11.1, as well as the other characteristic values. The radius obtained for sample S2 is smallest, in comparison with other. The obtained values for surface area and solubility of Ag NPs indicated that the solubility of NPs is greater for the smaller particles.

The investigation of swelling properties of pure PVA and Ag/PVP hydrogel nanocomposites was conducted in SBF at 37±1^{o}C. Swelling capacity of PVA and nano-Ag/PVA hydrogel device increased over the time and reached constant values of equilibrium swelling degree (SD_{eq}) after ~ 30 h (Table 11.2). The isothermal swelling capacity was higher for nano-Ag/PVA hydrogel device (samples S1−S3) compared to that obtained for PVA hydrogel (S7). This property is important in biomedical application of nanocomposite hydrogels for wound dressing applications, because Ag nanocomposite hydrogels, compared to pure hydrogel, can further absorb a slight to moderate amounts of the wound exudates by swelling. This helps in rapid healing of certain types of wounds. An increase in the absorption of surrounding fluid by nano-Ag/PVA hydrogel device is probably caused by the presence of some amounts of dissolved Ag^+ ions. This changes the composition of the medium and the chemical environment of the network [11.11, 11.12]. On the other hand, for the higher molar concentration of Ag NPs (samples S4−S6) swelling capacity decrease compared to pure PVA hydrogel. This is probably caused by the restriction of the larger scale segmental motion of polymer chains.

TABLE 11.2. VALUES OF THE EQUILIBRIUM SWELLING DEGREE (SD_{eq}), KINETIC CONSTANT (k) AND DIFFUSION EXPONENT (n) FOR THE POWER LAW MODEL, FIRST ORDER KINETICS AND SECOND ORDER KINETICS

Sample	SD_{eq}^{exp} (%)	power law kinetics			first-order kinetics			second-order kinetics		
		k ($1/h^n$)	n	R^2	SD_{eq}^{cal} (%)	$k_{F\text{-}O}\times10^4$ (1/s)	R^2	SD_{eq}^{cal} (%)	ν_0 (%/min)	R^2
S1	737	0.283	0.56	0.98	654	0.63	0.99	769	5.74	0.99
S2	811	0.263	0.57	0.99	730	0.59	0.99	855	5.42	0.99
S3	867	0.285	0.54	0.99	766	0.60	0.99	909	6.37	0.99
S4	317	0.758	0.35	0.98	300	2.12	0.90	318	5.14	0.99
S5	165	0.671	0.46	0.99	155	2.26	0.98	167	7.79	0.99
S6	135	0.733	0.40	0.96	123	1.38	0.79	136	5.91	0.99
S7	576	0.299	0.55	0.98	518	0.67	0.99	595	4.97	0.99

Diffusion coefficients (D) for both PVA hydrogel and nano-Ag/PVA hydrogel device were determined by the models based on solutions of Fick's law which assumes diffusion in one dimension with constant boundary conditions, using three aproximations: early-time

approximation (valid for the first 60% of sorption), late-time approximation (valid for the latter 40%), and Etters approximation [11.13]. An example of the model fits is shown in Fig. 11.2. and is representative of the reported data. The results are listed in Table 11.3.

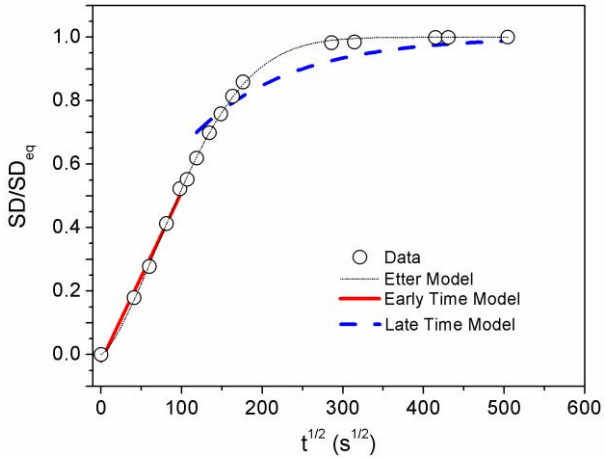

FIG. 11.2. Representative model fits for the early-time, late-time, and Etters approximations of diffusion through the samples (sample S3 in SBF at 37°C).

TABLE 11.3. MEDIA DIFFUSION COEFFICIENTS.

Sample	early time approximation		late time approximation		Etters model approximation	
	D×10^7 (cm^2/s)	R^2	D×10^7 (cm^2/s)	R^2	D×10^8 (cm^2/s)	R^2
S1	1.40	0.98	1.32	0.99	4.66	0.99
S2	1.16	0.99	1.19	0.99	7.32	0.99
S3	1.25	0.99	1.25	0.99	5.46	0.99
S4	8.51	0.98	8.14	0.98	5.33	0.99
S5	4.26	0.99	4.49	0.98	4.78	0.99
S6	4.81	0.98	5.17	0.85	0.12	0.98
S7	1.49	0.99	1.41	0.99	5.24	0.99

Sustained, steady supply of active Ag is important property of antimicrobial material. In the case of the investigated nano-Ag/PVA hydrogel device, the main released form of Ag is ionic, because Ag NPs are encapsulated in the matrix which prevents their releasing in the environment in larger amounts. It was observed, recently, that Ag NPs are unstable under physiological conditions, to some extent, due to the large ionic strength, which modifies the particle formal charge [11.13]. But, in general, studies have shown that the most of the Ag^+ ions are formed by oxidation of the zerovalent metallic particles, typically by reaction with dissolved O_2 and mediated by protons and other components in the surrounding fluid phase [11.14]. The NPs undergo the redox reaction ($2Ag_{(s)} + 1/2O_{2(aq)} + 2H^+ \rightarrow 2Ag^+_{(aq)} + H_2O_{(aq)}$) and release of Ag^+ ions. Because the release of soluble silver from nAg surfaces is primarily a heterogeneous oxidation reaction involving the cooperative effects of dissolved oxygen and protons, this suggests surface area dependence and the potential to control release through particle size control [11.15]. The obtained values of *in vitro* release of silver from nano-Ag/PVA hydrogel devices are shown in Table 11.4.

TABLE 11.4. CUMULATIVE IN VITRO Ag^+ IONS RELEASE FROM NANO-Ag/PVA HYDROGEL DEVICE.

Cumulative Silver Release/mass of HG NC (ppm/g)						
t (days)	S1	S2	S3	S4	S5	S6
1	5.8	6.6	5.4	29.8	95.0	212.1
3	9.5	10.0	11.1	47.6	183.7	336.9
5	12.4	12.5	15.1	59.1	193.6	356.3
7	15.5	15.4	18.7	70.6	199.6	364.8
9	18.9	18.5	22.3	80.4	206.1	377.9
%/g HG NC	16	19	11	4	4	7

For smaller initial molar concentration of Ag NPs, sample S2, the release profile showed the initial rapid release of the silver in comparison to the release of sample S3 despite containing less amount of Ag (Fig. 11.6a). The higher initial release in duration of 3 days from sample S2, could be associated with the smaller particle size, greatest surface area, of the Ag NPs and consequently their greater solubility, as shown in Table 11.1. For higher molar concentration of Ag NPs, samples S4–S6, an initial rapid release of Ag^+ ions was obserwed for all samples. This initial burst of Ag^+ ions was found to be critical in relation to the antibacterial properties of materials. It enables achieving immediate antibacterial concentrations in contact with body fluids folowed by lower and maintened release, sufficient to preserve the antibacterial concentrations of Ag^+ ions over a period of time and to reduce the initial bacterial attachement [11.16].

Given that the experiments are performed at physiological pH and are buffered, the overall cell voltage and the Gibbs free energy are calculated according to Nernst expression. The cell voltage mainly increases with the initial concentration of silver (Fig. 11.5(a)). The highest value obtained for the sample S4 is probably the result of the greatest fluid diffusion coefficient, *D*, as shown in Table 11.3. It seems that the cell potential depends on the diffusion characteristics of the fluid. The obtained results for the Gibbs free energy (Fig. 11.5c) show that the driving force for the oxidation increases as the initial concentration of silver, and the diffusion characteristics of the fluid, and the largest is for sample S4.

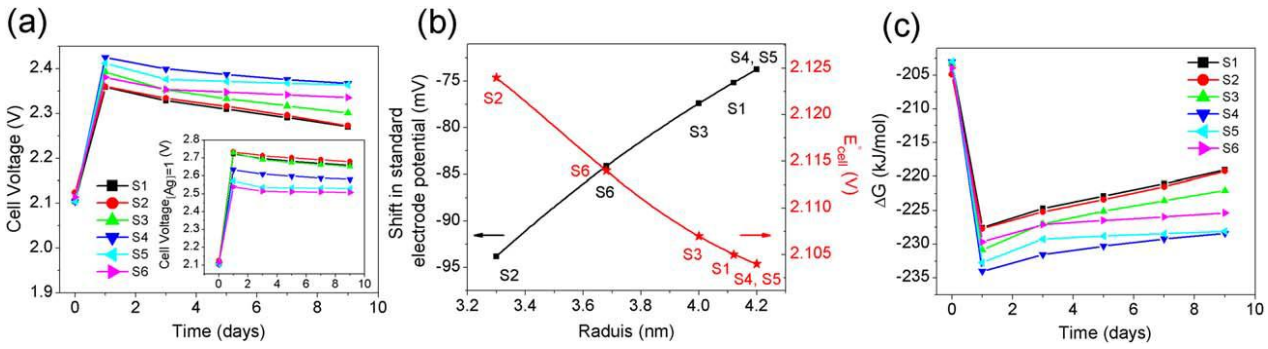

FIG. 11.5. (a) Cell potential, (b) plot of the shift in the standard electrode potential of the Ag NPs and corresponding standard cell electrode potentials (E^0_{cell}), and (c) Gibbs free energy (ΔG).

Throughout the duration of the experiment i.e. after 9 days, there was a difference in the final cumulative silver released throughout the study. The percentage of released Ag^+ ions declines along with increasing the total concentration of Ag^+ ions doped in the device, as shown in Table 11.4. The release of Ag^+ ions from nano-Ag/PVA hydrogel device, for higher molar

concentration of Ag NPs, can be inhibited by the oxygen depletion or by a high concentrations of free Ag^+ ions, that can interact with the surfaces of the NPs and inhibit surface reactions [11.17].

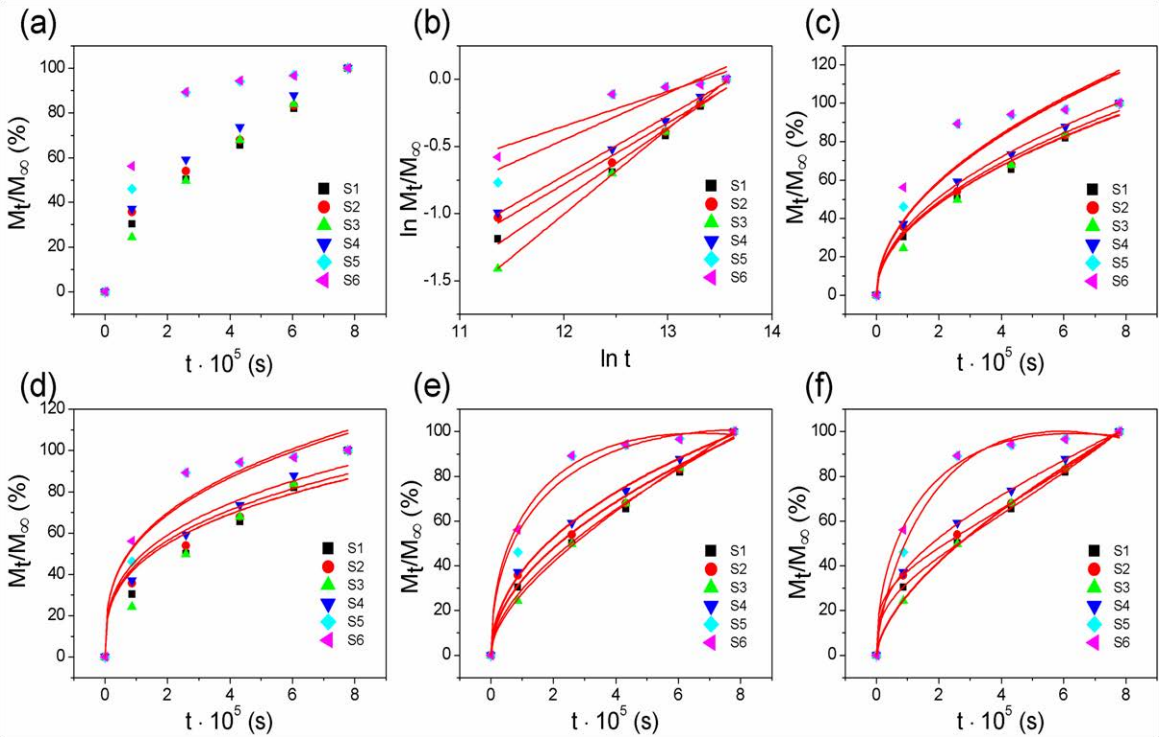

FIG. 11.6. Mathematical modeling of Ag^+ ions release from nano-Ag/PVA hydrogel device: (a) cumulative released amount of Ag^+ ions, (b) Korsmeyer-Peppas, (c) Higuchi, (d) Hixson-Crowel, (e) Kopcha, (f) Makoid-Banakar.

According to previous reports, silver has a bactericidal activity at concentrations as low as 0.035 ppm without toxic effects to mammalian cells [11.18]. But the typical minimum inhibitory concentration (MIC) and minimum bactericidal concentration (MBC) against standard reference cultures as well as multidrug-resistant organisms were 0.78-6.25 ppm and 12.5 ppm, respectively [11.19]. A silver concentration up to 1.2 ppm had no citotoxic effect on fibroblasts in-vitro, which play a critical role in wound healing. However, in general the citotoxic effect seem to be dose-depenent [11.20]. The maximum toxic concentration for human cells is around 10 ppm [11.21]. But some authors sugest that for topical use Ag NPs induce apoptosis at concentrations up to 250 μg/mL (ppm), which could favor scarless wound healing [11.19]. Except for the use as a antimicrobial topical dressings, nano-Ag/hydrogel systems could be applied for orthopedics implants such as artificial cartilage, interverterbral disc and artificial meniscus [11.22], or tissue expander device. Many biomaterials are being developed to be used for cartilage including meniscus substitution and hemiarthroplasty implants, but crosslinked PVA hydrogel due to its good biocompatibility and extraordinary properties such as low elastic modulus and high resilient and a similar biphasic lubrication mechanism is promising kind [11.23-11.25].

The curvilinear nature of the cumulative percentage of released silver versus time plots (Fig. 11.6a) suggests that silver release from the hydrogel does not follow zero-order kinetics. The Korsmeyer-Peppas, Higuchi, Hixson-Crowell, Kopcha and Makoid-Banakar's pharmacokinetic models used to fit obtained Ag^+ ions release data are [11.26, 11.27]. The models which give the best fit-solution are Kopcha and Makoid-Banakar's models, (Fig. 11.6.

and Table 11.5). Moreover, the Hixson-Crowell model suggests that the Ag NPs surface area changes as a function of time.

TABLE 11.5. RESULTS OF THE MODEL FITTING OF Ag^+ IONS RELEASE PROFILES.

Sample	Korsmeyer-Peppas			Higuchi		Hixson-Crowel		Kopcha			Makoid-Banakar			
	k_{KP} (%/s^n)	N	R^2	k_H (%/s$^{1/2}$)	R^2	k_{HC} (%/s$^{1/3}$)	R^2	A (%/s$^{1/2}$)	B×10^5 (%/s)	R^2	k_{MB} (%/s)	n	c×10^7	R^2
S1	0.071	0.53	0.98	0.106	0.99	0.942	0.93	0.083	3.09	0.99	0.597	0.34	-6.22	0.99
S2	0.189	0.46	0.98	0.109	0.99	0.969	0.96	0.104	0.68	0.99	1.899	0.25	-6.71	0.99
S3	0.018	0.64	0.99	0.107	0.98	0.943	0.91	0.072	4.63	0.99	0.022	0.62	-0.55	0.99
S4	0.231	0.45	0.99	0.114	0.99	1.014	0.98	0.123	-1.24	0.99	0.483	0.38	-2.20	0.99
S5	0.975	0.35	0.83	0.132	0.89	1.183	0.96	0.222	-12.2	0.98	0.023	0.68	11.50	0.99
S6	3.099	0.26	0.86	0.133	0.85	1.199	0.96	0.243	-14.8	0.99	0.245	0.49	7.71	0.99

The data in Table 11.5. clearly show that the value of *A* is far greater than that for B for all investigated nanosystems, suggesting that Ag^+ ions release from the nano-Ag/PVA hydrogel device is predominantly controlled by a diffusion process. Moreover, from Table 11.5. it can be seen that Makoid-Banakar's parameter n_{MB} (related to the shape of the function) is smaller for sample S2. When the parameter n_{MB} is smaller, the faster Makoid-Banakar's function rumps up, i.e. the rapid release of Ag^+ ions. The above analysis indicates that the kinetic of Ag^+ ions release is related to the size of NPs, namely, the smaller particles show faster Ag^+ ions release. It is in accordance with previous assumption that the release of Ag^+ ions depends on the surface area of NPs [11.21].

And finally, the kinetic models can be used to predict the performance and the possible lifetime of nano-Ag/PVA hydrogel device applied in different environments. In clinical practice the antimicrobial wound dressings are changed after 48 h or 72 h. It has been recommended that silver containing antimicrobial dressings should be used for two weeks initially and then, the wound, the patient and the management should be re-evaluated [11.28]. The released Ag^+ ions concentration, after 48 h, from the samples S1, S2 and S3 would be in the range of MIC, while from the samples S4, S5 and S6 they would be in the range of MBC. On the other hand, after 72 h all investigated samples would release Ag^+ ions in the MBC range. According to obtained released data, investigated nano-Ag/PVA hydrogel device, samples S1, S2 and S3, can be safely used as antimicrobial topical dressing in duration of 15 days. Even with higher molar concentratons of Ag NPs, sample S4 can be used safely if the scarless wound healing is needed. Moreover, the Makoid-Banakar's model was used to predict performance and the possible life time of nano-Ag/PVA hydrogel device if applied as soft tissue implant (meniscus) in a synovial joint e.g. knee. The results shows that concentrtions of Ag^+ ions, released from the samples S1, S2 and S3, would be sufficient to preserve post-operation sterilty of implanted device. In addition, they are below the maximum toxic concentration for human cells (around 10 ppm) [11.16].

In order to investigate the possibility to predict antibacterial potential using cumulative silver release study, the antibacterial potential of nano-Ag/PVA devices was investigated against gram-positive *Staphylococcus aureus* and gram-negative *Escherichia coli* cultures. The obtained result indicates that concentration level and the conditions for achieving significant antimicrobial activity are not met in duration of the experiment (24 h), for the samples with the lower amount of Ag NPs (S1, S2, and S3). On the other hand, samples with the higher amount of Ag NPs (S4, S5 and S6) possess excellent antimicrobial properties, and retained them even after ageing in buffered solution for two weeks and two months, despite smaller or larger loss of silver.

To prevent clusters collision and their growth into bigger NPs during formation, the polymer molecules with functional groups that have a great affinity for metals need to be added. In the case of CS and PVA, the amino ($-NH_2$) and hydroxyl (–OH) groups interact with the atoms on the surface of metal NPs and thus stabilize them, preventing their further growth [11.28-11.30]. In this study, the possibility of synthesis and stabilization of Ag NPs in CS/PVA blend system, with the different mass ration of CS and PVA, was investigated. The obtained results indicate that the formed Ag NPs are spherical in shape, with the face centered cubic crystal structure and diameter in the range of 11–14 nm. Fig. 11.5. represent the XRD pattern and SEM micrograph of uncrosslinked Ag-CS/PVA (40/60) nanocomposite. The characteristic values for Ag NPs stabilized by CS/PVA blends were calculated from the UV-Vis absorption spectra, using the software "MiePlot v.3.4", and presented at Table 11.6. According to the values of Ag NPs radii it can be observed that smaller NPs were produced when the PVA content in the blend is greater than 50%, which implies that the size of Ag NPs can be controlled by the changing of mass ratio of CS and PVA in the blend system.

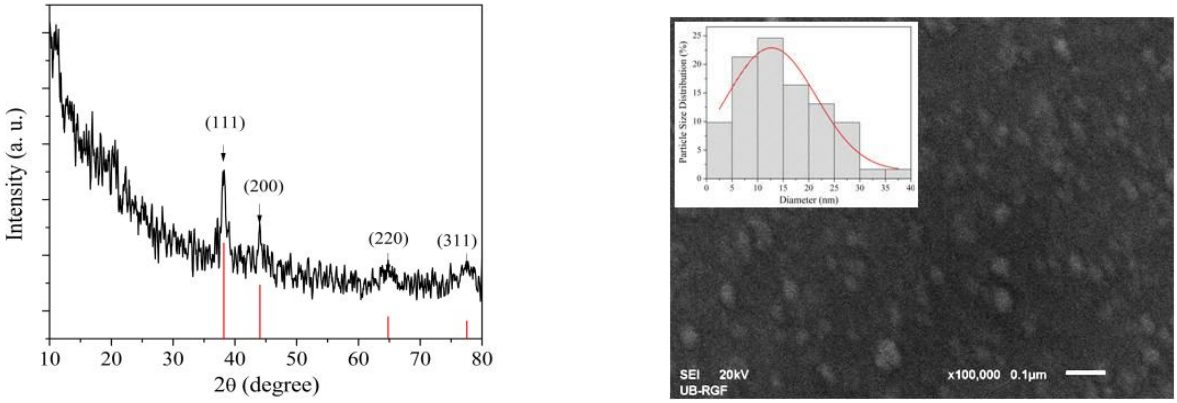

FIG. 11. 5. XRD patern (left) and SEM micrograph (right) of Ag-CS/PVA (40/60) nanocomposite.

TABLE 11.6. VALUES FOR THE PARAMETERS OF Ag NPS STABILIZED BY CS/PVA BLENDS: RADIUS (r_{exp}), AVERAGE NUMBER OF ATOMS (N_{AV}), DENSITY IN COLLOIDS (D), MOLAR CONCENTRATION IN COLLOIDS (C) AND THEORETICAL EFFECTIVE SURFACE AREA ($S.A.$).

CS/PVA	FWHM (nm)	r_{exp} (nm)	N_{av}	D (NPs/cm^3)	C (mol/dm^3)	S.A. (m^2/g)
100/0	91.3	6.74	74961	$4.02 \cdot 10^{12}$	$6.67 \cdot 10^{-9}$	42.39
80/20	91.2	6.73	74666	$4.03 \cdot 10^{12}$	$6.69 \cdot 10^{-9}$	42.45
60/40	90.8	6.70	73858	$4.08 \cdot 10^{12}$	$6.77 \cdot 10^{-9}$	42.64
40/60	83.8	6.18	58024	$5.19 \cdot 10^{12}$	$8.61 \cdot 10^{-9}$	46.23
20/80	80.1	5.91	50694	$5.94 \cdot 10^{12}$	$9.86 \cdot 10^{-9}$	48.34
0/100	74.8	5.52	41203	$7.31 \cdot 10^{12}$	$12.10 \cdot 10^{-9}$	51.76

After the successful synthesis of Ag NPs stabilized by CS/PVA blends, the next step in the investigation was the synthesis of crosslinked hydrogel nanocomposite based on Ag NPs as a filler and CS and PVA as matrix components. The different amounts of commercially available CS (water insoluble) were added to PVA (PVA/CS weight ratios were 100/0, 97/3, 95/5, 93/7 and 90/10) to investigate the possibility of crosslinking CS/PVA blends. The crosslinking of these CS/PVA blend systems were achieved in some extent due to the presence of PVA, but the obtained hydrogel blends possess the poor mechanical properties. It is well known that commercially available CS (water insoluble) doesn't crosslinked under the influence of γ-irradiation, and because of that the preparation of water soluble CS was the

next step in our investigation. The acetic acid solution of CS was exposed to γ-irradiation to perform reduction of molecular weight from 94.8±8.74 kDa down to 31.3±4.73 kDa, and after neutralization with NaOH, the obtained supernatant was the water soluble CS (wsCS). Thus obtained wsCS was used for the further preparation of the PVA/wsCS hydrogels.

Then, the 8 wt.% PVA and mixtures containing 8 wt% PVA/2 wt% wsCS and 8 wt% PVA/4 wt% wsCS were exposed to γ- irradiation in order to induced crosslinking of polymers. After the absorption of 25 kGy only the PVA hydrogel was formed (sample S8), while the 8 wt% PVA/2 wt% wsCS and 8 wt% PVA/4 wt% wsCS samples were further irradiated with 25 kGy. After the absorbed dose of 50 kGy, the formation of polymer network was observed for 8 wt% PVA/4 wt% wsCS (sample S10), but with poor mechanical properties, while in the case of 8 wt% PV A/2 wt% wsCS the crosslinking is still not achieved. Therefore, these samples were irradiated with an additional portion of 25 kGy, and after the absorption of 75 kGy the 8 wt% PVA/4 wt% wsCS (sample S11) and 8 wt% PVA/2 wt% wsCS (sample S9) hydrogels were obtained. In order to prepare the hydrogels with the better mechanical properties, and to prevent dissolution of wsCS during in situ synthesis of AgNP the γ-irradiation was followed by four freeze-thawing cycles. Fluorescence spectroscopy confirms the presence of wsCS in extracted wsCS/PVA matrix. Thus formed polymeric networks were used as a matrix for γ-irradiation *in situ* synthesis of Ag NPs, and obtained hydrogel nanocomposites are labeled as Ag-S8, Ag-S9, Ag-S10 and Ag-S11, respectively. The formation of Ag NPs in PVA/wsCS hydrogels was confirmed by UV-Vis spectral studies. The obtained Ag NPs are spherical in shape with the diameter around 12 nm.

Fig. 11.6a shows the FTIR spectra of the modified wsCS and the initial CS. In general, the free amine groups on deacetylated units and the hydroxyl groups on the C3 and C6 carbons on acetylated or deacetylated units of CS can be grafted. The two peaks at 1593 cm^{-1} and 1418 cm^{-1} of wsCS are the characteristic absorption bands of the carboxyl group (v_{as} $-COO^-$ and v_s $-COO^-$), which indicate that the carboxymethyl group is grafted onto the molecular chain of CS. Fig. 11.6b shows that PVA/wsCS blend xerogel served as stabilizing agent for AgNPs. Decreasing in intensity and red-shift of observed bands indicates possible formation of a coordination bond between AgNPs and $-COO^-$, $-NH_2$ and –OH groups in PVA/wsCS matrix.

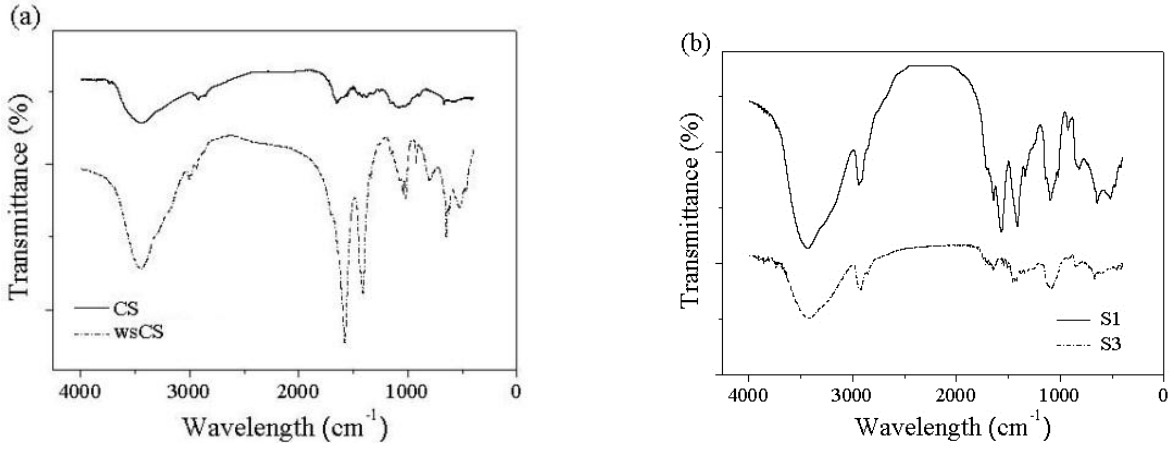

FIG. 11.6. FTIR spectra of (a) pure carboxymethyl wsCS, and (b) nanocomposite xerogel, Ag-S9, in comparing with pure S9 xerogel.

Fluorescence spectroscopy was employed to investigate the emission of crosslinked PVA/wsCS blend after extraction in water (Fig. 11.7a). Fig. 11.7b shows the optical extinction spectra of Ag-PVA/wsCS which are experimentally obtained (solid line) and obtained by simulation according to the Mie theory (dashed line). AgNPs radii can be determined by applying the computational analysis using the software "MiePlot v.3.4". Morphological properties of Ag-PVA/wsCS nanocomposites were examined by scanning electron microscopy (SEM). The obtained micrographs of network (sample Ag-S11) and spherical particles (sample Ag-S9) are shown in Fig. 11.7c.

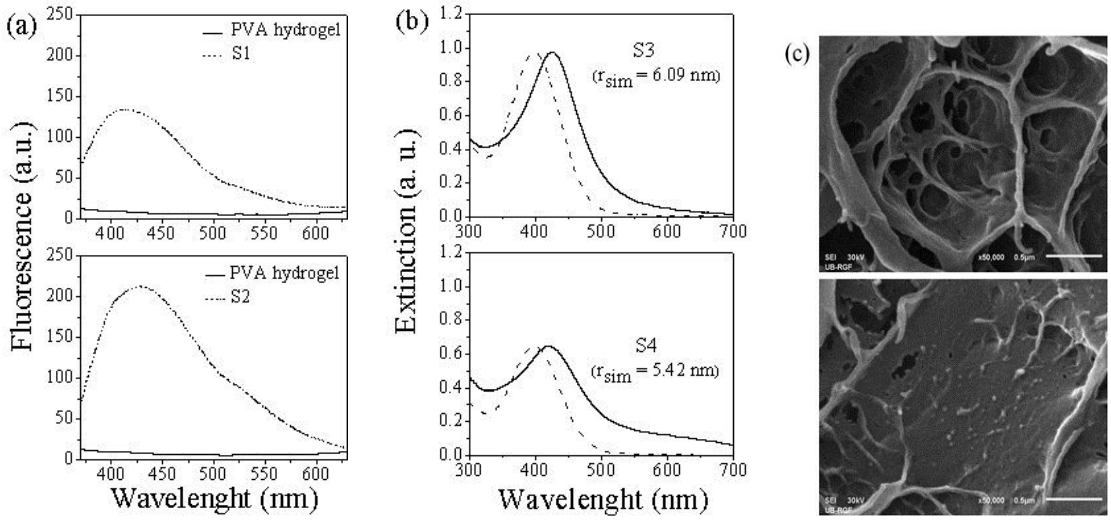

FIG. 11.7. (a) Fluorescent emission detection of grafted wsCS in PVA/wsCS blend hydrogels; (b) experimentally obtained UV-vis extinction spectra (solid line) and obtained by simulation according to the Mie theory (dashed line); SEM micrographs of Ag-S11 (c) (up) and Ag-S9 (c) (down).

The investigation of swelling properties of PVA/wsCS hydrogels as well as Ag-PVA/wsCS hydrogel nanocomposites was conducted in water at 25±1^{o}C, and compared with the pure PVA and Ag-PVA hydrogels. The maximum swelling values SD_{eq} calculated by the theoretical model (first and second order kinetics) for each samples are close to the experimental values (Table 11.7) [11.31-11.34].

TABLE 11.7. VALUES OF THE EQUILIBRIUM SWELLING DEGREE (SD_{eq}), KINETIC CONSTANT (k) AND DIFFUSION EXPONENT (n) FOR THE POWER LAW MODEL, FIRST ORDER KINETICS AND SECOND ORDER KINETICS.

Sample	SD_{eq}^{exp} (%)	power law kinetics			first-order kinetics			second-order kinetics		
		k ($1/h^n$)	n	R^2	SD_{eq}^{cal} (%)	$k_{F\text{-}O}\times10^4$ (1/s)	R^2	SD_{eq}^{cal} (%)	ν_0 (%/min)	R^2
S8	345	0.377	0.40	0.98	286	0.65	0.99	361	3.29	0.99
S9	402	0.473	0.46	0.96	335	0.70	0.97	417	4.89	0.99
S10	410	0.495	0.39	0.98	387	1.29	0.99	418	9.56	0.99
S11	351	0.433	0.40	0.98	300	0.77	0.97	361	4.99	0.99
Ag-S8	414	0.303	0.51	0.98	347	0.58	0.99	437	3.08	0.99
Ag-S9	566	0.364	0.43	0.99	454	0.60	0.97	592	5.35	0.99
Ag-S10	610	0.508	0.33	0.98	530	0.88	0.96	625	11.85	0.99
Ag-S11	497	0.421	0.37	0.99	406	0.66	0.97	515	5.91	0.99

It was evident that the initial concentration of wsCS, as well as initial concentration of Ag NPs incorporated into the hydrogel and increasing absorbed dose of irradiation directly have influence on the maximum of the swelling values. In general, the swelling values SD_{eq} is higher for silver nanocomposites (samples Ag-S8 – Ag-S11), in comparison with the pure systems (samples S8 - S11). Opposite, additional radiation up to the absorbed dose from 50 kGy to 75 kGy for samples S11 and Ag-S11, significantly decreases the values of SD_{eq} in comparison with samples S10 and Ag-S10, probably due to additional crosslinking of the polymer chains.

In addition, the simultaneous curing of polymers and formation of Ag NPs by γ-irradiation was investigated. The mixtures of $AgNO_3$/PVA (8 mM/8 wt%, labeled as Ag-S12) and $AgNO_3$/PVA/wsCS mixtures (8mM/8 wt%/2 wt% and 8mM/8 wt%/4 wt%, labeled as Ag-S13 and Ag-S14, respectively) were exposed to γ- irradiation up to the 200 kGy. The absorbed dose was divided in several portions (50+40+40+40+30) in order to monitor the crosslinking of polymers and reduction of Ag^+ ions. After the absorbed dose of 50 kGy, the systems didn't show any changes. The first change, the initial crosslinking was observed after absorbed of 90 kGy, but only for the sample Ag-S14. During the further irradiation and after absorbed dose of 130 kGy, the initial formation of polymer network was noticed for samples Ag-S12 and Ag-S13, while the crosslinked hydrogel was obtained for sample Ag-S14, but with poor mechanical properties. Moreover, at the absorbed dose of 130 kGy, the formation of Ag NPs was observed for sample Ag-S12, which is confirmed by the appearance of characteristic SPR band around 413 nm (Fig. 11.8a). The crosslinked polymer network with the good mechanical properties was obtained for all samples after the absorption of the last two portions of irradiation, i.e. after the absorbed dose of 170 kGy and 200 kGy. UV-Vis absorption spectra of Ag-PVA/wsCS hydrogel nanocomposites after the absorbed dose of 170 kGy and 200 kGy were presented at Figs. 11.8b and 11.8c, respectively.

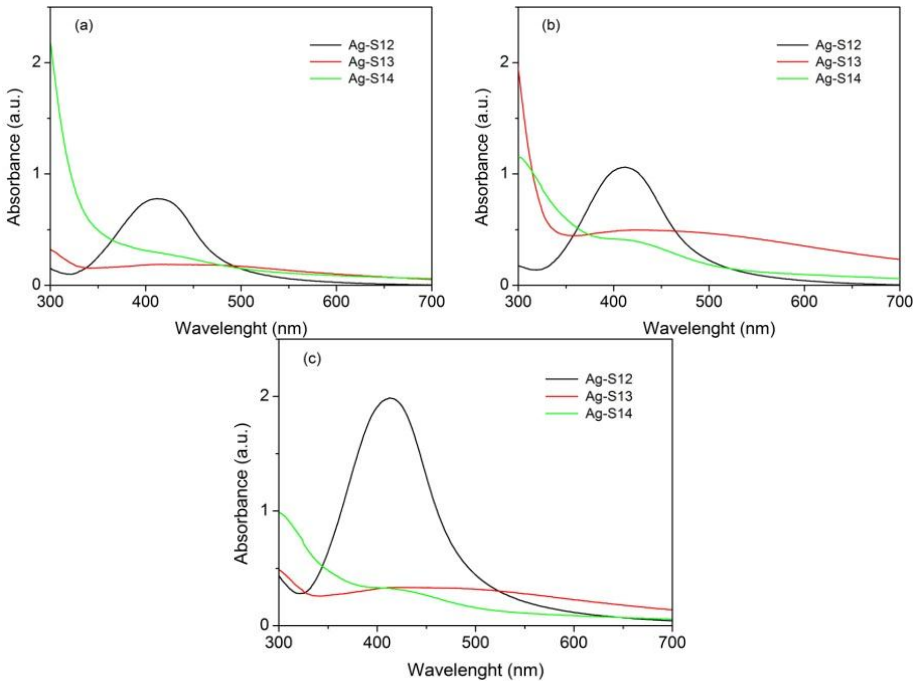

FIG. 11.8. UV-Vis absorption spectra of Ag-PVA/wsCS hydrogel nanocomposites, obtained by simultaneous crosslinking of polymers and formation of Ag NPs, after absorbed dose of (a) 130, (b) 170 and (c) 200 kGy.

From Fig. 11.8, it can be observed that in the case of sample Ag-S12 (black curve) which is control AgPVA sample, increasing of absorbed dose induced the increasing of absorbance, indicating the increase of Ag NPs concentration. On the other hand, for samples Ag-S13 (red curve) and Ag-S14 (green curve) only the very weak absorption in the range 400-450 nm can be noticed. Due to the fact that all the samples contain the same initial amount of silver and that they were irradiated under the same conditions, we assume that the absence of intense absorption for the samples Ag-S13 and Ag-S14 is caused by the formation of small Ag clusters instead of Ag NPs. Some preliminary investigation of these systems has already been done, but the more detailed analysis will be performed in order to confirm the formation of Ag clusters.

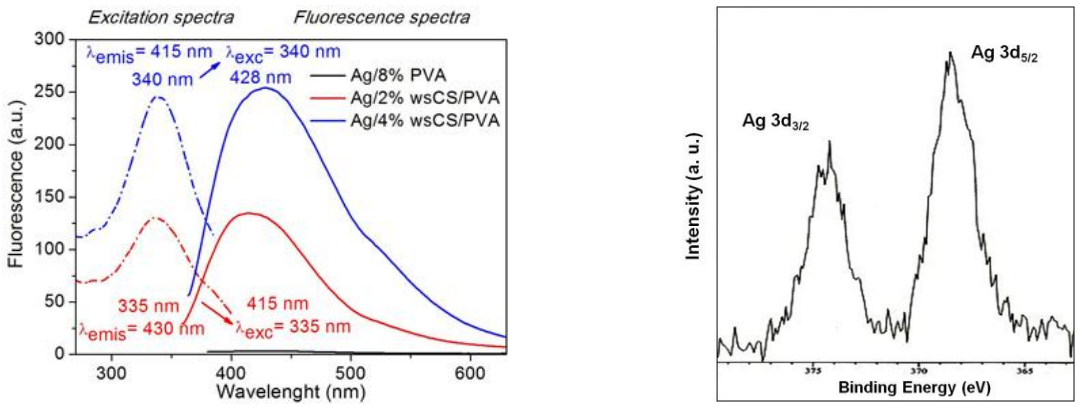

FIG. 11.9. Fluorescence spectra of Ag-PVA/wsCS hydrogel nanocomposites (left) and high resolution XPS spectra for Ag 3d core-level of the in situ Ag/2% wsCS/PVA nanocomposites (right).

The fluorescence spectra of Ag-PVA/wsCS hydrogel nanocomposites are presented on Fig. 11.9 (left), and clearly shows that the fluorescence of Ag clusters and CS were coupled. According to these results we cannot claim that we have particles less than 2 nm with

fluorescence in the same range as wsCS. On the other hand they implied that the Ag/PVA/wsCS hydrogel nanocomposites might be utilized as a new kind of fluorescence material. In order to obtain more precise results, we performed the XPS measurements of Ag/PVA/wsCS hydrogel nanocomposites. XPS spectrum (Fig. 11.9. right) shows the core-level binding energies of the doublet for Ag $3d_{3/2}$ and Ag $3d_{5/2}$ at 368 eV and 374 eV, respectively. These results clearly demonstrate that the Ag clusters embedded in the hydrogel are in the metallic state.

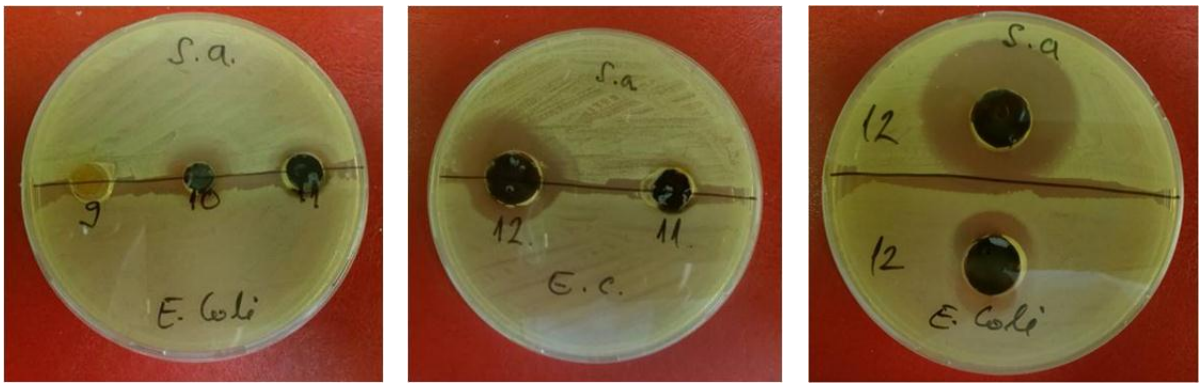

FIG. 11.10. Test of the antibacterial activity against Escherichia coli and Staphylococcus aureus: sample S11 (No. 9), sample Ag-S11 (No. 10), sample Ag-S12 (No. 11) and sample Ag-S14 (No. 12).

Antibacterial activity of synthesized nanocomposites based on wsCS, show enhanced antibacterial potential in comparing with Ag-PVA nanocomposites or PVA/wsCS matrix only. It is known that CS derivatives with the quaternary ammonium groups posses high efficacy against bacteria and fungi. The target site of these cationic polymers is the cytoplasmic membrane of bacterial cells. For *in situ* Ag/PVA/wsCS nanocomposites zone of inhibition is grater against *Staphylococcus aureus* which is important for the treatment of the wound infections in diabetic patients which are mainly caused by aerobic gram-positive *cocci*. These promising results give possibility for development and optimization of Ag/PVA/wsCS delivery system through therapeutic window.

11.4. CONCLUSIONS

Nano-Ag/PVA hydrogel device as a model system was synthesized by *in situ* γ-irradiation, with the aim to design a hydrogel controlled release system of Ag^+ ions for antibacterial purposes, utilizing the advantages of radiolytic method. The *in vitro* Ag^+ ions release study showed sustained and controlled release in the solution similar to the pH of biological fluids, with the absolute amount of the Ag^+ ions released in the antimicrobial ppm concentration range. The elements of the drug delivery paradigm were applied for the study of Ag^+ ions release kinetics. The models, which give the best fit-solution between experimental observations and the nonlinear function are Kopcha and Makoid-Banakar's pharmacokinetic dissolution model. It was foud that the release of Ag^+ ions is predominantly controlled by a diffusion process, i.e. the mass transport rate due to a concentration gradient of Ag^+ ions (Fickian diffusion). The Ag^+ ions release characteristics were the result not only of the molar concentration but the size of Ag NPs. However, it appears that the cell potential depends on the diffusion characteristics of the fluid. The antimicrobial testing has shown the correlation between the observed Ag^+ ions release potential and the antimicrobial properties of the nano-Ag/PVA hydrogel device against gram-positive *Staphylococcus aureus* and gram-negative *Escherichia coli*. According to obtained results, it could be expected that used mathematical

models could be routinely applied to help the optimization of the novel nano-Ag/hydrogels dosage forms. This is not only of academic interest, but a pre-requisite for an efficient improvement of the safety of the silver pharmaco-treatments.

Moreover, it was showed that the ration of PVA and CS in the blend systems can be used to control the size of Ag NPs. The obtained result indicated that the smaller Ag NPs were produced when the PVA content in the blend is greater than 50%. The crosslinking of these CS/PVA blend systems were achieved in some extent due to the presence of PVA, but the obtained hydrogel blends possess the poor mechanical properties.

The water soluble chitosan (wsCS) was prepared by γ-irradiation induced acidic degradation of commercially available product, and used in further synthesis of crosslinked nanocomposite systems. The PVA/wsCS hydrogels were synthesized also by the γ-irradiation followed by freeze-thawing cycles, in order to obtain the appropriate matrix for incorporation of Ag NPs. The different absorbed dose was applied to optimize the process of polymer crosslinking. The *in situ* incorporated Ag NPs were spherical in shape with the radius less than 12 nm. Kinetic aspects and diffusion model of the swelling process of pure hydrogels and hydrogel nanocomposites show that at the initial stage of swelling systems show Fickian diffusion.

Finally, the simultaneous curing of polymers and formation of Ag NPs by γ-irradiation was investigated. The optimization of the irradiation process is carried out in terms of the determination of the total absorbed dose required for the simultaneous crosslinking of polymers and formation of Ag NPs. According to the results, there are indications that in the Ag-PVA/wsCS hydrogel nanocomposites the small Ag clusters were formed instead of Ag NPs, and the further investigation will be performed.

Antibacterial activity of synthesized nanocomposites based on wsCS, show enhanced antibacterial potential in comparing with Ag-PVA nanocomposites or PVA/wsCS matrix only.

REFERENCES TO CHAPTER 11

[11.1] HILTON, J.R., WILLIAMS, D.T., BEUKER, B., MILLER, D.R., HARDING, K.G., "Wound dressings in diabetic foot disease", Clin. Infect. Dis. 39 (2004) 100-103.

[11.2] XIU, Z., ZHANG, Q., PUPPALA, H.L., COLVIN, V.L, ALVAREZ, P.J., "Negligible particle-specific antibacterial activity of silver nanoparticles", J. Nano Lett. 12 (2012) 4271-4275.

[11.3] LIU, J., SONSHINE, D.A., SHERVANI, S., HURT, R.H., "Controlled release of biologically active silver from nanosilver surfaces", ACS Nano 4 (2010) 6903-6913.

[11.4] SINGH, B., "Psyllium as therapeutic and drug delivery agent", Int. J. Pharmaceut. 334 (2007) 1-14.

[11.5] JOVANOVIĆ, Ž., KRKLJEŠ, A., STOJKOVSKA, J., TOMIĆ, S., OBRADOVIĆ, B., MIŠKOVIĆ-STANKOVIĆ, V., KAČAREVIĆ-POPOVIĆ, Z., "Synthesis and characterization of silver/poly(N-vinyl-2-pyrrolidone) hydrogel nanocomposite obtained by in situ radiolytic method", Radiat. Phys. Chem. 80 (2011) 1208-1215.

[11.6] KRKLJEŠ, A., NEDELJKOVIĆ, J., KAČAREVIĆ-POPOVIĆ, Z., "Fabrication of Ag–PVA hydrogel nanocomposite by gamma irradiation", Polym. Bull. 58 (2007) 271-279.

[11.7] KAČAREVIĆ-POPOVIĆ, Z., DRAGAŠEVIĆ, M., KRKLJEŠ, A., POPOVIĆ, S., JOVANOVIĆ, Ž., TOMIĆ, S., MIŠKOVIĆ-STANKOVIĆ, V., "On the Use of Radiation Technology for Nanoscale Engineering of Silver/Hydrogel Based Nanocomposites for Potential Biomedical Application", The Open Conference Proceedings Journal., 1 (2010) 200-206.
[11.8] RANCE, G.A., MARSH, D.H., KHLOBYSTOV, A.N., "Extinction coefficient analysis of small alkanethiolate-stabilised gold nanoparticles", Chem. Phys. Lett. 460 (2008) 230-236.
[11.9] VEENAS, C.L., NISSAMUDEEN, K.M., SMITH, S.L., BIJU, V., GOPCHANDRAN, K.G., "Off-axis PLD: A novel technique for plasmonic engineering of silver nanoparticles", J. Optoelectron Adv. M. 11 (2009) 114-122.
[11.10] STEPANOV, A.L., HOLE, D.E., TOWNSEND, P.D., "Modiffcation of size distribution of ion implanted silver nanoparticles in sodium silicate glass using laser and thermal annealing", Nucl. Instrum. Meth. B 149 (1999) 89-98.
[11.11] CAN, H.K., DENIZLI, B.K., KAVLAK, S., GUNER, A., "Preparation and swelling studies of biocompatible hydrogel systems by using gamma radiation-induced polymerization", Radiat. Phys. Chem. 72 (2005) 483-488.
[11.12] KAPLAN, H., GUNER, A., "Characterization and determination of swelling and diffusion characteristics of poly(n-vinyl-2-pyrrolidone) hydrogels in water", J. Appl. Polym. Sci. 78 (2000) 994-1000.
[11.13] ALARCON, E.I., BUENO-ALEJO, C.J., NOEL, C.W., STAMPLECOSKIE, K.G., PACIONI, N.L., POBLETE, H., SCAIANO, J.C., "Human serum albumin as protecting agent of silver nanoparticles: role of the protein conformation and amine groups in the nanoparticle stabilization", J. Nanopart. Res. 15 (2013) 1374-1377.
[11.14] MA, R., LEVARD, C., MARINAKOS, S.M., CHENG, Y., LIU, J., MICHEL, F.M.; BROWN, G.E.; LOWRY, G.V., "Size-controlled dissolution of organic-coated silver nanoparticles", Environ. Sci. Technol. 46 (2012) 752-759.
[11.15] LEE, Y.J., KIM, J., OH, J., BAE, S., LEE, S., HONG, I.S., KIM, S.H., "Ion-release kinetics and ecotoxicity effects of silver nanoparticles", Environ. Toxicol. Chem. 31 (2012) 155-159.
[11.16] JAMUNA-THEVI, K., BAKAR, S.A., IBRAHIM, S., SHAHAB, N., TOFF, M.R.M., "Quantification of silver ion release, in vitro cytotoxicity and antibacterial properties of nanostuctured Ag doped TiO2 coatings on stainless steel deposited by RF magnetron sputtering", Vacuum 86 (2011) 235-241.
[11.17] LIU, J., HURT, R.H., "Ion Release Kinetics and Particle Persistence in Aqueous Nano-Silver Colloids", Environ. Sci. Technol. 44 (2010) 2169-2175.
[11.18] HARDES, J., AHRENS, H., GEBERT, C., STREITBERGER, A., BUERGER, H., ERREN, M., GUNSEL, A., WEDEMEYER, C., SAXLER, G., WINKELMANN, W., GOSHEGER, G., "Lack of toxicological side-effects in silver-coated megaprostheses in humans", Biomaterials 28 (2007) 2869-2875.
[11.19] JAIN, J., ARORA, S., RAJWADE, J.M., OMRAY, P., KHANDELWAL, S., PAKNIKAR, K.M., "Silver nanoparticles in therapeutics: development of an antimicrobial gel formulation for topical use", Mol. Pharmaceut. 6 (2009) 1388-1401.
[11.20] JOVANOVIĆ, Ž., RADOSAVLJEVIĆ, A., KAČAREVIĆ-POPOVIĆ, Z., STOJKOVSKA, J., PERIĆ-GRUJIĆ, A., RISTIĆ, M., MATIĆ, I., JURANIĆ, Z., OBRADOVIĆ, B., MIŠKOVIĆ-STANKOVIĆ, V., "Bioreactor validation and biocompatibility of Ag/poly(N-vinyl-2-pyrrolidone) hydrogel nanocomposites", Colloid Surfaces B 105 (2013) 230-235.

[11.21] Wounds International. International Consensus: Appropriate Use of Silver Dressings in Wounds. http://www.woundsinter national.com/clinical-guidelines/international-consensusappropriate-use-of-silver-dressings-in-wounds (accessed 2012).
[11.22] KOBAYASHI, M., HYU, H.S., "Development and Evaluation of Polyvinyl Alcohol-Hydrogels as an Artificial Atrticular Cartilage for Orthopedic Implants", Materials 3 (2010) 2753-2771.
[11.23] KOBAYASHI, M., TOGUCHIDA, J., OKA, M.K., "Development of an artificial meniscus using polyvinyl alcohol-hydrogel for early return to, and continuance of, athletic life in sportspersons with severe meniscus injury. II: animal experiments", Knee 10 (2003) 53.
[11.24] BAKER, M.I., WALSH, S.P., SCHWARTZ, Z., BOYAN, B.D., "A review of polyvinyl alcohol and its uses in cartilage and orthopedic applications", J. Biomed. Mater. Res. B 100B (2012) 1451-1457.
[11.25] AYDIN, R.S.T., PULAT, M.R., "5-Fluorouracil Encapsulated Chitosan Nanoparticles for pH-Stimulated Drug Delivery: Evaluation of Controlled Release Kinetics", J. Nanomater. vol. 2012 Article ID 313961, 10 pages, 2012. doi:10.1155/2012/313961
[11.26] KHAMANGA, S.M., WALKER, R.B., "In Vitro Dissolution Kinetics of Captopril from Microspheres Manufactured by Solvent Evaporation", Dissolut. Technol. 3 (2012) 42-51.
[11.27] LI, F.; SU, Y.; WANG, J.; WU, G.; WANG, C., "Influence of dynamic load on friction behavior of human articular cartilage, stainless steel and polyvinyl alcohol hydrogel as artificial cartilage", J. Mater. Sci.: Mater. Med. 21 (2010) 147-154.
[11.28] HUANG, N.M., RADIMAN, S., LIM, H.N., KHIEW, P.S., CHIU, W.S., LEE, K.H., SYAHIDA, A., HASHIM, R., CHIA, C.H., "γ-ray assisted synthesis of silver nanoparticles in chitosan solution and the antimicrobial properties", Chem. Eng. J. 155 (2009) 499-507.
[11.29] BELLONI, J., MOSTAFAVI, M., REMITA, H., MARIGNIER, J.L., DELCOURT, M.O., "Radiation-induced synthesis of mono- and multi-metallic clusters and nanocolloids", New J. Chem. 22 (1998) 1239-1255.
[11.30] GACHARD, E., REMITA, H., KHATOURI, J., KEITA, B., NADJO, L., BELLONI, J., "Radiation-induced and chemical formation of gold clusters", New J. Chem. 22 (1998) 1257-1265.
[11.31] JOVANOVIĆ, J., ADNAĐEVIĆ, B., "Influence of poly(acrylic acid) xerogel structure on swelling kinetics in distilled water", Polym. Bull. 58 (2007) 243-252.
[11.32] MULLARNEY, M.P., SEERY, T.A.P., WEISS, R.A., "Drug diffusion in hydrophobically modified N,N-dimethylacrylamide hydrogels", Polymer 47 (2006) 3845-3855.
[11.33] RITGER, P.L., PEPPAS, N.A., "A simple equation for description of solute release II. Fickian and anomalous release from swellable devices", J. Control. Release 5 (1987) 37-42.
[11.34] KATIME, I., VELADA, J.L., NOVOA, R., DÍAZ DE APODACA, E., PUIG, J., MENDIZABAL E., "Swelling kinetics of poly(acrylamide)/poly(mono-n-alkyl itaconates) hydrogels", Polym. Int. 40 (1996) 281-286.

Chapter 12

PREPARATION AND CHARACTERIZATION OF POLY(LACTIC ACID)-STARCH BIODEGRADABLE COMPOSITES VIA RADIATION PROCESSING

K. HEMVICHIAN, P. SUWANMALA
Thailand Institute of Nuclear Technology

W. KANGSUMRITH
Department of Industrial Engineering, Faculty of Engineering,
Thammasat University

T. PONGPRAYOON
Department of Chemical Engineering,
Faculty of Engineering,
King Mongkut's University of Technology

Bangkok,
Thailand

Abstract

This research aims to modify the surface of cassava starch (CS) to make it more compatible with polylactic acid (PLA). The research is divided into 3 parts. In the first part, radiation-induced crosslinking of PLA was investigated. Results showed that the presence of a suitable crosslinking agent (TAIC) enables PLA to undergo crosslinking induced by gamma radiation. The optimum condition for radiation-induced crosslinking of PLA was determined. TMA results revealed that PLA crosslinked by gamma radiation has higher thermal stability, compared to unirradiated PLA. For the second part, the surface modification of CS was carried out via esterification reaction using L-lactic acid to yield surface modified starch (SMS). SMS was used to react further with L-lactide to yiled PLA grafted onto starch (PLA-g-CS). PLA-g-CS was used as a compatibilizer for the blending between PLA and CS. Results from mechanical tests of PLA-CS blends showed that the compatibilizer did hot help improve the mechanical properties of the blends. In the third part, an alternative method to increase the compatibility between PLA and CS was also investigated. Admicellar polymerization was used to modify the sucface of CS to make it more hydrophobic and hence more compatible with PLA. Poly(methyl methacrylate) (PMMA) film was coated on the surface of CS by admicellar polymerization. PMMA-modified starch (MS) was blended with PLA. Results have shown that, at the same TPS content, mechanical properties of PLA-MS blends were much better than those of PLA-CS blends.

12.1. OBJECTIVE OF THE RESEARCH

The specific objective of this research is to apply the use of radiation processing to prepare biodegradable composites from PLA and CS, a natural polymer that is inexpensive and abundant, especially in Thailand. CS will be used as starting material. CS will be modified first in order to render starch more compatible with PLA. In order to further improve the thermal properties, the blends will be subjected to radiation to induce crosslinking between the molecules of PLA and CS.

12.2. INTRODUCTION

Poly(lactic acid) or polylactide (PLA) is a compostable thermoplastic obtained by ring-opening polymerization of lactide monomers which can be derived from renewable resources [12.1], such as starch or sugarcanes. In recent years, PLA has been receiving a great deal of attention, essentially due to its degradability. For this environmental-friendly profile, along with a highly transparent

appearance, similar to that of polyethylene terephthalate (PET), PLA has undoubtedly become one of the most promising alternatives to non-biodegradable synthetic polymers conventionally derived from petroleum-based chemicals. Nonetheless, two of the most important factors that prevent PLA from being commercially and widely used are its low thermal stability [12.2-12.3] and high cost, compared to commercial plastics such as polyethylene (PE) or PET commonly used in packaging materials. Renewable resources such as starch are relatively inexpensive and therefore able to offer a competitive commercial strategy. The proposed blending between PLA and starch derivatives is designed to combine the processability and PET-like properties of PLA with the high thermal stability of starch derivatives. This work intends to utilize radiation processing as a means to overcome the aforementioned shortcomings associated with PLA, by blending PLA with starch derivatives and using radiation-induced cross-linking to improve thermal stability of the blends.

Chen et al. [12.4] developed a new method for the surface modification of starch by esterification reaction of the hydroxyl groups on starch molecules with lactic acid. The surface modified starch (SMS) was then used as a macromolecular initiator for the ring-opening polymerization of L-lactide to synthesize the starch grafted PLA copolymer (PLA-g-CS). The amphiphilic character of PLA-g-CS showed good adhesion between the two components and therefore was a good compatibilizer for blending hydrophobic PLA with hydrophilic starch. When subjected to radiation, PLA undergoes degradation processes [12.5]. However, a number of researchers [12.6-12.9] have discovered that, with a suitable crosslinking agent, radiation can induce crosslinking between PLA molecules. This research aims to modify CS surface to make it more compatible with PLA and to find an optimum condition for radiation-induced crosslinking of the blends by gamma irradiation.

Besides the synthesis of PLA-g-CS to be used as a compatibilizer, an alternative method to make CS more compatible with PLA by admicellar polymerization was proposed. Admicellar polymerization was first introduced by Wu et al. in 1987 [12.10]. Admicellar polymerization consists of a four-step process; admicelle formation on the surface, monomer adsolubilization, polymerization of the monomer dissolved in admicelles, and surfactant removal to expose the surface of polymer film, as shown in Figure 12.1.

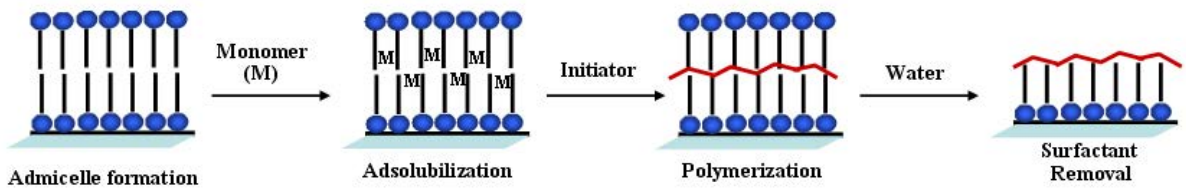

Fig. 12.1. Admicellar polymerization.

Admicellar polymerization is a well-known technique to improve surface of materials by coating the surface with nanoscale polymeric thin film [12.11-12.14]. The thin film is formed by polymerization of monomers inside the admicelles. In this work, admicellar polymerization was used to form PMMA film on CS surface to enhance the adhesion between CS and PLA.

12.3. MATERIALS AND METHODS

12.3.1. Materials

Commercial cassava starch was obtained from Bangkok Inter Food Co., Ltd. Polylactic acid (PLA 2002D) was purchased from Nature Works® (USA). Lactic acid was purchased from Merck. Triallyl isocyanurate (TAIC), (3S)-Cis-3,6-Dimethyl-1,4-dioxane-2,5-dione (L-

lactide), tin(II)-2-ethylhexanoate and methyl methacrylate (MMA) were supplied by Aldrich (USA). Glycerol and ammonium persulphate [$(NH_4)_2S_2O_8$] were acquired from Ajax Finechem Pty. Ltd. (New Zealand). Cetyltrimethylammonium bromide ($[CH_3(CH_2)_{15}N(CH_3)_3]Br$ or CTAB) (Fluka, Switzerland) was used as received. Chloroform (Lab Scan), ethanol (Fisher Scientific) and acetone (Merck) were used without further purification.

12.3.2. Synthesis of surface modified starch (SMS)

The surface modification of starch with L-lactic acid is shown in Figure 12.2. 30 g of cassava starch was dispersed in 100 ml of THF. Lactic acid was gradually dropped into the suspension. The mixture was heated to 60 °C and maintained for 30 min. The THF solvent was removed by evaporator and 150 ml of toluene was added into the mixture. The mixture was heated to 150 °C and kept for 10 h. The water formed was removed by azeotropic dehydration with toluene. The mixture was washed five times by THF and ethyl acetate, respectively, to remove non-grafted lactic acid. The mixture was then filtrated and dried in vacuum oven at 60 °C for 24 h to remove the residual solvent.

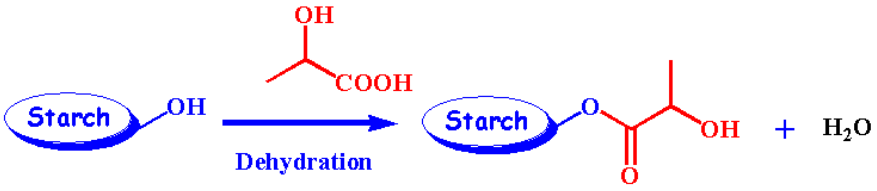

FIG. 12.2. The surface modification of starch with lactic aicd.

12.3.3. Synthesis of PLA-g-starch (Compatibilizer)

Radiation-induced grafting polymerization of L-lactide onto the surface of SMS, Figure 12.3, was carried out with 0.1 wt% $Sn(Oct)_2$ as catalyst under nitrogen atmosphere at 4 different doses: 5, 10, 15 and 20 kGy. The feed ratio of SMS to L-lactide in weight is 1:1. The product was washed five times with ethanol to remove unreacted L-lactide and residual catalyst. The product was the mixture of PLA-g-CS and PLA homopolymer. Toluene extraction was used to separate PLA-g-CS from PLA homopolymer. The product was put into a 50 ml toluene in a bottle. The mixture was stirred at 20 ^oC for 24 h and then filtered. The remaining solids were washed with toluene for three times. The above process was repated once again. The solid after toluene extraction were considered as PLA-g-CS. PLA-g-CS was dried in a vacuum oven and characterized by FTIR.

FIG. 12.3. Polymerization of L-lactide with surface modified starch.

12.3.4. Synthesis of MS (CS modified by PMMA by admicellar polymerization)

CTAB was dissolved in 1000 ml of distilled water. The amount of CTAB used was 7.5 mmole, according to the adsorption isotherm in our previous study. 1 g of cassava starch was dispersed in 50 ml of CTAB solution. The mixture was stirred at room temperature for 24 hr. MMA and 0.94 ml of ethanol was added. The molar ratio of CTAB to MMA was varied (1:30, 1:40 and 1:50). The mixture was continuously stirred at room temperature for 24 hr. Then, 0.017 g of ammonium persulphate was added. The mixture was gradually heated to 30 °C and kept for 48 h under stirring to induce polymerization. The modified starch was subsequently filtered and washed many times with distilled water until the redundant surfactant and the upper layers of admicelle formed on silica surface were completely removed. After the washing steps have been thoroughly done, the removal of the outer-layered surfactant was confirmed by floating test. Once the outer-layered surfactant has been removed, the surface will be hydrophobic and therefore the samples will be floating on the water surface. On contrary, if there is some remaining outer-layered surfactant, the surface will still be hydrophilic and the samples will be sinking down at the bottom. The silica samples were later dried in an air oven at 40^{o}C for 3 days, before the characterization.

12.3.5. Sample preparation and irradiation: PLA samples

Pure PLA samples with varied contents of crosslinking agent were prepared to find the optimum condition for radiation-induced crosslinking. PLA pellets were dried in a vacuum oven at 75^{o}C for 24 h. A co-current twin-screw extruder (Lab Tech, LTE16-40, Thailand), equipped with segmented screw of diameters of 16 mm and L/D ratio of 40, was used to mix PLA with TAIC at different concentrations: 0, 1, 3 and 5 phr. The composition and abbreviated name of these samples are shown in Table 12.1. The temperatures of barrel heating zone I, II, III, IV and V of the die of the extruder were set to 155, 175, 185, 195, and 200°C, respectively. The TAIC-containing PLA pellets were then compressed by a compression molder (Lab Tech, Thailand) to form 150 mm x 150 mm x 0.2 mm films. The pellets were pre-pressed and full-pressed at 200°C for 8 and 2 min, respectively, followed by cold-pressing at room temperature for 2 min. The film samples were irradiated using a Co-60 gamma irradiator (Gamma Chamber 5000, BRIT, India) at 0, 20, 40, 60, 80 and 100 kGy, under vacuum.

TABLE 12.1. COMPOSITION AND ABBREVIATED NAME OF PLA SAMPLES, PLA-CS AND PLA-MS BLENDS

Sample Name	PLA (g)	TPS from CS (g)	TPS from CS Modified by PMMA (g)	TAIC (phr)	PLA-g-CS (phr)
P100 T0	100	-	-	0	-
P100 T1	100	-	-	1	-
P100 T3	100	-	-	3	-
P100 T5	100	-	-	5	-
P90 CS T3	90	10	-	3	-
P80 CS T3	80	20	-	3	-
P70 CS T3	70	30		3	-
P80 CS T3 G3	80	20	-	3	3
P80 CS T3 G5	80	20	-	3	5
P90 MS T3	90	-	10	3	-
P80 MS T3	80	-	20	3	-
P70 MS T3	70	-	30	3	-

12.3.6. Sample preparation and irradiation: PLA-CS and PLA-MS blends

Thermoplastic starch (TPS) was first prepared from CS or MS (CS modified by PMMA by admicellar polymerization) and glycerol using a High Speed Mixer (Lab Tech, Thailand). The screw speed was set at 3,000 rpm. The ratio of CS to glycerol was 70:30. The melt blending of PLA and TPS was performed using the same prodecure for pure PLA samples, except that the temperatures of barrel heating zone I, II, III, IV and V of the die of the extruder were set to 135, 150, 160, 170, and 180°C, respectively. The composition and abbreviated name of different blends between PLA and TPS, with varied contents of TPS, crosslinking agent and compatibilizer, are tabulated in Table 12.1. The film samples were prepared using the same prodecure for compression molding and irradiated using the same gamma irradiator at the same doses.

12.3.7. Characterization

Chemical characterization was done using a Fourier transform infrared spectrometer from Bruker (Tensor 27). Spectra were collected with 16 co-added at a resolution of 4 cm^{-1}. Scanning electron microscope (SEM) by JEOL (Model JSM-5410LV) was used to study surface morphology. Samples were put on a brass plate where Au coating was applied.

12.3.8. Mechanical properties

The mechanical properties were measured at room temperature on a tensile tester (AG-100kNG, Shimadzu, Japan) at a crosshead speed of 10 mm/min. Sample preparation was done using a SD-type lever-controlled sample cutter (SDL-100, Dumbbell Co., Ltd., Japan) and a super dumbbell cutter (SDMK-1000-D, Dumbbell Co., Ltd., Japan), according to the ASTMD-638-IV. For each blend composition at each condition, ten samples were tested and the results were averaged. A thermomechanical analyzer (Mettler Toledo, TMA/SDTA 841^e) was used to study the thermo mechnical properties of the samples. Sample films (thickness 0.2mm) was fixed to the sample holder under a constant load of 0.5 g (0.004 Newton) and heated from 0°C to 260°C at a heating rate of 10°C/min. The deformation (%) was recorded against the temperature.

12.4. RESULTS AND DISCUSSION

12.4.1. PLA samples

Figure 12.4 shows the tensile strength and elongation at break of PLA samples irradiated under vacuum as a function of crosslinking agent content and dose. Tensile strength of P100 T0 drastically decreased with dose, especially after 60 kGy, while P100 T1 remained roughly the same from 0 to 80 kGy. P100 T3 slightly increased with dose, whereas P100 T5 obviously increased with dose. Similar trends were observed for elongation at break of PLA samples. The results showed that, with optimum amount of crosslinking agent, irradiation under vacuum brought about enhancement in mechanical properties of PLA samples.

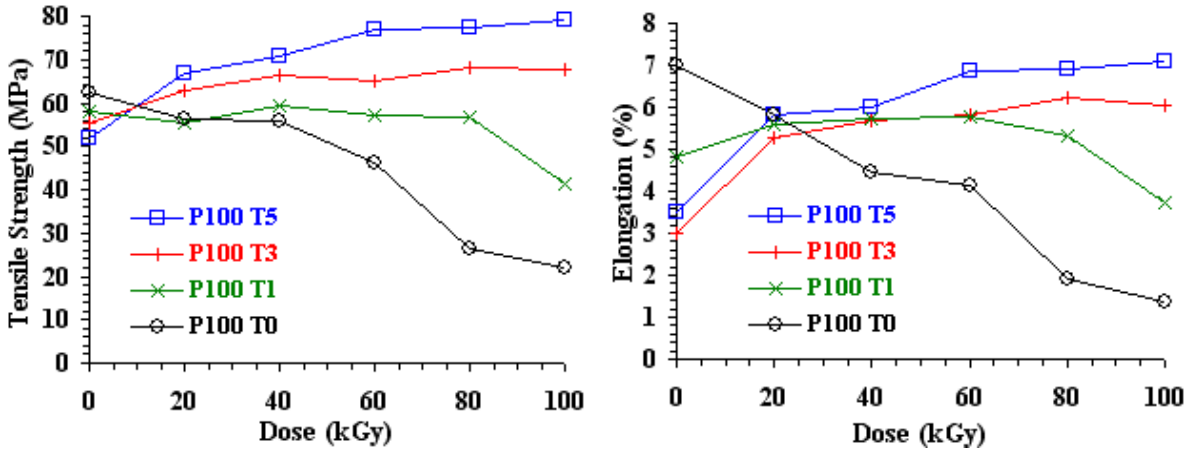

FIG. 12.4. Tensile strength (left) and elongation at break (right) of PLA samplesirradiated at different contents of crosslinking agent and doses.

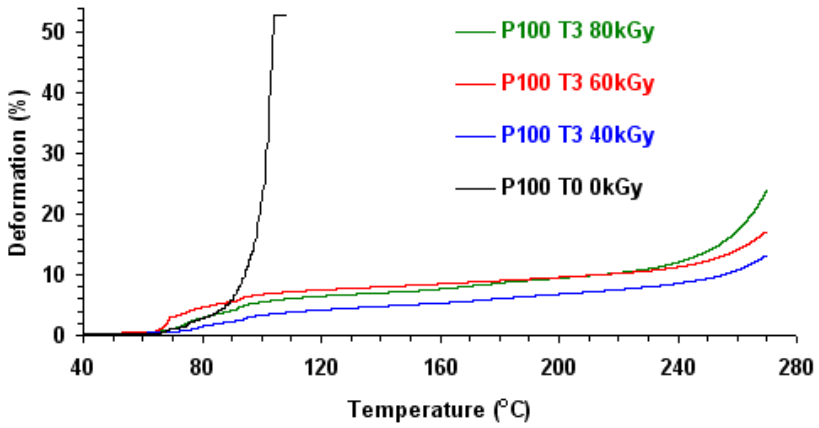

FIG. 12.5. TMA thermograms of P100 T3 samples irradiated at different dose under vacuum.

Figure 12.5 shows the TMA thermograms of P100 T3 samples irradiated at 0, 40, 60 and 80 kGy. Unirradiated P100 T3 sample started its initial elongation slightly after 60°C, continued its gradual elongation to higher temperatures and showed its drastic deformation at approximately 100°C, after which it finally fractured. The significant elongation reflects the softening of the sample. All P100 T3 samples irradiated in vacuum at 40, 60 and 80 kGy also showed initial elongation at around 70°C and continued to show their gradual deformation to higher temperatures. All P100 T3 samples were thermally stable even after 200°C and showed approximately less than 15% of deformation even at 250 °C, without breaking. These results hence, once again, confirmed the radiation-induced of PLA samples irradiated as well as their higher thermal stability.

12.4.2. PLA-CS blends (without the compatibilizer)

The effect of starch content on the tensile strength and elongation at break for the PLA-CS blends, without the compatibilizer, is shown in Figure 12.6.

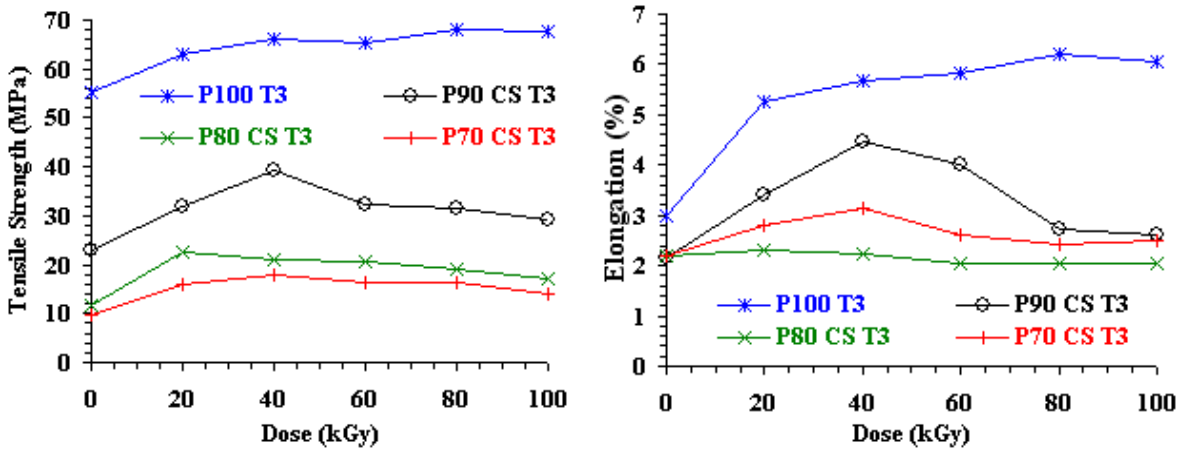

FIG. 12.6. Tensile strength (left) and elongation at break (right) of PLA-CS blends (without compatibilizer) irradiated at different doses.

For unirradiated samples, the tensile strength of the blends decreased markedly from roughly 55 to 10 MPa, as the starch content is increased from 0 to 30%. Similar trend was observed for the elongation at break of the blends. The deterioration in mechanical properties of PLA-CS blends is most likely due to poor compatibility between PLA and CS. Figure 12.5. also demonstrates the effect of radiation on the tensile strength and elongation at break of the blends. At high starch content, radiation showed slight effects on both the tensile strength and elongation at break of the blends. At low starch content, the effects of radiation became more evident. For P90 T3 samples, both the tensile strength and elongation at break initially increased with dose, but started to drop off after 40 kGy. This can be explained from the fact that at low doses, crosslinking is dominant, while at high doses, intensive chain scissions lead to dominance of degradation over crosslinking.

12.4.3. PLA-CS blends (with the compatibilizer)

PLA-g-CS was synthesized in large scale and used as the compatibilizer for blending PLA with CS. Due to the difficulties and complications of the multi-step synthesis of PLA-g-CS, the amount of synthesized PLA-g-CS was not enough to be used as the compatibilizer for all ratios of PLA:TPS (90:10, 80:20 and 70:30). Therefore, the ratio of PLA:TPS at 80:20 was chosen, based on the ratio of PLA-g-CS:TPS which is similar to that of samples studied in previous works [12.4, 12.15]. To study the effect of the amount of the compatibilizer on the properties of the blends, two concentrations of PLA-g-CS were used; 3 and 5 phr. The composition of the blends is detailed in Table 12.1.

Tensile and elongation at break of the blends with the compatibilizer, along with those of pure PLA sample and the blends with the same ratio of PLA:TPS (80:20) but without the compatibilizer are shown in Figure 12.7.

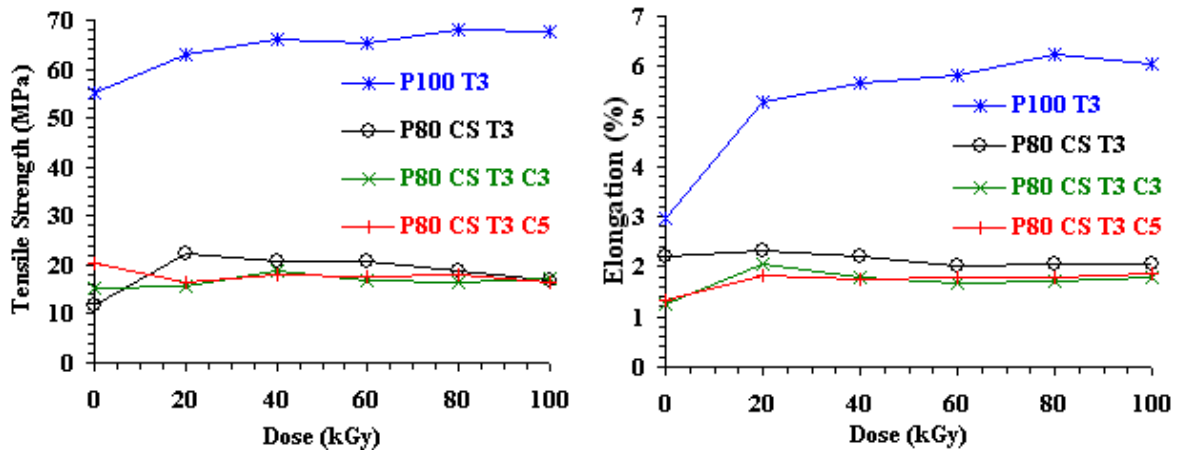

FIG. 12.7. Tensile strength (left) and elongation at break (right) of PLA-CS blends (with compatibilizer) irradiated at different doses.

The results showed that the compatibilizer did not help improve the mechanical properties of the blends. Tensile of the blends with the compatibilizer was a little better than that of the blend without the compatibilizer, but was lower after irradiation. Elongation at break of the blends with the compatibilizer was lower than that of the blend without the compatibilizer, both before and after irradiation. The drop in mechanical properties of PLA-CS blends with the compatibilizer may stem from the fact that the grafting rate of PLA-g-CS was relatively low, when compared with those reported in previous work [12.15], whose maximum grafting rate was as high as 64%. This low grafting efficiency along with low concentration of PLA-g-CS used (3 and 5 phr) may not be enough to induce good interfacial adhesion between PLA and CS.

12.4.4. Characterization of MS (CS modified by PMMA by admicellar polymerization)

Chemical characterization of MS was done using FTIR. The result was shown in Figure 12.8, in comparison with FTIR spectra of CS and PMMA. The FTIR spectrum of PMMA shows a strong, characteristic peak at 1722 cm^{-1} corresponding to C=O stretching in ester. FITR spectrum of MS shows similar peak commonly found in that of CS, with an additional peak at 1726 cm^{-1}, hence confirming the presence of PMMA in MS.

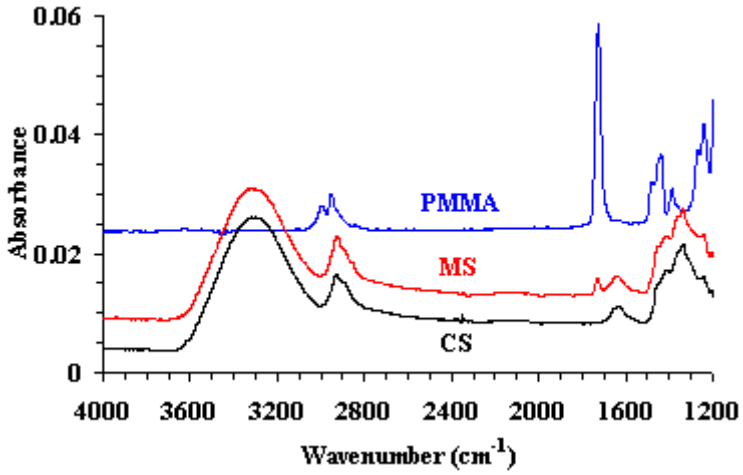

FIG. 12.8. FTIR spectra of CS, MS and PMMA.

After the synthesis, hydrophobicity of CS and MS was examined and compared by a floating test. The results are shown in Figure 12.9.

FIG. 12.9. Flotation test of CS (left) and MS (right).

MS was able to float on the water surface for a while, wherears CS immediately sank to the bottom of the beaker when they were placed on the water surface. Obviously, the results showed that MS is more hydrophobic than CS, thus confirming the film formation of PMMA on starch surface. In order to confirm the modification of starch surface, iodine test was performed. Iodine solution is well known to react with starch, resulting in a purple black color. The color can be detected visually. The results are shown in Figure 12.10. Obviously, CS reacted with iodine solution, yielding purple black color. However, the intensity of the color was much less in MS. These results clearly sybstantiated the modification of starch surface.

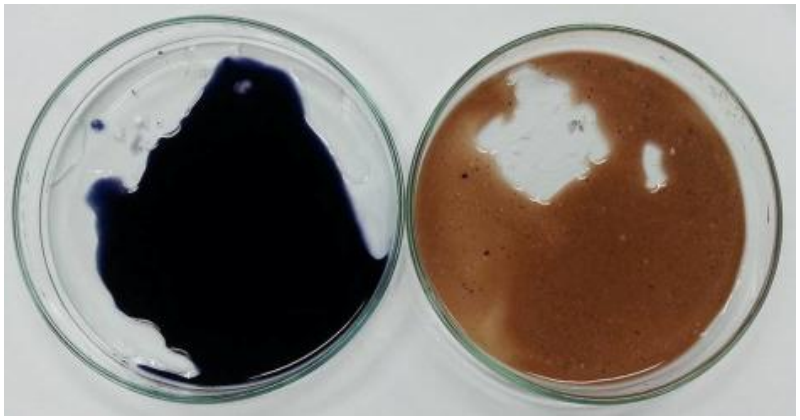

FIG. 12.10. Iodine test of CS (left) and MS (right).

SEM was used to compare the surface morphology of CS and MS. Figure 12.11. shows relatively smooth surface of CS and displays comparatively rough surface of MS, confirming the modification of starch surface.

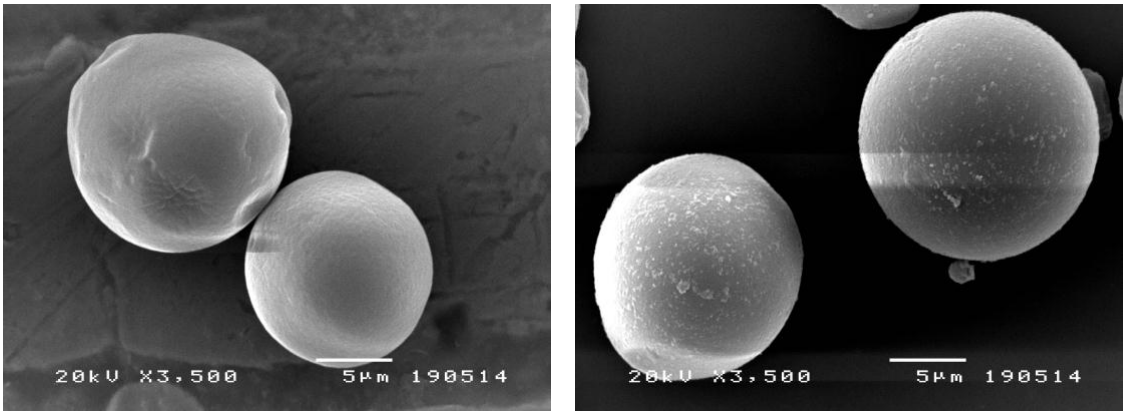

FIG. 12.11. SEM images of CS (left) and MS (right).

12.4.5. PLA-MS blends

The mechanical properties of PLA-MS blends are shown in Figure 12.12. Tensile strength of PLA-MS blends also decreased with increasing TPS content. Nevertheless, unlike PLA-CS blends, PLA-MS blends did not show drastic decrease of mechanical properties, but rather displayed gradual decline. Before irradiation, the tensile strength of the blends with 0, 10, 20 and 30% of starch content was about 55, 47, 34 and 26 MPa, respectively. At the same TPS content, they are much better than those of PLA-CS blends, both with (Figure 12.7) and without the compatibilizer (Figure 12.6). The tensile strength of the PLA-CS blends (without compatibilizer) with 0, 10, 20 and 30% of starch content was about 55, 23, 12 and 10 MPa, in that order. Elongation at break data offer interesting results. For unirradiated samples and samples irradiated at 20 and 40kGy, elongation at break of each PLA-MS blend is even higher than that of pure PLA sample. These results simply imply improved compatibility between PLA and MS. This can be explained from the fact that PLA is generally brittle,

while TPS is usually more flexible. The improved compatibility between PLA and MS makes it possible for PLA matrix to transfer stress formed during mechanical tests to dispersed phase of MS, thus leading to higher elongation of the PLA-MS blends.

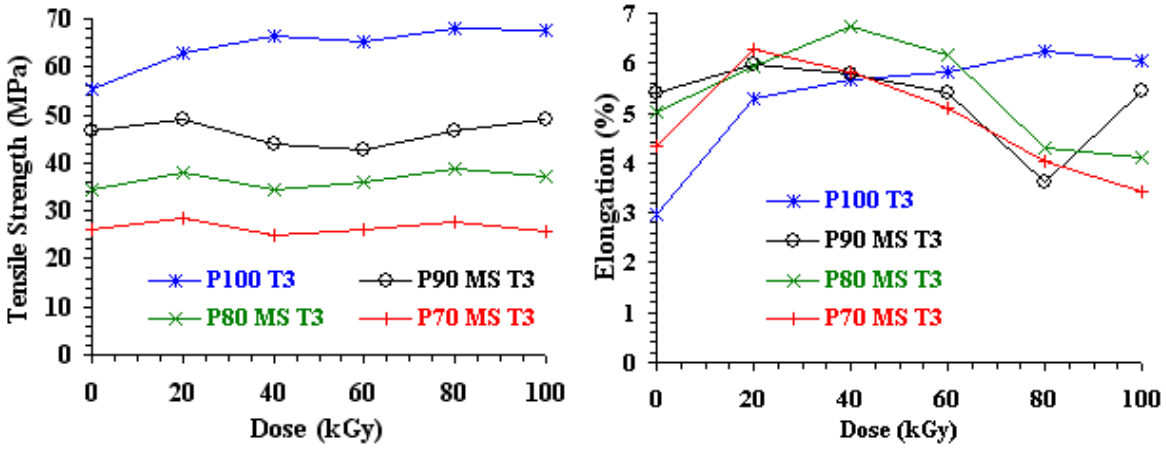

FIG. 12.12. Tensile strength (left) and elongation at break (right) of PLA-MS blends irradiated at different doses.

SEM was used to compare the surface morphology of PLA sample, PLA-CS and PLA-MS blends with PLA:TPS ratio at 70:30.

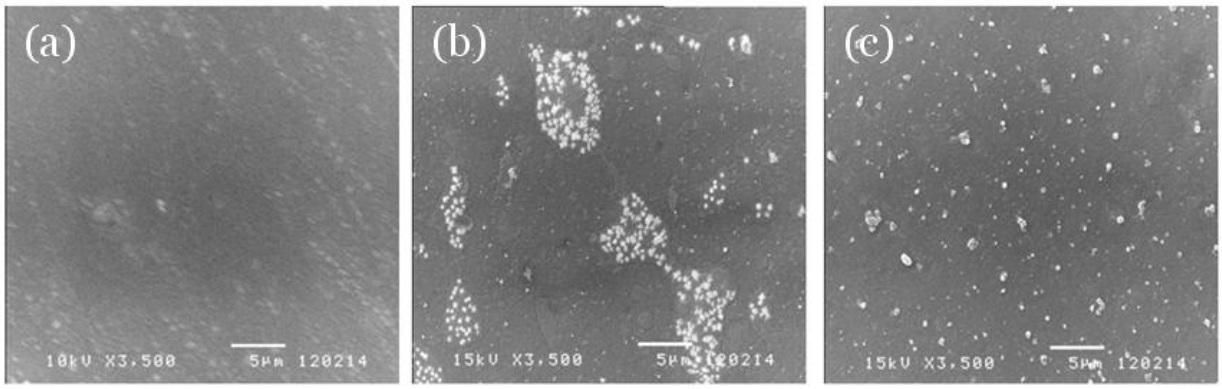

FIG. 12.13. SEM images of (a) PLA pure sample (P100 T3), (b) PLA-CS blend (P70 CS T3) and (c) PLA-MS blend (P70 MS T3).

Figure 12.13a shows relatively smooth surface of PLA sample. Figure 12.13b and 12.13c display distribution of CS and MS inside PLA matrix, respectively. Starch particles in PLA-CS blend obviously accumulated into big groups, resulting in poor dispersion. This is simply due to the fact that the surface of starch is full of hydroxyl groups. These hydrophilic groups tend to have strong interactions, thus resulting in agglomerates. Unlike PLA-CS blend, PLA-MS blend displays less agglomerates, offering much better dispersion. This stems from the fact that the surface of MS is coated with PMMA which is thick with ester groups. These ester groups have less interaction with each other, hence resulting in less agglomeration.

These ester groups also are less hydrophilic and more compatible with the surface of PLA, thus leading to improved compatibility between PLA and MS.

12.5. CONCLUSION

PLA-g-CS was synthesized to be used as a compatibilizer for PLA and CS blends. However, the results showed that mechanical properties of PLA-CS blends, both with and without compatibilizer, drastically decreased with increasing starch content. The decline in mechanical properties of PLA-CS blends with the compatibilizer may be due to low grafting rate of PLA-g-CS. Moreover, the multi-step synthesis of PLA-g-CS was proved to be complicated, making it quite difficult for large-scale synthesis.

Admicellar polymerization was proposed as an alternative technique to modify starch surface with PMMA. Having ester groups, PMMA is highly compatible with PLA. The characterization proved that MS (PMMA-modified starch) was successfully prepared by admicellar polymerization. This technique is much simpler and less complex, while offering scale up capability.

Tensile strength of PLA-MS blends also decreased with increasing TPS content. However, unlike PLA-CS blends, PLA-MS blends did not show drastic decrease of mechanical properties, but rather displayed gradual decline. At the same TPS content, mechanical properties of PLA-MS blends were much better than those of PLA-CS blends, both with and without compatibilizer. In comparision with PLA-CS blends, the results from both mechanical properties and SEM analysis confirmed the improved compatibility between PLA and MS, simply due to the presence of PMMA in MS which has excellent compatibility with PLA.

REFERENCES TO CHAPTER 12

[12.1] R. M. RASAL, A. V. JANORKAR, D. E. HIRT, Poly(lactic acid) modifications, Progress in Polymer Science 35 (2010) 338-356.

[12.2] H. XU, C. Q. TENG, M. H. YU, Improvements of thermal property and crystallization behavior of PLLA based mutiblock copolymer by forming stereocomplex with PDLA oligomer, Polymer 47 (2006) 3922-3928.

[12.3] M. SHIBATA, N. TERAMOTO, Y. INOUE, Mechanical properties, morphologies, and crystallization behavior of plasticized poly(L-lactide)/poly(butylenes succinate-co-L-lactate) blends, Polymer 48 (2007) 2768-2777.

[12.4] L. CHEN, X. QIU, M. DENG, Z. HONG, R. LUO, X. CHEN, X. JING, The starch grafted poly(L-lactide) and they physical properties of its bleding composites, Polymer 46 (2005) 5723-5729.

[12.5] M. C. GUPTA, V. G. DESHMUKH, Radiation effects on poly(lactic acid), Polymer 24 (1983) 827-830.

[12.6] T. M. QUYNH, H. MITOMO, N. NAGASAWA, Y. WADA, F. YOSHIL, M. TAMADA, Properties of crosslinked polylactides (PLLA & PDLA) by radiation and its biodegradability, European Polymer Journal 43 (2007) 1779-1785.

[12.7] N. NAGASAWA, A. KANEDA, S. KANAZAWA, T. YAGI, H. MITOMO, F. YOSHII, M. TAMADA, Application of poly(lactic acid) modified by radiation crosslinking, Nuclear Instruments and Methods in Physics Research B 236 (2005) 611-616.
[12.8] H. MITOMO, A. KANEDA, T. M. QUYNH, N. NAGASAWA, F. YOSHII, Improvement of heat stability of poly(L-lactic acid) by radiation-induced crosslinking, Polymer 46 (2005) 4695-4703.
[12.9] P. RYTLEWSKI, R. MALINOWSKI, K. MAROCZEWSKI, M. ZENKIEWICZ, Influence of some crosslinking agents on thermal and mechanical properties of electron beam irradiated polylactide, Radiation Physics and Chemistry 79 (2010) 1052-1057.
[12.10] J. WU, J. H. HARWELL, E. A. O'REAR, Two-dimensional solvents: Kinetics of styrene polymerization in admicelles at or near saturation, Journal of Physical Chemistry 91 (1987) 623-634.
[12.11] P. M. KARLSSON, N. B. ESBJORNSSON, K. HOLMBERG, Admicellar polymerization of methyl methacrylate on aluminum pigments, Journal of Colloid and Interface Science 337 (2009) 364-368.
[12.12] Y. ZHAO, J. QIU, H. FENG, M. ZHANG, L. LEI, X. WU, Improvement of tensile and thermal properties of poly(lactic acid) composites with admicellar-treated rice straw fiber, Chemical Engineering Journal 173 (2011) 659-666.
[12.13] T. PONGPRAYOON, N. YANUMET, S. SANGTHONG, Surface behavior and film formation analysis of sisal fiber coated by poly(methyl methacrylate) ultrathin film, Colloids and Surfaces A: Physicochem. Eng. Aspects 320 (2008) 130-137.
[12.14] L. LEI, J. QIU, E. SAKAI, Preparing conductive poly(lactic acid) with poly(methyl methacrylate) (PMMA) functionalized graphene (PFG) by admicellar polymerization, Chemical Engineering Journal 209 (2012) 20-27.
[12.15] L. CHEN, X. QIU, Z. XIE, Z. HONG, J. SUN, X. CHEN, X. JING, Poly(L-lactide)/starch blends compatibilized with poly(L-lactide)-g-starch copolymer, Carbohydrate Polymers 65 (2006) 75-80.

Chapter 13

RADIATION-INDUCED MODIFICATION OF NANOCLAY AND POLYMER FOR ENHANCING MUTUAL COMPATIBILTY FOR THE PREPARATION OF NANOCOMPOSITES AND PREPARATION OF POLYMER/NANOMETAL COMPOSITES

O. GÜVEN, F. ZENGIN, T. ÇAĞLAYAN, A. BAKAR,
Department of Chemistry,
Hacettepe University,
Turkey

Abstract

Polymer/clay nanocomposites are new generation materials that bring significant changes in mechanical, thermal and permeation properties of base polymers by low clay loading. In this study, polypropylene/montmorillonite (PP/MMT) and poly(ethylene-co-vinylacetate) / montmorillonite (EVA/MMT) nanocomposites were prepared by melt intercalation method by using batch type mixer. Radiation degraded and oxidized polypropylene granules were used as compatibilizer and unmodified clay (Na^+ montmorillonite, MMT) as the filler. 10 kGy was determined to be the most suitable irradiation dose for the best compatibilizing effect. Radiation degraded (chain scissioned and oxidized) PP has been found to show very good compatibilizing effect for the natural montmorillonite/polypropylene composites. Polymer/clay nanocomposites were also prepared by melt intercalation of pristine poly(ethylene-co-vinyl acetate) (EVA 18) and clay modified by in-situ radiation polymerization of a charged monomer. Monomer polymerized in between the silicate layers caused a separation allowing the diffusion of EVA chains forming intercalated strautures. Structures of nanocomposites were characterized by ATR-FTIR, TEM (Transmission Electron Microscopy), XRD (X-Ray Diffraction) and PALS (Positron Annihilation Lifetime Spectroscopy). Tensile tests made on nanocomposites showed improvement in the range of 25-50% in elastic modulus compared to neat polymer.

13.1. INTRODUCTION

The addition of nanoclays to a polymer matrix has been proven to bring large improvement in the mechanical properties, thermal stability, fire resistance, gas barrier properties of starting polymeric materials [13.1]. Heat distortion temperature of Nylon6 has been shown to be increased from 60 ^oC to 150 ^oC with the addition of a few weight percent of montmorillonite [13.2]. Modest addition of clay provided substantial increases in tensile strength, tensile modulus and storage modulus with almost no decrease in impact resistance. Polymer/clay composites based on layered silicates are generally classified into three types depending on the extent of separation of silicate layers and interspersing of polymer chains. These are conventional composites, intercalated nanocomposites and exfoliated nanocomposites. If the clay layers are completely separated from each other to create a disordered array with polymer chains entering into galleries, the composite is said to be exfoliated. The extent of dispersion of clay in polymer matrix depends on the properties of polymer and clay, interactions between polymer, clay, and modifying agents, processing conditions. The significant improvement in mechanical properties of Nylon6/clay nanocomposites was explained to be due to the presence of an exceptionally high interfacial surface area generated by exfoliation and to the formation of ionic and/or hydrogen bonding between the organic polymer and inorganic silicate. When polymer and clay are used without being modified however, the interaction and dispersion becomes less likely due to the incompatibility of the two. The preparation of fully exfoliated polymer/clay nanocomposites therefore depends on

the successful modification of polymer and/or clay to make them compatible[13.3]. The inorganic and hydrophilic nature of clay layers can be modified by exchanging of cations in the galleries by quaternary ammonium compounds whereas organic and fully hydrophobic nature of polymers such as PE, PP can be modified by grafting of these polymers with suitable monomers such as maleic anhydride.

Polymers and clay are not generally fully interspersed to form nanocomposites and modification of either the clay or the polymer is mostly necessary. Montmorillonite (MMT), frequently used clay for example in polymer/clay nanocomposites is modified by quaternary ammonium compounds to make an intercalated nanocomposite exfoliate. Clays are generally modified by cation exchange. As for the modification of polymers, grafting of maleic anhydride onto PE or PP enhances the compatibility of these fully hydrophobic polymers with unmodified clay[13.4]. In either approach the main goal is to increase the dispersion of polymer chains within the layered structure of silicates.

In this work for the preparation of Polypropylene/MMT nanocomposites, radiation degraded/oxidized PP has been used as the compatibilizer between the PP matrix and unmodified MMT. The level of chain scission and oxidation induced in PP can be controlled by gamma irradiation in air of PP granules to optimize the formulations for improving the mechanical properties of a ternary mixture of PP/γ-PP/MMT. In this approach host polymer itself was aimed to be modified by ionizing radiation to enhance compatibility by lowering molecular weight of the pristine polymer as well as its surface oxidation. A different approach has been considered for the preparation of poly(ethylene-co-vinyl acetate)(EVA)/clay nanocomposites by radiation-induced polymerization of a charged monomer [2-(Methacryloloxy)ethyl]-trimethyl ammonium chloride absorbed inside the galleries of montmorillinite thus making the clay more compatible for further mixing with the EVA copolymer. The improvement in mechanical properties has been followed by mechanical tests and newly acquired properties were explained by structural analysis of nanocomposites by employing Small Angle X-Ray Scattering (SAXS), Transmision Electron Microscopy (TEM), Positron Annihilation Lifetime Spectroscopy (PALS), X-Ray Diffraction (XRD) and Differential Scanning Calorimetry (DSC) techniques.

Metal-polymer nanocomposites (materials based on metallic nanoparticles embedded in polymeric matrices) attracted considerable interest in recent years due to their unique and tunable functional properties, including specific catalytic activity, sensor properties, and optical, magnetic and other characteristics. Common approaches to the synthesis and investigation of such materials have been reviewed in a number of monographs [13.5, 13.6]. The most convenient route to the fabrication of metal nanoparticle embedded polymer thin films involves in-situ generation of the nanoparticles through reduction or decomposition of appropriate precursors inside the polymer film. Among the most convenient precursors of nanoparticles for such techniques are metal cations, which can be reduced by chemical, electrochemical, photochemical and *radiation-induced chemical* methods. The latter method makes it possible to reduce a wide variety of metal ions in aqueous solutions, polymer matrices and heterogeneous systems, because it is basically free of limitations resulting from reduction potentials of non-noble ions, limited diffusion of reducing reagent molecules, optical absorption properties of ions and some other factors, which often present problems for other methods. From physical and technical points of view, the radiation-induced processes are characterized by potential tuning ability (using variations in radiation parameters, i.e., type of radiation, energy, dose rate and total dose) and easy operational control of the process, which is impossible in chemical procedure. From the chemical point of view, the

radiation-induced reduction in aqueous media and swollen polymer matrices exploits unique properties of hydrated electron (e_{aq}) characterized by high reduction potential, high diffusion coefficient and absence of additional reaction products (commonly occurring in chemical reduction). The radiation-chemical method has thus been proven to be a promising tool to obtain various-type metal nanoparticles in polymer matrices starting from properly organized precursor systems. Among various metal ions studied so far by not only radiation but also other techniques it has been observed that copper presents a special case being not so stable against oxidation in nanosize. The main aim of this work is to investigate different polymer matrices in binary and ternary combinations in the presence of copper ions to control size, distribution and oxidative stability of metallic copper nanoparticles. The polymers selected are poly(acrylic acid), poly(allyl amin) due to their inherent characteristics in forming complexes with copper ions in aqueous solutions. To see the effect of type of ionizing radiation and dose rate, gamma irradiation and X-rays are used in the experiments.

13.2. EXPERIMENTAL PART

13.2.1. Materials

As polymeric matrix polypropylene with two different melt flow rates were used namely, PETOPLEN MH 418 and PETOPLEN EH 102 from PETKIM company, Turkey, with MFIs 4-6 g/10 min and 9-13 g/10 min respectively both measured at 2.16 kg/230^{o}C conditions. Poly(ethylene-co-vinyl acetate), containing 18% wt. vinyl acetate (EVA18) was obtained from Innospec Active Chemical, England, with melt flow index (MFI) 12.415±0.045 g/10 min. measured at 2.16 kg/190°C conditions. Unmodified Na-montmorillonite (Na-MMT), with a cation exchange capacity (CEC) value of about 145 meq/100g, was obtained from Nanomer/PGV Company. Clay modifying monomer [2-(Methacryloyloxy) ethyl]-trimethyl amonium chloride, with concentration 80% wt. was obtained from Sigma Aldrich.

13.2.2. Preparation of nanocomposites

Finely ground PP granules were irradiated in air in a GammaCell 220 ^{60}Co gamma irradiator at a dose rate of 0.08 kGy/h to three different total absorbed doses of 5, 10 and 20 kGy. By irradiating in air, PP was simultaneously oxidized and extensively chain scissioned which was determined by measuring the melt flow rate. PP/Clay/compatibilizer ternary systems were thus prepared by using 20% by weight compatibilizer gamma irradiated PP(γ-PP), 1-5% clay and pristine PP to make up the total 100 by using a torque rheometer.

The modified clays were prepared by cation exchange reaction between Na-MMT and [2-(Methacryloyloxy) ethyl]-trimethyl ammonium chloride in aqueous solution. The aqueous suspension solution containing 20 g Na-MMT and 16 ml [2-(Methacryloyloxy) ethyl]-trimethyl amonium chloride was prepared in 100 ml of distilled water. The suspension was stirred at 25°C for 24 h and nitrogen gas was passed from this solution for 5 min. Then this solution was irradiated to 10 kGy to induce radiation polymerization of monomer inside the clay particles. The modified clay was washed and filtered with distilled water to remove polymers which formed outside the clay particles. Then the product was dried in vacuum oven at 60°C for 24h.

13.2.3. Characterization of properties

The most important property to be investigated to see the effect of modes of preparation of ternary blends is their mechanical properties. Stress-strain tests were carried out by using a universal mechanical testing device, ZWICK Z010 following the ASTM D638 standard.

The oxidation of PP granules either due to irradiation or ozonation was determined by using a Nicolet iS10 Diamond ATR-FTIR spectrometer.

The Melt Flow Rates of original and irradiated and ozon treated PP samples were measured by using CEAST Modular Melt Flow Rate apparatus at 190 ^{o}C and 2.16 kg operational conditions.

XRD patterns were obtained by using a Japanese Rigaku D/Max-2200/PC X-ray diffractometer equipped with graphite mono-chromatized CuKα radiation (λ =0. 15406 nm). The scanning range was 2°-15° with a scanning rate of 2°/min.

The microstructures of nanocomposites were imaged using a Tecnai G2 F30 (300 kV) Transmission Electron Microscopy (TEM). The samples for TEM were cut to 200 nm thick sections with a diamond knife microtome (Leica Microsystems, Model EMUC6 + EMFC6).

13.2.4. Preparation of polymer/metal nanocopper composites

Polymer/metal ion double complex was prepared from the aqueous solutions of 0.3 M PAlAm and 0.15 M $CuSO_4.5H_2O$ by adding a few drops of formic acid to reduce pH of the solution to 4.32. Physical appearance of double complex solution is homogeneous. Molarity of polymer solutions is based on the concentration of repeating units.
To prepare polymer/metal ion triple complex, first 0.3 M PAlAm and 0.3 M PAA solutions were mixed in equimolar ratio to prepare stoichiometric inter polyelectrolyte complex (IPEC). In order to prevent the formation of large complex agglomerates, formic acid is used as a shielding solvent and pH is reduced to 3.2. Then, IPEC was mixed with 0.15 M $CuSO_4.5H_2O$ which formed a suspension with a pH of 3.55.
After addition of ethanol (10% by volume), double and triple systems were bubbled with pure argon and irradiated with X-rays using a 5-BKhV-6(W) tube with a tungsten anode (30 kV, 70 mA). The solutions and suspensions were irradiated in plastic cells with wall thickness of ca. 5 mm. The estimated total absorbed dose was ca. 140 kGy after 2 hours of irradiation.

13.3. RESULTS AND DISCUSSION

13.3.1. PP/MMT nanocomposites

Polyolefines and clay are not fully interspersed to form nanocomposites and modification of either the clay or the polymer is mostly necessary. Montmorillonite (MMT), frequently used clay for example in polymer/clay nanocomposites is modified by quaternary ammonium compounds to make an intercalated nanocomposite exfoliate. Clays are generally modified by cation exchange. As for the modification of polymers, PE or PP grafted with maleic anhydride enhances the compatibility of these fully hydrophobic polymers with unmodified clay. In either approach the main goal is to increase the dispersion of polymer chains within the layered structure of silicates to form exfoliated layers providing maximum interaction of the polymer with the silicate layers shown below.

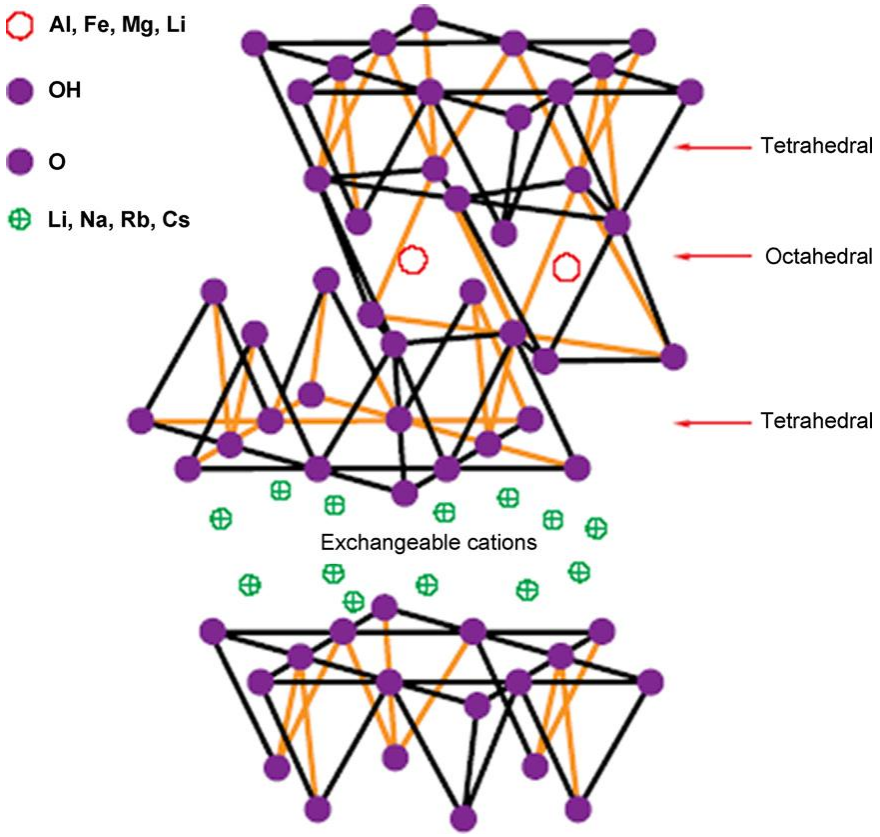

The success of preparing polyolefin/clay nanocomposites relies totally on the extent of insertion of polymer chains into layer occupied by the exchangeable cations. Organo-modified clays are generally prepared by replacing exchangeable cations (Na^+ or K^+) by quaternized alkyl ammonium salts, phosphonium salts, etc. [13.7].

Ternary blends of PP/clay/g-PP were prepared by using PP MH418, natural montmorillonite and gamma-irradiated polypropylene. Fine PP granules irradiated to 5, 10 and 20 kGy doses were used as compatibilizer. PP nanocomposite sheets were prepared from ternary blends obtained in a double screw extruder for mechanical tests. The evaluation of stress-strain curves yielded the major mechanical properties such as elastic modulus, tensile strength and elongation at break. E-modulus and tensile strength values for the ternary blends prepared by using 10 kGy irradiated PP show the best results, hence 10 kGy has been considered as the optimum dose in the preparation of ternary blends. Next step is to compare the mechanical properties of these blends with PP nanocomposites to be prepared using maleic acid grafted PP. Figs. 13.1-13.3. compares the mechanical properties of three different PP nanocomposites.

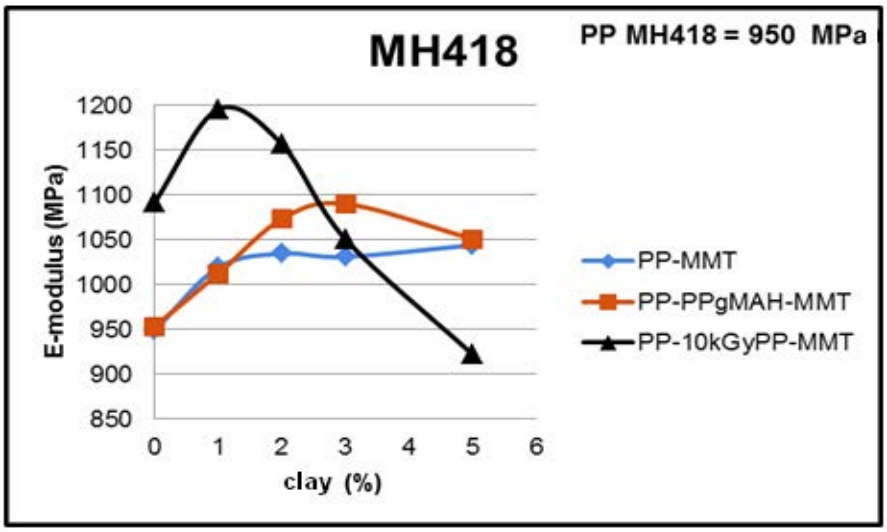

FIG. 13.1. E-modulus values for three different PP nanocomposites

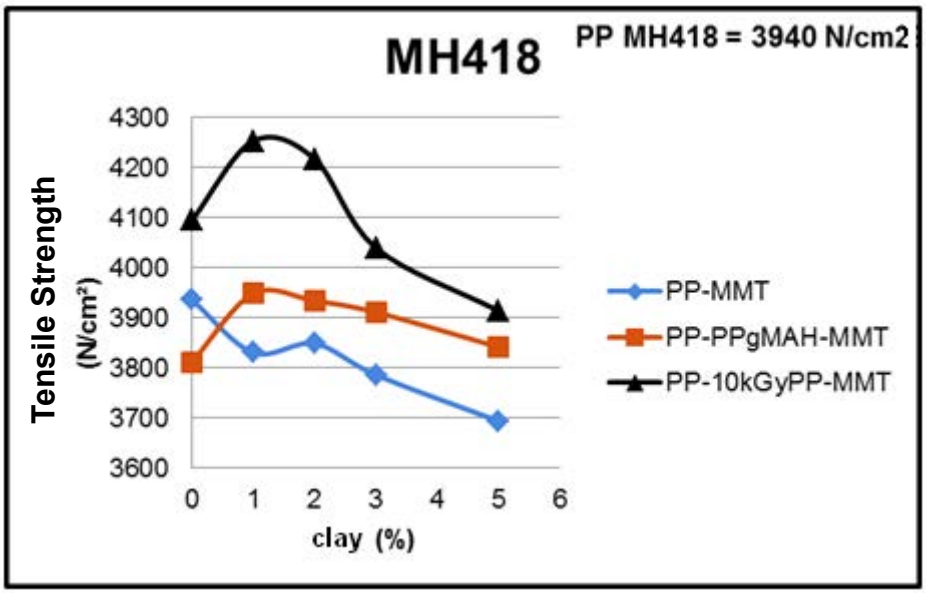

FIG. 13.2. Tensile strength values for three different PP nanocomposites

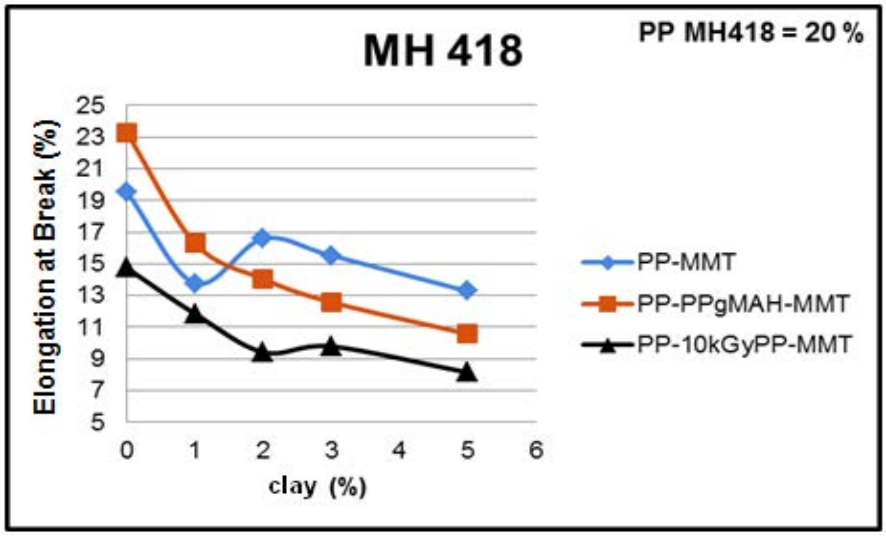

FIG. 13.3. Elongation at Break values for three different PP nanocomposites

These three diferent PP nanocomposites were prepared by using the pristine PP as the major ingredient, clay in 1-5 % varying compositions. One sample was prepared without compatibilizer (PP-MMT), the second one by using Maleic Anhydride grafted PP (PP-MAH) and the third one by using 10 kGy irradiated PP. As it is clearly seen from Figs. 13.1. and 13.2. the best results were obtained when 10 kGy irradiated PP was used as the compatibilizer. Nanocomposites prepared by using 1% clay show significant improvement in their E-modulus and Tensile strengths. The elongation at break values, Fig. 13.3., however were found to be inferior which is an expected result considering the inverse relation between the modulus and elongation.

13.3.2. EVA/MMT Nanocomposites

Unmodified MMT was interacted with a charged monomer [2-(Methacryloloxy) ethyl]-trimethyl amonium chloride in presence of water and through ion exchange reaction monomer filled the space between the silicate layers. Later, this mixture was irradiated 10 kGy, 20 kGy, 30 kGy for in-situ polymerization of the monomer. The formation of polymer inside the MMT silicate layers has been followed gravimetrically and found that 7.2, 7.7. and 8.1 g polymer formed in 20 g clay after 10, 20 and 30 kGy irradiation which corresponds to 36, 39, and 41% polymer loading respectively.

Binary blends of EVA18/clay were prepared by using EVA 18, and natural montmorillonite, the same modified by 10, 20, 30 kGy irradiation in the presence of the charged monomer and two commercial organo-modified clays I31PS and I44P. The evaluation of stress-strain curves yielded the major mechanical properties such as elastic modulus, tensile strength and elongation at break. The Figures 13.4.-13.6. show the changes in these mechanical properties as a function of clay composition in the range of 1-5%. All the EVA18/clay nanocomposites exhibited some improvement in both E-Modulus and tensile strength. E-Modulus and tensile strength values for EVA18/30 kGy composite samples show better results than EVA18/10 kGy, EVA18/20 kGy, EVA18/I44P and EVA18/Na-MMT composite samples. When compared with EVA18/I31PS, similar results were obtained for EVA18/30 kGy irradiated modified clay. E-Modulus and tensile strength values of composite samples increased with

increasing clay content. The elongation at break values for composite samples were found to be inferior which is an expected result considering the inverse relation between the modulus and elongation. The elongation at break values for composite samples decreased with decreasing clay content. Clay is modified to obtain organophilic structure. Thus, distance between layers increase and the interaction between polymer and clay increases. Intercalated and exfoliated nanocomposites are obtained by using modified clays. Intercalated and exfoliated structures give better results compared to the microcomposites. The results show that observed improvements in the mechanical properties are due to the presence of both intercalated and exfoliated structures.

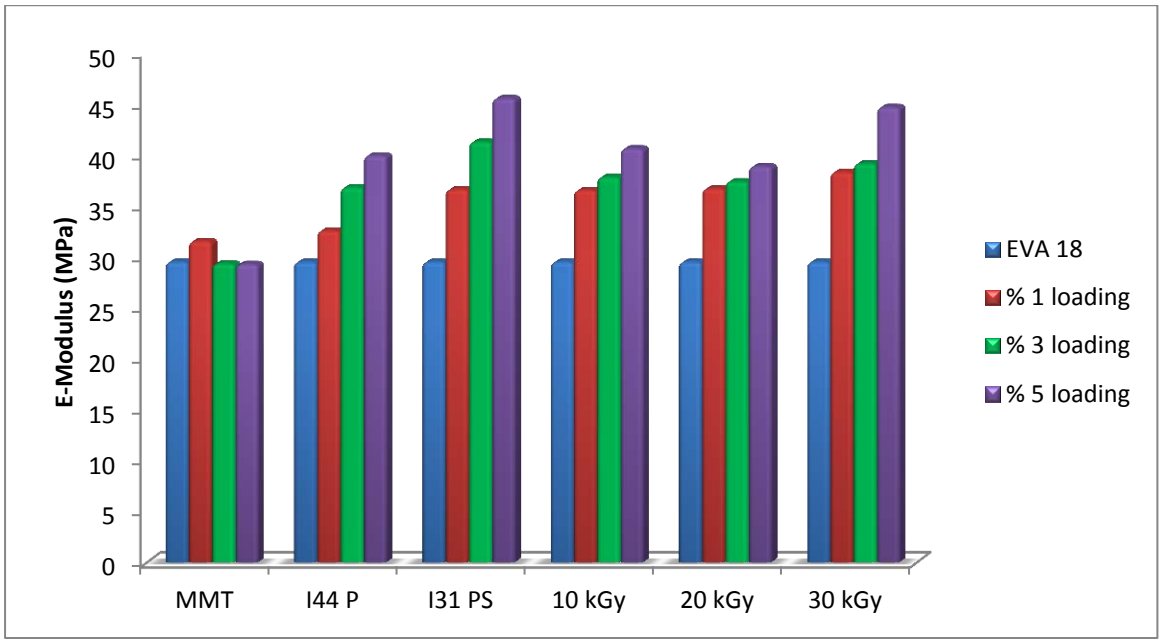

FIG 13.4. Change of E-Modulus of EVA18/clay nanocomposites loaded with different clays.

In Figs 13.4.-13.6. the abbreviations used as 144P and 131PS refer to two commercially available organo-modified MMTs used in the preparation of EVA nanocomposites.

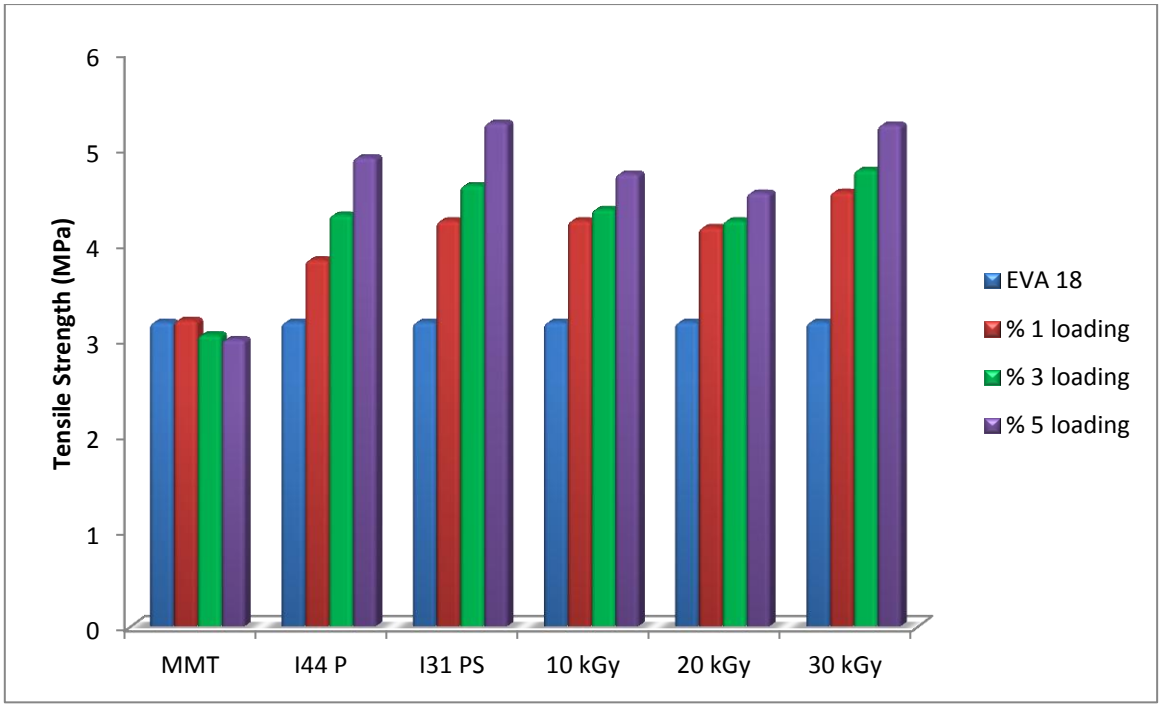

FIG.13.5. Change of Tensile Strength values of EVA18/clay nanocomposites with different type and amount of clay loading.

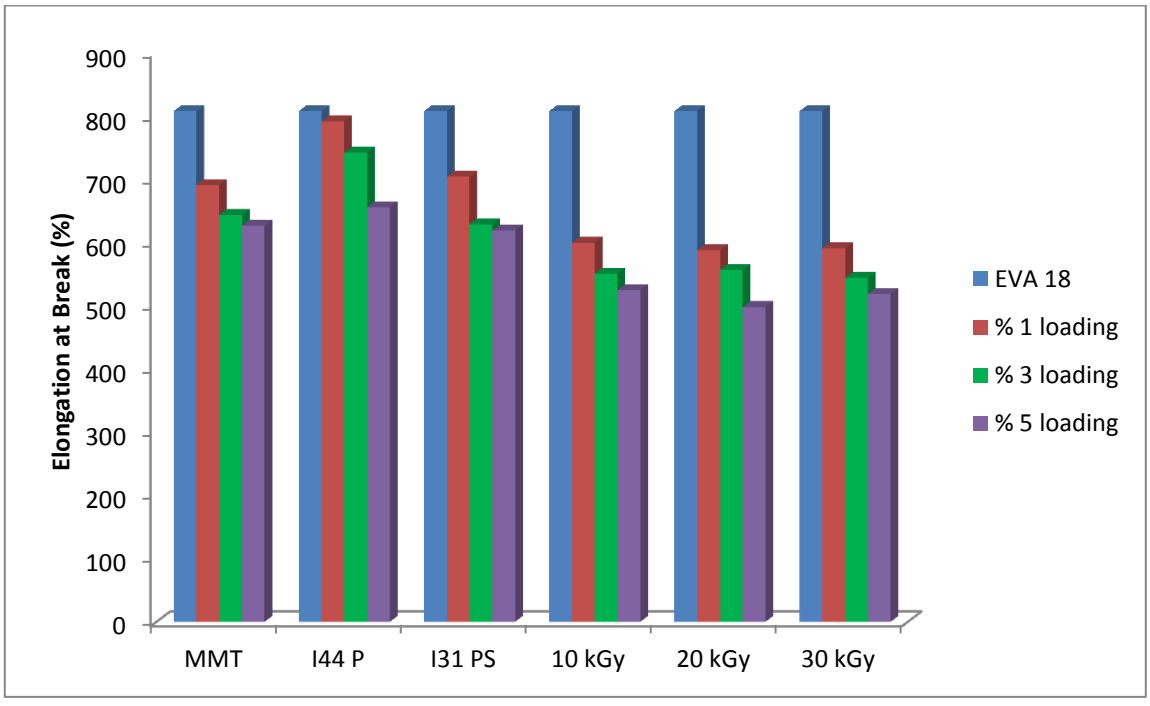

FIG. 13.6. Change of Elongation at Break values of EVA18/clay nanocomposites.

Every nanocomposite sample was analyzed by X-Ray Diffraction (XRD) in order to investigate whether intercalation and/or exfoliation occur. The distance between layers of the modified and unmodified clays and composite samples were calculated from Bragg's equation and are given in Table 13.1. below. Figure 13.7. shows the X-ray diffraction (XRD) pattern of Na-MMT and 10, 20 and 30 kGy modified clays. For 10, 20 and 30 kGy modified

clays; there are intense peaks at 4.38, 4.18 and 3.84° respectively, which are shifted from the diffraction peak of the Na-MMT at 6.98°. This confirms that polymer, which was obtained from charged monomer by irradiation, intercalated into the layers of the clay and increased the distance between layers.

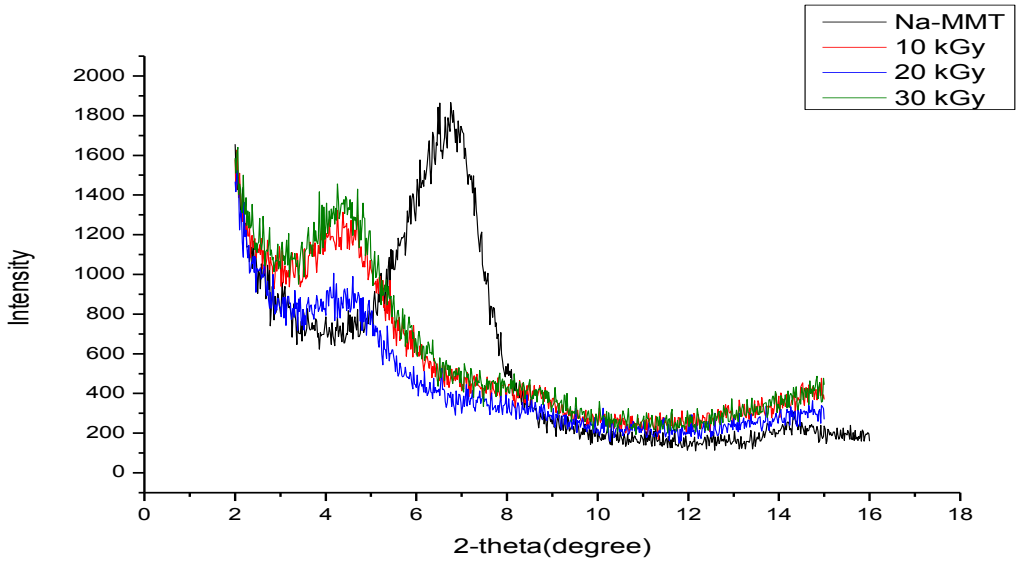

FIG. 13.7. X-ray diffraction (XRD) pattern of Na-MMT and 10, 20 and 30 kGy modified clays.

TABLE 13.1. VALUES OF DISTANCE BETWEEN LAYERS OF THE CLAYS AND COMPOSITE SAMPLES

	MMT	I44 P	I31 PS	10 kGy	20 kGy	30 kGy
$d_{spacing}$	1,27 nm	2,54 nm	2,10 nm	2,01 nm	2,11 nm	2,29 nm
	EVA 18-MMT	EVA 18-I44 P	EVA 18-I31 PS	EVA 18-10 kGy	EVA 18-20 kGy	EVA 18-30 kGy
%1 $d_{spacing}$	1,28 nm	3,48 nm	3,11 nm	2,35 nm	3,03 nm	3,18 nm
%3 $d_{spacing}$	1,32 nm	3,30 nm	3,48 nm	3,11 nm	3,45 nm	-------
%5 $d_{spacing}$	1,31 nm	2,98 nm	3,49 nm	3,50 nm	-------	-------

Polymer-Nanometal Composites

In this work, we prepared double polymer/metal ion complex system from the solution of PAlAm-Cu(II) and triple polymer/metal ion complex system from a mixture of solutions of PAlAm-PAA-Cu(II) and then irradiated in aqueous-alcohol mixture by X-rays at room temperature. PAlAm was used for the first time in this work as a chelating ligand which has a primary amin functional group in the side chain[13.8].

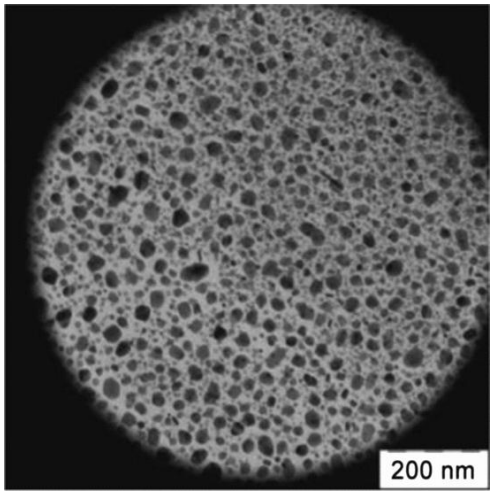

FIG. 13.8. TEM image of irradiated solution of double metal polymer complex (0.3 M PAlAm – 0.15 M Cu^{2}+, 10% ethanol (by volume), pH=4.32 , irradiation dose 140 kGy).

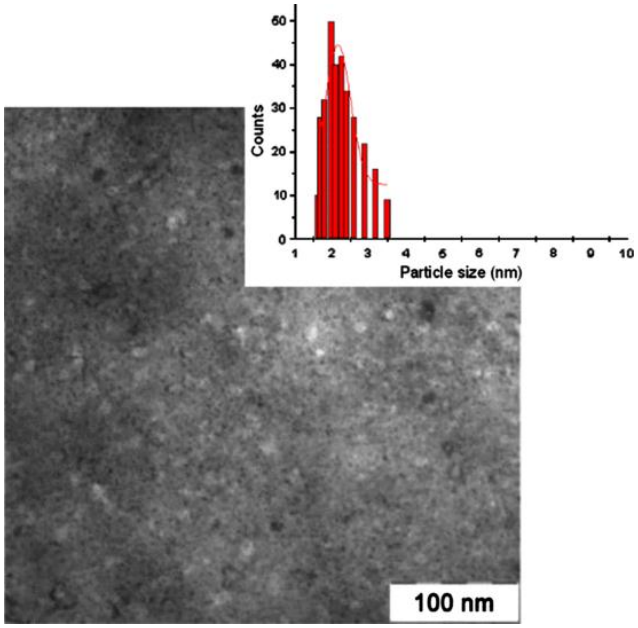

FIG. 13.9. TEM image and particle size distribution diagram of irradiated solution of triple metal polymer complex (0.3 M PAlAm – 0.3 M PAA-0.15 M $Cu^{2}Cu^{2+}$,+, 10% %10 ethanol (by volume), pH=3.55, pH = 3.55, irradiation dose 140 kGy).

For both double and triple systems irradiation leads to effective reduction of copper ions as evidenced by dramatic change in the sample color from blue to red and decay of absorption at 780 nm. TEM pictures taken from the double and triple complexes irradiated to 140 kGy are shown in Figs. 13.8. and 13.9, respectively. The TEM image obtained for double system, Fig. 13.8. demonstrates formation of both small and large nanoparticles.

Light blue color of copper sulphate solutions turned deeper blue upon forming binary and ternary complexes. Irradiation of these solutions turned them into deep copper red, indicating the transformation of copper ions into metallic copper, Fig. 13.10.

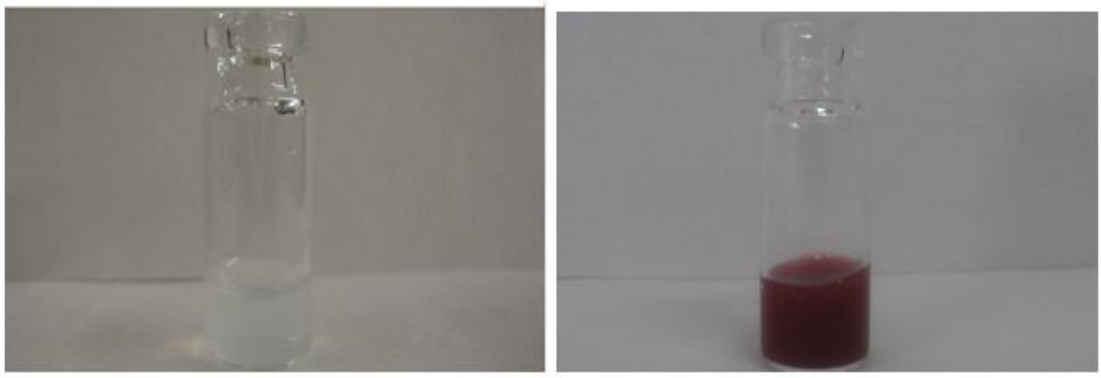

FIG. 13.10. Light blue color of PAlAm-Cu(II) complex on the left is turned into deep red indicating the conversion of Cu(II) into Cu^0

The solutions of 0.3 M PAlAm (M_W of 15,000) (based on concentration of repeating units), 0.3 M PAA (Mw=230,000) and 50wt.% of aqueous formic acid were poured into polystyrene petri dishes and dried at room temperature. Triple complex films were obtained by immersing into aqueous solution of 1.0 M $CuSO_4.5H_2O$ (Scheme 1). Films of triple systems in aqueous-alcohol mixture (10% ethanol) were bubbled with pure argon and irradiated with X-rays using a 5-BKhV-6(W) tube with a tungsten anode (30 kV, 70 mA) and Co-60 gamma source (1.44 kGy/h dose rate).

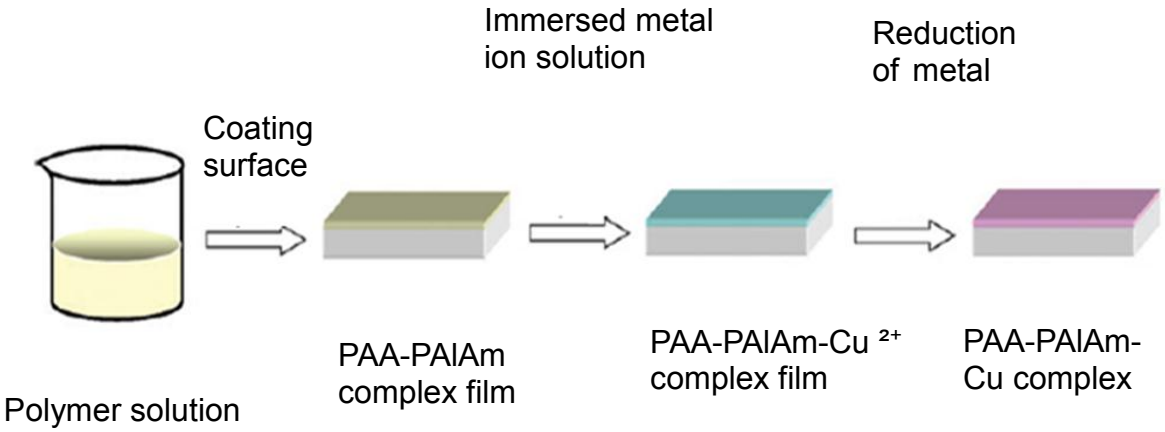

Scheme 13.1. Preparation of triple triple complex films

In this work, we prepared triple polymer/metal ion complex films from solutions of PAlAm-PAA-Cu(II) which were obtained by immersing preformed PAlAm-PAA films into aqueous solution of $CuSO_4.5H_2O$. Films were irradiated in aqueous-alcohol mixture by gamma and X-ray sources at room temperature. PAlAm was used for the first time in this work as a chelating ligand which has a primary amin functional group in the side chain. Complex formation leads to blue coloration of initially colorless interpolyelectrolyte complex (IPEC) films, as a result of incorporation of metal ions. This coloration of IPEC is a qualitative indicator of transformation of IPEC to triple interpolyelectrolyte complex. Triple interpolyelectrolyte complex irradiation by gamma and X-ray sources leads to effective

reduction of copper ions as evidenced by dramatic change in the sample color from blue to red, shown in Figure 13.11.

FIG. 13.11. Blue colored PAlAm-PAA-Cu(II) film (left) changes into deep metallic copper red (right) after irradiation.

REFERENCES TO CHAPTER 13

[13.1] PAVLIDOU, S., PAPASPYRIDES, C.D., A review on polymer-layered silicate nanocomposites, *Progress in Polymer Science*, 33(2008) 1119-1198.

[13.2] KATO, M., MATSUSHITA, M., FUKUMORI, K., Development of a new production method for a PP-Clay nanocomposite, *Polym. Eng. Scien*., 44(2004) 1205-1211.

[13.3] NGUYEN, Q.T., BAIRD, D.G., Preparation of polymer-clay nanocomposites and their properties, *Adv. Polym. Scien*., 25(2006) 770-785.

[13.4] RAY, S.S., OKAMOTO, M., Polymer/layered slicate nanocomğposites: a review from preparation to processing, *Progress in Polymer Science*, 28(2003) 1539-1641.

[13.5] NICOLAIS, L., (editor) 2004, Metal-Polymer Nanocomposites. NY: Wiley & Sons Inc.

[13.6] MAI, Y., YU Z., 2006, Polymer Nanocomposites. Woodhead Publishing.

[13.7] GAO, F., Clay/polymer composites: the story, *Materialstoday*, Nov(2004) 50-55.

[13.8] BAKAR, A., GÜVEN,O., ZEZIN, A.A., FELDMAN,V.I., Controlling the size and distribution of copper nanoparticles in double and triple polymer-metal complexes by X-ray irradiation, Rad. Phys. Chem., 94(2014)62-65.

Chapter 14

RADIOLYTIC SYNTHESIS OF MAGNETIC NANOCOMPOSITES

Radiation Curing of Composites for Enhancing their Features and Utility in Healthcare and Industry

M. AL-SHEIKHLY, A. BARKATT
Department of Materials Science and Engineering,
University of Maryland,
College Park, MD,
United States of America

Abstract

Magnetic nanocomposites, in which magnetic nanoparticles are encapsulated in polymeric matrices have important applications in medicine, imaging, electronics and mechanical devices. Radiation synthesis of ethyl hexyl acrylate (EHA) and acrylic acid (AA) copolymer-ferric ionomer, and approximately 20-nm Fe_3O_4 (magnetite) nanoparticles encapsulated in EHA-AA copolymer were obtained. The kinetics of copolymerization was measured using pulse radiolysis. Pulse radiolysis of 2-EHA shows that transient absorption at 330 nm, attributable to 2-EHA$^{\bullet}$ radicals, forms within 0.01 μs, probably due to reaction of trace amounts of water present in the 2-EHA with 2-EHA$^{-\bullet}$ radicals. The decay of the absorption over a time scale of $1 \cdot 10^{-8}$ to $1 \cdot 10^{-4}$ s follows second order kinetics with a gradually decreasing rate constant as the polymer radical grows in mass. At very short durations the rate constant reaches an upper limit of $(2.0 \pm 0.2) \cdot 10^{10}$ $M^{-1}s^{-1}$. The $(EHA\text{-}AA\text{-}Fe^{3+})_n$ ionomer and $(EHA\text{-}AA\text{-}Fe_3O_4)_n$ nano-composite exhibit interesting magnetic properties.
The magnetization measurements on the $(EHA\text{-}AA\text{-}Fe_3O_4)_n$ nano-composite show a combination of ferromagnetic behavior (hysteresis) at relatively small magnetic fields with superparamagnetic behavior at large fields. The ferromagnetic behavior can be attributed to the presence of larger nanoparticles and the superparamagnetic behavior to smaller nanoparticles. As expected, the magnetization increases with magnetite concentration up to about 10% Fe (in the form of Fe_3O_4). Above this concentration, the magnetite apparently no longer forms a uniform suspension in the 2-EHA/AA copolymer.
Our results also show that $(EHA\text{-}AA\text{-}Fe^{3+})_n$ ionomer exhibit a positive deviation from the Curie's Law dependence at low temperature. This deviation can be attributed to a mutual spin alignment contribution to the magnetization. In nano-particulate materials both a superparamagnetic behavior (due to very small particles) and cooperative behavior (due to larger particles) contribute to the total magnetization; such combined effect is indeed clearly visible in our results. The ferromagnetic behavior is expected to be more noticeable at lower temperatures, where thermal motion is least likely to disrupt mutual spin orientation. This is indeed reflected in our results. It should be noted that that specific magnetization of the $FeCl_3$ ionomers is much lower than the one observed with the $(EHA\text{-}AA\text{-}Fe_3O_4)_n$ nano-composite. This is to be expected in view of the strong tendency of magnetite to exhibit ferromagnetic behavior. However, it is remarkable that some mutual spin alignment takes place within the $FeCl_3$ ionomers.

14.1. INTRODUCTION

Magnetic nanocomposites, in which magnetic nanoparticles are encapsulated in polymeric matrices, have important applications in medicine, electronics and mechanical devices. However, the development of processes leading to magnetic nanocomposites with desirable, predictable and reproducible properties has turned out to be a difficult challenge. To date, most studies have concentrated on a magnetic oxide, primarily magnetite (Fe_3O_4), as the encapsulated phase. However, the synthesis of batches of magnetite with homogeneous properties at reasonably low temperature is a delicate operation. Indeed, commercial lots of

magnetite powder, despite having bulk Fe_3O_4 stoichiometry, turn out to have large variations in structure and in magnetic properties. The difficulties in controlling the product are greatly magnified when the particle size is in the nanometer range [14.1].

One possible approach to the production of magnetic nanocomposites is to aim for the encapsulation of particles of metal rather than oxide. The magnetic properties of a metal cluster of a given size can be expected to be much more predictable and controllable than those of oxides. Several magnetic metal candidates can be considered for inclusion in a polymeric matrix. These include iron, cobalt and nickel. One route to the preparation of metal clusters is reductive radiolysis of the corresponding metal salts, a technique that has been previously demonstrated. In preliminary experiments, an aqueous suspension of metallic cadmium was radiolytically produced from cadmium salts, so long as an alcohol was added to scavenge OH radicals. Nickel salts were also observed to produce metal suspensions, albeit at a lower yield than in the cases of cadmium and lead [14.2]. De-oxygenation of the solutions promoted higher yields and enhanced stability of the suspensions. Copper nanoclusters were also produced by gamma radiolysis [14.3]. Cobalt nanoparticles were prepared by gamma radiolysis in the forms of an aqueous sol, a self-supporting powder, and in dispersion on an alumina surface [14.4]. The production of nickel nanoparticles by means of irradiation with synchrotron x-ray radiation was also reported [14.5]. Because nickel is the least reactive of the three magnetic metals towards water, nickel nano-particles should be the easiest to prepare upon starting from aqueous salt solutions.

The production of the polymer in which the magnetic nanoparticles are to be encapsulated may also be initiated by ionizing radiation. For instance, the polymerization of acrylate esters is known to be initiated by a pulsed electron beam [14.6]. For the present study, if a nickel salt is introduced into a medium consisting of an organic monomer and OH radical scavengers, the ionizing radiation might be expected to produce both nanoparticles of metallic nickel and an acrylic polymer. Because both the nickel nanoparticles and acrylate matrix are produced in close proximity, it is possible that the metal clusters would be encapsulated *in situ*, resulting in a stable metal-polymer nanocomposite.

It is proposed that the addition of an organic monomer may improve the yield of the magnetic metal clusters. During reductive radiolysis of metal salts, the metal is susceptible to oxidation or re-dissolution in water. If the concentration of water is reduced, the yield and stability of metal clusters are likely to be greatly enhanced. Utilizing an organic monomer as the main component of the reaction medium allows the reduction to take place in a solution with much reduced water content. For instance, a nickel salt can be combined with a medium consisting of an acrylate ester, an alcohol OH radical scavenger, and just enough water to solubilize the metal salt. If nickel is introduced in the form of an organic salt, solvents which are miscible with the monomer can be used, possibly eliminating the water entirely, as long as the system is sufficiently polar to generate solvated electrons. Even if some water is necessary, its amount would be small enough to minimize the extent of its reaction with the metal particles.

The nanocomposites produced in this study would be characterized by means of a combination of chemical, magnetic and microscopic techniques. Following the synthesis of iron-based nanocomposies, further experiments will be conducted possibly on cobalt-based and nickel-based systems.

14.2. EXPERIMENTAL PROCEDURE

The work presented in this study involves a synthesis of a copolymer composed of 2-ethylhexyl acrylate (2-EHA) and acrylic acid (AA) using gamma and pulsed electron beam

radiation. The structure of thethis copolymer and the kinetics of its formation were investigated using ^{1}H nuclear magnetic resonance (NMR), electron pulse radiolysis with kinetic spectroscopic detection (PR-KSD), and Fourier transform infrared spectroscopy (FTIR). The effects of total dose, dose rate, and acrylic acid content on the polymerization reaction were studied. The conversion of 2-EHA monomer into polymer at a given total dose was found to be enhanced at lower dose rates and higher concentrations of acrylic acid.

2-Ethylhexyl acrylate/Acrylic acid (2-EHA/AA) co-polymers were prepared by mixing together 2-EHA (75-100 mol%) and AA (0-25 mol%) in a conical flask sealed with a rubber septum, bubbling with argon gas, transferring aliquots of the mixture to glass vials in a glove box, and irradiating the vials using either the University of Maryland's 100 kCi Co-60 gamma source or the University of Maryland's pulsed electron beam linear accelerator (LINAC).

Iron-poly(2-EHA-co-AA) ionomers were produced by dissolving the irradiated 2-EHA/AA mixtures in THF, mixing with $FeCl_3$, and performing dialysis by means of a cellulose membrane to remove unassociated ions, such as chloride, from the co-polymer. Chloroform and methanol were used as solvents in the dialysis.

The experimental procedure of the ionomer synthesis is shown in Figure 14.1. below.

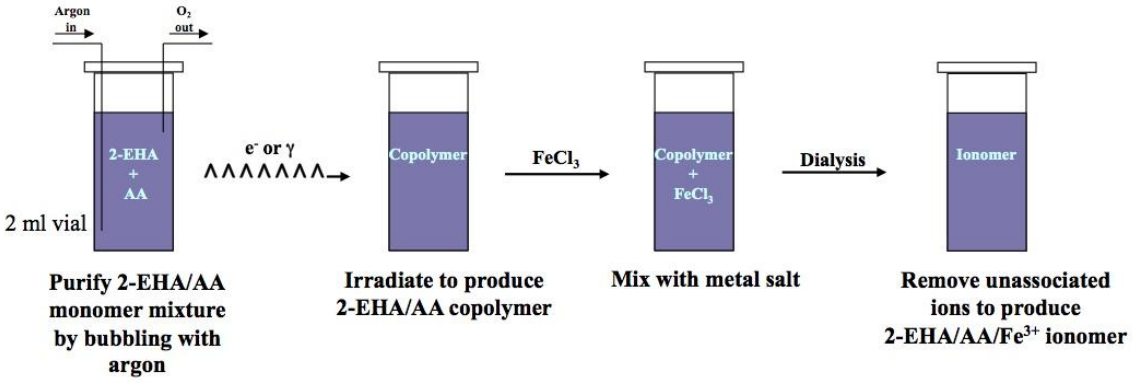

FIG 14.1. Experimental Procedure for Ionomer Synthesis

Nanocomposites were produced by mixing the 2-EHA/AA polymer with a suspension of nanoparticles of magnetite (Fe_3O_4) in kerosene, sonicating the mixture for several hours, and allowing it to dry in air.

14.3. RESULTS AND DISCUSSION

14.3.1. Characterization of ionomers

As described above, Fe^{3+} ionomers were prepared by dissolving the radiation-produced poly(2-EHA-co-AA) in THF, mixing the solution with a solution of anhydrous $FeCl_3$ in THF, and dialyzing the mixture through a cellulose membrane. Different concentrations of the Fe^{3+} ionomer were prepared by using different volumes of $FeCl_3$ solution in THF. It was observed that it was possible to obtain ionomers with concentrations of $FeCl_3$ corresponding to as high as (1.00 $\pm$ 0.05) % Fe (mass percent) without indications of non-uniformity resulting from exceeding the solubility of $FeCl_3$ in the acrylic co-polymer. On the other hand, when it was attempted to raise the concentration of $FeCl_3$ to 2 % based on Fe (mass percent), it was

observed that the solubility was exceeded as indicated by the fact that different portions of the sample had widely different concentrations of Fe as determined by using an ICP-AES spectrometer (see below). Thus, it was concluded that the solubility of $FeCl_3$ in the co-polymer, expressed in wt. % Fe^{3+}, was between 1 and 2 % Fe. A concentration of 1 % by wt. of Fe corresponds to 2.7 mole % Fe in the 3:1 EHA-AA co-polymer. The concentration of Fe in the ionomers was determined by dissolving the samples in a mixture of HCl and HNO_3 and analyzing these solutions using an ICP-AES spectrometer. Evidence for the formation of ionomers was provided by the observation that the FTIR spectrum of the samples, most noticeable in the case of the sample with the highest Fe^{3+} content of 1.00 % Fe^{3+}, exhibited peaks which were not observed in the base co-polymer. The most noticeable of these peaks was the one at 1374 cm^{-1}, as shown in Figure 14.2. This peak indicates the incorporation of the metal ion in a co-polymer.

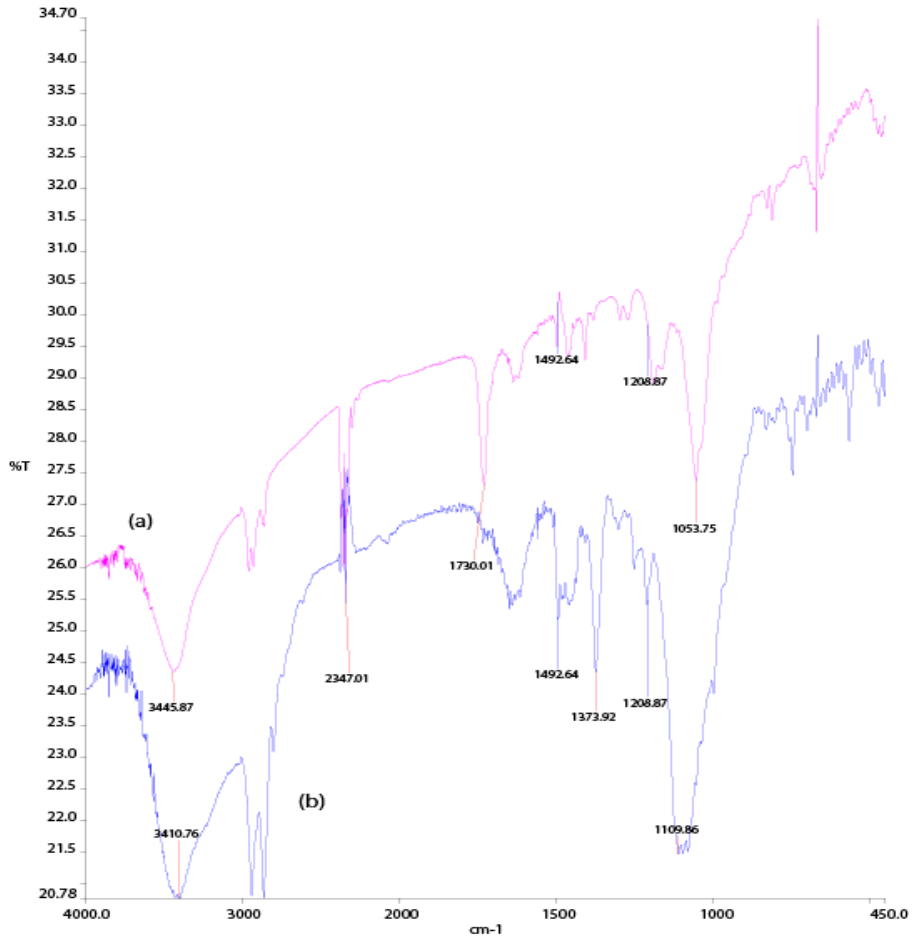

FIG 14.2. FTIR spectra of 2-EHA-co-AA co-polymers. (a) Pure co-polymer 2.7 mol % Fe ionomer in a 75 mol % 2-EHA/25 mol % AA, produced by exposure of monomer mix to 100 Gy of Co-60 gamma radiation at a dose rate of 13 Gy · min^{-1}; (b) Same co-polymer after reaction with $FeCl_3$ to produce a 73.0 mol % 2-EHA/24.3 mol % AA/2.7 mol % Fe^{3+} ionomer.

Oxygen 1s XPS spectra of poly(2-EHA-co-AA) before and after mixing with $FeCl_3$ exhibit shifts of the C-O and C=O peaks to higher energies when iron is present (Figure 14.3). The

relative intensity of the C-O peak decreases when $FeCl_3$ is added, and a peak corresponding to Fe^{3+}-O appears at 530.6 eV.

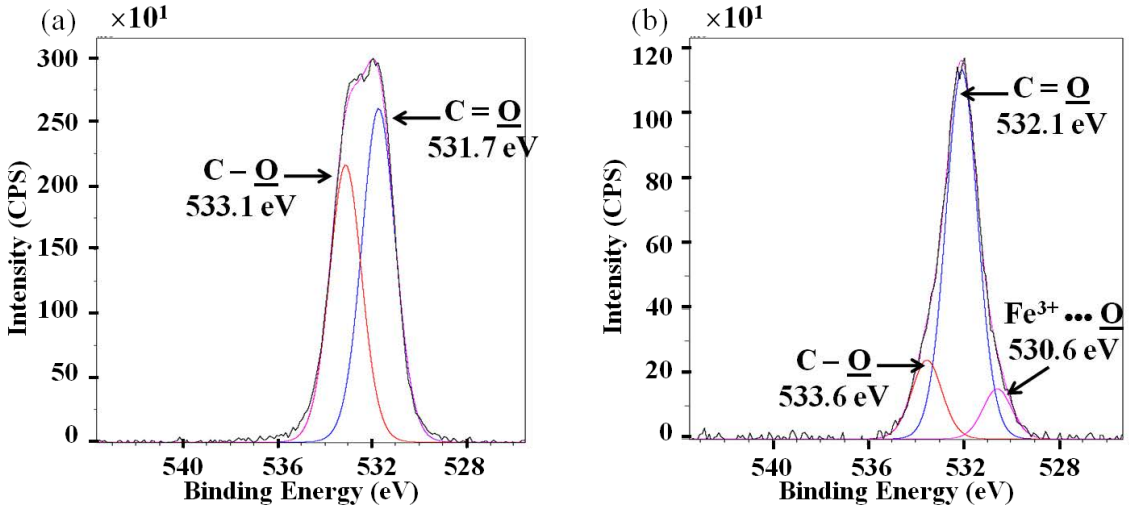

FIG 14.3. O 1s XPS spectra of 2-EHA-co-AA co-polymers: (a) without adding $FeCl_3$, (b) after mixing with $FeCl_3$ and dialyzing the product.

A TEM micrograph of the iron salt with poly(2-EHA-co-AA) is shown in Figure 14.4. This micrograph shows the presence of nanometer-size clusters of iron species.

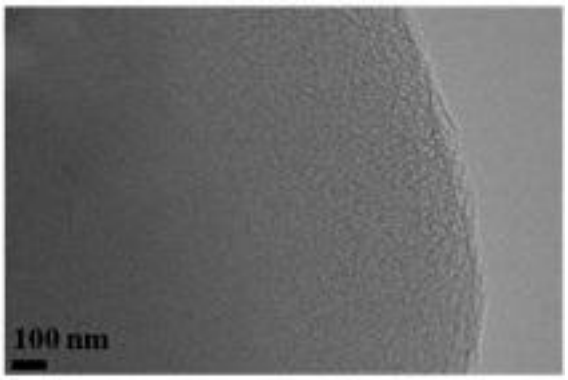

FIG 14.4. TEM micrograph of ionomer of 2-EHA-co-AA co-polymer.

The proposed mechanism of the formation of iron-based monomer in 2-EHA/AA co-polymer is represented in the following schematic diagram:

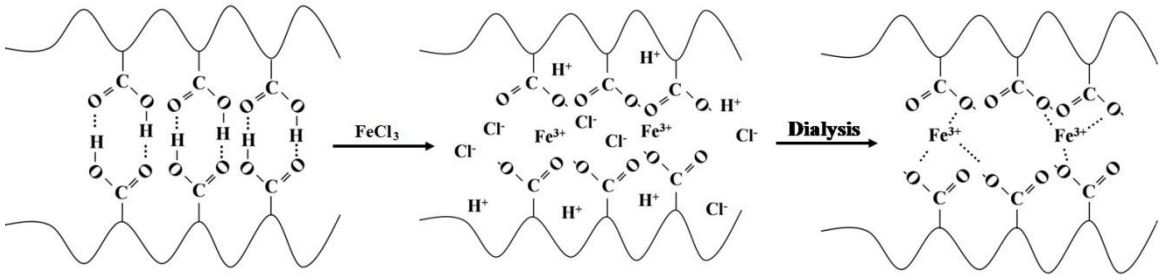

As mentioned above, a strong indication of the formation of the ionomer is furnished by the observation of the appearance of the peak at 1374 cm^{-1} in the IR spectrum (Figure 14.8). This peak may be associated with a C-H bending vibration that is not observed in the base co-polymer due to the fact that the latter has a more rigid structure because of the presence of hydrogen bonds. Another indication is the observation of the 530.6-eV peak in the XPS spectrum of poly(2-EHA-co-AA) after mixing with $FeCl_3$. This peak apparently results from interaction between ferric ions and the oxygen atoms of AA. The TEM micrographs of these systems show the presence of Fe-rich regions with a linear dimension of the order of 100 nm. These regions may consist of clustered ionomers.

14.3.2. Synthesis and characterization of magnetic nanocomposites

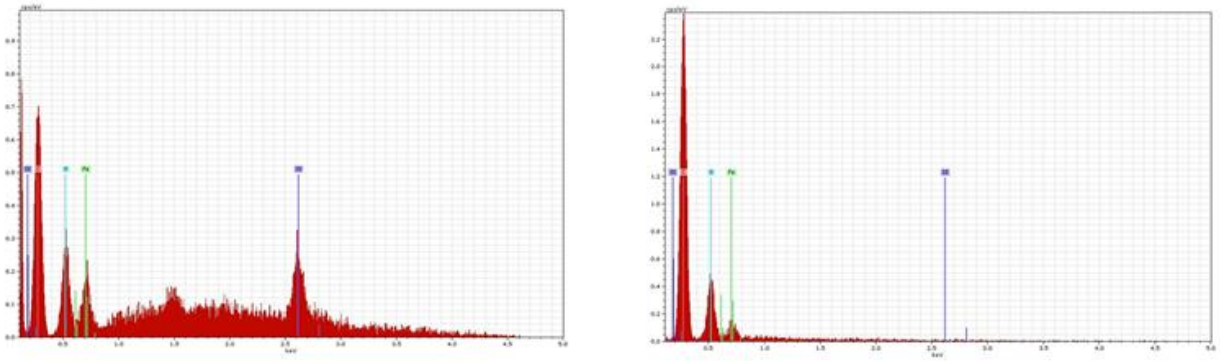

FIG. 14.7. Energy Dispersive X-ray Analysis: Fe3O4 (1% Fe) Nanocomposite (left) and Fe3O4 (1% Fe) Nanocomposite (right)

Magnetic measurements were performed on the poly(2-EHA-co-AA)/iron samples which are shown in the figures below.

In nanoparticles which are smaller than the domain size but not extremely small, there is a mixed ferromagnetic/superparamagnetic behavior as reflected in the Langevin equation (Figure 14.8).

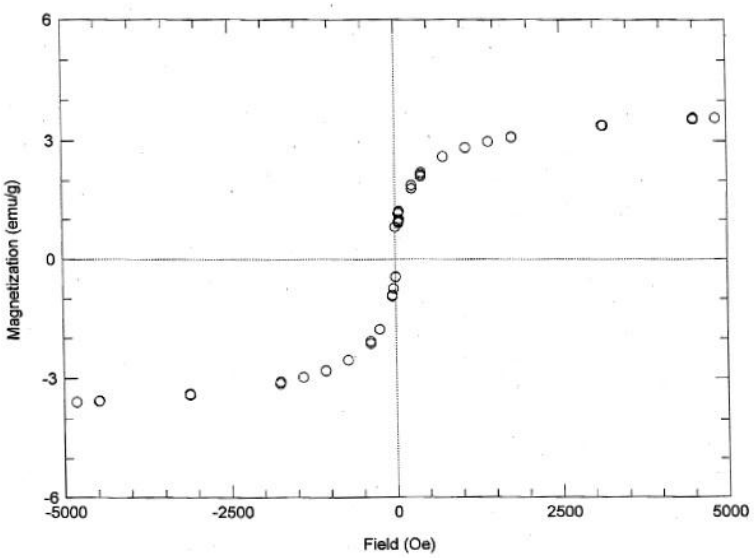

FIG. 14.8. Magnetization Measurements: Magnetite Nanocomposite (1%) – 15nm

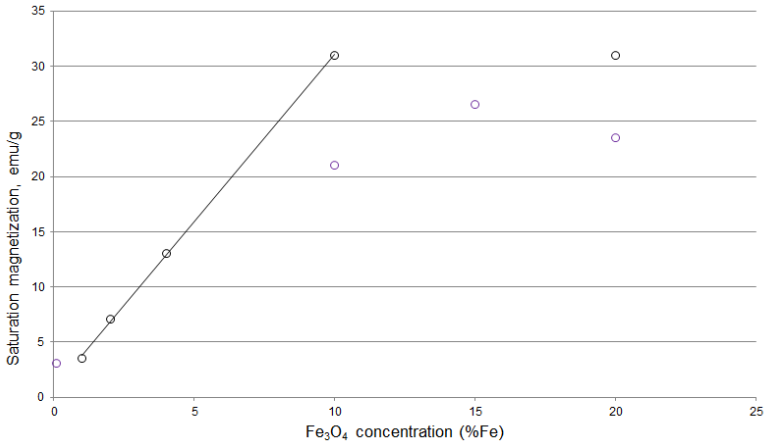

FIG. 14.1. Magnetization of Fe3O4 samples in 2-EHA/AA co-polymer: Various Nanocomposite Concentrations

The magnetization results for the magnetite nanocomposites show a combination of ferromagnetic behavior (hysteresis) at relatively small magnetic fields with superparamagnetic behavior at large fields. The ferromagnetic behavior can be attributed to the presence of larger nanoparticles and the superparamagnetic behavior to smaller nanoparticles. As expected, the magnetization increases with magnetite concentration up to about 10% Fe (in the form of Fe_3O_4). Above this concentration, the magnetite apparently no longer forms a uniform suspension in the 2-EHA/AA co-polymer.

14.3.3. Calculation of particle size from magnetic measurements

14.3.3.1. General

Ferromagnetic materials consist of particles that have a size that is larger than, or at least equal to, the size of a magnetic domain. A typical domain size is around 100 nm or 0.1 μm.

If the individual particles are smaller, i.e., they are subdomain in size, then the observed magnetic behavior is no longer ferromagnetic. Above a certain temperature called the blocking temperature (T_B), except at very high fields, the magnetization (M) of subdomain particles continues to rise with increasing applied magnetic field, and drops to zero, similar to paramagnetic behavior, once the external field is removed. This behavior is called superparamagnetism.

The blocking temperature T_B is the temperature at which the time it takes the spins to flip due to thermal fluctuations becomes comparable to the time of the measurement. T_B depends on the nature of the material, the particle size, and the applied magnetic field H. T_B increases with increasing particle size and with decreasing H. For instance, in the case of magnetite with particle size of $\geq$ 100 nm and very weak H the limiting value of T_B is 580 ^oC. For a particle with a size of 5 nm and a field of 500 G, T_B can be as low as 45 K.

14.3.3.2. Equations (The transition from ferromagnetic to superparamagnetic behavior in nanoparticles)

The Langevin Function

$$M_T = M_s + N_{sp}\mu\{[\cosh(\mu H/kT)/\sinh(\mu H/kT)] - (kT/\mu H)\}$$

where,
M_T = Total magnetization
M_s = Saturation magnetization of particles larger than, or close to, domain size
N_{sp} = Number of superparamagnetic particles (much smaller than domain size)
μ = Magnetic moment of superparamagnetic particles

For $T > T_B$, μ can be found from curve fitting.
$V = \mu/\sigma$
V = Particle volume
σ = Specific magnetization (materials property)
T is the temperature of the experiment
k is the Boltzmann constant (Gas constant/Avogadro's Number)

The Bean-Livingston equation

$$H_C = (2KV/\mu)[1 - 5(kT/KV)^{1/2}]$$

where,
K = Anisotopic energy
V = Particle volume
H_C = Coercive force (magnetic field that has to be applied in the opposite direction in order to reduce the magnetization to zero)

For $T < T_B$, μ can be found by plotting H_C vs. $T^{1/2}$ and calculate the slope and intercept.
$V = \mu/\sigma$
V = Particle volume
σ = Specific magnetization (materials property)
T is the temperature of the experiment
k is the Boltzmann constant (Gas constant/Avogadro's Number)

14.3.3.3. How do we decide if $T < T_B$ or $T > T_B$?

a. We plot the magnetization M against the applied field H and obtain the hysteresis curve. We increase H until M no longer changes significantly with H , i.e., M reaches its saturation value. The coercive force H_c is the field that we have to apply in the opposite direction in order to bring the magnetization back to zero after the sample has reached its saturation magnetization.
b. If $T < T_B$, H_c depends on the temperature of the experiment T. If $T > T_B$, H_c is independent of the temperature.

14.3.3.4. Determination of Particle Size for the case of $T > T_B$

a. Find σ, the specific magnetization, of the material in question from the literature or from measurements on large particles.
b. Plot the total magnetization M_T against H.
c. At low fields, M increases quickly with H, mostly due to the contribution of the large (ferromagnetic) particles. At high fields, the dependence becomes much weaker, because it is only due to the superparamagnetic particles, while the contribution of the large particles to M_T has become saturated. Thus, it is easy to draw a horizontal line at the level of M_T where this contribution becomes constant. This represents the value of the saturation magnetization, M_s. The continued weak dependence of M_T on H represents $M_T - M_s$, i.e., the component of the magnetization due to the superparamagnetic (subdomain) particles.
d. Plot $M_T - M_s$ as a function of $\{[\cosh(\mu H/kT)/\sinh(\mu H/kT)] - (kT/\mu H)\}$. The slope will yield $N_{sp}\mu$. (Actually, we plot $M_T - M_s$ against H at constant T or against 1/T at constant H and perform curve fitting to find $N_{sp}\mu$ using Equation (1)).
e. N_{sp} can be found from the number of magnetic moments (based on the number of iron atoms) associated with the superparamagnetic (subdomain) particles. This is obtained by calculating the total number of magnetic moments based on the concentration of the iron species (e.g., magnetite) in the sample on one hand, and the number of unpaired spins per formula unit (e.g., number of unpaired spins per Fe_3O_4 unit) on the other. From the total number of magnetic moments we subtract the number of magnetic moments associated with ferromagnetic (multidomain) particles, which is obtained by dividing the saturation magnetization, M_s, by the specific magnetization (paragraph 4a). The difference corresponds to the number of magnetic moments associated with the superparamagnetic component.
f. Now we can find a value for μ. $\mu = \sigma V$. Since we know σ (see paragraph 4a), we can calculate V, the particle volume, and from it the diameter d of the particle R [$V = 4\pi(d/2)^3/3$].

Comment: When we are studying nanoparticle dispersions, no large (multidomain) particles are present, and this greatly simplifies the procedure, since M_s is not significant and we can calculate N_{sp} directly without having to subtract the number of magnetic moments corresponding to M_s.

14.3.3.5. Determination of Particle Size for the case of $T < T_B$

a. Same as *14.3.3.4*. under a.
b. Plot H_c against $T^{½}$.
c. The slope of the line obtained in paragraph V(b) is $S = (-10/\mu)(kKV)^{½}$. The intercept (H_c extrapolated to T = 0) is $I = 2KV/\mu$.
d. Based on paragraph V(c), $\mu = 50kI/S^2$. Thus we do not need to know K.
e. Same as IVf.

Magnetic measurements were performed on the poly(2-EHA-co-AA)/iron samples which are shown in the figure below. Ionomer formulated composition used for these measurements was based on 2:1 mole ratio Fe^{2+}:AA.

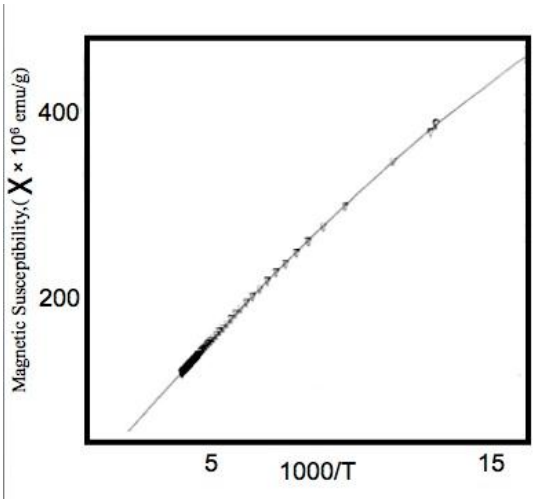

FIG. 14.2. Magnetic susceptibility in the function of temperature for 2-EHA/AA co-polymer

The vibrating sample magnetometry analysis indicated that poly(2-EHA-co-AA)/iron ionomer contained magnetic clusters with an average diameter of 4.7 nm. The magnetic cluster characterization was determined using the method and equations described above in the "Calculation of Particle Size from Magnetic Measurements" section.

14.4. COLLABORATIONS

Collaboration has been established with the following colleagues:

1. Dr. Cecilia Evora and Dr. Leonardo Silva -Brazil:

The collaboration is based on the synthesis of nanocomposites of functionalized carbon nano fibers and metals ions such as ferric. During the implementation of this collaboration, Mrs. Cecilia Evora visited the University of Maryland during the period of

August 26- 30, 2013, and Mr. Mohamad Al-Sheikhly visited IPEN-Brazil during March 18-31, 2014. During these two visits, experiments and discussions were performed.

2. Professor Xavier Coqueret- Université de Reims Champagne Ardenne
Institut de Chimie Moléculaire de Reim- France

The collaboration is based on synthesis and characterization of magnetic nanocomposite of NVP-AllylNVP-Fe^{3+} and NVP-Allyl NVP-gadolinium nanocomposite. Mr. Mohamad Al-Sheikhly visited the Institut de Chimie Moléculaire de Reim for the period of May 11-June 8-2014 to discuss the details of this project. Samples of NVP-Allyl NVP were prepared at Reim-France were sent to Maryland to incorporate the metal ions.

3. Professor Cleilia Dispenza- University of Palermo-Italy

Mr. Al-Sheikhly visited University of Palermo for the period of November 12-16, 2013 to discuss the progress of the collaboration of the magnetic nano composite. Two graduate students from Palermo visited and worked in Maryland.

14.5. CONCLUSION

Magnetic nano-composite and magnetic ionomers of 2-ethyl hexyl acrylate and acrylic acid copolymer were synthesized and characterized.

The implications of magnetization results for magnetite nanocomposites can summarized as follows:

- The magnetization results show a combination of ferromagnetic behavior (hysteresis) at relatively small magnetic fields with superparamagnetic behavior at large fields.
- The ferromagnetic behavior can be attributed to the presence of larger nanoparticles and the superparamagnetic behavior to smaller nanoparticles.
- As expected, the magnetization increases with magnetite concentration up to about 10% Fe (in the form of Fe_3O_4). Above this concentration, the magnetite apparently no longer forms a uniform suspension in the 2-EHA/AA copolymer.

The implications of magnetization results for $FeCl_3$ ionomers can be summarized as follows:

- When the fit to Curie's Law for paramagnetic materials is examined, our results show a positive deviation from the Curie's Law dependence at low temperature.
- This deviation can be attributed to a mutual spin alignment contribution to the magnetization.
- In nanoparticulate materials both a superparamagnetic behavior (due to very small particles) and cooperative behavior (due to larger particles) contribute to the total magnetization; such combined effect is indeed clearly visible in our results.
- The ferromagnetic behavior is expected to be more noticeable at lower temperatures, where thermal motion is least likely to disrupt mutual spin orientation. This is indeed reflected in our results.
- Note that specific magnetization of the $FeCl_3$ ionomers is much lower than the one observed with the magnetite nanoparticles. This is to be expected in view of the

strong tendency of magnetite to exhibit ferromagnetic behavior. However, it is remarkable that some mutual spin alignment takes place within the $FeCl_3$ ionomers.

REFERENCES TO CHAPTER 14

[14.1] NURMI, J.T.; TRATNYEK, P.G.; SARATHY, V.; BAER, D.R.; AMONETTE, J.E.; PECHER, K.; WANG, C.; LINEHAN, J.C.; MATSON, D.W.; PENN, R.L.; DRIESSEN, M.D. ,"Characterization And Properties Of Metallic Iron Nanoparticles: Spectroscopy, Electrochemistry, And Kinetics", Environ. SCI. XXX (2005) XXX

[14.2] BARKATT, A.; RABANI, J., Metal Precipitation From Pulse Irradiated Solutions Of Cadmium(Ii) And Similar Cations, J. Phys. Chem., **79** (1975) 1359-1362.

[14.3] JOSHI, S.S.; PATIL, S.F.; IYER, V.; MAHUMUNI, S., Radiation Induced Synthesis And Characterization Of Copper Nanoparticles, Nanostructured Mater. **10** (1998) 1135-1144.

[14.4] KAPOOR, S.; SALUNKE, H.G.; PANDE, B.M.; KULSHRESHTHA, S.K.; MITTAL, J.P., Mater Res. Bull. **33** (1998) 1555-1562.

[14.5] LEE, H.J.; JE, J.H.; HWU, Y.; TSAI, W.L., Synchrotron X-Ray Induced Solution Precipitation Of Nanoparticles, Nucl. Instr. Meth. Phys. Res. Part B, 199 (2003) 342-347.

[14.6] FENG, H.; AL-SHEIKHLY, M.; SILVERMAN, J.; WEISS, D.E.; NETA, P., Polymerization Of Neat 2-Ethylhexyl Acrylate Induced By A Pulsed Electron Beam, J. Polym. Sci. A Polym. Chem, 41 (2003) 196-203.

Chapter 15

STUDY ON SYNTHESIS OF SILVER NANOPARTICLES BY Γ-IRRADIATION AND THEIR FIXING IN POROUS CERAMIC FOR APPLICATION AS ANTIMICROBIAL FILTER

NGUYEN QUOC HIEN, DANG VAN PHU, LE ANH QUOC, NGUYEN NGOC DUY
Research and Development Center for Radiation Technology,
Vietnam Atomic Energy Institute,
Ho Chi Minh City,
Vietnam

Abstract

The colloidal silver nanoparticles (AgNPs) solution with concentration of 500 mg/L and the AgNPs diameter of 10 – 15 nm was synthesized on pilot scale of 100 L/batch by gamma irradiation method using polyvinylpyrrolidone as stabilizer. Porous ceramic (PC) samples and porous ceramic candle filter (PCCF) product with the specific surface area of 1.83 m^2/g and the average pore size of 61.9 Å were functionalized by treatment with an aminosilane (AS) agent (3-aminopropyltriethoxysilane) and then impregnated in AgNPs solution for fixing through coordination bonds between $–NH_2$ groups of the AS and the silver atoms. The AgNPs content attached in PC (AgNPs/PC) and in PCCF (AgNPs/PCCF) was of about 200–250 mg/kg. Owing to strong bonding of silver atoms to the wall of PC, the contents of silver released from AgNPs/PCCF into filtrated water by flow test were less than 10 μg/L, it is satisfactory to the WHO guideline of under 100 μg/L for drinking water. The antimicrobial effect of AgNPs/PCCF for *E. coli* was carried out by flow test with an inoculated initial contamination of *E. coli* in water of about 10^6 CFU/100ml. Results showed that the contamination of *E. coli* in filtrated water through AgNPs/PCCF (up to 500 L) was less than 1 CFU/100ml compared to 3×10^4 CFU/100ml for bare PCCF (only up to 40 L). Thus, AgNPs/PCCF with the silver content of 200 – 250 mg/kg, the specific surface area of 1.51 m^2/g and the average pore size of 48.2 Å has highly antimicrobial effect and suitably released silver content that can be applied for point-of-use drinking water treatment.

15.1. INTRODUCTION

The presence of toxic metals and pathogenetic microbes in drinking water is a potential health risk. According to WHO, at least one billion people in the worldwide do not have access to clean, potable water sources [15.1]. Therefore, the development of innovative drinking water quality control strategies is of the utmost importance. Recently, considerable interest has arisen in the use of silver nanoparticles (AgNPs) based on gigantic high antimicrobial and biofouling improvement for water disinfection [15.2]. In particular, the formation of by-products into water by conventional treatment techniques and the increasing of resistance of some pathogens to conventional disinfectants have encouraged researchers to explore the antimicrobial activity of AgNPs [15.3]. The reliability and ease of operation of membrane-based water filtration systems such as polyurethane foam [15.4], polysulfone [15.5], paper [15.1], and porous ceramic [15.6] have led to enlarging utilization for water treatment. Numerous investigations have been carried out on loading AgNPs with the functionalized polymer membrane as an effectively antimicrobial agent for water treatment [15.4]. Unfortunately, the AgNPs were commonly inert with polymer or PC surfaces [15.7], so that silver releases into water filtrate with overdoses compared to the limit of 100 μg/L at maximum for drinking water, according to the WHO guideline [15.8]. Several approaches were studied to improve on loading and holding abilities of AgNPs onto polymer and PC filters, mainly by using a binder, coupler and/or surface modification by appropriate agents containing functional groups which have affinity with AgNPs [15.6, 15.7].

In this study, the domestic commercialized porous ceramic candle filter (PCCF) product was used for fixing with AgNPs through coordination bonds between $–NH_2$ groups and silver atoms by using an aminosilan as coupling agent. The silver content released from AgNPs/PCCF into filtrated water and the antimicrobial effect of AgNPs/PCCF was also investigated by flow test. Owing to highly antimicrobial effect and acceptable level of silver content released in water, AgNPs/PCCF can be potentially further developed for point-of-use drinking water treatment.

15.2. EXPERIMENTAL

15.2.1. Materials and chemicals

Silver nitrate ($AgNO_3$) is pure grade product from China. Polyvinylpyrrolidone (PVP) K90 is a pharmaceutical grade product from BASF, Germany. Absolute ethanol (C_2H_5OH) is pure product of Truong Thinh Company, Vietnam. Aminosilane (AS), namely 3-aminopropyltriethoxysilane, NH_2-C_3H_6-$Si(OC_2H_5)_3$ is a product of Merck, Germany. Distilled water was used in all experiments. Porous ceramic (PC) samples supplied by a domestic Ceramic Company, Hai Duong, Vietnam with the specific surface area of 1.83 m^2/g, the average pore size of 61.9 Å and total pore volume of 2.8×10^{-3} cm^3/g measured by BET method. The Luria-Bertani medium for bacteria incubation was purchased from Himedia, India. The *Escherichia coli ATCC 6538* (*E. coli*) was provided by University of Medicine-Pharmacy, Ho Chi Minh City, Vietnam.

15.2.2. Methods

15.2.2.1. Synthesis of colloidal AgNPs solution

PVP and ethanol (EtOH) were dissolved in distilled water to prepare solution with the concentration of 1% (w/v) for PVP and 5% (v/v) for EtOH. Silver nitrate was then dissolved in the above prepared solution to obtain final formulation: 5 mM Ag^+/1% PVP/5% EtOH/water to 100 ml on experimental scale and to 100 L divided into 4 plastic cans (25 L/can) on pilot scale. The gamma irradiation of Ag^+ solution for the synthesis of AgNPs was carried out on a Co-60 irradiator with dose rate of about 1.2 kGy/h measured by the ethanol-chlorobenzene dosimetry system [15.9] at VINAGAMMA Center, Ho Chi Minh City. UV-vis absorption spectra of irradiated AgNPs solution were taken on an UV-vis spectrophotometer model Jasco V-630, Japan. The size of the AgNPs was measured using a transmission electron microscope (TEM) model JEM 1010, JEOL, Japan.

15.2.2.2. Treatment of PC samples with AS

PC samples dimensions of approximately $3.0\times2.5\times0.8$ cm^3 were treated in 10% sulfuric acid at 60°C for 1 h, washed with water and dried at 110°C. Then the PC samples were impregnated in 2% (v/v) AS in EtOH solution with different time duration. The PC samples impregnated with AS were dried at room temperature and then heated at 110°C in an oven (Memmert, Germany) for 2 h to silanol bonding functionalization between PC and AS.

15.2.2.3. Impregnation of AS functionalized PC in AgNPs solution

The AS functionalized PC samples were further impregnated in AgNPs solution for 24 h, washed in ultrasonic bath for 15 min and then by water for several times. Drying of AgNPs/PC samples was performed in a forced air oven (DNF 410, Yamato, Japan) at 80°C

till to dry. The obtained PC samples were specified as antimicrobial AgNPs/PC. The content of silver in AgNPs/PC was determined by inductively coupled plasma-atomic emission spectroscopy (ICP-AES) on a Perkin-Elmer, Optima 5300 DV. The presence of silver in AgNPs/PC was also assessed by energy-dispersive X-ray spectroscopy (EDX) on a JEOL 6610 LA. The specific surface area, the average pore size and total pore volume were measured by BET method (Quantachrom Nova 1200) using N_2 as the adsorbate. The absorption spectrum of the AgNPs/PC was also taken on an UV-vis spectrophotometer model Jasco V-630, Japan using AgNPs/PC powder suspended in 1% PVP aqueous solution. The same AgNPs fixing process was also carried out for PCCF product (Length: 20 cm, Diameter: 4 cm; and Thickness: 0.8 cm) denoted as AgNPs/PCCF.

15.2.2.4. Determination of silver release from AgNPs/PCCF

The AgNPs/PCCF was connected to tap water with the flow rate of ~5 L/h up to 500 L. The filtrated water samples were collected for determination of the silver content by neutron activation analysis method at nuclear research reactor, Dalat.

15.2.2.5. Antimicrobial effect

In vitro test of AgNPs/PC

To examine the antimicrobial effect of AgNPs/PC, 1 ml of ~10^7 CFU/ml (CFU: colony-forming units) *E. coli* suspension was separately added to 99 ml LB medium in 3 conical flasks (250 ml). The cultures were shaken at 150 rpm for 20 min at room temperature. Then 5 g of AgNPs/PC powder was introduced into one of the 3 tested flasks with the silver content of about 10 mg/L. The same weight of bare PC powder was added to the second flask, and the third flask was used as the blank control. All flasks were shaken at 150 rpm for 30 min, and then diluted tenfold in distilled water to 1×10^{-5} of initial concentration. 0.1 ml of each diluted solution was spread on LB agar plates, and incubated at 37^{o}C for overnight (~16 h). The counts of bacterial colonies were the surviving numbers of *E. coli* [15.10].

Flow test of AgNPs/PCCF

The inlet water was inoculated with *E. coli* of about 10^6 CFU/100ml. The antimicrobial effect of AgNPs/PCCF was investigated with the flow rate of ~5 L/h. The output water samples passed through AgNPs/PCCF were collected up to 500 L for assessment of the *E. coli* contamination (CFU/100ml) according to ISO 9308-1: 2000 [15.11].

15.3. RESULTS AND DISCUSSION

15.3.1. Synthesis of colloidal AgNPs solution

Many methods for the synthesis of AgNPs with different stabilizers have been developed [15.12]. The method using ionizing radiation (gamma ray and electron beam) provides several advantages compared to other methods, such as: (1) the process is carried out at room temperature; (2) reducing agents occur fairly uniformly in the solution; (3) the reaction rate can be controlled by varying absorbed dose (irradiation time); (4) pure AgNPs can be produced without contamination of excessive reductant and Ag^+ residue; (5) The particle size can be controlled by selection of initial Ag^+ concentration; and (6) large scale production can be carried out at a comparatively reasonable cost [15.12]. The mechanism of the gamma Co-

60 irradiation method was described by Belloni et al. [15.13]. Briefly, Ag^+ ions were reduced by hydrated electron (e^-_{aq}) and hydrogen atom ($H^\bullet$) which were generated by γ-radiolysis of aqueous solution as presented in Equation (1).

$$H_2O \xrightarrow{\wedge\wedge\wedge} e^-_{aq}, H^\bullet, {}^\bullet OH, H_2O_2, H_2, H_3O^+ \quad (1)$$

The reduction reaction process can be written as follows:

$$Ag^+ + e^-_{aq} \rightarrow Ag^o \quad (2)$$

$$Ag^+ + H^\bullet \rightarrow Ag^o + H^+ \quad (3)$$

$$Ag^o + Ag^+ \rightarrow Ag^+_2 \quad (4)$$

$$Ag^+_2 + e^-_{aq}\,(H^\bullet) \rightarrow Ag^o_2 \rightarrow Ag^+_n \rightarrow Ag^o_n \quad (5)$$

The hydroxyl radical (${}^\bullet OH$) reacts with alcohol (e.g. methanol, ethanol, isopropanol,) yielding hydroxyalkyl radical which is able to reduce Ag^+ ions absorbed on clusters to Ag^o [15.12, 15.14].

Fig. 15.1. shows the effect of dose on optical density (OD) and the maximum absorbed wavelength (λ_{max}) at saturated conversion dose. It can be observed from Fig. 15.1. that the conversion dose ($Ag^+ \rightarrow Ag^o$) is of about 15 kGy and $\lambda_{max} \sim 400$ nm.

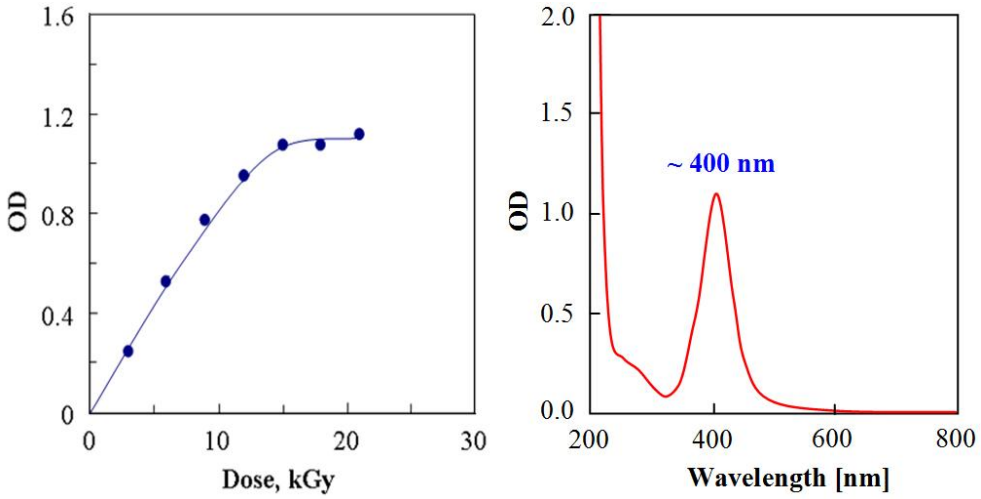

FIG. 15.1. The values of OD with doses and UV-vis spectrum of 5mM AgNPs solution

TEM image and particles size distribution of AgNPs prepared on experimental scale for the silver concentration of 5 mM stabilized with 1% PVP K90 was presented in Fig. 15.2. The average AgNPs size was of 9.5 ± 0.8 nm. According to results reported by Phu et al. [15.15], the AgNPs size ~10 nm exhibited highly antimicrobial activity with the efficiency of 99.99% at 5 ppm of AgNPs content.

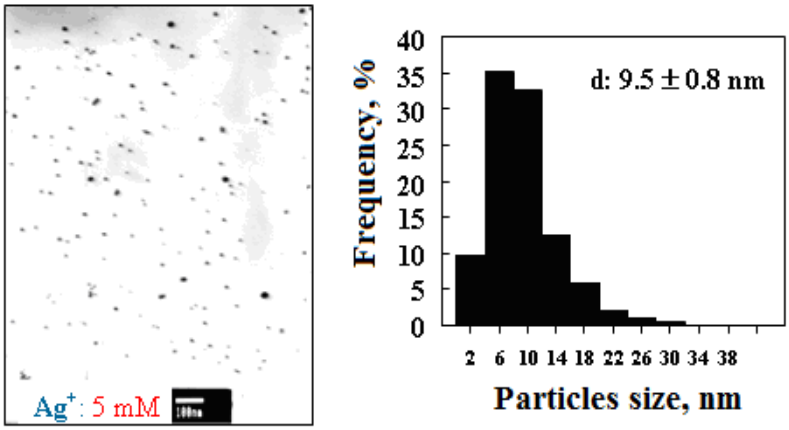

FIG. 15.2. TEM image and histogram of AgNPs size distribution

Results in Table 15.1. show the parameters of AgNPs prepared on pilot scale. The particle sizes (10 – 15 nm) were slightly bigger compared with that from experimental scale. The reason may be due to the dose rate was different from the outside to the center of the irradiation solution volume.

TABLE 15.1: CHARACTERISTICS OF AgNPs 5 mM ON PILOT SCALE BY GAMMA IRRADIATION

Parameters	Dose, kGy	λ_{max}, nm	OD	d, nm
Values	15 – 20	397 – 401	0.9 – 1.1	10 – 15

15.3.2. Optimization of treatment time of PC with AS

TABLE 15.2. EFFECT OF AS TREATMENT TIME ON SILVER CONTENT IN AgNPs/PC

AS treatment time, min	30	60	90	120	150	180
Ag content in PC, mg/kg	200	205	228	226	222	231

Results in Table 15.2. indicated that the optimal treatment time of PC with AS was of 90 – 120 min and AgNPs content fixed in PC samples was of 226 – 228 mg/kg. Table 15.3. showed the AgNPs content, particularly of 227.3 ± 15.2 mg/kg fixed in PCCF product.

TABLE 15.3. THE SILVER CONTENT IN AgNPs/PCCF

AS treatment time, min	120	120	120
Ag content in PCCF, mg/kg	226	234	222

Thus, AgNPs fixed in PCCF through coordination bonds between $–NH_2$ groups of the AS and the silver atoms have been prepared for further investigation of silver release and antimicrobial effect by flow test. Lv et al. also studied to fix AgNPs in PC for water treatment, but they only prepared samples of 1×1×0.5 cm^3 [15.6]. They did not used

commercial PCCF products so that to restrict the development for the practical application purpose.

As described in Scheme 1, the $–NH_2$ groups at the top of AS molecules fixed to porous ceramic coordinated with silver atoms of AgNPs and formed a AgNPs/PC composite [15.6]. Gianni et al. explained that the coordination bonding of the $–NH_2$ group with silver atoms is due to silver has an empty orbital and nitrogen a lone electron pair [15.16].

a) Hydrolyzation of AS

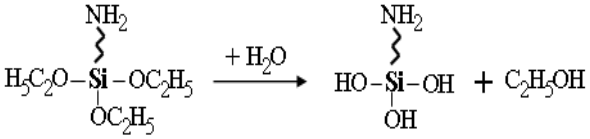

b) Dehydration

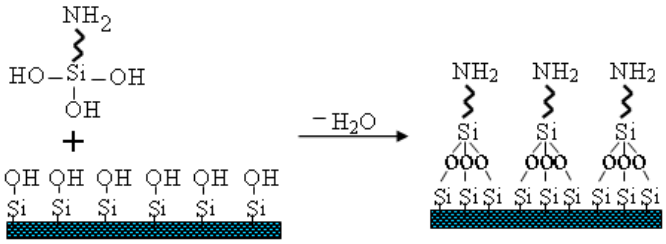

c) Impregnation in AgNPs solution, 25°C, 24 – 32 h

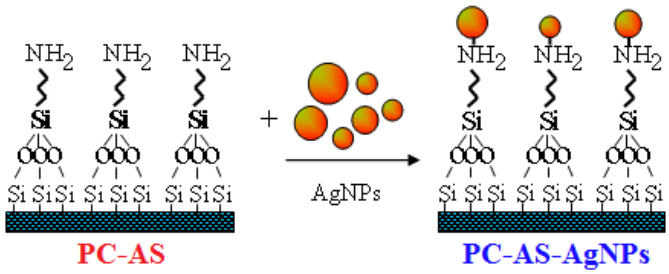

SCHEME 15.1. Reaction process of fixing AgNPs in PC though AS coupling agent

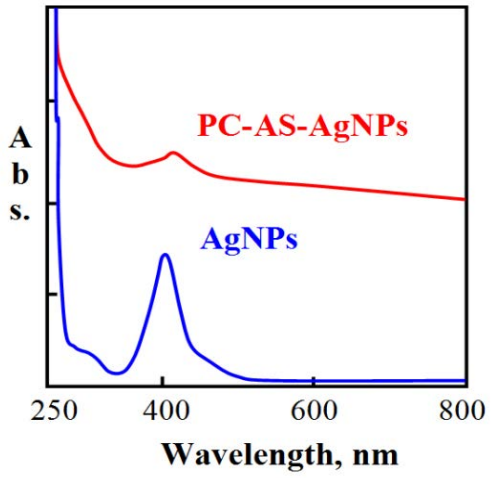

FIG. 15.3. UV-vis spectra of AgNPs/PC and AgNPs

Results in Fig. 15.3. showed that λ_{max} of AgNPs/PC was at about 405 nm with broad peak compared to that of the original AgNPs, the reason may be due to the influence of the ceramic carrier. Thus, this peak indicated that AgNPs are present in the PC as reported by Lv et al. [15.6], however, the λ_{max} of AgNPs/PC in their study was shifted to the shorter wavelength from 429 to 422 nm.

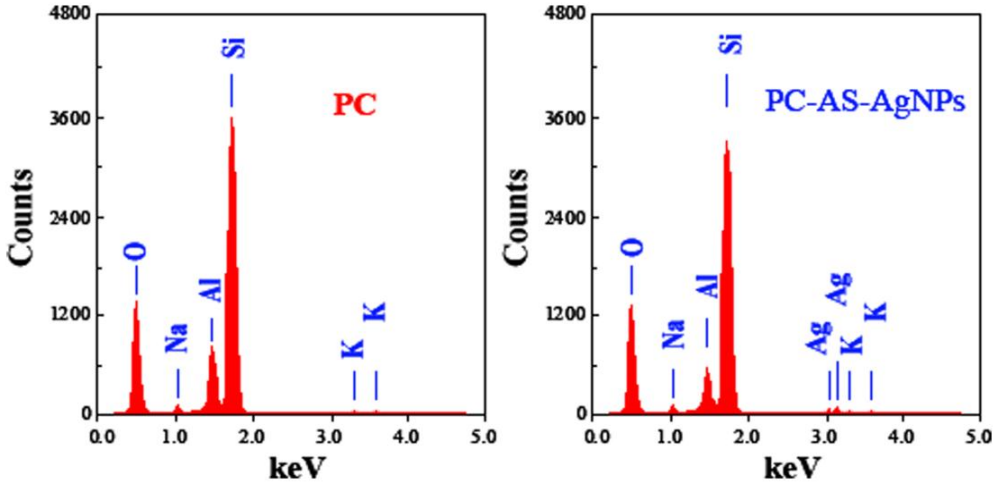

FIG. 15.4. EDX spectra of bare PC and AgNPs/PC

Results in Fig. 15.4. showed that the composition of PC consists of three main elements particularly silicon, aluminium, oxygen and small amount of sodium and potassium, but without any trace of silver. After fixing AgNPs in PC, the peak at 3 keV appeared in EDX spectrum confirming the presence of silver in the composition of AgNPs/PC. In the study of Klemenčič et al. [15.17] and Gusseme et al. [15.3], the EDX spectrum was also used to confirm the presence of AgNPs in cellulose and polyvinylidene fluoride samples.

15.3.3. Content of silver release from AgNPs/PCCF into filtrated water

TABLE 15.4. RESULT OF SILVER CONTENT IN THE FILTRATED WATER RELEASED FROM AgNPs/PCCF

Volume of filtrated water, L	20	40	80	100	200	300	400	500
Ag content, µg/L	9.04	7.49	4.12	2.66	0.64	0.66	0.34	0.92

Results in Table 15.4. proved that the contents of the silver releasing from AgNPs/PCCF in the filtrated water by flow test with the rate of ~5 L/h was less than 10 µg/L determined by neutron activation analysis method. The silver contents are far below the WHO guideline of 100 µg/L silver for drinking water [15.8]. Oyanedel-Craver et al. [15.18] and van Halem et al. [15.19] also studied of silver-impregnated porous ceramic pot filter for low-cost household drinking water treatment. However, they did not used coupling agent like AS to fix AgNPs to the ceramic wall, therefore silver was easily leaching from the pot and the antimicrobial effect should be decreased with the filtration time. Thus, it was recommended that the life

time of the silver-impregnated porous ceramic pot filter without coupling agent was of 1 – 2 years [15.19], but the risk of over dose of silver release into water had not been reported.

TABLE 15.5. CHARACTERISTICS OF BLANK PCCF AND AgNPs/PCCF

Parameters	PCCF	AgNPs/PCCF
Silver content (mg/kg)	Not detected	200 – 250
Specific surface area (m^2/g)	1.83	1.51
Average pore size (Å)	61.9	48.2
Total pore volume (cm^3/g)	2.8×10^{-3}	1.8×10^{-3}

Results in Table 15.5. indicated that the specific surface area, total pore volume and average pore size of AgNPs/PCCF were reduced compared to that of PCCF. The reason may be explained that the presence of AS and AgNPs caused the pore size smaller and when the pore size is smaller, concurrently the specific surface area and the total pore volume will also be decreased. Sui & Huang reported the average pore size of the ceramic candle filter was of about 1,500 Å that is very large pore size compared to ours [15.20]. However, this type of porous ceramic candles was reported to exhibit highly antibacterial effect for water filtration with regularly cleaning to avoid fouling. The reason to achieve such a highly antibacterial efficiency was not elucidated.

15.3.4. Antimicrobial effect

15.3.4.1. In vitro test of AgNPs/PC

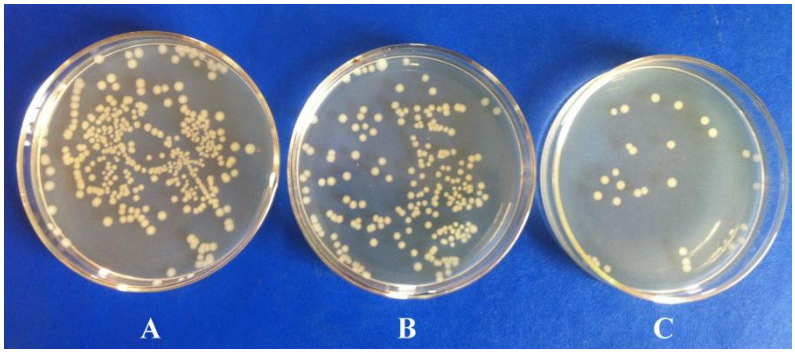

FIG. 15.5. E. coli colonies forming on LB agar from 0.1 ml (1×10^{-3} diluted solutions):

(A) control sample, (B) blank PC, and (C) AgNPs/PC

The surviving number of *E. coli* in the tested medium was of 3.35×10^6; 3.33×10^6 and 2.75×10^5 CFU/ml for control, blank PC and AgNPs/PC samples, respectively as shown in Fig. 15.5. The *in vitro* test results indicated that AgNPs/PC has antimicrobial effect against *E. coli*.

15.3.4.2. Flow test of AgNPs/PCCF

TABLE 15.6. THE COUNTS OF *E. coli* IN FILTRATED WATER BY FLOW TEST THOUGH BLANK PCCF AND AgNPs/PCCF

Volume of filtrated water, L		10	20	40	160	260	300	400	500
Counts of *E. coli* (CFU/100ml)	AgNPs/PCCF	< 1	<1	<1	<1	<1	<1	<1	<1
	PCCF	6×10^4	4×10^4	3×10^4	-	-	-	-	-

Result in Table 15.6. indicated that the water filtrated though AgNPs/PCCF up to 500 L did not contaminate of *E. coli* (< 1 CFU/100 ml) that is generally accepted for drinking water in comparison to 3×10^4 CFU/100 ml (up to 40 L) for blank PCCF.

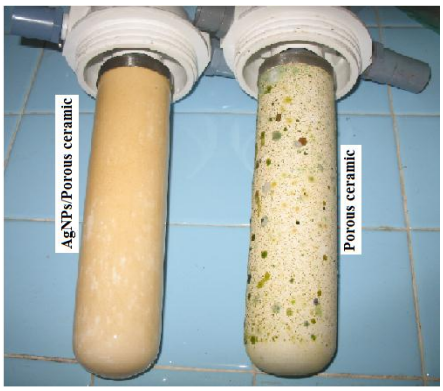

FIG. 15.6. The outside appearance of blank PCCF and AgNPs/PCCF after flow test

Fig. 15.6. showed that the outside of the AgNPs/PCCF had almost no growth of microorganisms compared to the blank (bare) PCCF. This observation confirmed again the highly antimicrobial property of the AgNPs/PCCF.

Among the water treatment materials, ceramic filters (disk, candle and pot) proved to be one of the best treatment options for reducing bacteria by more than 99% [15.21]. And according to Sui & Huang [15.20], the porous ceramic candle filter can be used to filtrate more than 50 M^3 of drinking water. As the results obtained in our work, the as-prepared AgNPs/PCCF contained of about 100 mg AgNPs. The silver content released into water was of about 10 μg/L as calculated from the results in Table 15.4. Thus, theoretically one AgNPs/PCCF can be used for filtration of about 10 M^3 water with regard to the AgNPs content of AgNPs/PCCF. Therefore, the AgNPs/PCCF prepared in this study using AS as coupling agent to fix AgNPs to the wall of PC with highly antimicrobial effect is promising to apply for point-of-use drinking water treatment.

15.4. CONCLUSIONS

The colloidal AgNPs solution with the particles size of 10 – 15 nm and the AgNPs concentration of 500 mg/L was synthesized by γ-irradiation method. The fixing of AgNPs in porous ceramic samples and porous ceramic candle filter through coordination bonds

between $-NH_2$ groups of aminosilane and silver atoms was performed. Results of flow test with the rate of ~5 L/h on silver release and antimicrobial effect for *E. coli* indicated that the silver content in filtrated water was less than 10 μg/L, and it is far below the WHO guideline of 100 μg/L for drinking water and the contamination of *E. coli* was of <1 CFU/100ml. Thus, the as-prepared AgNPs/PCCF with the silver content of 200 – 250 mg/kg, the specific surface area of 1.51 m^2/g, the average pore size of 48.2 Å and the total pore volume of 1.8×10^{-3} cm^3/g have highly antimicrobial effect that can be applied for point-of-use drinking water treatment.

ACKNOWLEDGEMENTS

This research work was supported in part by the International Atomic Energy Agency (IAEA) under Research Contract no. 16719. We would like to thank VINAGAMMA Center for γ-irradiation to prepare colloidal silver nanoparticles solution. We also gratefully thank Mr. Nguyen Trong Viet, Hai Duong Ceramic Co. Ltd. for providing porous ceramic candle filter samples.

REFERENCES TO CHAPTER 15

[15.1] DANKOVICH, T.A., GRAY, D.G., Bactericidal paper impregnated with silver nanoparticles for point-of-use water treatment, *Environmental Science and Technology* 45 (2011) 1992-1998.

[15.2] ZODROW, K., BRUNET, L., MAHENDRA, S., LI, D., ZHANG, A., LI, Q., ALVAREZ, P.J.J., Polysulfone ultrafiltration membranes impregnated with silver nanoparticles show improved biofouling resistance and virus removal, *Water Research* 43 (2009) 715-723.

[15.3] GUSSEME, B.D., SINTUBIN, L., BAERT, L., THIBO, E., HENNEBEL, T., VERMEULEN, G., UYTTENDAELE, M., VERSTRAETE, W., BOON, N., Biogenic silver for disinfection of water contaminated with viruses, *Applied and Environmental Microbiology* 76 (2010) 1082-1087.

[15.4] JAIN, P., PRADEEP, T., Potential of silver nanoparticle-coated polyurethane foam as an antibacterial water filter, *Biotechnology and Bioengineering* 90 (2005) 59-63.

[15.5] TAUROZZI, J.S., ARUL, H., BOSAK, V.Z., BURBAN, A.F., VOICE, T.C., BRUENING, M.L., TARABARA, V.V., 2008. Effect of filler incorporation route on the properties of polysulfone-silver nanocomposite membranes of different porosities, *Journal of Membrane Science* 325 (2008) 58-68.

[15.6] LV, Y., LIU, H., WANG, Z., LIU, S., HAO, L., SANG, Y., LIU, D., WANG, J., BOUGHTON, R.I., Silver nanoparticle-decorated porous ceramic composite for water treatment, *Journal of Membrane Science* 331 (2009) 50-56.

[15.7] TSENG, C.H., WANG, C.C., CHEN, C.Y., 2006. Polypropylene fibers modified by plasma treatment for preparation of Ag nanoparticles, *The Journal of Physical Chemistry B* 110 (2006) 4020-4029.

[15.8] World Health Organization, Guidelines for Drinking-Water Quality, First Addendum to Third Edition, 2006, Vol. 1 Recommendations, Geneva.

[15.9] Practice for use of the ethanol-chlorobenzene dosimetry system, ISO/ASTM 51538:2002, Standards on dosimetry for radiation processing, ASTM International, 2004, 87-97.

[15.10] CHEN, C.Y., CHIANG, C.L., Preparation of cotton fibers with antibacterial silver nanoparticles, *Materials Letters* 62 (2008) 3607-3609.

[15.11] ISO 9308-1:2000, 2000. Water quality - detection and numeration of *Escherichia coli* and coliform bacteria.

[15.12] DU, B.D., PHU, D.V., DUY, N.N., LAN, N.T.K., LANG, V.T.K. et al., Preparation of colloidal silver nanoparticles in poly(N-vinylpyrrolidone) by γ-irradiation, *Journal Experimental Nanoscience* 3 (2008) 207-213.
[15.13] BELLONI, J., MOSTAFAVI, M., REMITA, H., MARIGNIER, J.L., DELCOURT, M.O., Radiation induced synthesis of mono- and multi-metallic clusters and nanocolloids, *New Journal of Chemistry*, (1998) 1239-1255.
[15.14] TEMGIRE, M.K. AND JOSHI, S.S., 2004. Optical and structural studies of silver nanoparticles, *Radiation Physics and Chemistry* 71 (2004) 1039-1044.
[15.15] PHU, D.V., LANG, V.T.K, LAN, N.T.K., DUY, N.N. et al., Synthesis and antimicrobial effects of colloidal silver nanoparticles in chitosan by γ-irradiation, *Journal Experimental Nanoscience* 5 (2010) 169-179.
[15.16] GIANNI, C., MAURIZION, M.M., Density functional study on the adsorption of pyrazole onto silver colloidal particles, *The Journal of Physical Chemistry B* 106 (2002) 6875-6880.
[15.17] KLEMEČIČ, D., SIMONČIČ, B., TOMŠIČ, B., OREL, B., Biodegradation of silver functionalized cellulose fibers, *Carbohydrate Polymers* 80 (2010) 427-436.
[15.18] OYANEDEL-CRAVER, V.A. AND SMITH, J.A., Sustainable colloidal-silver-impregnated ceramic filter for point-of-use water treatment, *Environmental Science and Technology* 42 (2008) 927-933.
[15.19] VAN HALEM, D., VAN DER LAAN, H., HEIJMAN, S.G.J., VAN DIJK. J.C., AMY, G.L., Assessing the sustainability of the silver-impregnated ceramic pot filter for low-cost household drinking water treatment, *Physics and Chemistry of the Earth* 34 (2009) 36-42.
[15.20] SUI, X., HUANG, X., The characterization and water purification behavior of gradient ceramic membranes, *Separation and Purification Technology* 32 (2003) 73-79.
[15.21] SIMONIS, J.J., BASSON, A.K., Evaluation of a low-cost ceramic micro-porous filter for elimination of common disease microorganism, *Physics and Chemistry of the Earth* 36 (2011) 1129-1134.

LIST OF CONTRIBUTORS

Abd El-Rehim, H.	Egyptian Atomic Energy Authority (EAEA) National Centre for Radiation Research and Technology (NCRRT) Egypt
Al-Sheikhly, M.	Department of Materials Science and Engineering University of Maryland United States Of America
Bauer, F.	Institut für Technische Chemie Universitaet Leipzig Germany
Coqueret, X.	Institut de Chimie Moleculaire de Reims Université de Reims Champagne Ardenne France
Dispenza, C.	Dipartimento di Ingegneria Chimica, Gestionale, Informatica, Meccanica (DICGIM) Università di Palermo Italy
Dubey, K.	Department of Atomic Energy (DAE) Bhabha Atomic Research Centre (BARC) India
Evora, M.C.	Instituto de Pesquisas Energeticas e Nucleares (IPEN) Comissão Nacional de Energia Nuclear (CNEN) Brazil
Güven, O.	Department of Chemistry Hacettepe University Turkey
Hemvichian, K.	Nuclear Research and Development Group Thailand Institute of Nuclear Technology (TINT) Thailand
Lacroix, M.	INRS-Institut Armand-Frappier Canada

Nguyen, Q.H.	Vietnam Atomic Energy Institute (VINATOM); Research and Development Centre for Radiation Technology Vietnam
Nik Salleh, N.	Malaysian Nuclear Agency Malaysia
Przybytniak, G.	Centre for Radiation Research and Technology Institute of Nuclear Chemistry and Technology Poland
Radosavljevic, A.	Laboratory for Radiation Chemistry and Physics "Gamma", 030 Vinca Institute of Nuclear Sciences Serbia
Safrany, A.	International Atomic Energy Agency Department Nuclear Sciences and Applications Austria
Yasin, T.	Department of Metallurgy and Materials Engineering Institute of Engineering and Applied Sciences Pakistan

IAEA
International Atomic Energy Agency

No. 23

ORDERING LOCALLY

In the following countries, IAEA priced publications may be purchased from the sources listed below or from major local booksellers.

Orders for unpriced publications should be made directly to the IAEA. The contact details are given at the end of this list.

AUSTRALIA
DA Information Services
648 Whitehorse Road, Mitcham, VIC 3132, AUSTRALIA
Telephone: +61 3 9210 7777 • Fax: +61 3 9210 7788
Email: books@dadirect.com.au • Web site: http://www.dadirect.com.au

BELGIUM
Jean de Lannoy
Avenue du Roi 202, 1190 Brussels, BELGIUM
Telephone: +32 2 5384 308 • Fax: +32 2 5380 841
Email: jean.de.lannoy@euronet.be • Web site: http://www.jean-de-lannoy.be

CANADA
Renouf Publishing Co. Ltd.
5369 Canotek Road, Ottawa, ON K1J 9J3, CANADA
Telephone: +1 613 745 2665 • Fax: +1 643 745 7660
Email: order@renoufbooks.com • Web site: http://www.renoufbooks.com

Bernan Associates
4501 Forbes Blvd., Suite 200, Lanham, MD 20706-4391, USA
Telephone: +1 800 865 3457 • Fax: +1 800 865 3450
Email: orders@bernan.com • Web site: http://www.bernan.com

CZECH REPUBLIC
Suweco CZ, spol. S.r.o.
Klecakova 347, 180 21 Prague 9, CZECH REPUBLIC
Telephone: +420 242 459 202 • Fax: +420 242 459 203
Email: nakup@suweco.cz • Web site: http://www.suweco.cz

FINLAND
Akateeminen Kirjakauppa
PO Box 128 (Keskuskatu 1), 00101 Helsinki, FINLAND
Telephone: +358 9 121 41 • Fax: +358 9 121 4450
Email: akatilaus@akateeminen.com • Web site: http://www.akateeminen.com

FRANCE
Form-Edit
5 rue Janssen, PO Box 25, 75921 Paris CEDEX, FRANCE
Telephone: +33 1 42 01 49 49 • Fax: +33 1 42 01 90 90
Email: fabien.boucard@formedit.fr • Web site: http://www.formedit.fr

Lavoisier SAS
14 rue de Provigny, 94236 Cachan CEDEX, FRANCE
Telephone: +33 1 47 40 67 00 • Fax: +33 1 47 40 67 02
Email: livres@lavoisier.fr • Web site: http://www.lavoisier.fr

L'Appel du livre
99 rue de Charonne, 75011 Paris, FRANCE
Telephone: +33 1 43 07 50 80 • Fax: +33 1 43 07 50 80
Email: livres@appeldulivre.fr • Web site: http://www.appeldulivre.fr

GERMANY
Goethe Buchhandlung Teubig GmbH
Schweitzer Fachinformationen
Willstätterstrasse 15, 40549 Düsseldorf, GERMANY
Telephone: +49 (0) 211 49 8740 • Fax: +49 (0) 211 49 87428
Email: s.dehaan@schweitzer-online.de • Web site: http://www.goethebuch.de

HUNGARY
Librotade Ltd., Book Import
PF 126, 1656 Budapest, HUNGARY
Telephone: +36 1 257 7777 • Fax: +36 1 257 7472
Email: books@librotade.hu • Web site: http://www.librotade.hu

INDIA
Allied Publishers
1st Floor, Dubash House, 15, J.N. Heredi Marg, Ballard Estate, Mumbai 400001, INDIA
Telephone: +91 22 2261 7926/27 • Fax: +91 22 2261 7928
Email: alliedpl@vsnl.com • Web site: http://www.alliedpublishers.com

Bookwell
3/79 Nirankari, Delhi 110009, INDIA
Telephone: +91 11 2760 1283/4536
Email: bkwell@nde.vsnl.net.in • Web site: http://www.bookwellindia.com

ITALY
Libreria Scientifica "AEIOU"
Via Vincenzo Maria Coronelli 6, 20146 Milan, ITALY
Telephone: +39 02 48 95 45 52 • Fax: +39 02 48 95 45 48
Email: info@libreriaaeiou.eu • Web site: http://www.libreriaaeiou.eu

JAPAN
Maruzen Co., Ltd.
1-9-18 Kaigan, Minato-ku, Tokyo 105-0022, JAPAN
Telephone: +81 3 6367 6047 • Fax: +81 3 6367 6160
Email: journal@maruzen.co.jp • Web site: http://maruzen.co.jp

NETHERLANDS
Martinus Nijhoff International
Koraalrood 50, Postbus 1853, 2700 CZ Zoetermeer, NETHERLANDS
Telephone: +31 793 684 400 • Fax: +31 793 615 698
Email: info@nijhoff.nl • Web site: http://www.nijhoff.nl

Swets Information Services Ltd.
PO Box 26, 2300 AA Leiden
Dellaertweg 9b, 2316 WZ Leiden, NETHERLANDS
Telephone: +31 88 4679 387 • Fax: +31 88 4679 388
Email: tbeysens@nl.swets.com • Web site: http://www.swets.com

SLOVENIA
Cankarjeva Zalozba dd
Kopitarjeva 2, 1515 Ljubljana, SLOVENIA
Telephone: +386 1 432 31 44 • Fax: +386 1 230 14 35
Email: import.books@cankarjeva-z.si • Web site: http://www.mladinska.com/cankarjeva_zalozba

SPAIN
Diaz de Santos, S.A.
Librerias Bookshop • Departamento de pedidos
Calle Albasanz 2, esquina Hermanos Garcia Noblejas 21, 28037 Madrid, SPAIN
Telephone: +34 917 43 48 90 • Fax: +34 917 43 4023
Email: compras@diazdesantos.es • Web site: http://www.diazdesantos.es

UNITED KINGDOM
The Stationery Office Ltd. (TSO)
PO Box 29, Norwich, Norfolk, NR3 1PD, UNITED KINGDOM
Telephone: +44 870 600 5552
Email (orders): books.orders@tso.co.uk • (enquiries): book.enquiries@tso.co.uk • Web site: http://www.tso.co.uk

UNITED STATES OF AMERICA
Bernan Associates
4501 Forbes Blvd., Suite 200, Lanham, MD 20706-4391, USA
Telephone: +1 800 865 3457 • Fax: +1 800 865 3450
Email: orders@bernan.com • Web site: http://www.bernan.com

Renouf Publishing Co. Ltd.
812 Proctor Avenue, Ogdensburg, NY 13669, USA
Telephone: +1 888 551 7470 • Fax: +1 888 551 7471
Email: orders@renoufbooks.com • Web site: http://www.renoufbooks.com

United Nations
300 East 42nd Street, IN-919J, New York, NY 1001, USA
Telephone: +1 212 963 8302 • Fax: 1 212 963 3489
Email: publications@un.org • Web site: http://www.unp.un.org

Orders for both priced and unpriced publications may be addressed directly to:

IAEA Publishing Section, Marketing and Sales Unit, International Atomic Energy Agency
Vienna International Centre, PO Box 100, 1400 Vienna, Austria
Telephone: +43 1 2600 22529 or 22488 • Fax: +43 1 2600 29302
Email: sales.publications@iaea.org • Web site: http://www.iaea.org/books

International Atomic Energy Agency
Vienna
ISBN 978–92–0–103815–9
ISSN 1011–4289